AD-784 130

TECHNOLOGY DEVELOPMENT REPORT: RESULTS OF STATIC ELECTRICITY DISCHARGE SYSTEM TESTS (ACTIVE AND PASSIVE) - HEAVY LIFT HELICOPTER

John B. Solak, et al

Boeing Vertol Company

Prepared for:

Army Air Mobility Research and Development Laboratory

May 1974

EUSTIS DIRECTORATE POSITION STATEMENT

The passive static electricity dissipation concept described in the report offers a workable solution to the problem within the context of Heavy Lift Helicopter program constraints. The experimental designs and hardware were substantiated during full-scale testing in a desert environment of heavy triboelectric charging and provided the basis for the design of prototype hardware.

The conclusions contained herein are concurred in by this Directorate.

Technical monitorship for this effort was jointly provided by Mr. S. B. Poteate, Jr., Maintenance and Analysis, Military Operations Technology Division, and Mr. J. A. Vichness, Heavy Lift Helicopter Project Office, Systems Support Division.

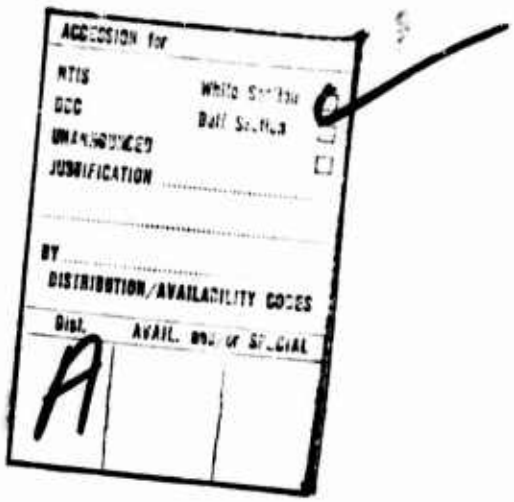

DISCLAIMERS

The findings in this report are not to be construed as an official Department of the Army position unless so designated by other authorized documents.

When Government drawings, specifications, or other data are used for any purpose other than in connection with a definitely related Government procurement operation, the United States Government thereby incurs no responsibility nor any obligation whatsoever; and the fact that the Government may have formulated, furnished, or in any way supplied the said drawings, specifications, or other data is not to be regarded by implication or otherwise as in any manner licensing the holder or any other person or corporation, or conveying any rights or permission, to manufacture, use, or sell any patented invention that may in any way be related thereto.

Trade names cited in this report do not constitute an official endorsement or approval of the use of such commercial hardware or software.

DISPOSITION INSTRUCTIONS

Destroy this report when no longer needed. Do not return it to the originator.

Unclassified

SECURITY CLASSIFICATION OF THIS PAGE (When Data Entered)

REPORT DOCUMENTATION PAGE		READ INSTRUCTIONS BEFORE COMPLETING FORM
1. REPORT NUMBER USAAMRDL-TR-74-22	2. GOVT ACCESSION NO.	3. RECIPIENT'S CATALOG NUMBER AD 784130
4. TITLE (and Subtitle) TECHNOLOGY DEVELOPMENT REPORT - RESULTS OF STATIC ELECTRICITY DISCHARGE SYSTEM TESTS (ACTIVE AND PASSIVE) - HEAVY LIFT HELICOPTER		5. TYPE OF REPORT & PERIOD COVERED Final report 6. PERFORMING ORG. REPORT NUMBER T301-10194-1 and -2
7. AUTHOR(s) John B. Solak Gregory J. Wilson		8. CONTRACT OR GRANT NUMBER(s) Contract DAAJ01-71-C-0840 (P40)
9. PERFORMING ORGANIZATION NAME AND ADDRESS Boeing Vertol Company A Division of The Boeing Company Philadelphia, Pennsylvania 19142		10. PROGRAM ELEMENT, PROJECT, TASK AREA & WORK UNIT NUMBERS
11. CONTROLLING OFFICE NAME AND ADDRESS U. S. Army Aviation Systems Command St. Louis, Missouri 63166		12. REPORT DATE May 1974 13. NUMBER OF PAGES 235
14. MONITORING AGENCY NAME & ADDRESS(if different from Controlling Office) Eustis Directorate U. S. Army Air Mobility R&D Laboratory Fort Eustis, Virginia 23604		15. SECURITY CLASS. (of this report) Unclassified 15a. DECLASSIFICATION/DOWNGRADING SCHEDULE

16. DISTRIBUTION STATEMENT (of this Report)

Approved for public release; distribution unlimited.

17. DISTRIBUTION STATEMENT (of the abstract entered in Block 20, if different from Report)

18. SUPPLEMENTARY NOTES

19. KEY WORDS (Continue on reverse side if necessary and identify by block number)

Helicopters
Electricity
Electric fields
Turbines
Dissipation

20. ABSTRACT (Continue on reverse side if necessary and identify by block number)

This document presents the findings of a three-phase program consisting of laboratory tests, ground tests, and a full-scale flight test program to evaluate methods for active dissipation of the static electricity buildup on the Heavy Lift Helicopter (HLH). Remote helicopter-borne electric field mills were also evaluated as sensors of the electrical potential between the hovering helicopter and the ground.

DD FORM 1 JAN 73 1473 EDITION OF 1 NOV 65 IS OBSOLETE

Unclassified

SECURITY CLASSIFICATION OF THIS PAGE (When Data Entered)

20. Continued.

Flight tests were conducted on a CH-47 helicopter, since the HLH is currently in its development stage.

This document also presents the final results of the static electricity drainage tests for the Heavy Lift Helicopter (HLH) Advanced Technology Component (ATC) development program. Included are:

1. Summary of active static electricity discharge system tests.

2. Detailed description and findings of passive static electricity discharge system tests.

3. Final program conclusions and a recommended design for the HLH static electricity system hardware.

TABLE OF CONTENTS

		Page
1.0	ACTIVE STATIC ELECTRICITY DISCHARGE SYSTEM . .	1
1.1	INTRODUCTION	1
1.2	TEST SEQUENCE AND PROCEDURE	2
1.3	TEST DATA COLLECTION/PROCESSING/ANALYSIS . . .	2
1.4	TASK CONCLUSIONS	3
1.5	RECOMMENDATIONS	4
2.0	DESCRIPTION AND FINDINGS OF PASSIVE STATIC ELECTRICITY PROGRAM	5
2.1	BACKGROUND	5
2.2	OBJECTIVE	5
2.3	DESIGN APPROACH	5
2.4	HARDWARE DESCRIPTION	6
2.4.1	GROUNDING LINE	6
2.4.2	GROUNDING POLE	8
2.5	FLIGHT TEST EVALUATION PROGRAM	9
2.6	TASK CONCLUSIONS	11
2.7	DESIGN OF HLH RESISTIVE GROUNDING LINK	12
2.8	RECOMMENDATIONS	15
2.8.1	PASSIVE STATIC ELECTRICITY HARDWARE	15
2.8.2	ARCTIC INVESTIGATION	15
3.0	REFERENCES	16

APPENDIXES

		Page
I.	Nanevicz, J. E., and Douglas, D. G., ELECTROSTATIC DISCHARGE SYSTEM, Stanford Research Institute, Final Report, November 1972.	17
II.	Douglas, D. G., and Nanevicz, J. E., FLIGHT TEST EVALUATION OF HELICOPTER CARGO HANDLING SYSTEMS - PASSIVE STATIC ELECTRICITY DRAINAGE, Final Report, Stanford Research Institute, September 1973.	152
III.	HLH STATIC ELECTRICITY SYSTEM HARDWARE DESIGN.	227

TECHNOLOGY DEVELOPMENT REPORT
RESULTS OF STATIC ELECTRICITY DISCHARGE SYSTEM TESTS (ACTIVE AND PASSIVE)-HEAVY LIFT HELICOPTER (HLH)

1.0 ACTIVE STATIC ELECTRICITY DISCHARGE SYSTEM

1.1 INTRODUCTION

With the contract award to develop advanced technology components for the Heavy Lift Helicopter (HLH), The Boeing Company, with Stanford Research Institute (SRI) as subcontractor, undertook the assignment of solving the most troublesome static electricity problem affecting a helicopter:

- Potential equalization between a hovering helicopter and the ground or a cargo handler standing on the ground.

The design objective is to limit energy transfer on contact to 1 millijoule. For a heavy lift helicopter of 120,000 pounds gross weight and the electric capacity of the order of 2,000 picofarads, this is equivalent to no more than about 1,000 volts potential difference.

All previous tests have indicated that the maximal charging rates are of the order of 300 microamperes for a 40,000-pound helicopter gross weight. For the 120,000-pound heavy lift helicopter, an estimated charging rate of 600 microamperes was set as the design objective for dissipating capability.

The design objective for an HLH active automatic system can, therefore, be stated as follows: not more than 1 millijoule discharge (potential difference less than 1,000 to 2,000 volts) under 600 microamperes natural charging conditions.

There are two basic approaches to the solution of the large hovering helicopter problem:

- Sensing and actively dissipating proper polarity and amperage charges into the surrounding air to counteract the natural charging of the helicopter. This method is commonly called an active system, since a high-voltage power supply is used to produce the discharge.

- Reducing the helicopter voltage by means of passive corona points and grounding the helicopter by means of droplines (passive system).

This section is concerned only with active dissipation systems.

Basic approaches selected for the remote sensing and active dissipation investigations described in this report are:

- To sense the potential between the winch-mounted cargo hook and the ground by locating an electric field mill on the hook and evaluating accuracy (fidelity) as a function of height of this field mill above the ground.

- To dissipate currents up to 600 microamps into the exhaust plumes of the helicopter turboshaft engines, thereby taking advantage of the high flow velocities in this region to overcome space charge limitations close to the active dissipator electrodes and to provide a mechanism for blowing the free ions away from the helicopter.

1.2 TEST SEQUENCE AND PROCEDURE

The test program, which was formulated in Reference 1 of Section 3.0, was divided into three phases:

1. Laboratory dissipator tests using a low-speed wind tunnel and a full-scale mock-up of an engine exhaust and aft helicopter fuselage.

2. Helicopter ground tests of selected active dissipator configurations to evaluate the thermal, acoustic, soot, and flow field effects of an actual engine exhaust plume.

3. Full-scale flight tests on a CH-47 helicopter at the U. S. Army Yuma Proving Ground to evaluate active dissipators and remote sensors under conditions of actual helicopter triboelectric charging while hovering in a dust cloud.

1.3 TEST DATA COLLECTION/PROCESSING/ANALYSIS

Success or failure of the active dissipation system was predicated on solution of two basic problems:

1. Dissipation of a continuous charging current of 600 microamperes into the air surrounding the hovering helicopter.

2. Correct sensing of the potential difference between the helicopter and the ground while actively dissipating high charging currents.

It was anticipated by Boeing Vertol that the dissipation problem could be solved, but that the question of correct sensing might encounter basic limitations from the physics of ion clouds and from remote sensor concepts, since potentials are inferred rather than actually measured directly. For this reason, Boeing Vertol went to the technical community for expertise in static electricity dissipation in the form of a request for quote (RFQ) on the Reference 1 program.

Bids were received from two technically qualified organizations: Dynasciences Corporation and Stanford Research Institute. The sensing problem dictated emphasis on basic electrostatic physics rather than on hardware. Stanford Research Institute (SRI) was selected to perform the program and prepare a final report.

Test data collection, processing, and analysis are contained in the comprehensive subcontractor final report by Dr. Joseph E. Nanevicz and Mr. D. G. Douglas of SRI, entitled "Electrostatic Discharge System" which is provided as Appendix I to this document.

1.4 TASK CONCLUSIONS

Appendix I contains the conclusions derived from this program. A brief summary of the major conclusions is provided below.

1. Sensing Accuracy - Under heavy triboelectric charging conditions, the ion cloud which surrounds a large helicopter as a result of natural charging, active dissipation, and electrification of the ground surface can falsify readings from sensors located on the helicopter fuselage and on a simulated cargo hook lowered to within 5 feet of the ground. The residual discharge energy on the helicopter resulting from these sensor errors can reach 10 joules (Table IV, Page 110) on the fuselage and 1.0 joule on the cargo hook (Table VII, Page 145). This lack of sensor accuracy, at large helicopter charging levels, prevents any active dissipation system from meeting the system safety objective of the heavy lift helicopter.

2. Dissipation - It will be feasible to actively dissipate 200 microamperes into each turbine exhaust of the HLH for a combined total of 600 microamperes using a bipolar power supply of 200,000 to 250,000 volts potential. Dissipation from corona points extending from the fuselage into the rotor downwash could also provide currents in excess of 600 microamperes but would require approximately 8 corona points located a minimum of 6 feet away from any conductive surface of the helicopter.

3. Resistance of the Ground - Prior to the June 1972 Yuma desert tests, the resistance of a dry desert was considered to be of the order of 10^9 ohms (References 2 and 3). Measurements at Yuma in May and June 1972, near the end of a 159-day dry spell, have shown that desert resistance is seldom higher than 10^6 ohms and never exceeds 10^7 ohms. This throws new light on the feasibility of passive dropline discharging techniques in lieu of active dissipation as shown below:

Ground Resistance	Charging Current	Residual Helicopter Voltage
10^9 ohms	600 μA	600,000
10^7 ohms	600 μA	6,000
10^6 ohms	600 μA	600

1.5 RECOMMENDATIONS

1. Based on the findings of this program, it is recommended that the Heavy Lift Helicopter Advanced Technology Component static electricity dissipation program be reoriented from active dissipation to passive dissipation and grounding techniques.

2. Primary objective of a passive grounding system should be protection of the ground handler during cargo hookup operations. A reasonable amount of sparking should be accepted upon grounding.

3. Cargo unloading should be protected by contact grounding directly through the cargo itself.

4. For the special case of dry snow, where high surface resistance could prevent successful ground, a winterization kit approach should be used consisting of a projectile and trailing wire to pierce the insulating layer.

2.0 DESCRIPTION AND FINDINGS OF PASSIVE STATIC ELECTRICITY PROGRAM

2.1 BACKGROUND

Based on the findings of the active dissipation program, the static dissipation program was redirected to a passive system. The passive system was developed and subsequently demonstrated in May/June 1973 at the U. S. Army Yuma Proving Ground. Appendix II to this report fully describes the tests and demonstration. Subsequent paragraphs summarize the passive static electricity system development program.

2.2 OBJECTIVE

The primary objective of the passive system is the protection of the cargo handler during cargo hookup operations. This objective presents a design compromise:

1. A highly conductive grounding link (such as a low-resistance wire) between the helicopter and the ground surface will leave the minimum residual voltage on the helicopter. However, in case of inadvertent contact with the cargo handler (prior to contact with the ground surface), it will expose the cargo handler to the full discharge energy stored by the helicopter.

2. If a resistor of several megohms is inserted in the grounding line, it will protect the cargo handler against very high voltages on the helicopter (e.g., 10 Mohms will allow a contact up to 120,000 volts, 20 Mohms over 200,000 volts, etc.) but will leave a residual voltage under heavy charging conditions due to the ohmic voltage drop. At the HLH design maximum charging current of 600 microamperes, a total resistance between the helicopter and ground of 10 Mohms will leave a residual voltage of 6,000 volts on the helicopter, and 20 Mohms will leave a residual voltage of 12,000 volts.

2.3 DESIGN APPROACH

Two pieces of grounding hardware were considered for the HLH. The first is a resistive grounding link, commonly called a grounding line, which is attached to one cargo coupling and dangles approximately 7 feet below it. As the HLH winches are used to lower the cargo coupling for load hookup, the grounding line contacts the cargo or the ground and thereby discharges the helicopter prior to any handling of the cargo coupling by ground hookup personnel. The second hardware item is a

resistive grounding pole intended to be used under the special circumstances of a depot location and a requirement to handle or guide cargo before it touches the ground. In this situation, the grounding pole, which is a loose piece of ground handling equipment, is used to contact the cargo and to thereby discharge the cargo and the helicopter, making it safe for ground handler manipulation.

Designs were formulated by Boeing Vertol for the grounding line (Reference 4) and grounding pole (Reference 5). Fabrication bids were solicited from static electricity discharger manufacturers. Successful bidder was The Truax Company, Fort Myers, Florida.

2.4 HARDWARE DESCRIPTION

The grounding line and grounding pole hardware are shown in Figure 1.

2.4.1 GROUNDING LINE - The grounding line consists of the following elements:

1. Cargo coupling attachment fitting
2. Damage-resistant leader
3. Disconnect coupling
4. 10 megohm resistive element
5. Disconnect coupling
6. Grounding element
7. Corona discharge element

Electrical conductivity is provided from end-to-end of the grounding line.

Cargo Coupling Attachment Fitting - This item consists of an L-shaped aluminum bracket which attaches to the cargo coupling and provides a horizontal mounting surface for the remainder of the grounding line.

Damage-Resistant Leader - This item consists of a 3/16-inch-diameter steel cable encased in a 1/2-inch-outside-diameter rubber hose sealed with RTV type sealant at each end. Steel threaded shafts are swaged to both ends of the cable to provide attachment means for the elements above and below. The purpose of this item is to absorb, in a harmless manner, any accidental impacts which might occur if the cargo coupling is dropped on the ground or on top of cargo, or if it is swung into the side of cargo or other obstacles.

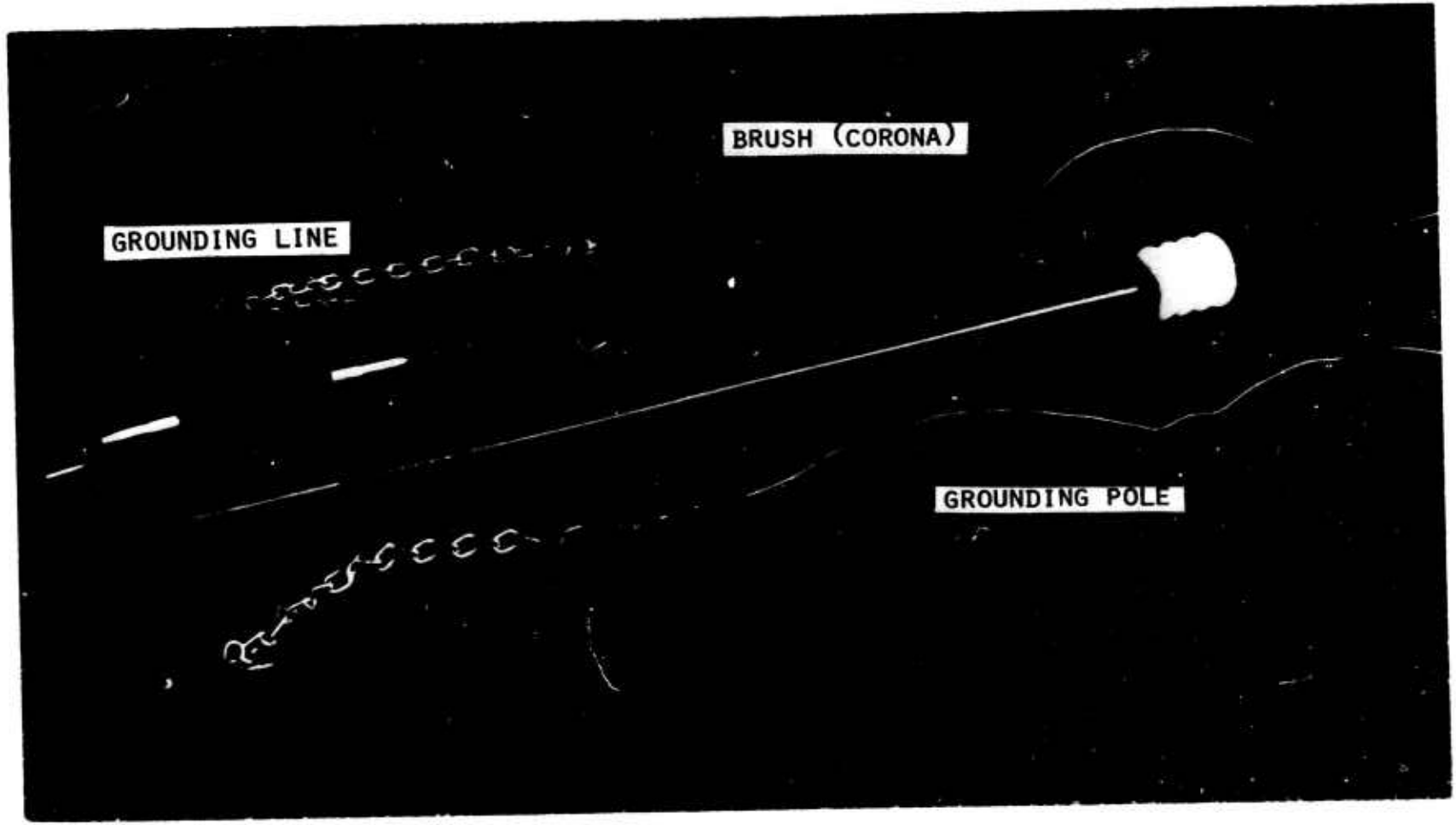

FIGURE 1. PASSIVE STATIC ELECTRICITY DISCHARGE SYSTEM.

Disconnect Coupling - This item consists of a standard pair of MS electrical connectors. It serves the dual purpose of providing a convenient means of replacing damaged elements rather than the entire grounding line and acts as a yield feature to free the cargo coupling in the event that the grounding line becomes snagged in ground obstacles or is trapped under cargo. Tensile force for complete severance is 300 to 700 pounds.

Ten Megohm Resistive Element - This item consists of a 1/4-inch-diameter stranded nylon rope, dipped in polyurethane doped with a carbon dust of sufficient content to provide the required resistance and flexibility. Heat-shrinkable Teflon tubing is used to jacket the nylon rope in order to prevent shorting of the element by rain droplets. Teflon was selected as the jacketing material because of its high resistance to carbon tracking, a phenomenon which shorts high-voltage insulators. The resistive element is designed to carry continuous currents up to 600 microamperes without deterioration. The purpose of this element is to limit sparking on ground contact and also to act as a shock limiter in the event the grounding line is accidentally touched before it contacts the ground.

Disconnect Coupling - Same as prior disconnect coupling.

Grounding Element - This item consists of a 2-foot length of cadmium-plated steel chain. Welded tabs are provided on each end link for compatibility with forked bolts which in turn are attached to disconnect couplings. A feed-through wire is provided to ensure end-to-end electrical conductivity. Its purpose is to provide a flexible, damage-resistant multiple contact element to ground the helicopter under widely varying conditions of surface composition. An additional consideration is to minimize the danger of injury to ground handlers or damage to cargo if inadvertently struck.

Corona Discharge Element - This item consists of either a metal brush made up of 300 steel wires of 0.010 inch diameter shaped to form a hemisphere, or a standard fixed-wing aircraft passive electrostatic discharger (Truax Company Model ESD-2A). The purpose of this item is to decrease the magnitude of spark discharge prior to ground contact by providing a low corona threshold element which will reduce the helicopter potential as it descends to within 5 feet of the ground.

2.4.2 GROUNDING POLE - The grounding pole consists of the following elements:

1. Conductive contact element
2. One megohm resistive element
3. Lead wire
4. Ground contact element
5. Insulating rod

Conductive Contact Element - This item consists of a 1/4-inch-diameter anodized aluminum rod threaded at one end and bent into the shape of a shepherds crook. Its purpose is to contact the cargo and to accept direct spark discharges which are then carried to the ground. It also provides a means for gripping or hooking onto most types of external cargo.

One Megohm Resistive Element - This item consists of a 12-inch-long rigid tubular fiberglass center-body overcoated with polurethane doped with a carbon dust content sufficient to provide the required resistance. Attachments are provided at each end to maintain electrical conductivity with the conductive contact element and the lead wire.

Lead Wire - This item consists of a 120-inch piece of No. 6 AWC copper braid inside an equal length of heat-shrinkable Teflon tubing. Disconnect couplings of the MS electrical type are provided at each end to permit field replacement if the lead wire becomes damaged. The purpose of this element is to carry the static discharge from the conductive contact element to the ground and also to serve as a drain for a lightning strike to the helicopter after the grounding pole has been attached to the cargo.

Ground Contact Element - This item consists of a 2-foot length of cadmium-plated steel chain. Welded tabs are provided on each end link for compatibility with forked bolts which in turn are attached to disconnect couplings. A feed-through wire is provided to ensure end-to-end electrical conductivity. The purpose of this element is to provide a reasonable contact electrical path to ground under widely varying terrain conditions in the presence of hovering helicopter rotor downwash.

Insulating Rod - This item consists of a hollow insulating fiberglass pole 6 feet in length covered with heat-shrinkable Teflon tubing for water repellency. Its resistance exceeds 100 megohms. A series of polypropylene water droplet collars is provided to prevent rain from forming a continuous conductive path down the length of the pole. A rubber handgrip is provided at the lower end to facilitate one-hand usage. The purpose of the insulating rod is to protect the ground handler from the shock energy levels of helicopter discharging.

2.5 FLIGHT TEST EVALUATION PROGRAM

The static electricity hardware was evaluated under simulated operational conditions during a series of U. S. Army flight tests at Yuma Proving Ground, using a CH-47 Chinook helicopter.

The helicopter was hovered over typical surfaces such as macadam, concrete, hard-packed desert, plowed-up desert, and the contact was established by the grounding line, lowered on a simulated cargo hook (aluminum block) or by the grounding pole. Different grounding electrodes (chain) and resistive elements were tested, under actual service conditions (whipping in the helicopter downwash, deployment by dropping the line, manhandling by grounding pole). In addition, the resistance between the grounding electrode and the good ground was measured and plotted in function of applied voltage. The detailed description of these tests is contained in Appendix II. It soon became obvious that the grounding resistance is sufficiently low to insure acceptable residual voltage after ground contact was made, but that the grounding line and the grounding pole hardware as supplied by The Truax Company are unsuitable for reasons outlined below.

1. Grounding Line

   a) Damage Resistive Leader - The steel cable should be encased in vulcanized rubber to exclude water ingress and corrosion.

   b) MS Connectors should be replaced by more rugged and more permanent coupling. A yield feature should be included as a separate design element (500 lb. $\pm$ 100 lb.).

   c) The flexible resistive element failed under test conditions. Subject to strain of deployment from the helicopter, whipping in the helicopter downwash or hooked accidentally by the grounding pole, its resistance has invariably increased by a factor of 3 to 4 (30 to 40 Mohms). Such high resistance would leave 18 to 24 KVolt residual voltage under 600 microamperes charging and is therefore unacceptable. The transition from resistive coating to connector was by means of a copper wire, which was failing under normal handling. For the above reason, the tests were completed using a rigid ceramic resistor with good resistance stability, but unsuitable for the incorporation in the actual design. The redesign of the resistive element (and the whole grounding line) is contained in Appendix III. Full redesign considerations are given in Paragraph 2.7 of this report.

   d) Grounding Chain - Its length will be increased from 2 feet to 3 feet, to allow for more vertical motion of the hovering helicopter.

e) The Corona Discharge Elements will be eliminated because the tests have shown that its contribution to RFI cannot be detected in presence of other RFI generated under triboelectric charging conditions.

2. Grounding Pole - As stated in Paragraph 2.6, Item c of this report, it was concluded that the use of the grounding pole is not warranted. The deficiencies of the grounding pole are reported below in case some user has a requirement for the grounding pole rather than the grounding line (e.g.; U. S. Coast Guards are using the grounding pole for shipboard operation).

a) The contact hook should be replaced by some form of a clip-on device, which would prevent accidental breaking of the grounding contact and thus free the cargo handler from holding the contact unbroken (Note: If the contact is accidentally broken, the helicopter regains full voltage in 1 to 2 seconds).

b) 1.0 Mohm Resistor should be eliminated. Its reduction of sparking of the grounding chain is insignificant. To limit the danger of spilled fuel ignition, a much higher resistance is required, which would defeat the voltage lowering process.

c) Water droplet collar must be lighter.

d) The grip must be of larger diameter and longer, to allow holding the pole with both hands.

2.6 TASK CONCLUSIONS

The following conclusions have been drawn from the flight evaluation of passive static electricity hardware:

1. The concept of a resistive grounding link between a hovering Heavy Lift Helicopter and the ground for static electricity potential equalization is viable for typical moderate climate surfaces.

2. A passive grounding line with a 10-megohm series resistance should be employed on the HLH to protect ground handlers from static electricity during cargo hookup operations. The design of the grounding line should be revised to provide 10 Mohm resistance stable within ±1 Mohm under temperature, voltage, and strain variations, retaining its flexibility and providing good protection against service abuse (Appendix III and Paragraph 2.7 of this report). All other improvements outlined in Paragraph 2.5, Item 1., should be included.

3. A grounding pole should not be used with the HLH, since ground personnel could receive severe shocks if contact were inadvertently lost with the cargo.

2.7 DESIGN OF HLH RESISTIVE GROUNDING LINK

1. General. Due to lack of firm data on stability of flexible resistors (temperature, voltage, mechanical strain) it was decided to take the following approach on the design of the grounding line.

   a) Long Term Solution - Flexible resistor, fully tested for environmental conditions will be used when it is offered by the resistor industry.

   b) Short Term Solution - Fixed resistive elements of suitable stability, properly protected from service life abuse will be used.

   The short term solution is discussed below and shown in Appendix III.

2. Basic Design. The resistive line will consist of 3 elements 3.3 Mohm each, 70 KVolt each, 7 inches long. Each resistor will be incased in a strong protective tubing for mechanical protection, and potted on ends to exclude water ingress and corrosion. The resistors are chosen from the products of the Resistance Products Co. in Harrisburg. Their resistors were used by Princeton University and ECOM in experiments described in Ref.5. (NOTE: Other companies equally qualified are Victoreen Resistors, Cleveland, Ohio, and International Resistance Company.)

3. Resistance Stability Requirements. The resistor must hold its resistance within ±10% from -65°F to 160°F (per HLH specifications) under maximum voltage of 200 KVolt (120 KVolt for dry climate, measured in Yuma desert, 200 KVolt anticipated for the Arctic).

4. Industry Standards. The resistor industry uses definitions given below:

   a) Temperature Stability - Percentage per °C

   b) Voltage Stability - Resistance is measured at 1/10 voltage, then at full voltage. The resistance change per volt is defined as

$$\frac{R \text{ at } 0.1 \text{ volts} - R \text{ full volts}}{\text{Volts} - 1/10 \text{ Volts}}$$

5. Types of Resistors Available. Two resistance types are available from the resistor industry, namely:

- Carbon film deposited on fiberglass. This resistance has the advantage of a flexible rod (fiberglass), but the carbon coating exhibits large temperature and voltage coefficients.

- Metal oxide film deposited on ceramic. This resistance has the disadvantage of rather brittle rod (alum. oxide) but the oxide deposit has superior temperature and voltage characteristics. It is pointed out that ± 1.0 Mohm resistance change is rather conservative and probably ± 2.0 Mohm resistance change would be acceptable in service. In Items a) and b) below, the two resistance types are described in more detail.

a) Carbon Deposited on Fiberglass - 3.3 Mohm, 70 KVolt, 126°C Temperature Range.

- Resistance change with temperature

10^{-3} per °C
10^{-3} x 126 = 12.6% = 1.26 Mohm for 10 Mohm

- Resistance change with voltage

3×10^{-6} Per Volt
Change: $3 \times 10^{-6} \times 7 \times 10^{4}$ Volt x 3.3 Mohm = 0.7 Mohm
2.1 Mohm for 10 Mohm
Total change: 3.36 Mohm

This resistor could be used if nothing better was available, but was rejected for a better one which is described in the following.

b) Metal Oxide (RPC Type X7071) on Ceramic (alum. oxide).

- Resistance change with temperature

200×10^{-6} per °C = 2×10^{-4} per °C
for 126°C and 10 Mohms = 0.25 Mohms
(Note: Victoreen claims 3.5×10^{-4} per °C)

- Resistance change due to voltage:

10^{-6} per volt.
10 Mohms x 10^{-6} x 180 x 10^{3} = 1.8 Mohms
(Note: Victoreen claims 5×10^{-6} per Volt)

Total Resistance Change: 2.0 Mohms approx., which corresponds to ± 1 Mohm change. This type of resistor was selected.

6. Resistor Data. Length 7.0 inches, which corresponds to 10 Volt/mil, customary in resistor design (an insulating sleeving can be provided, e.g., heat-shrinkable Teflon tubing, if service tests show flashover problem exists).

Continuous current carrying capability - 1 mA, maximum 1.6mA. Surge capability - 1.4 A for 1 microsecond (approximately). Total Resistance Change Due to Temperature and Voltage: less than ± 1.0 Mohm.

End caps, stainless steel or nickel, 0.1 wide. Thickness: 15 mil ± 1 mil (Pigtails spot welded on both ends to end caps).

7. Problem of Thermal Expansion and Potting. The aluminum oxide is not flexible; hence it must be protected from mechanical abuse. Enclosing the resistor inside a Teflon cylinder would provide good water-repellency and a strong case. Potting looks like a very attractive solution against water ingress and dielectric strength. Unfortunately, the difference in thermal expansion of the materials in question excludes potting of the whole resistor length (see Table 1 below).

TABLE 1.

Material	Linear Thermal Expansion Coeff.	Total Expansion on 7" Length for 126°C	Expansion for 126°C
Alum.Oxide	7×10^{-6} per °C	6.3 mil	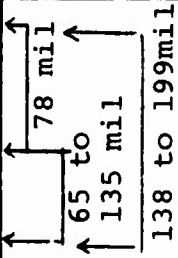
Fiberglass	8×10^{-6} per °C	8.0 mil	
Teflon	95×10^{-6} per °C	84 mil	
Potting Compound BAC 5550	160 to 230 x 10^{-6} per °C	142 to 205 mil	

It is obvious that potting the whole length of 7" would present very difficult packaging. The 40-mil expansion difference between the Teflon and aluminum oxide presents a problem, which would require some flexible

bellows on both sides of the resistor. A suitable compromise is a fiberglass case, covered with heat shrinkable Teflon tubing or polyolefine tubing (for water repellency, carbon tracking), and potting of both ends of the tube only.

2.8 RECOMMENDATIONS

2.8.1 PASSIVE STATIC ELECTRICITY HARDWARE

1. The resistive grounding link design presented in Appendix III should be adopted for the HLH.

2. The HLH/ATC development program does not include full hardware qualification. The resistive grounding link (Appendix III) should be subjected to military qualification prior to production.

2.8.2 ARCTIC INVESTIGATION

The significance of arctic climates on grounding surface resistance is unknown. Since surface resistance affects the performance of the resistive grounding link, typical arctic surface resistances should be established at HLH residual static electricity potentials to extend hardware application to these climates.

Survey of the literature in the United States, United Kingdom, and Canada has shown that there is no data available on contact resistance of a grounding element at voltages up to 14 KVolt and currents of the order of 600 microamperes. Some physicists (Prof. J.R. Addison of McGill University) believe that surface conduction of the snow crystals at such elevated voltages will be more significant than the relatively low conductivity measured for conduction through the ice crystal's body. It is quite possible that the grounding contact resistance will be sufficiently low to assure operational feasibility of the passive method even under worst (dry snow) condition.

3.0 REFERENCES

1. Solak, B. J., and Wilson, G. J., CRITICAL ITEM DEVELOPMENT SPECIFICATION FOR HLH ADVANCED TECHNOLOGY COMPONENT (ATC) PROGRAM - STATIC DISCHARGE SYSTEM - STAGE I, Report S301-10011, Rev. B, The Boeing Vertol Company, Philadelphia, Pa., March 1972.

2. USAAVLABS Technical Report 69-90, INVESTIGATION OF CH-54A ELECTROSTATIC CHARGING AND OF ACTIVE ELECTROSTATIC DISCHARGER CAPABILITIES, AD865988, Eustis Directorate, U.S. Army Air Mobility Research and Development Laboratory, Fort Eustis, Virginia, January 1970.

3. ECOM Research and Development Report, ECOM-02412-6, THE PRINCETON PENNSYLVANIA ARMY AVIONICS RESEARCH PROGRAM, PRINCETON TASKS, September 1970.

4. Boeing Vertol's S301-10050 Design Specification - CARGO HANDLING SYSTEM - STATIC ELECTRICITY DRAINAGE-GROUNDING LINE.

5. Boeing Vertol's S301-10051 Design Specification - CARGO HANDLING SYSTEM - STATIC ELECTRICITY DRAINAGE-GROUNDING POLE.

6. ECOM Research and Development Report ECOM-02412-10, THE PRINCETON PENNSYLVANIA ARMY AVIONICS RESEARCH PROGRAM, FINAL TASK REPORT, A FUNDAMENTAL STUDY OF STATIC ELECTRIC PHENOMENA (APPLIED TO HELICOPTERS), March 1972.

APPENDIX I

ELECTROSTATIC DISCHARGE SYSTEM

FOREWORD

This report was prepared by Stanford Research Institute, Menlo Park, on Army Contract DAAJ01-71-C-0840(P40), subcontract P.O. CH-700377. The work was administered under the direction of The Vertol Division, Boeing Company, Philadelphia, Pa. Mr. B. J. Solak was the technical monitor.

The studies presented began in December 1971 and concluded in September 1972. This report describes research performed by the Electronics and Radio Sciences Division, Electromagnetic Sciences Laboratory of Stanford Research Institute. The principal investigator, Dr. J. E. Nanevicz, was responsible for research activity under SRI Project 1657.

ABSTRACT

Laboratory and flight tests were performed to investigate various active discharger systems, and the sensing problem as it relates to the Boeing 301 HLH Helicopter. Excellent agreement between laboratory studies and flight tests were obtained.

The experiments show that while high-net-current (> 600 μA) discharger designs were probably feasible for the HLH helicopter, the accurate sensing of the helicopter potential (with respect to ground) would be very difficult when the helicopter was operated in an external space-charge environment.

CONTENTS

FOREWORD 17

ABSTRACT 18

LIST OF ILLUSTRATIONS 20

LIST OF TABLES 24

I INTRODUCTION 25

II LABORATORY INVESTIGATION OF DISCHARGER DESIGNS 29

III HELICOPTER GROUND TESTS OF DISCHARGER DESIGNS 52

IV FLIGHT TESTS 65

A. Instrumentation Calibration 70
B. Ground-Conductivity Measurements 71
C. Flight Tests of Discharging Elements 73
D. Sensor-Fidelity Flight Tests 92

V CONCLUSIONS 118

APPENDICES

A LABORATORY ELECTROSTATIC MEASUREMENTS 121

B A STATISTICAL EXAMINATION OF THE ELECTRIC FIELDS MEASURED BY A HELICOPTER HOVERING IN A DUSTY ENVIRONMENT 127

ACKNOWLEDGMENTS 148

REFERENCES 149

DD Form 1473

ILLUSTRATIONS

2	SRI Wind-Tunnel Facility to Permit Active-Discharger Testing	31
3	Laboratory Mock-up of CH-47 Helicopter Fuselage and Engine	32
4	Velocity-Profile Measurements of Engine-Simulator Output	33
5	Schematic Representation of Voltage and Currents Measured in the Laboratory Simulation Facility	36
6	Performance of Various Discharger Designs at 125-ft/s Wind Speed in Laboratory Mock-up	37
7	General Results of Experiments with Discharger Configurations Involving a Single Point for Wind Speed = 125 ft/s	40
8	Results of Experiments on the Use of a Long Element as a Discharger for Wind Speed = 125 ft/s	41
9	General Results of Experiments Involving Rings as Discharging Elements for Wind Speed = 125 ft/s	43
10	Variation of Current with Power-Supply Voltage for Single-Point Discharger for a Wind Speed of 125 ft/s	46
11	Variation of Current with Wind Speed for a Single-Point Discharger	47
12	Relationships Among Currents as Power-Supply Voltage is Varied	48
13	Relationship Between Currents as Airspeed is Varied	50
14	Instrumentation Configuration for CH-47 Ground Tests at Boeing Vertol	54
15	Photograph of Arrangement for Ground Tests	55
16	Comparison of Laboratory Data for a Single-Point Discharger with Ground-Test Measurements	57

17 Comparison of Laboratory Data for Dual-Ring Discharger with Ground-Test Measurements 58

18 Recirculation-Current Studies During Ground Tests with a Power-Supply Voltage of 120 kV for a Ring Discharger and for a Single Corona Point on Center Line 59

19 Laboratory Investigation of Extended Discharger Spacing 62

20 Supersonic Nozzle Configuration Used During Laboratory Tests to Investigate the Utility of Auxiliary Air Flows 63

21 Photograph Showing Airborne Instrumentation 66

22 Photograph Showing Airborne Instrumentation (Front View of Helicopter Showing Radar-Altimeter Antennas and #2 Field-Meter Installation) 67

23 Photograph Showing Airborne Instrumentation (Side View of Helicopter Showing Field Meters #3 and #4 and Recirculation Patches) 68

24 Layout of Instrumentation for Dissipator Tests 74

25 Photograph of CH-47 Flight-Test Aircraft 75

26 Photograph of Single-Point Discharger Mounted Three Exhaust Diameters Behind the Left Turbine Exhaust 77

27 Sign Conventions for Currents and Fields 78

28 Flight-Test Comparison of Single-Ring and Single-Point Dischargers in Engine Exhaust (Clean Environment) 79

29 Flight-Test Investigation of Effects of Discharging Element as a Function of Distance Aft of Engine Exit Plane (Clean Environment) 81

30 Flight-Test Comparison of Discharge Current from Discharging Elements in One vs. Two Engine Exhausts (Clean Environment) 82

31 Flight-Test Investigation of Discharge Current as a Function of Hover Altitude for the Ring Discharger Mounted in the Left Exhaust, Five Diameters Behind the Exit Plane (Clean Environment). . . . 84

32	Flight-Test Investigation of Outrigger Discharger Currents as Affected by Helicopter Hover Altitude (Clean Environment)	85
33	Maximum-Dissipation Flight Tests Using Outrigger System and Single Ring at d = 5D (Clean Environment) . . .	86
34	Photograph Showing Flight-Test Operation at Phillips Drop Zone	88
35	Flight-Test Investigation of Current Dissipation Using Outrigger Dischargers, as Affected by Helicopter Hover Altitude (Dust Environment)	89
36	Flight-Test Investigation of Current Dissipation Using Turbine Discharger as Affected by Helicopter Hover Altitude (Dust Environment)	90
37	Comparison of SRI Flight and Ground Discharger Tests with Previous Flight-Test Data	91
38	Flight-Test Calibration of Cargo-Hook Field Meter	94
39	Flight-Test Calibtation of Helicopter Field Meters	96
40	Sensor-Fidelity Flight Tests with Outrigger Discharger (Clean Area).	99
41	Sensor-Fidelity Flight Tests Using Ring at 5D for Artificial Charging	101
42	Helicopter Fly-by Investigation of Dust-Dust Triboelectric-Charging Effects	104
43	Observation of Electric Fields on Various Sensors Measured as a Function of Time	106
44	Measured Electric Field as a Function of Time During Ground-Disconnect Experiment while Hovering in Dust	112
45	Measured Electric Field as a Function of Time During Ground-Disconnect Experiment while Hovering in a Clean Area	115
46	Flight-Test Comparison of Effects of Wind on Field-Meter Readings During Nulling Experiment	117
47	Comparison of Responses of Flush-Mounted Field Meter with Responses of Protruding Field Meter	122
48	Laboratory Calibration of Field Meter Location	125

49 Typical Oscillograph Record (Raw Data) Showing Field-Meter Data, Ground Current, Radar Altimeter, and Clock Signal as Functions of Time 131

50 Electric-Field Histogram for Helicopter Hover Operation in Dusty Environment--Field Meter #1 H = 25 ft, h = 15 ft 132

51 Potential Histogram for Helicopter Hover Operation in Dusty Environment--Field Meter #1, H = 25 ft, h = 15 ft 134

52 Potential Histogram for Helicopter Hover Operation in Dusty Environment--Field Meter #2, H = 25 ft 135

53 Potential Histogram for Helicopter Hover Operation in Dusty Environment--Field Meter #3, H = 25 ft 136

54 Potential Histogram for Helicopter Hover Operation in Dusty Environment--Field Meter #4, H = 25 ft 137

55 Potential Histogram for Helicopter Hover Operation in Dusty Environment--Field Meter #1, H = 50 ft, h = 25 ft 138

56 Potential Histogram for Helicopter Hover Operation in Dusty Environment--Field Meter #2, H = 50 ft 139

57 Potential Histogram for Helicopter Hover Operation in Dusty Environment--Field Meter #3, H = 50 ft 140

58 Potential Histogram for Helicopter Hover Operation in Dusty Environment--Field Meter #4, H = 50 ft 141

59 Ground-Current Histogram for Helicopter Hover Operation in Dusty Environment--A/C Grounded, H = 25 ft 142

60 Ground-Current Histogram for Helicopter Hover Operation in Dusty Environment--A/C Grounded, H = 50 ft 143

61 Measured Ground Current vs. Inferred Potential from Field-Meter #2 for Helicopter Hover Operations in a Dusty Environment, H = 50 ft 145

TABLES

I	Surface Resistance as Determined by Megger Method (V_{PS}= 4 kV)	72
II	Relationships Between Outrigger Voltage and Electric Field at Various Sensor Locations	100
III	Statistical Compilation of Data Measured by Airborne Field Meters While Hovering in Dust at 25 ft and 50 ft.	109
IV	Discharge-Energy Probability Calculations Inferred from Field-Meter Data for a Helicopter Hovering in the Dust	110
V	Comparison of Electric Fields Measured on a Model and on a Full-Scale CH-47	126
VI	Statistical Summary of Observed Ground Current During Helicopter Hover Operations in a Dusty Environment	135
VII	Charging Current and Available Record Time, H=25 ft, h=5 ft	146
VIII	Discharge Energy Probability H=25 ft, h=5 ft.	146

I INTRODUCTION

For many years it has been known that when an aircraft (fixed or rotary-wing) operates in an environment containing particles (snow, ice crystals, rain, dust, etc.) there is a high probability that the aircraft will become electrified due to triboelectric (i.e., frictional) charging. This charging can increase the potential of the aircraft to a point, beyond which further charging results in corona discharges from various parts of the airframe to the surrounding air. These uncontrolled high-energy discharges can interfere with radio equipment and/or prematurely detonate explosive devices or ignite inflammable materials.

Considerable effort has been expended in recent years in identifying and solving this problem on fixed-wing aircraft. The solution has generally been to install corona-discharge devices that lower the aircraft potential, through passive or active means, to acceptable levels. These devices utilize a non-recirculating discharge system in which the rapid flow of air over the aircraft surfaces is used to carry away the ions created by the corona discharge to allow a reduction in potential to low energy levels.

A hovering helicopter, however, presents a different problem not easily solvable by conventional means. There is no slipstream into which ions may be injected and suitably carried away from the aircraft. The hovering helicopter and its rotor down-wash tend to form a "closed loop" system--i.e., ions injected into the rotor wash tend to recirculate back to the airframe through the convective processes beneath the helicopter.

With the increased use of helicopters in cargo operations, the electrostatic discharge encountered when the cargo is grounded poses a serious hazard to ground personnel and to explosive or inflammable materials. This hazard continues to increase as helicopters become larger, since the capacitance of the helicopter (and hence the energy released on discharge) is proportional to the size of the helicopter.

The program described below was undertaken in an attempt to define a few optimum discharger designs that might be used on the Boeing 301 HLH, and to determine the feasibility of correctly sensing the helicopter-to-ground potential using electric-field meters.

When considering the problem of maintaining the potential of a hovering helicopter near zero (with respect to ground) it becomes apparent that the most crucial problems are (1) devising a scheme for accurately measuring the helicopter-to-ground potential in the presence of charged particles, discharged ions, and external electric fields, and (2) designing and positioning a discharging element on the helicopter capable of removing from the aircraft the required discharge current. There are many other problems associated with the development of a functioning active discharging system, such as designing a high-voltage supply capable of operating in the helicopter environment, and designing a stable servo system, but unless the problems of sensing and discharging have been solved, all other problems are academic.

A review of the general problem quickly indicated that any approach to this investigation must lean heavily on experiment. The geometry of the helicopter is sufficiently complicated that a purely analytical approach to a study of the electrostatic fields in its vicinity is difficult. The problem is further complicated by the fact that a hovering helicopter may not be located in a field-free, charge-free region, but can be surrounded by charged particles of various kinds,

(ice, dust, discharged ions, etc.) severely complicating the sensing problem. The primary limit on current discharged from an element is established by the ion cloud formed about the element by the discharge products. Accordingly, to determine discharge-current levels, it is mandatory that the airflows about the helicopter (which are responsible for carrying away the discharge products) be known or simulated accurately. Proper description of all of these parameters in sufficient detail to permit an accurate analytic solution appeared impossibly difficult, so that a highly experimental approach was followed instead.

In further planning the possible approaches, it was observed that flight tests can be very expensive and marginally productive unless they are carefully planned to eliminate as much as possible random testing involving a wide variety of configurations. This consideration dictated that flight tests be preceded by thorough laboratory and ground tests to serve as a guide in determining the ultimate course of the flight tests.

With the above arguments in mind, it was decided that the program would be conducted in three phases. In the first, laboratory simulations were carried out at SRI to investigate likely approaches, and to weed out those that proved to be undesirable. The laboratory tests also provided an opportunity to vary certain parameters such as size and spacing to investigate their effect on system performance and to do these things economically. In the second phase, ground tests were carried out on a CH-47 helicopter at Boeing Vertol in Philadelphia to verify the laboratory results and gain additional insight into the discharging processes as they apply to the CH-47. The ground tests also afforded the opportunity to investigate the workability of proposed flight-test systems in an actual helicopter environment. In the third phase, flight tests were conducted at the Yuma Proving Ground, Yuma, Arizona, using an instrumented CH-47 helicopter. During these tests, conducted in May and June, 1972, the best of the discharger designs

selected in the laboratory and ground tests were thoroughly examined. Concurrent with the discharger evaluations in the flight-test phase, airborne and ground field meters were used to determine the feasibility of accurately inferring the potential of the helicopter with respect to ground.

II LABORATORY INVESTIGATION OF DISCHARGER DESIGNS

Experience in designing aircraft discharging systems has indicated that it is essential that the discharge products (ions) be injected into a high-velocity airstream to carry them away and minimize the limitation of the discharge by the presence of the discharge ion cloud, or space charge. In addition, it is important that the discharge products be directed away from any field-sensing devices being used to measure aircraft potential, because these charged particles may introduce a measurement error. In casting about for likely locations for discharging elements, one is immediately led to the rotor-blade tips since these are regions of clearly defined, high-velocity airflow. This technique was not studied because locating active discharging elements on the rotor blades greatly complicates rotor design, and the costs involved were beyond the scope of the present program. A second, smaller and slower region of directed airflow away from the helicopter exists in the turbine engine exhausts. The feasibility of locating discharging elements here was investigated on the present program. A third region of directed airflow away from the helicopter is located amidship in the region where the two rotors intersect. The functioning of a discharging element in this location was also investigated.

In designing a discharging system, one must select a discharger configuration, a discharger location, and an operating potential. Many combinations of these parameters are possible, and to test all of the combinations during flight tests would be prohibitively expensive. It was decided, therefore, that a helicopter mock-up would be used in a laboratory program to investigate a wide variety of discharger arrangements, and to select the most promising for further investigation during the ground and flight tests.

It was observed that, in order to expedite the investigation of the various design parameters, it would be desirable to have an operating full-scale model of the discharging system, aircraft, and engine available in the laboratory. This approach is far preferable to simply placing the engine mock-up in a uniform low-velocity airflow field, because the actual space-charge distributions expected can be more realistically simulated. This was accomplished at minimum cost by modifying an existing water-wave wind-tunnel facility in the Electromagnetic Sciences Laboratory at SRI. This facility employs two 30,000-cfm centrifugal blowers to generate a maximum wind velocity of 55 ft/s in a tunnel of 3-ft-by-5-ft cross section as shown in the sketch of Figure 2. By building an adapter section in the output plenum chamber and knocking a hole in the wall of the chamber, it was possible to use the air source to feed a 22-inch-diameter cylindrical tube simulating the CH-47 helicopter engine exhaust. The "engine" and a full-scale mock-up of the aft part of the Chinook helicopter in the immediate vicinity of the engine were installed in the room beyond the plenum chamber.

A photograph of the laboratory set-up is shown in Figure 3. The mock-up consisted of a wooden framework covered with sheet metal to simulate the electrical characteristics of the helicopter fuselage. Provisions were made to electrically isolate the aft end of the engine tail-pipe and the helicopter mock-up to permit such parameters as local recirculation to be studied in the laboratory. A track made of PVC plastic pipe was used to support various discharging elements under study.

Once the "engine" was operational, a series of velocity-profile measurements were made at various stations behind the tail pipe. The results of these measurements are shown in Figure 4. It is seen from this figure that the modifications made to the wind tunnel allowed an increase in wind speed to about 125 ft/s. It is evident that at a

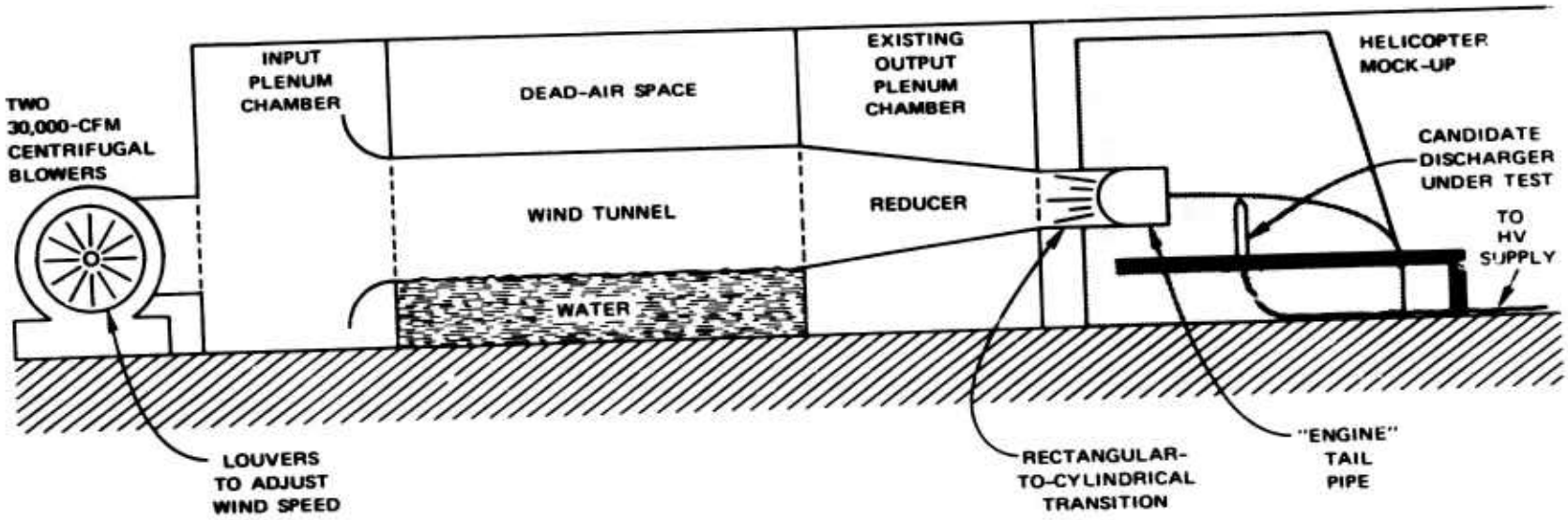

FIGURE 2 SRI WIND-TUNNEL FACILITY TO PERMIT ACTIVE-DISCHARGER TESTING

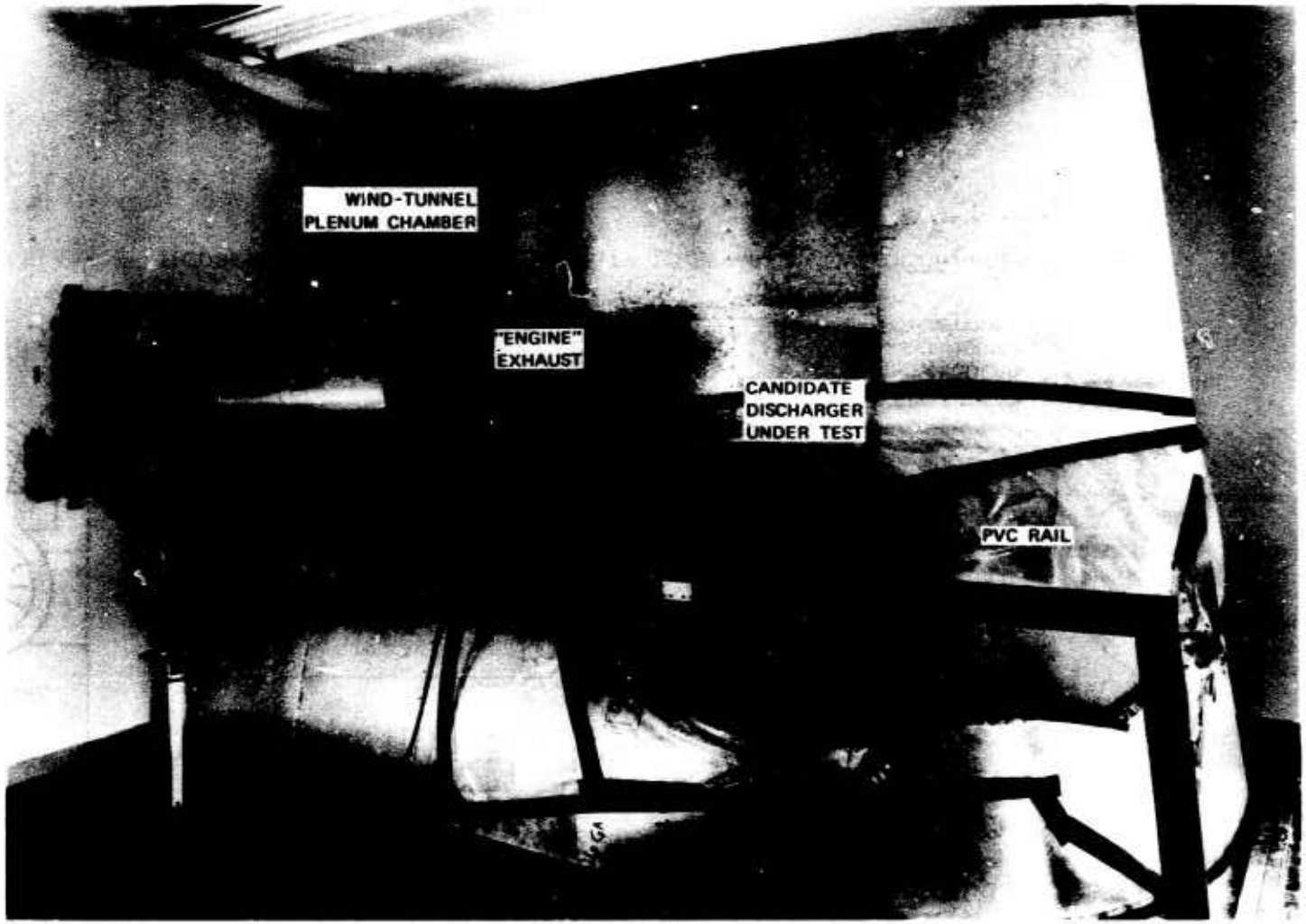

FIGURE 3 LABORATORY MOCK-UP OF CH-47 HELICOPTER FUSELAGE AND ENGINE

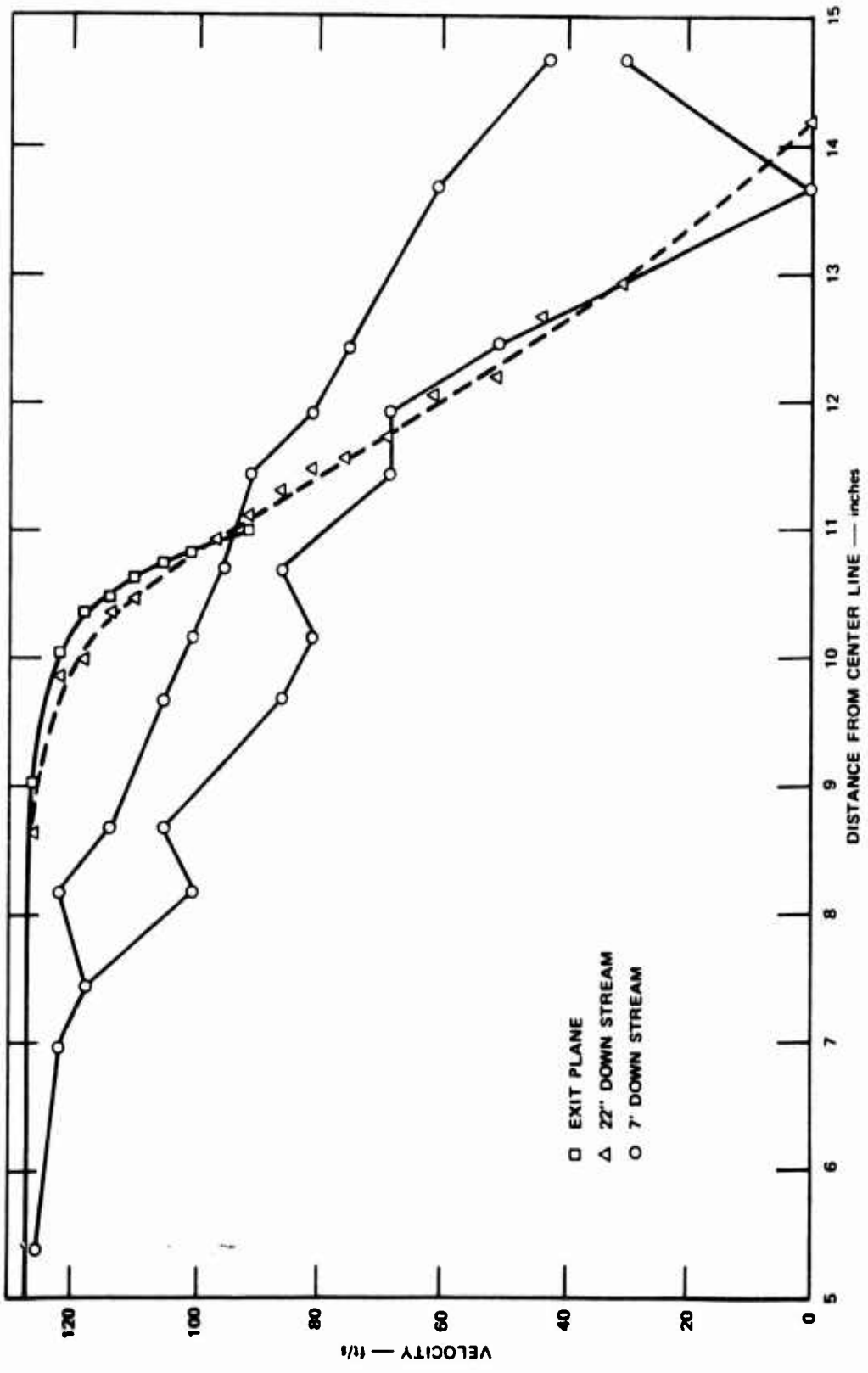

FIGURE 4 VELOCITY-PROFILE MEASUREMENTS OF ENGINE-SIMULATOR OUTPUT

position one tail-pipe diameter downstream of the exit plane the flow is still very clearly defined and has not grown appreciably in diameter. Farther downstream, however, the boundary of the flow becomes less clearly defined, and the flow becomes turbulent. These results are interesting, because they indicate that there is little flow actually impinging on the body of the helicopter to cause recirculation. Although the maximum flow velocity in the simulator engine is slower than the 300-ft/s turbine exhaust velocities on the CH-47, it was felt that the important aspects of various discharger design parameters could be adequately investigated with these speeds, and costly modification of the wind tunnel to increase wind speed would be avoided. A measure of the sensitivity of a particular parameter to wind speed could be obtained by repeating measurements at several wind speeds. Provisions were included in the existing tunnel to vary wind speed by adjusting louver settings on the centrifugal blower input.

During the laboratory discharger tests the candidate discharging electrodes were mounted on a PVC rail running parallel to the exhaust axis and positioned 22 inches below the axis. The rail was attached to the mock-up at the forward end and was mounted on a strut extending to the aft end as is shown in Figure 2.

The approach to testing in the facility was as follows. First, a variety of possible discharging-element designs were conceived and assembled. Some of these designs were mechanically awkward, while others appeared to be electrically less desirable than others. These "ugly ducklings" were deliberately included in the initial testing to make certain that no satisfactory design was accidentally discarded as the result of unjustified, preconceived bias. Next, each successive design was installed in the laboratory simulation facility and evaluated according to the following general procedure. The "engine exhaust"

wind speed was set at the maximum value of 125 ft/s and the power-supply voltage was then increased in steps to its maximum value. Next, while the power-supply voltage was held at its maximum value, the airspeed was decreased in steps to zero. Where appropriate, the position of the discharging element was varied from one to three nozzle diameters aft of the engine exhaust plane, and the test sequence was repeated. Measurements were made of wind speed, power-supply voltage, power-supply current, net discharge current, current recirculated to the helicopter body, recirculation current to an electrically isolated patch on the fuselage, and current arriving on a large metal screen located approximately 10 ft downstream from the aft end of the helicopter. The voltage and currents measured are illustrated schematically in Figure 5. Taking data in this way limits to a tractable quantity the number of combinations of supply voltage and wind speed that must be measured to specify the performance of a particular discharger design. With these measurements taken, it is possible to extrapolate the data both to higher wind speed and to higher power-supply voltage, to estimate ultimate performance capabilities.

A description of some of the more interesting designs investigated is given in Figure 6 along with an indication of the results observed for the maximum wind velocity. In Column 1 of the figure are shown the results for a single sharp point located on the axis of the engine and one nozzle diameter downstream of the exit plane. Comparing Column 2 with Column 1 we find that moving this same point to a position roughly four nozzle diameters downstream of the exit plane markedly reduces the current recirculating back to the airframe and increases the net current discharged from 23 to 60 μA. Column 3 demonstrates that some additional discharging capability is achieved by using three discharging points spaced over a line somewhat smaller than the exit-plane diameter.

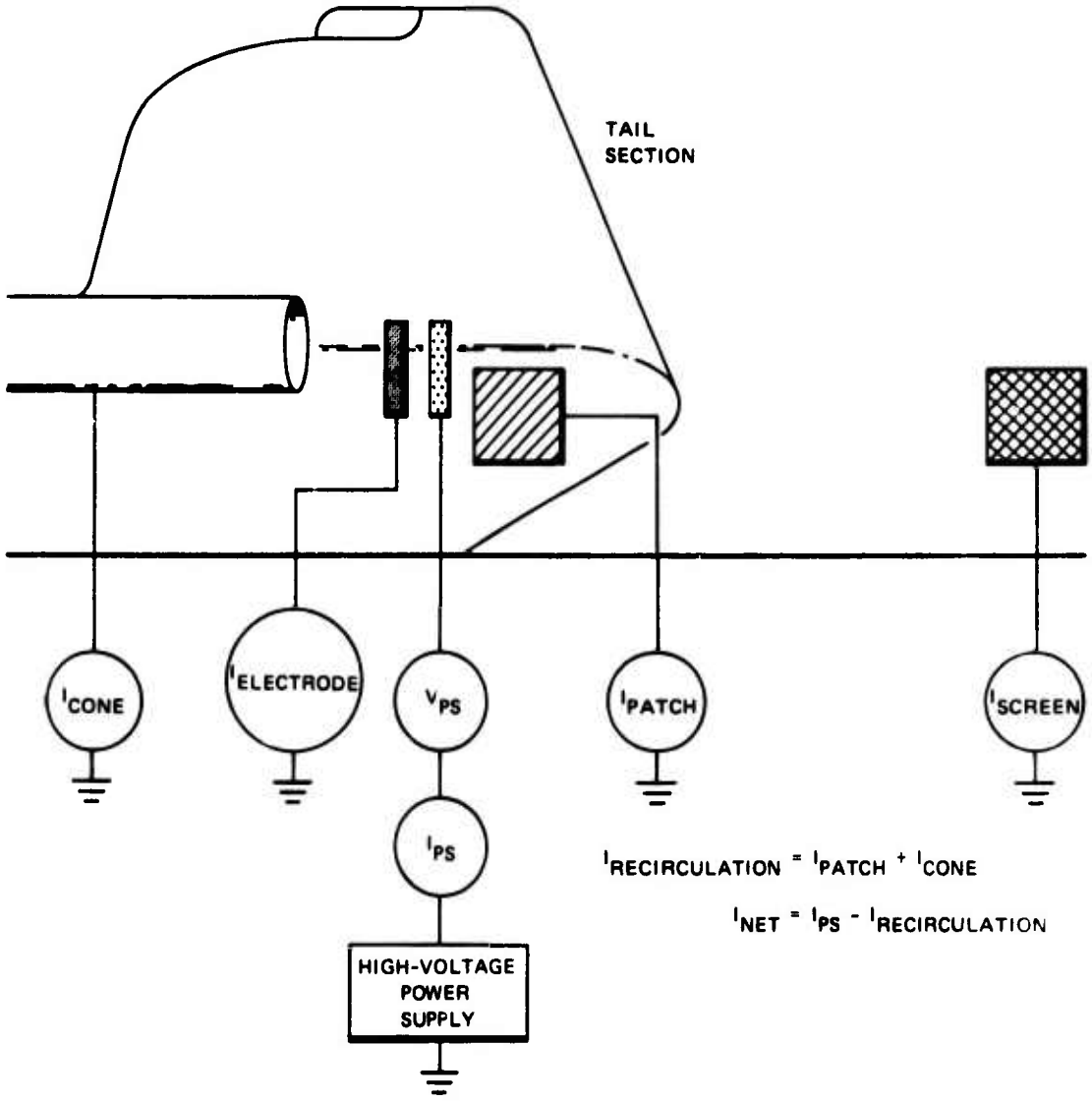

FIGURE 5 SCHEMATIC REPRESENTATION OF VOLTAGE AND CURRENTS MEASURED IN THE LABORATORY SIMULATION FACILITY

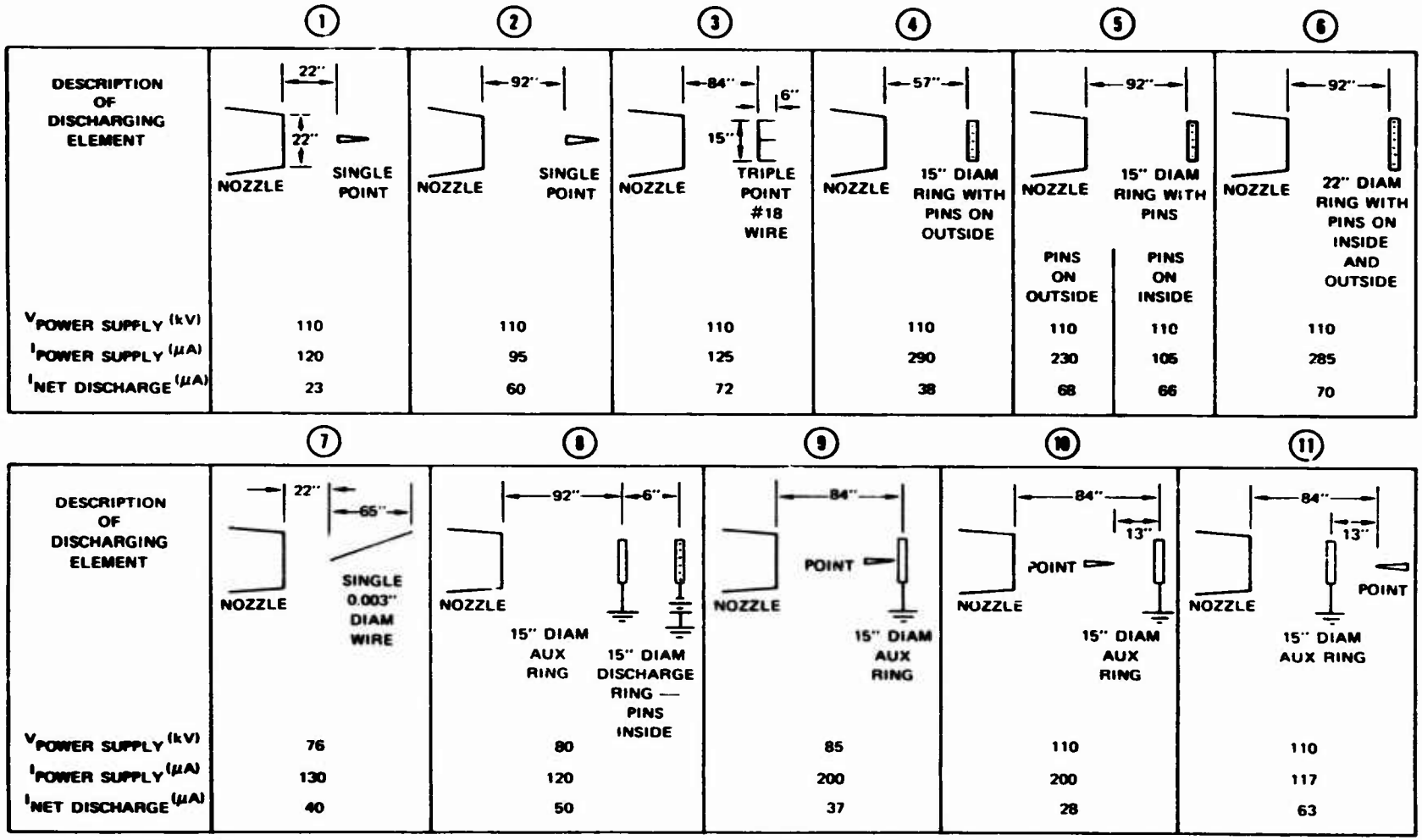

NOTE: When these measurements were completed, it was found that the model engine was located approximately 22 inches farther forward on the helicopter mock-up than is actually the case on the CH-47 helicopter.

FIGURE 6 PERFORMANCE OF VARIOUS DISCHARGER DESIGNS AT 125-ft/s WIND SPEED IN LABORATORY MOCK-UP

Columns 4 through 6 summarize a series of experiments using a discharging element consisting of a ring equipped with discharging points pointing inward or outward from its periphery. (This general design is interesting since, by proper location of the pins, it results in a low-noise discharging system.) Comparing Columns 4 and 5, we find again that moving the discharging element to a position roughly four nozzle diameters downstream of the exit plane decreases recirculation and increases the net discharge current. Within Column 5 we find that a ring fitted with inward-facing pins discharges roughly the same net current as one fitted with outward-facing pins, but that with the inward-facing pins, the power-supply current (and hence recirculating current) is half as high. Comparing Columns 5 and 6 indicates that by using a 22-inch-diameter ring with both inward- and outward-facing pins, one can achieve a slight increase in net discharge current while sustaining a substantial increase in recirculation current.

Column 7 gives the results of an experiment in which a single 0.0003-inch-diameter wire was used as the discharging element. For this test, the power-supply voltage was restricted to 76 kV, so that the current was lower than it would have been with 110 kV applied. At the higher voltage, the discharge current should approach that of the other discharger configurations tested ($\approx$ 60 μA).

Column 8 gives the results of the experiment in which an auxiliary grounded electrode was placed in proximity to the discharging electrode in an effort to achieve the desired discharge current at lower power-supply voltage. During these experiments great care was exercised to avoid arc-over, which might damage the power supply. Accordingly, the voltage was restricted to 80 kV in this configuration, giving a net discharge current of 50 μA. It appears that discharge currents of 60 to 70 μA could be achieved at a power-supply voltage somewhat below 110 kV.

The power-supply current for the configuration of Column 8 will be higher than that required for the same discharge current for a lone 15-inch ring with inward-facing pins as illustrated in Column 5.

The last three columns in the figure illustrate a set of experiments conducted to investigate the effectiveness of using an auxiliary grounded electrode to reduce the power-supply voltage requirements of a single-point discharger. In Columns 9 and 10 it is evident that the re-circulation current increases markedly when the point is even with or upstream of the auxiliary ring. Unfortunately the higher recirculation current is not accompanied by an increased discharge current. With the design of Column 11 it was possible to achieve a slightly higher discharge current than was achievable with a single point (see Column 2) for a given power-supply voltage.

Based on tests performed on the discharger configurations shown in Figure 6, more exhaustive tests were conducted on those dischargers showing promise electrically, and that might lend themselves, mechanically, to the ground- and flight-test program.

Although detailed data were taken for each discharger configuration, it is instructive to look first at only the data for top wind speed and highest supply voltage to see how discharge current varies with discharger design and location for these "more promising" configurations. Data for the single discharge point are presented in this abbreviated form in Figure 7. In Column 1 we see that as the discharge point is moved farther downwind from the "engine" exhaust plane, the power-supply current decreases and the net discharge current increases. These results indicate that the net discharge current achievable is limited by recirculation to the airframe in the immediate vicinity of the discharging element. For this reason, discharging elements positioned far back from the fuselage result in a higher net discharge current even though they are located in a region of somewhat reduced flow velocity.

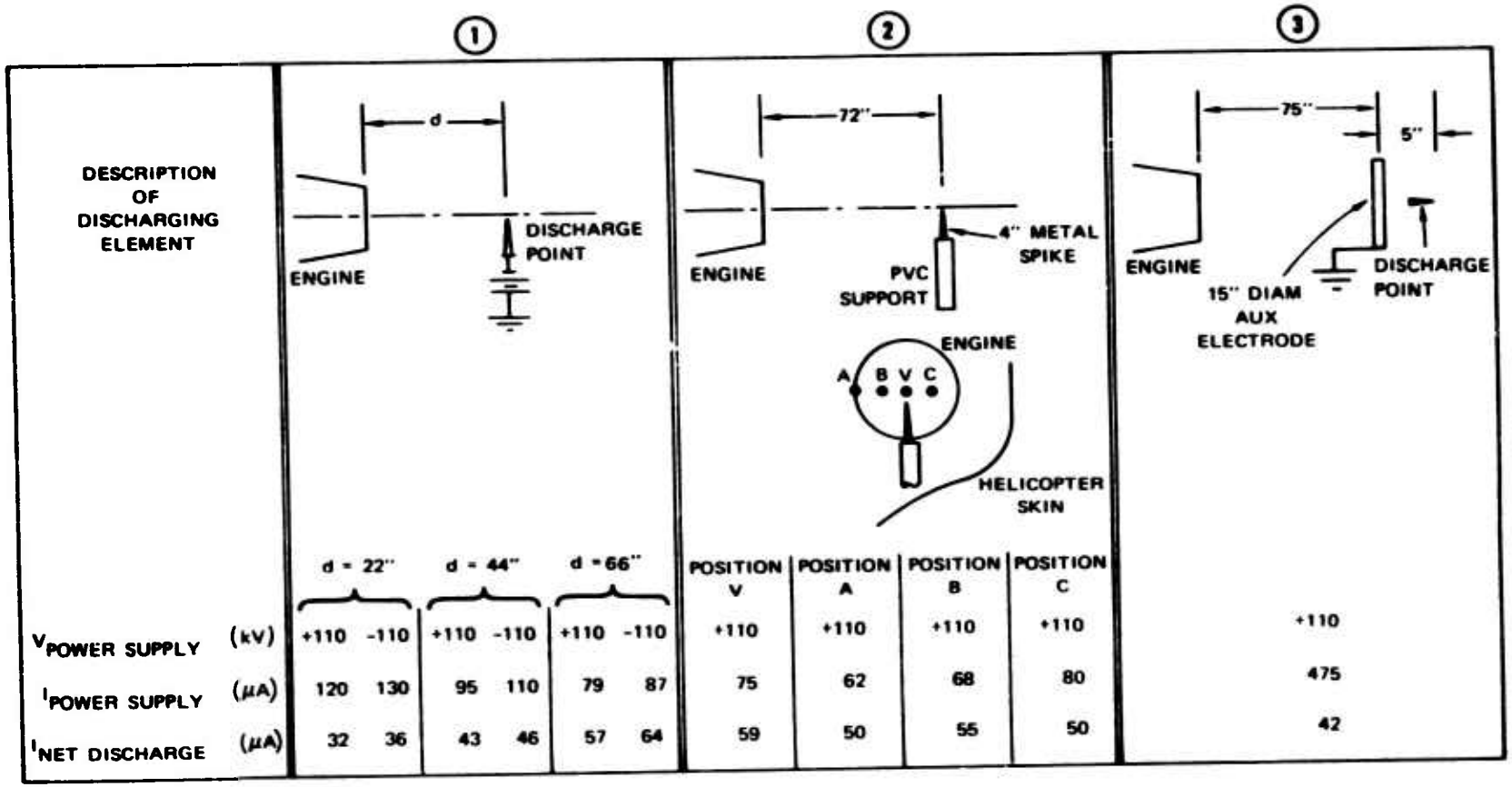

		d = 22"		d = 44"		d = 66"		POSITION V	POSITION A	POSITION B	POSITION C	
$V_{POWER\ SUPPLY}$	(kV)	+110	-110	+110	-110	+110	-110	+110	+110	+110	+110	+110
$I_{POWER\ SUPPLY}$	(μA)	120	130	95	110	79	87	75	62	68	80	475
$I_{NET\ DISCHARGE}$	(μA)	32	36	43	46	57	64	59	50	55	50	42

FIGURE 7 GENERAL RESULTS OF EXPERIMENTS WITH DISCHARGER CONFIGURATIONS INVOLVING A SINGLE POINT FOR WIND SPEED = 125 ft/s

In Column 2, the effect of moving the discharge point away from the center line of the engine is illustrated. Evidently the vertical position V along the center line results in maximum net discharge current. Although moving the point away from the skin to Positions A or B reduces the power-supply current, it also reduces the net discharge current. As might be expected, moving the point toward the skin to C increases the power-supply current (as the result of increased recirculation), but also reduces the net discharge current. Apparently discharge current is maximized when the ion density is uniformly distributed throughout the exhaust.

Column 3 illustrates the effect of using an auxiliary electrode in an effort to achieve the desired discharge current at lower power-supply voltage. Although the power-supply current is drastically increased, most of this current flows to the auxiliary ring, and the net current is lower than it would have been without the ring.

Column 1 of Figure 8 illustrates two sets of experiments using a

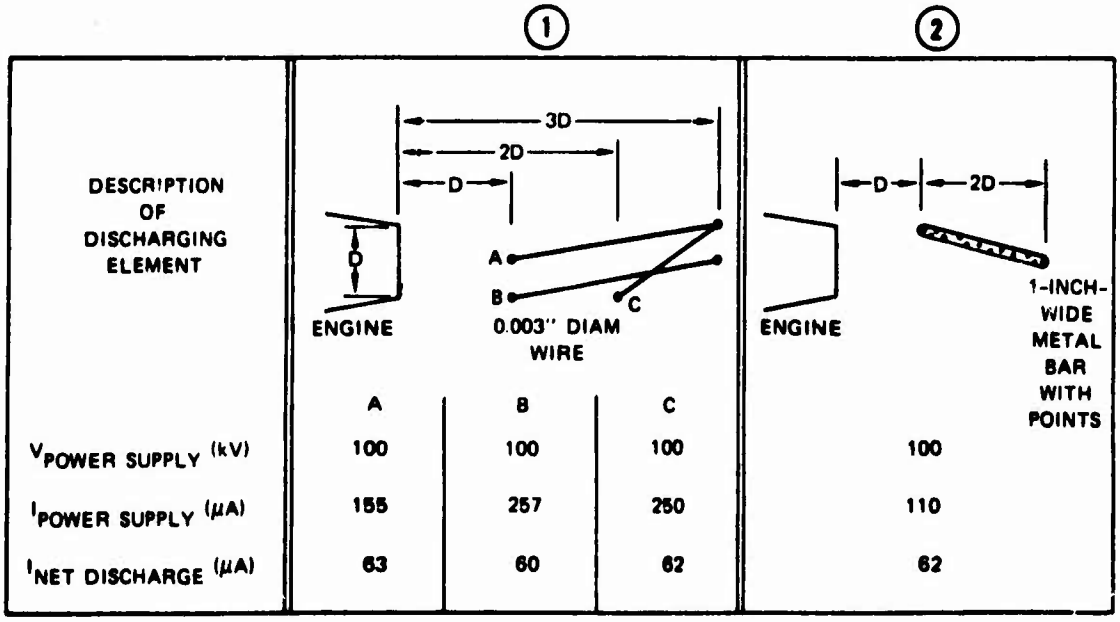

FIGURE 8 RESULTS OF EXPERIMENTS ON THE USE OF A LONG ELEMENT AS A DISCHARGER FOR WIND SPEED = 125 ft/s

single 0.003-inch-diameter wire as a discharging element. The purpose of these tests was to investigate the way in which discharging characteristics are affected by the length and placement of the wire. In Configuration A, the wire extended from a point on the center line of the exhaust at a distance one nozzle diameter downstream, to a point on the top of the exhaust three diameters downstream. To achieve Configuration B, the wire was merely translated down by one-half a nozzle diameter. The effect of this translation was to markedly increase the power-supply current while at the same time reducing the net discharge current. In Configuration C, a shorter wire was used to span the entire nozzle. There is very little difference in performance between Configurations B and C. The results of these experiments again indicate that bringing any part of the discharging element close to the fuselage increases the recirculation current and, often, decreases the net discharge current.

The second column in Figure 8 shows the results of an experiment in which a pin-filled metal bar was used as the discharging element. Its performance is similar to that of the 0.003-inch-diameter wire. The primary difference is that the power-supply current was lower with the bar than with any of the wires. This probably stems from the fact that the bar was tilted down at the back, making it roughly parallel with the contour of the helicopter in this region and maximizing the spacing between the discharger and the helicopter skin. The wire of Column 1, on the other hand, is tilted upward. It is probable that the power-supply current in Column 2 would also have approached 110 μA if the wire had been tilted downward.

Results of experiments with various combinations of ring-shaped discharging elements are presented in Figure 9. Column 1 indicates that the net discharging current is relatively independent of the diameter of a single ring used as the discharge element. It should also be noted

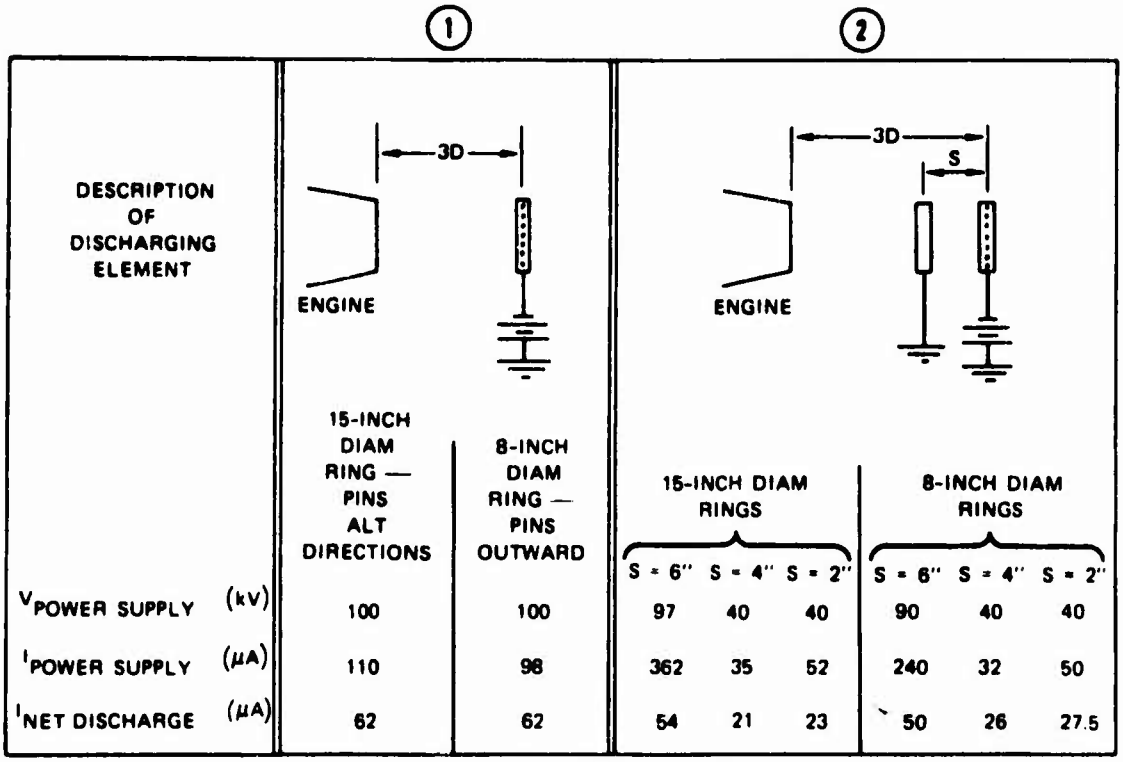

DESCRIPTION OF DISCHARGING ELEMENT		15-INCH DIAM RING — PINS ALT DIRECTIONS	8-INCH DIAM RING — PINS OUTWARD	15-INCH DIAM RINGS			8-INCH DIAM RINGS		
				S = 6"	S = 4"	S = 2"	S = 6"	S = 4"	S = 2"
$V_{POWER\ SUPPLY}$	(kV)	100	100	97	40	40	90	40	40
$I_{POWER\ SUPPLY}$	(μA)	110	98	362	35	52	240	32	50
$I_{NET\ DISCHARGE}$	(μA)	62	62	54	21	23	50	26	27.5

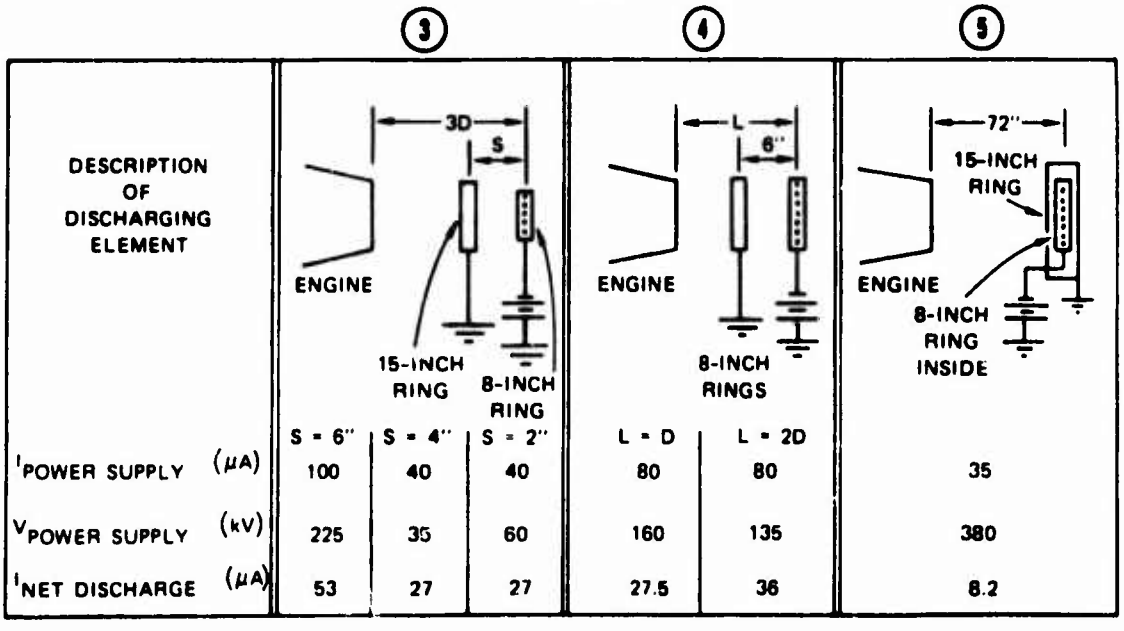

DESCRIPTION OF DISCHARGING ELEMENT		S = 6"	S = 4"	S = 2"	L = D	L = 2D	
$I_{POWER\ SUPPLY}$	(μA)	100	40	40	80	80	35
$V_{POWER\ SUPPLY}$	(kV)	225	35	60	160	135	380
$I_{NET\ DISCHARGE}$	(μA)	53	27	27	27.5	36	8.2

FIGURE 9 GENERAL RESULTS OF EXPERIMENTS INVOLVING RINGS AS DISCHARGING ELEMENTS FOR WIND SPEED = 125 ft/s

that this current is almost identical with that obtained with a single point in Column 1 of Figure 7 (positive polarity).

Column 2 of Figure 9 illustrates the results of experiments with discharging elements composed of a discharging ring and an auxiliary ring of the same diameter. Again the performance of the system is evidently not very sensitive to ring diameter. The spacing between the rings does affect system performance, since the spacing determines the maximum power-supply voltage that can be used without flashover. In the case of a 2-inch spacing, this is 40 kV. (40 kV was also used as the maximum voltage in the experiments with 4-inch spacing. It could have been higher, but the test matrix was set up for 40 kV). With 6-inch spacing it was possible to use 90 to 97 kV without flashover. These results indicate that spacings as low as 2 inches are impractical in that they do not permit significant power-supply current before flashover. Even a spacing of 6 inches is inadequate to avoid flashover at 110 kV. Finally, it is apparent that at the 125-ft/s exhaust velocity, substantial recirculation to the ground ring occurs, so that the net discharge current achieved is lower than with a single ring in Column 1.

The results of a series of experiments with rings of unequal size are summarized in Column 3. Although there is some variation in details between these data and those of Column 2, there appears to be no reason to choose one over the other.

Column 4 illustrates the reduction in net discharge current that occurs as the discharging assembly is moved closer to the engine. This is in agreement with the results obtained with a single discharge point in Column 1 of Figure 7.

The last experiment with ring-discharger configurations is illustrated in Column 5. It consisted of a pin-filled, 8-inch-diameter ring concentrically mounted inside a 15-inch-diameter auxiliary electrode.

For the wind speeds available, the recirculation with this arrangement is very high and the net discharge current is low.

In Figure 10 results are presented of a typical set of measurements exploring in detail the way in which discharger currents are related to power-supply voltage and discharger spacing aft of the engine exit plane. For each spacing, the net current increases nearly linearly with increasing power-supply voltage, with curves of higher slope corresponding to larger spacing. The net-power-supply-current curves, on the other hand, are definitely concave upward, indicating that the current varies as more than the first power of voltage. Also, the higher power-supply-current curves correspond to the lower discharger spacings. The behavior of the net-discharge-current curves is so regular that they can be extrapolated to voltages of 150 kV and beyond with considerable confidence.

For a single-point discharger, the interrelationships between currents, spacings, and "exhaust" speed are shown in Figure 11. It is evident that some net current is discharged even at zero exhaust speed, but that as speed is increased, the net current increases. At low values of wind speed, the curve is concave upward, but as speed is increased, the curve becomes very nearly linear. These net-current data, also, are sufficiently well behaved so that they can be extrapolated to considerably higher speed. Looking at the power-supply-current data, we observe that the power-supply current increases with increasing speed, and also tends to approach the net discharge current as exhaust speed is increased. Thus, not only does increasing speed increase the current leaving the point, but it gets the ions far away from the vehicle before they emerge from the flow field. In this way recirculation is progressively cut down.

Some of these physical relationships are more clearly illustrated in Figure 12, which presents data obtained using a single point at a

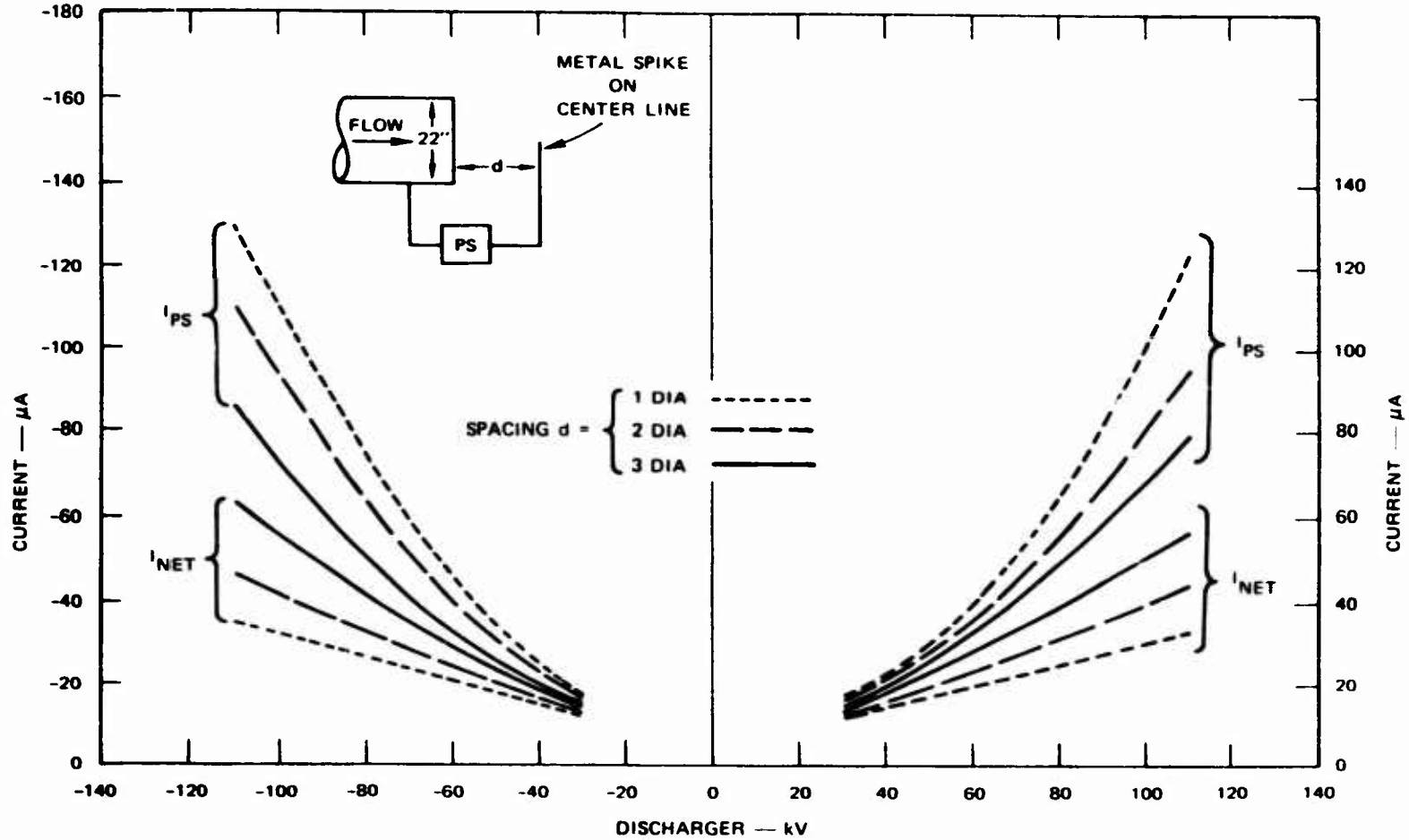

FIGURE 10 VARIATION OF CURRENT WITH POWER-SUPPLY VOLTAGE FOR SINGLE-POINT DISCHARGER FOR A WIND SPEED OF 125 ft/s

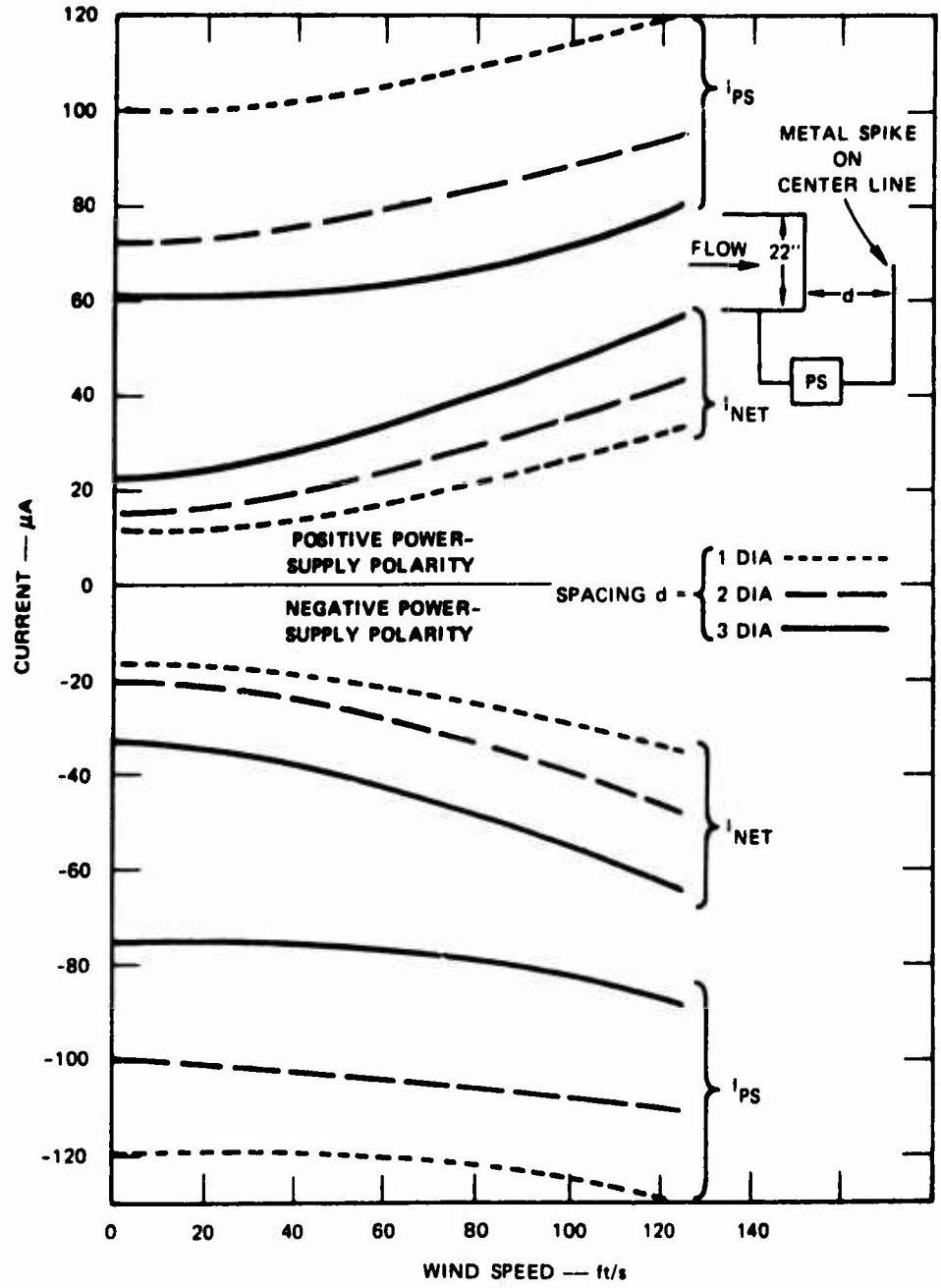

FIGURE 11 VARIATION OF CURRENT WITH WIND SPEED FOR A SINGLE-POINT DISCHARGER

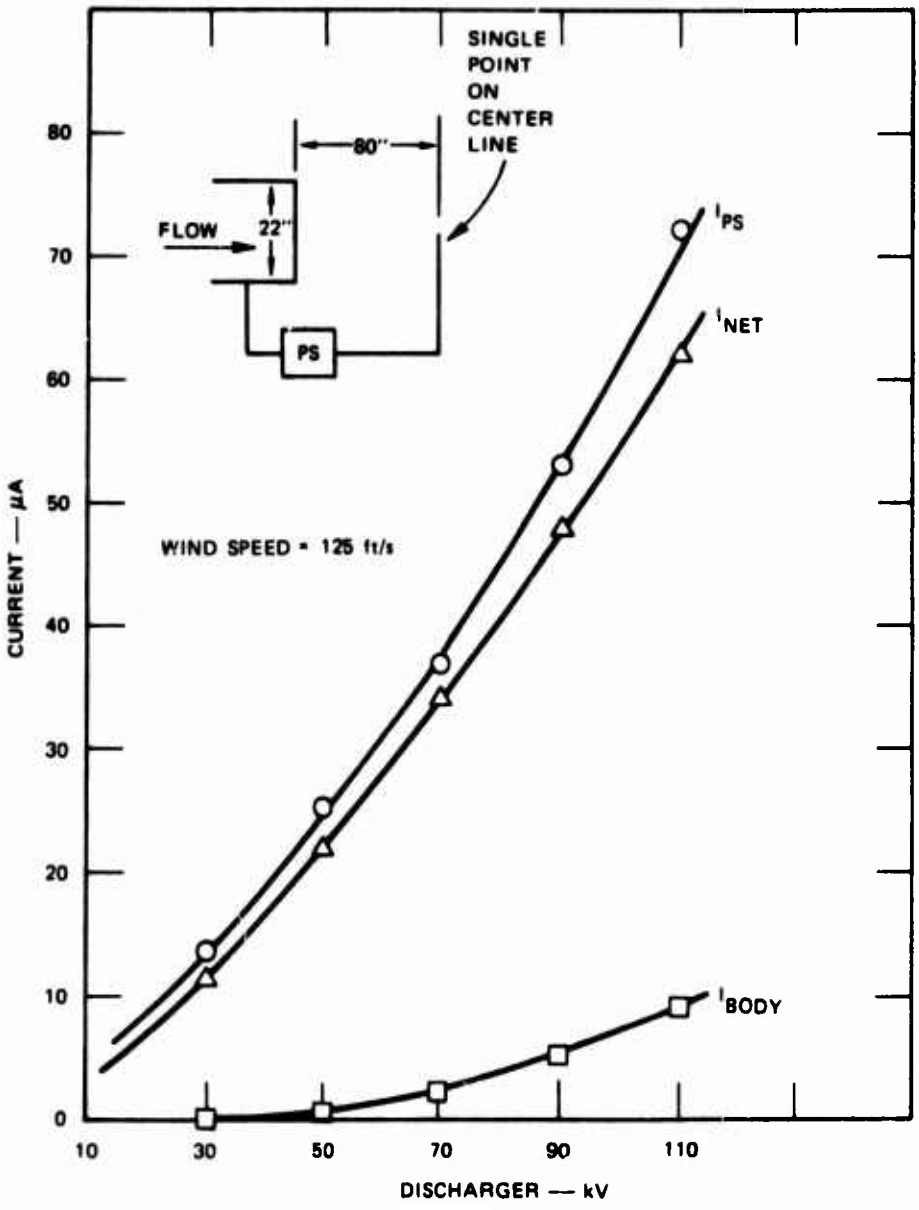

FIGURE 12 RELATIONSHIPS AMONG CURRENTS AS POWER-SUPPLY VOLTAGE IS VARIED

single spacing and varying power-supply voltage. Here the point was located 80 inches back of the exit plane, making the discharging process more efficient, so that some of the interrelationships are more clearly evident. With a high-voltage point this far from the nearest ground electrode, the current leaving the system is not being limited by ion space charge near the point--i.e., more ions generated by increased power-supply voltage are effective in increasing net discharge current. The behavior of the recirculated current, I_{body}, is also interesting. At low power-supply voltages, the electric field generated by the supply voltage on the discharging element and the coulomb force generated by the self charge on the ion beam itself are both low, resulting in low recirculating current. As power-supply voltage is increased, it increases the magnitude of both the field generated by the discharging element, and the coulomb forces generated by the increased charge density in the ion beam. The net result is that the recirculation current increases with increasing power-supply voltage. The increasing recirculation current manifests itself as a divergence between the net discharge current and the power-supply current. For the discharger geometry of Figure 12, the system is quite efficient even with a power-supply voltage of 110 kV (86% of the power-supply current is discharged), and the power-supply voltage could probably be doubled without requiring unacceptably high power supply currents.

Figure 13 illustrates the way in which various currents are affected by changes in exhaust velocity. Obviously, as velocity is increased, the net discharge current increases, first as a lower-than-first-power of velocity and then approaching a linear dependence. The recirculation current I_{body} is maximum at zero velocity when the applied field and coulomb field have unlimited time to act on the discharged ions to cause them to be recirculated. As the exhaust velocity is increased, the ions are carried away faster and the recirculation

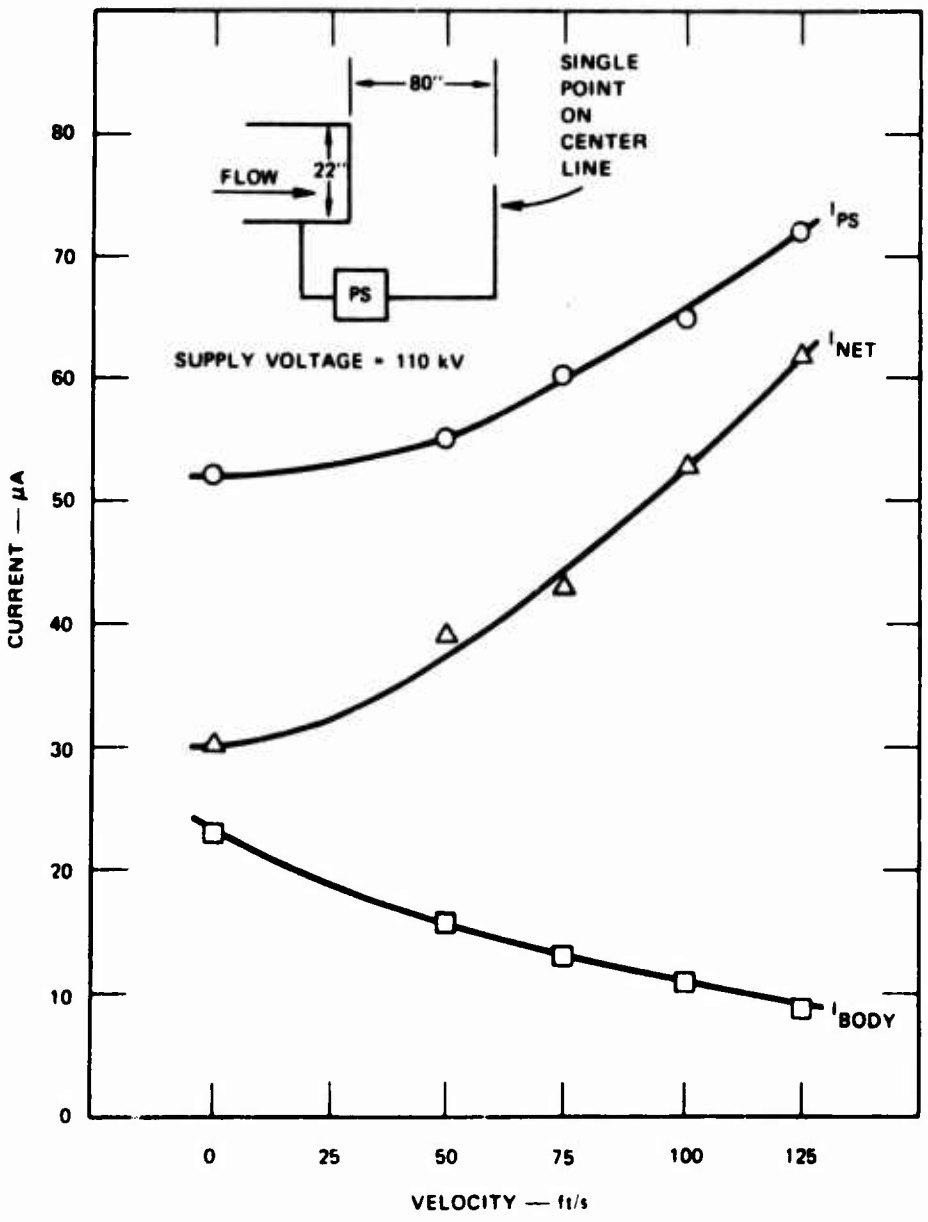

FIGURE 13 RELATIONSHIP BETWEEN CURRENTS AS AIR SPEED IS VARIED

current is diminished. The reduced recirculation current at high wind speeds causes the power-supply current to approach the net discharge current.

Subsequent to performing these tests, a report by Andrews and Forrest[1*] was received that confirmed the findings discussed above.

*References are listed at the end of the report.

III HELICOPTER GROUND TESTS OF DISCHARGER DESIGNS

When the discharging elements to be used in the CH-47 tests at Boeing Vertol in Philadelphia were chosen, all the laboratory data discussed above were borne in mind. It was felt that, throughout this program, as much as possible of the "blue sky" experimentation should be conducted in the laboratory, where it can be accomplished at minimum cost. Before the ground tests began, it was felt that they should be designed to verify laboratory results, to expose interesting discharging-element designs to a more nearly true in-flight environment (involving acoustic noise, high temperature, soot, etc.), and to look for unexpected developments. It was felt, furthermore, that the ground tests should be of clearly circumscribed scope, since they are considerably more expensive than the laboratory tests, but are not representative of the in-flight situation in all respects. Accordingly, it was decided that the discharging elements to be investigated would be confined to a single-point stainless-steel discharger and a 12-inch-diameter stainless-steel ring discharger, each of which would be used alone or in connection with a 12-inch-diameter auxiliary discharge electrode for a total of four different configurations. The single-point discharging element was chosen because of its extreme simplicity and good performance (compare Column 1, Figure 7 with Column 1, Figure 9). The ring-shaped discharging electrode was chosen because it too is a simple and rugged design, because physically it is markedly different from a single point, and because the ring discharging element produced the highest net discharge current (by a small factor) in the laboratory tests (see Column 1, Figure 9). A 12-inch ring diameter was chosen because, although the results of Column 1, Figure 9, indicate that net current is

not sensitive to ring size, it was realized that the voltage for flashover to the skin does depend on diameter (proximity to skin). Accordingly, a value of 12 inches (roughly the mean between 8 and 15 inches) was chosen for the ring diameter.

Although the discharger designs involving an auxiliary electrode appeared to be less satisfactory than single elements in the laboratory tests, it was felt that it was extremely important to test these configurations in the ground tests to determine the degree to which ground-test and laboratory data agree on both promising and unpromising designs. Thus, experiments with auxiliary electrodes were included in the CH-47 ground tests at Vertol. In considering the auxiliary-electrode separation for the ground tests, it was observed that the experiments summarized in Column 2, Figure 9, indicated that flashover voltage and net discharge current both increased with increasing distance between the electrodes up to the maximum spacing (6 inches) investigated in the laboratory, and that this spacing did not permit the application of 120 kV without flashover. It was decided, therefore, that for the ground tests the spacing would be set at 9 inches to permit the application of the full available 120-kV power-supply potential, and to maximize the net discharge current.

The set-up used for the ground tests is shown in Figure 14. A sheet of mylar (taped over a plywood sheet to preclude the possibility of rocks of other objects puncturing the mylar sheet) was placed under each of the four helicopter tires to insulate it from ground, to permit the net discharge current to be measured by means of a meter connected between the helicopter frame and a nearby ground stake. (The resistance between adjacent ground stakes 84 feet apart was measured to be 60 ohms, and the resistance between the helicopter and ground was measured to be greater than 60 megohms.) The 120-kV, 12-mA power supply used in these experiments was powered from the ship's Auxiliary Power Unit (APU)

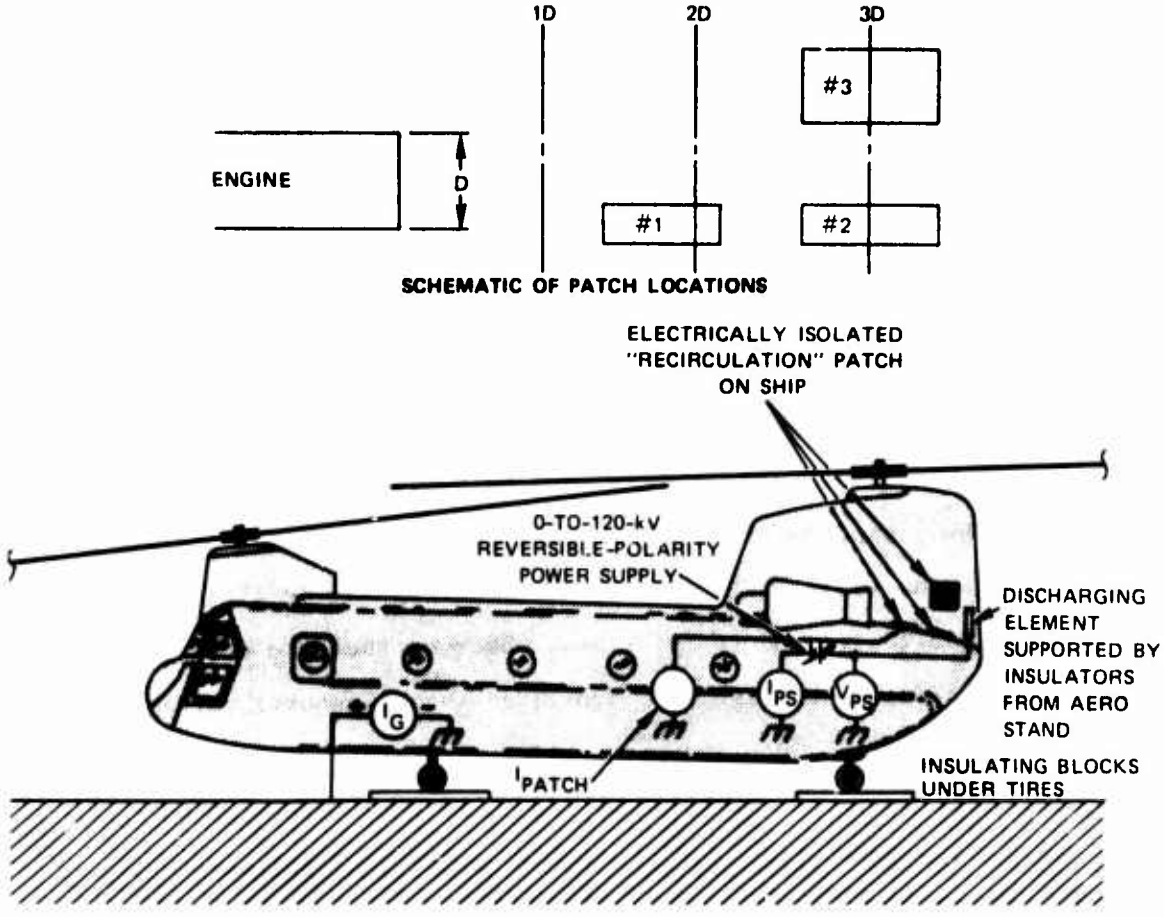

FIGURE 14 INSTRUMENTATION CONFIGURATION FOR CH-47 GROUND TESTS AT BOEING VERTOL

so that there were no external power sources or other wiring connected to the helicopter during the tests. The discharging element was supported in the jet-engine exhaust by means of Teflon insulating blocks attached to an aero stand that could be moved about on the ground to adjust the position of the discharging element. Also included in the instrumentation system was a set of five strategically located metal patches insulated from the skin, and positioned in the vicinity of the discharger to permit the measurement of current recirculated to the skin at the location of the patch. A photograph showing the general arrangement of the ground tests is shown in Figure 15.

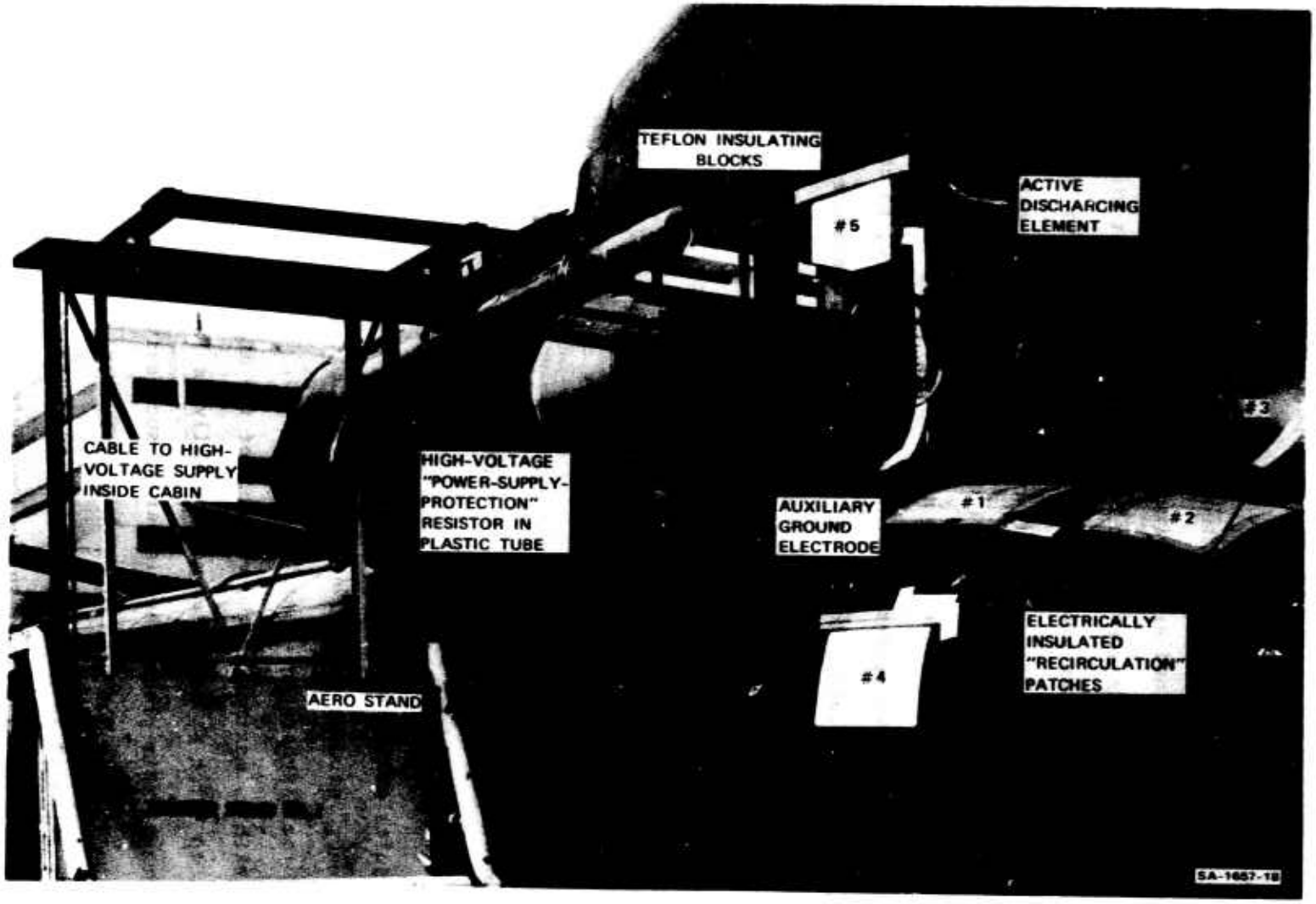

FIGURE 15 PHOTOGRAPH OF ARRANGEMENT FOR GROUND TESTS

Since the ground tests provided an opportunity to check the validity of the laboratory simulation facility, certain of the data obtained in the two tests are plotted for comparison in Figures 16 and 17. The results obtained with a single-point discharger are shown in Figure 16. The general trends are in good agreement, but the net discharge currents measured in the ground tests are appreciably lower than those measured in the laboratory, in spite of the fact that the exhaust velocity in the ground tests was twice as high. The low net current during the ground tests undoubtedly stems from the high temperature of the jet-engine exhaust gases, which reached 350 to 400°C, as compared to 20°C in the laboratory tests. At the elevated temperatures of the exhaust in the ground-tests the ion mobility is roughly twice that in the laboratory set-up, so that, for a given wind speed, recirculation in the ground tests will be much higher than in the laboratory.

The results obtained with a dual-ring discharger are shown in Figure 17. Again the trends of the laboratory and ground-test data are in good agreement. In this case too, the net discharge current obtained during the ground tests is appreciably lower than that measured in the laboratory mock-up.

Results of the recirculation-current studies and discharge "efficiency" studies are shown in Figure 18. It is evident that, regardless of the discharging-element configuration, the current recirculating to the skin is maximum in the vicinity of the discharger. Thus the current to Patch #1 decreases monotonically as the discharger is moved aft, because this places the discharger successively farther downstream of the patch. In the case of Patch #2, however, moving the discharger aft to a location two exhaust diameters downstream of the engine exit plane places the discharger in the immediate vicinity of Patch #2. Thus as the discharger is moved successively back, Patch #2 current first increases and then monotonically decreases.

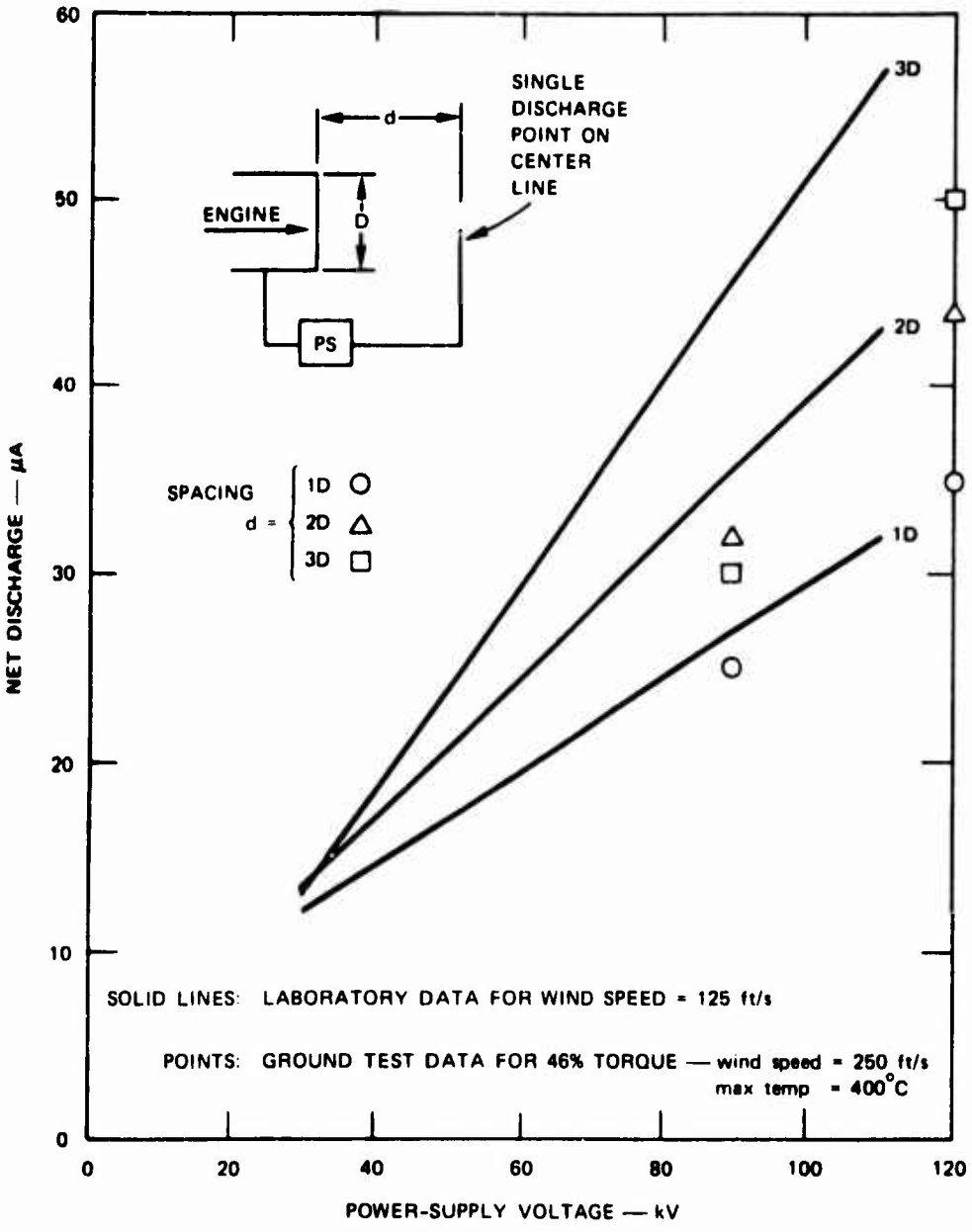

FIGURE 16 COMPARISON OF LABORATORY DATA FOR A SINGLE-POINT DISCHARGER WITH GROUND-TEST MEASUREMENTS

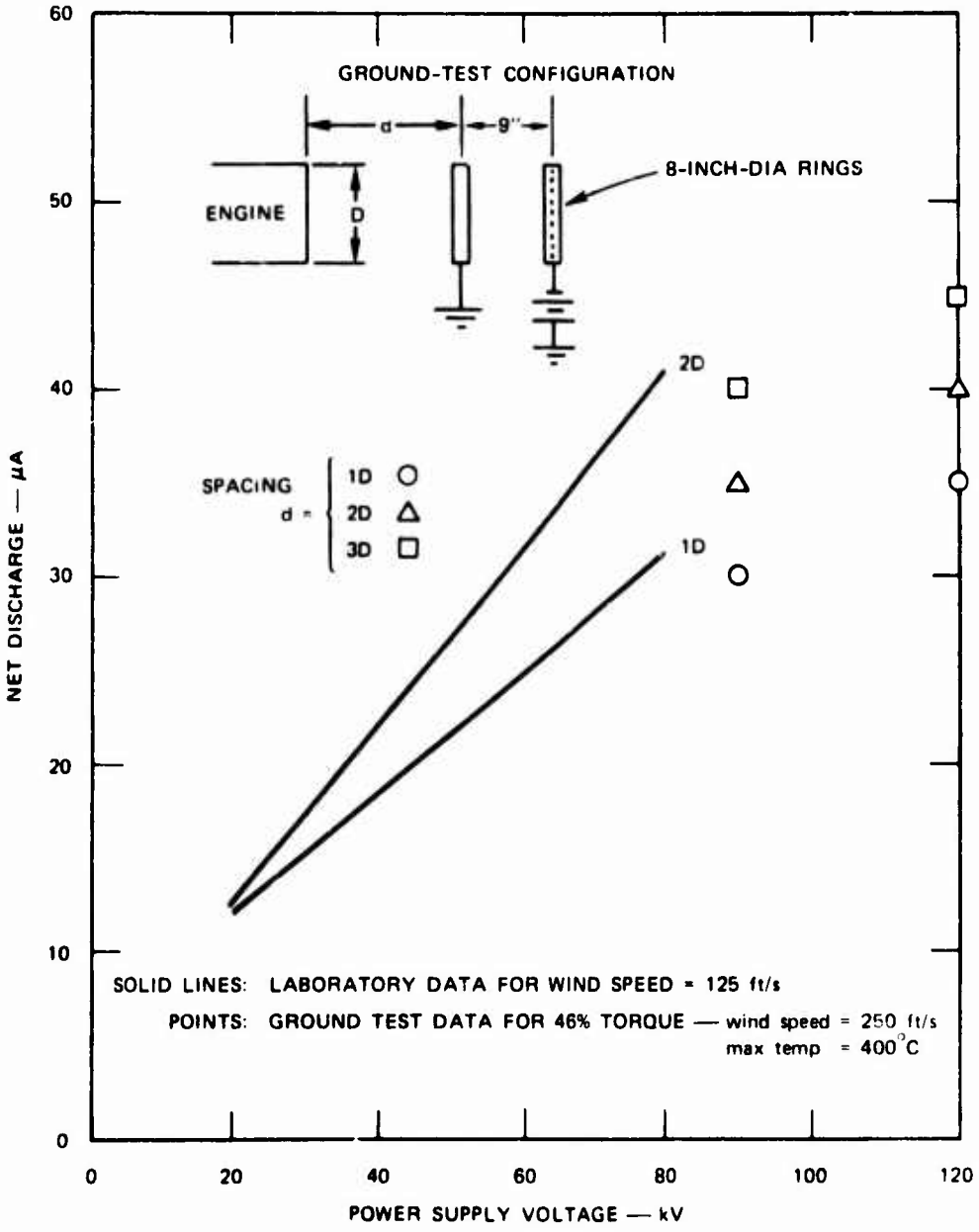

FIGURE 17 COMPARISON OF LABORATORY DATA FOR DUAL-RING DISCHARGER WITH GROUND-TEST MEASUREMENTS

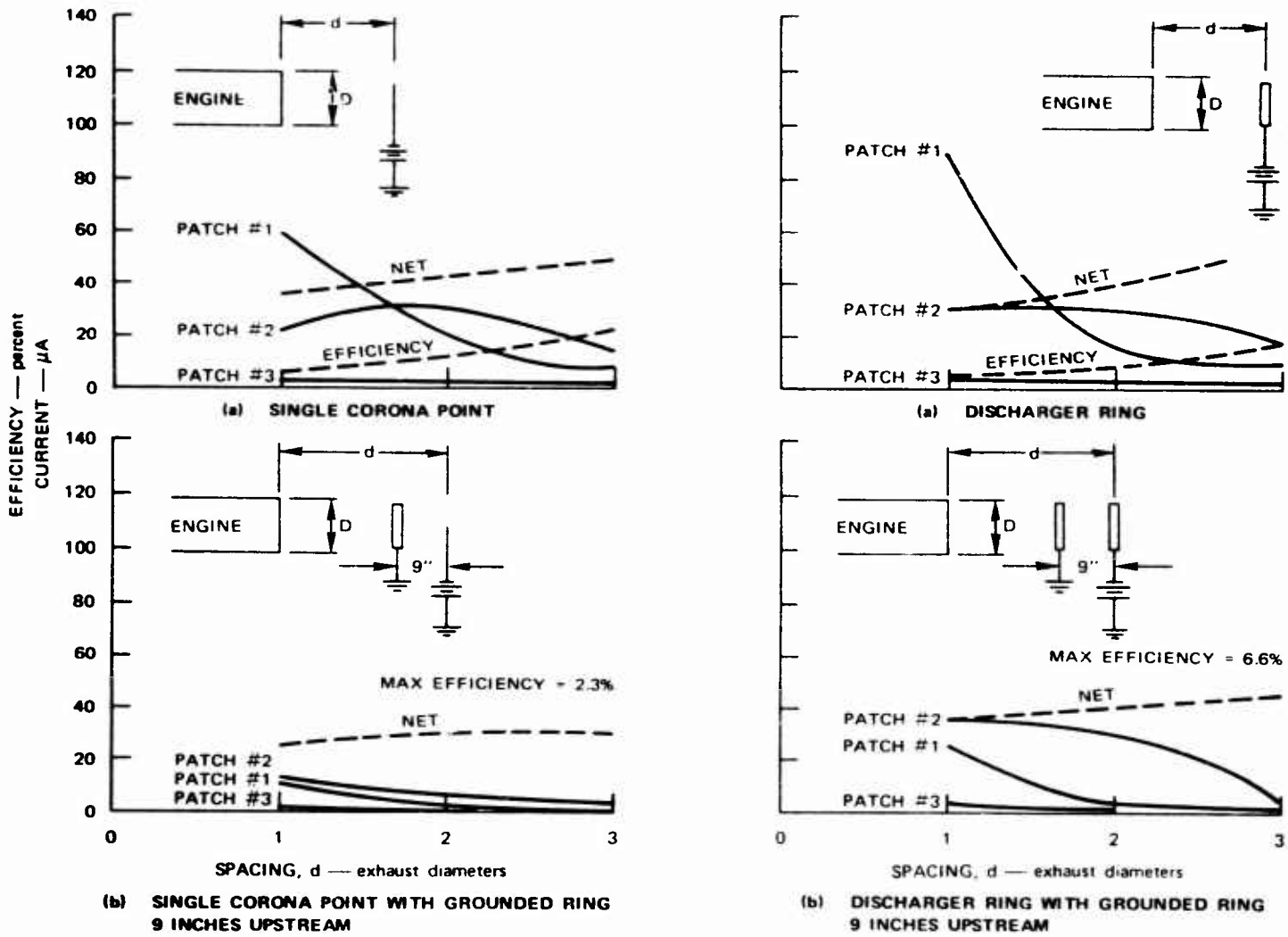

FIGURE 18 RECIRCULATION-CURRENT STUDIES DURING GROUND TESTS WITH A POWER-SUPPLY VOLTAGE OF 120 kV FOR A RING DISCHARGER AND FOR A SINGLE CORONA POINT ON CENTER LINE

The efficiency of the various discharger configurations at different locations is also of interest. Here, efficiency η is defined by

$$\eta = 100 \cdot \frac{I_{net}}{I_{PS}} \qquad - - - - - - - - - (1)$$

where $I_{net} = I_{PS} - I_{recirculation}$.

Consideration of the currents measured will reveal that I_{net} is a measure of the combined effectiveness of the discharger design and its location on the helicopter, while $I_{recirculation}$ is a measure of the effectiveness of the discharger location and the effects of airflow and exhaust temperature (i.e., ion mobility). It is clear, then, that the optimum discharger design and location will be the one giving the lowest $I_{recirculation}$ and highest I_{net} / I_{PS}. In the case of the simple discharging elements, all of the recirculation is to the helicopter skin, so that efficiency is markedly improved by moving the discharging elemen aft from the engine exhaust plane, thereby getting it away from the fuselage structure. Although there is considerably less current recirculated to the skin from the compound discharging elements located at d = 1D, there is considerable current flowing to the auxiliary grounded ring. Thus the efficiency of these configurations is only a few percent, as shown in Figure 18. This situation would, of course, be markedly improved if the exhaust velocity were higher and its temperature lower, for the reasons discussed earlier.

In general, the results of the ground tests confirmed the laboratory findings. Simple discharging elements (a single point or a single ring) were the best choices since they discharged most current for a given supply voltage. Also, their efficiency was highest. It also was demonstrated that the basic discharging-element designs were suitable for use in flight in that they operated satisfactorily in the engine-exhaust environment (acoustic noise, high temperature, soot, etc.).

At the conclusion of the ground tests, a review of the data available indicated that both the laboratory and the ground-test data were in good agreement, and that substantial increases in net discharge current accrued from increasing discharger spacing behind the engine exit plane, at least up to the maximum distance d = 3D investigated (see Figures 16 and 17). It was decided that the laboratory investigation should be extended to greater spacings to determine when the current ceases to increase. The results of this work are shown in Figure 18. It is evident that considerable improvement was achieved for each configuration tested, by increasing the spacing up to d = 5D. The discharger-efficiency curves also plotted in Figure 20 indicate that the increased discharger current is achieved largely by virtue of increased efficiency (i.e., reduced recirculation to the skin). Beyond a spacing of 5D, the improvement achieved by decreased recirculation resulting from increased distance to the skin is counterbalanced by degraded performance stemming from increased difficulty in getting discharge products removed as the result of immersing the discharging element in a region of low-speed, diffuse, and considerably turbulent flow.

In an attempt to optimize discharger performance, two additional experiments were performed in the laboratory. These experiments consisted of adding a high-velocity nitrogen blast, coaxial with the mock-up exhaust, to blow over a single corona point at different exhaust diameters aft of the exhaust nozzle. The experiments were conducted using auxiliary ground rings as well as one in which no ground ring was used. In the first experiment a small subsonic orifice was used to control the nitrogen mass flow rate. Although dm/dt was not measured, it is felt that it was about 1 gram/s, and the exit velocity was about 100 m/s. The results of this test indicated that when the ground ring was used, the net current dissipated was limited to approximately 10 μA because of the

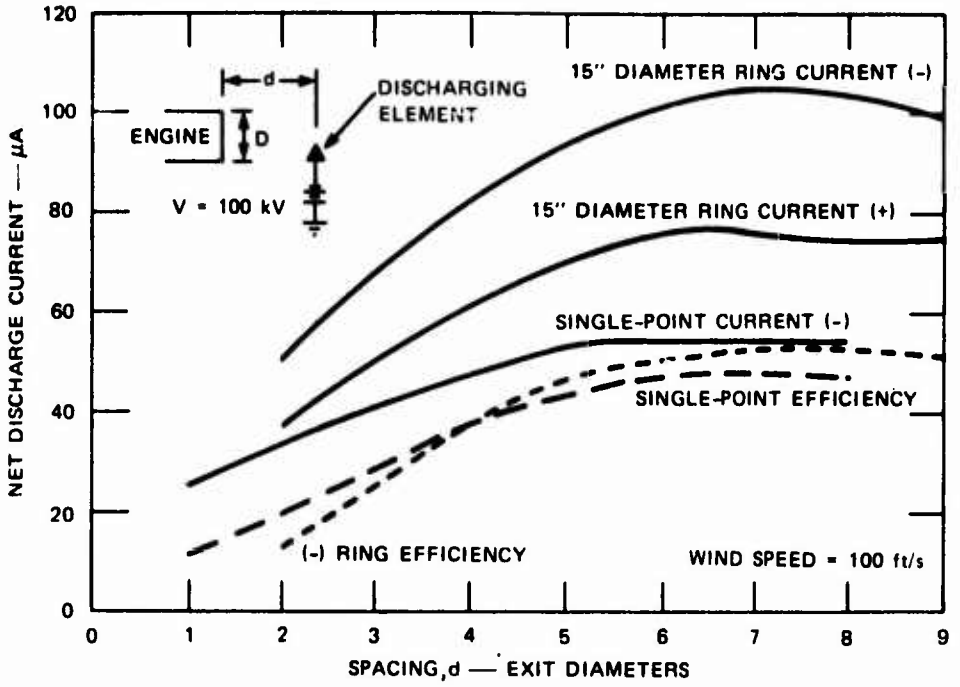

FIGURE 19 LABORATORY INVESTIGATION OF EXTENDED DISCHARGER SPACING

high-velocity convection that carried the discharge products into the grounded ring. In the tests performed without an auxiliary ground ring, using the subsonic orifice, the results were similar to those shown in Column 1 of Figure 7 for d = 66 inches, and the discharger efficiency obtained by using the high-velocity air blast was not increased over that obtained using the single-point discharger alone. In the second laboratory experiment, a large supersonic nozzle was designed and connected directly to the valve of a high-pressure nitrogen bottle (2400 psi, initially), and installed in such a way as to place the exiting high-velocity gas flow coaxial with the mock-up-engine exhaust flow. The nozzle had a 0.55-inch-diameter throat and a 1.0-inch-diameter exit aperture, and is illustrated in Figure 20. Although the exit velocity of the nitrogen from the nozzle aperture could not be accurately computed because of a mismatch in the reservoir, assumptions about the character of the mismatch led to reasonable velocity estimates of between 650 m/s

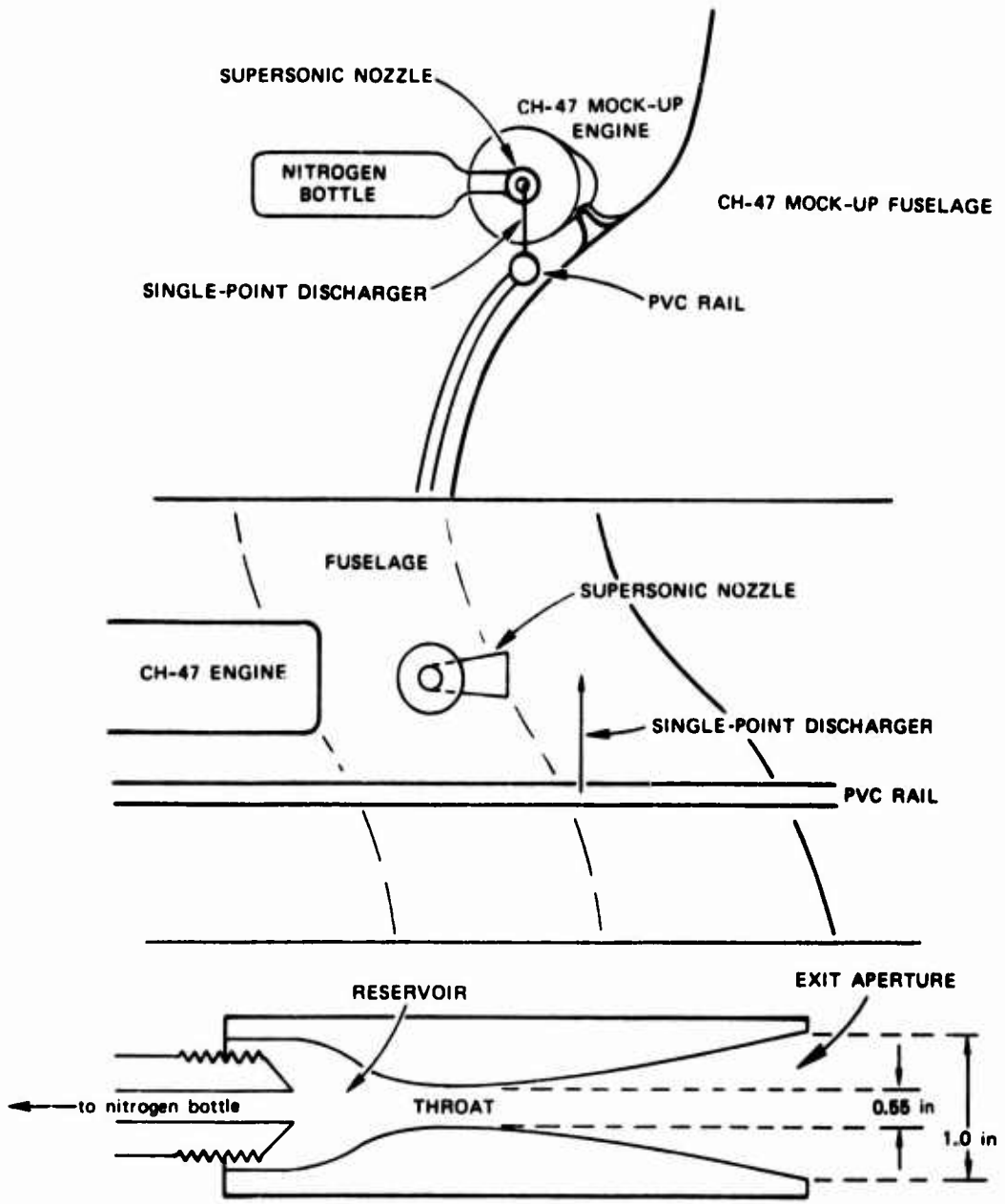

FIGURE 20 SUPERSONIC-NOZZLE CONFIGURATION USED DURING LABORATORY TESTS TO INVESTIGATE THE UTILITY OF AUXILIARY AIR FLOWS

and 750 m/s (i.e., ~ Mach 2). This high-velocity gas flow was accompanied by mass flow rates of about 0.11 kg/s, which depleted the 230-ft^3 nitrogen bottle in about 15 seconds.

The dissipation tests were conducted as described earlier, with the nitrogen bottle turned off, and then with it fully turned on. The single-point discharger was used, and it was placed 6 inches downstream from the supersonic-nozzle exit aperture.

The results of this test indicated that only a 10% improvement in the net current was obtained when the nitrogen was turned on, at the expense of large quantities of nitrogen.

The lack of performance of these high-velocity air flows in aiding the discharge process is attributed to the fact that the jets of nitrogen become turbulent shortly after leaving the nozzle and quickly slow and mix with the surrounding air and thus allow recirculation to the fuselage. This was particularly apparent when the supersonic nozzle was tested; three feet downstream from the nozzle the flow was only about 60 ft/s, and gas-dynamic data[2] indicate that the flow from this nozzle design becomes subsonic 4 inches downstream of the exit aperture.

The above experiments indicate that techniques using small-diameter, high-velocity auxiliary air flows to aid dissipation are not practical because of the enormous mass flow rates that would be required to significantly improve the net current.

IV FLIGHT TESTS

As discussed earlier, since the difficult geometry of a helicopter together with its complicated air flows prevent accurate evaluations of discharger designs to be made in the laboratory, the final analysis of the problems of discharging and sensing had to be made during actual helicopter hover operations. These tests were carried out during the months of May and June, 1972, at the Yuma Proving Grounds (YPG), Yuma, Arizona. Since the objectives of this program were to determine the feasibility of sensing and discharging a large helicopter, a Boeing CH-47 (s/n 169102) with a gross weight of about 30,000 lb (approximately 1/4 of the HLH gross weight) was chosen as the test vehicle.

The helicopter was instrumented with a Universal Voltronics BAL200-5.5-S power supply rated at 1.1 kVA (200,000 V at 5.5 mA) to provide ions during the sensor-fidelity phase of the tests, and to evaluate active dischargers during the dissipator tests. In addition to the power supply, the helicopter was instrumented with four field meters mounted in various places to measure electric fields, and a radar altimeter to obtain precise hover-altitude information. The helicopter was modified to allow various discharger designs to be installed in one or both turbine exhausts at different distances aft of the exhaust-nozzle exit plane. Recirculation "patches" were added in various places on the fuselage to allow measurements of the currents circulating from the discharger to the fuselage to be made. All the various measurements made were recorded on a CEC 5-119 oscillograph mounted in the helicopter, and were also presented to the aircraft test operator on a rack of panel meters mounted in the helicopter cargo bay. The instrumentation described above is shown in Figures 21, 22, and 23.

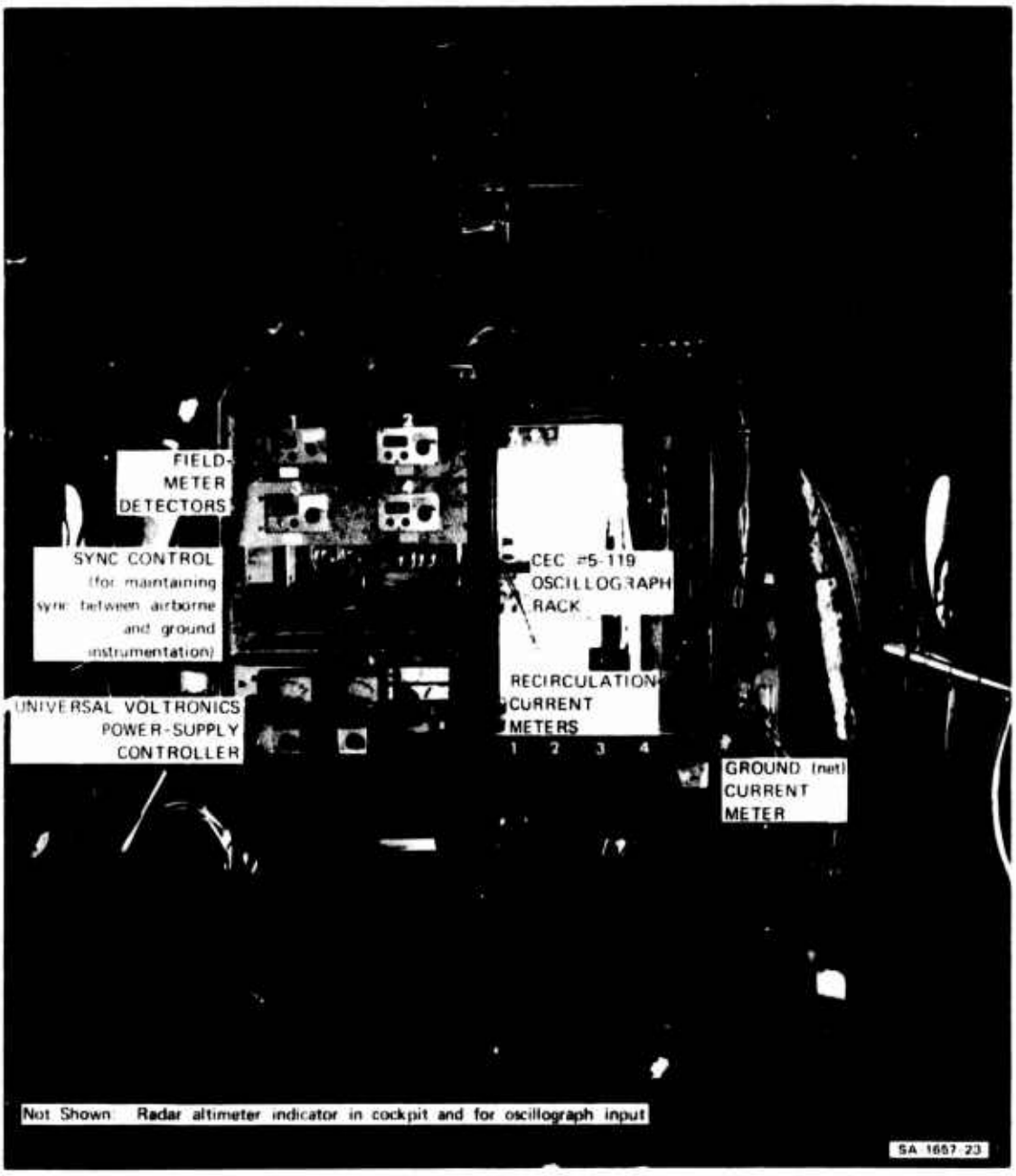

FIGURE 21 PHOTOGRAPH SHOWING AIRBORNE INSTRUMENTATION (instrument rack inside aircraft)

FIGURE 22 PHOTOGRAPH SHOWING AIRBORNE INSTRUMENTATION (front view of helicopter showing radar-altimeter antennas and #2 field-meter installation)

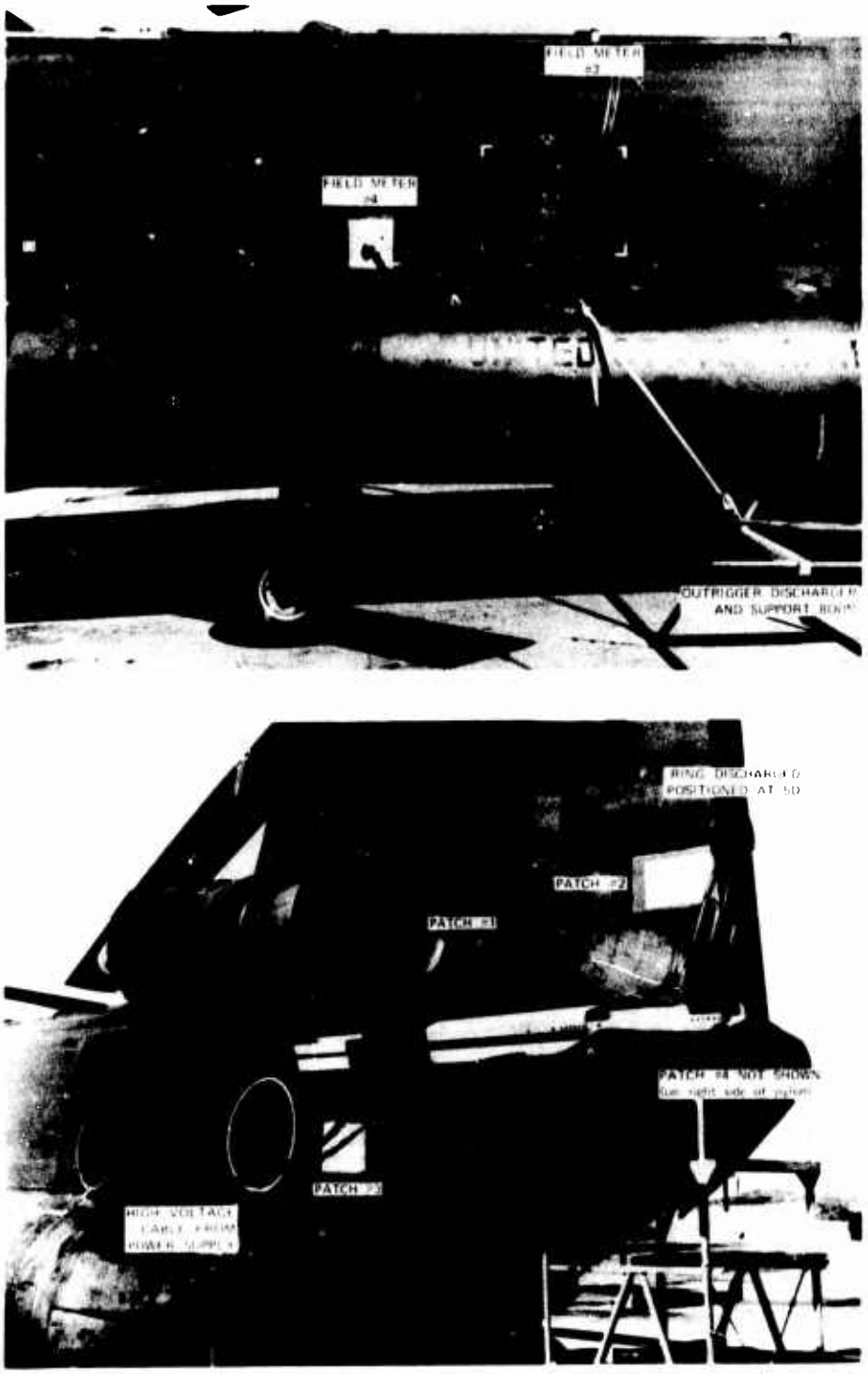

FIGURE 23 PHOTOGRAPH SHOWING AIRBORNE INSTRUMENTATION (side view of helicopter showing field meters #3 and #4 and recirculation patches)

In addition to the airborne electronics, a ground array of field meters, immediately beneath the hovering helicopter, was installed to observe the electric fields near the ground in the vicinity of the helicopter. These data were also recorded on a second CEC 5-119 oscillograph.

In order that a complete and accurate picture of the helicopter sensing and discharging problem could be drawn and explored, it was necessary to operate the helicopter in "clean" and "dirty" environments. The "clean" environment tests were performed on the C-130 tie-down pad at the Laguna AAF at YPG, and they allowed an investigation of sensing and discharging free of contamination from dust, in order to determine the ultimate capabilities of a sensing/discharging system. The "dirty" environment tests were conducted in the Phillips Drop Zone, a large expanse of plowed sand, at YPG. These tests simulated what might be an actual operating environment, and allowed the sensing/discharging problem to be fully investigated.

A Flight Test Plan[3] was prepared to serve as a guide in order that the tests could be conducted with a minimum of duplication and confusion. The test plan outlined the proposed schedule of flight operations and delineated the various discharger and field-meter configurations to be used. Shortly after the flight tests began it became apparent that, because of limitations on helicopter availability, not all the tests in the test plan could be accomplished as described in the plan. Since so many of the tests were essential to the successful completion of the investigation, it was decided that as many tests as possible would be combined in each flight. For example, the sensor-fidelity tests were combined with various discharger tests. In all but one of the tests, the ground array of field meters was used to measure the ambient electric field, as well as the electric fields beneath the hovering helicopter.

This arrangement, although severely complicating each flight mission, allowed most of the tests described in the Flight Test Plan to be completed and also allowed several additional tests to be made. These additional tests were done, at the expense of the less important tests described in the flight-test plan, so that questions arising during the course of testing might be answered. These additional tests are described below.

A. Instrumentation Calibration

Pre- and post-mission calibrations were performed on both the airborne and ground instrumentation. The power-supply voltage and current, the recirculation current patches, and the ground-current meters were calibrated using constant-voltage and constant-current sources.

The field meters were calibrated with a set of parallel plates separated by a distance, d. The parallel plate structure incorporated a hole in one of the plates to permit it to pass the field meter sensor vanes to simulate a flush-mounted field meter installation. A known voltage, V, was then applied and varied between these plates. The electric field intensity in the calibrating structure is given by

$$E = \frac{V}{d} \qquad \text{- - - - - - - - - - (2)}$$

As is discussed in more detail in Appendix A, the non-flush field sensor installation together with the calibration procedure followed resulted in a field meter output which indicated the magnitude of the field, E_{face}, at the field meter face. If one is interested in the field, E_{skin}, that would exist on the aircraft skin at the same location in the absence of the field meter (or the field that would be measured by a flush-mounted field meter at this location), the following relation should be used

$$E_{skin} = \frac{E_{face}}{2.5} \quad . - - - - - - - (3)$$

Throughout this report, all field meter data are presented in terms of E_{face}.

Since the field meters were to be operated in a region of heavy dust, and since these dust particles might be charged and collide with the sensor, it was important to use a field-meter design that minimizes error due to the dust current. The field meters used for the tests employed a synchronous detector, and used the field chopping vanes to generate the reference signal. With this scheme the "field" signal and the "dust current" signal are 90° out of phase with one another, and the detector discriminates against any "dust current" signal. For a description of the principle of operation of such an electric field meter the reader is referred to an earlier SRI report.[4]

B. Ground-Conductivity Measurements

Previous work[5] indicated extremely large values of resistance (about 2.5×10^9 ohms) between measured points during tests at the Yuma Proving Grounds. Since a "good" ground was essential to the accurate measurements of ground current (from natural or artificial charging) and of fields about the helicopter (the helicopter in most cases was to be grounded), a good deal of time was spent in measuring various ground resistances around YPG.

Two basic techniques were used to measure the resistance of the soil: "megger" tests when the resistance was high, and an ohmmeter when the resistance was low enough. Surprisingly, it was possible to use the ohmmeter in many of the tests because the soil resistivity was not as high as expected. On May 30, 1972, after 159 days of drought in Yuma, the resistance between two ground stakes 27 ft apart, 3 ft deep in the

concrete C-130 tie-down pad, was measured to be 10 k Ω, and two stakes, 3 ft deep and 270 ft apart measured 11 k Ω. The measurement was repeated over a period of two weeks with consistent results. On June 6, 1972, a thunderstorm brought rain to YPG. The "dusty"-environment hover tests were conducted after this rain, at the Phillips Drop Zone. One week after the rain, on June 13, and again on June 19 the ground resistance at Phillips was measured between two stakes, 30 ft apart, driven 2 ft deep. This resistance was determined to be 700 ohms on the 13th, and 1000 ohms on the 19th. On the 29th of June a surface-resistivity measurement was made by inserting the ohmmeter probes, about 24 inches apart, 2 inches into the soil. The resistance measured here was about 700 k Ω; when the probes were inserted 2 inches deep and 240 ft apart the resistance was measured to be 5 MΩ.

On June 9 surface-resistivity measurements were made in the vicinity of the hangar at Laguna AAF. The high-voltage power supply was used as the "megger"; one side of the supply was grounded through the grounding stake in the aircraft tie-down and the other side of the supply was connected to a 2-inch by-3-ft metal bar via a long piece of RG-58/U center conductor. The metal bar was dragged over various surfaces and the resistance determined. These data are shown in Table 1.

Table 1

SURFACE RESISTANCE AS DETERMINED BY MEGGER METHOD (V_{PS} = 4 kV)

Surface	Resistance
Dirt and gravel	2 - 8 MΩ
Concrete	3 - 8 MΩ
Macadam	≈ 10 MΩ

It is seen from the above data that the measured ground resistance was relatively low. If one assumes a charging current of about 100 μA to the helicopter (from natural or artificial causes), these low resistances would lead to actual helicopter potentials of 1 V or less if the helicopter was staked to ground, and a potential of about 200 V if the "ground" was only a conductor dropped to the surface.

It was determined from these measurements that the ground currents and fields measured during the hover tests would be accurate and uncontaminated by a poor ground.

C. Flight Tests of Discharging Elements

For the Yuma flight-test investigation of discharging elements, the basic instrumentation was essentially the same as that shown in Figure 14 for the Vertol ground tests, except that the wire to the ground stake was made longer to permit the measurements to be made with the aircraft in flight, and is illustrated in Figure 24. Tests were made of three basic discharging elements: a single point or ring located in one (and in some cases both) of the engine exhausts (these two configurations displayed the greatest promise in the ground tests of Figure 18), and an "outrigger" discharger shown in Figure 25. The outrigger discharger system consisted of a four-ft-long, 1-inch-diameter aluminum tube mounted amidship on each side of the helicopter 6 ft outboard from the skin. A sharpened wire was installed at each end of each bar to provide four widely-spaced, low-threshold corona points. Structural considerations required that 3 ft of the 6-ft outrigger supports be made of aluminum which somewhat reduced the electrical-breakdown strength of the outrigger system.

In view of the results of the laboratory tests shown in Figure 19, provisions were made on the flight-test aircraft to position the dis-

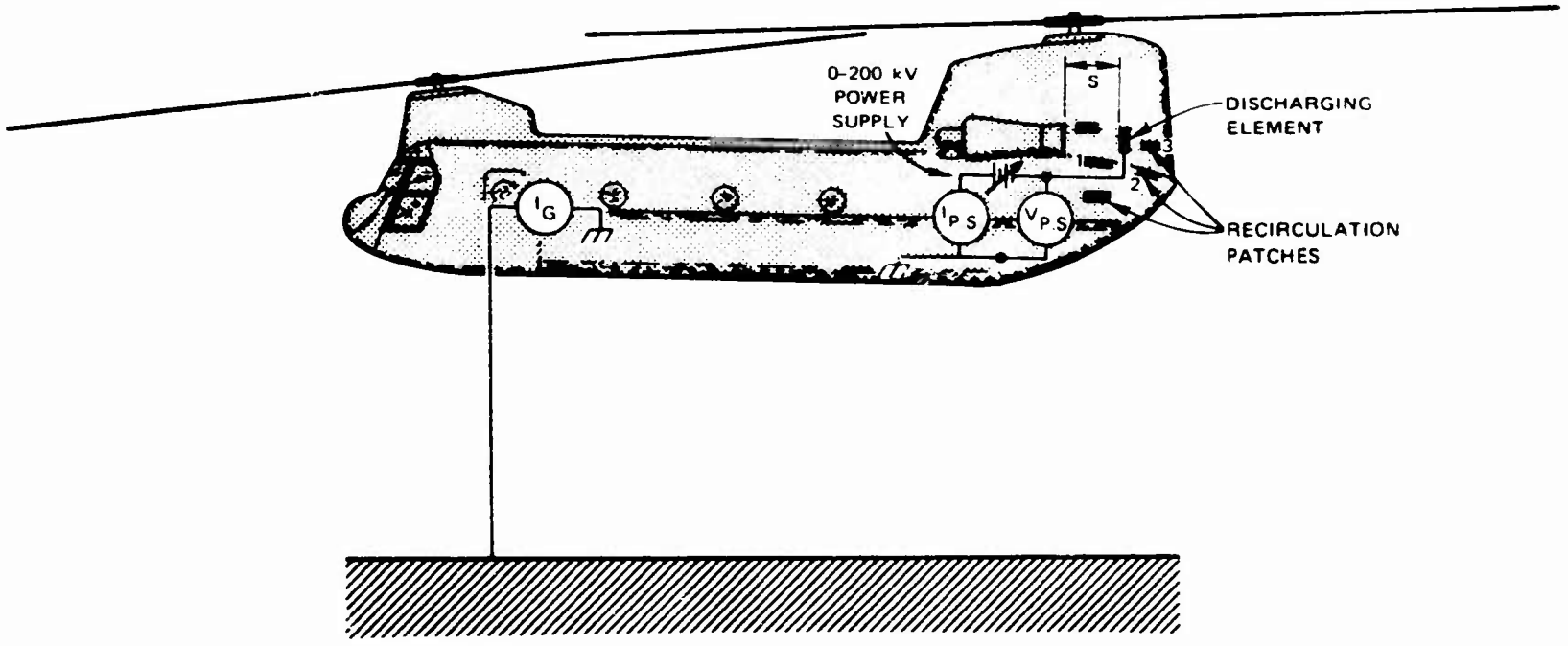

FIGURE 24 LAYOUT OF INSTRUMENTATION FOR DISSIPATOR TESTS

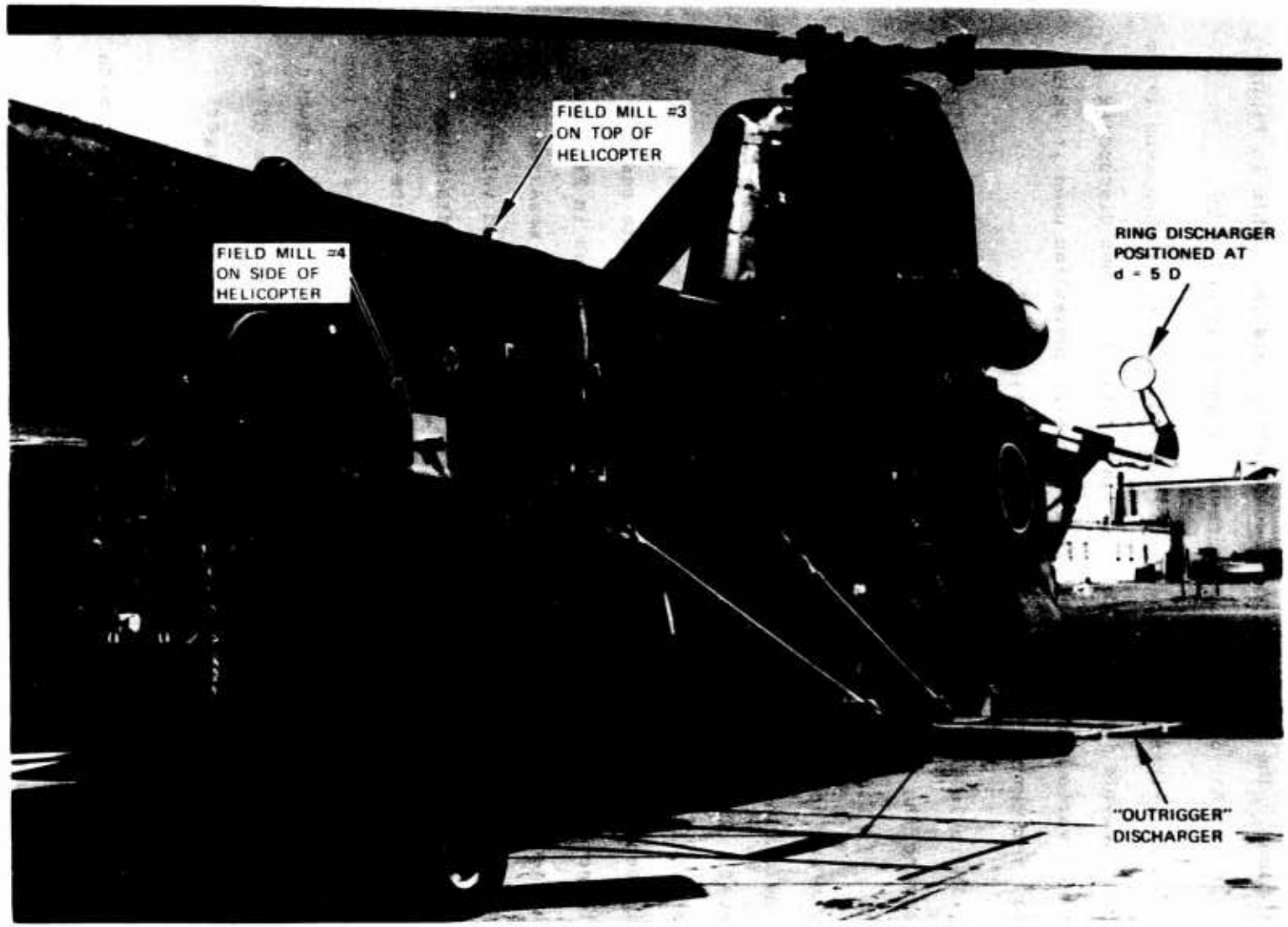

FIGURE 25 PHOTOGRAPH OF CH-47 FLIGHT-TEST AIRCRAFT

charging element up to five engine-exhaust diameters aft of the engine exit plane. The structure for accomplishing this is visible in Figure 25, and another discharger arrangement is shown in Figure 26.

In describing the various charging and discharging phenomena it is of considerable importance to agree on a convention when discussing the signs of various charged particles. The sign convention used in this report for currents and fields is shown in Figure 27.

In reviewing the results of the flight tests, it is interesting to determine the degree to which they agree with the laboratory and ground tests. In Figure 28, the net discharge current for a single-point discharger is plotted for comparison with the current discharged from a single ring at the same location (d = 5D) in the helicopter engine exhaust. The two sets of data obviously lie along the lines of best fit. This result substantiates the laboratory and ground-test data, which indicated that a single point and a single ring constitute equally satisfactory discharging elements. Shown for comparison in Figure 28 is a laboratory experimental curve of discharge current measured at the same spacing behind the engine exit plane, and with a wind velocity of 100 ft/s. The laboratory data predict a somewhat higher discharge current than was measured in flight. As was indicated in the discussion of the ground tests in Section III, this disparity probably stems from the difference in temperature between the laboratory "engine" exhaust and that of the actual aircraft engine. The higher temperature of the real engine exhaust implies higher ion mobility, permitting larger recirculation, which results in lower net discharge current.

With the effectively low directed wind velocities associated with the CH-47 turbine exhaust, it is necessary to move the discharging element far from the fuselage to reduce current recirculation to a tolerable level. This means that high power-supply voltages must be used to

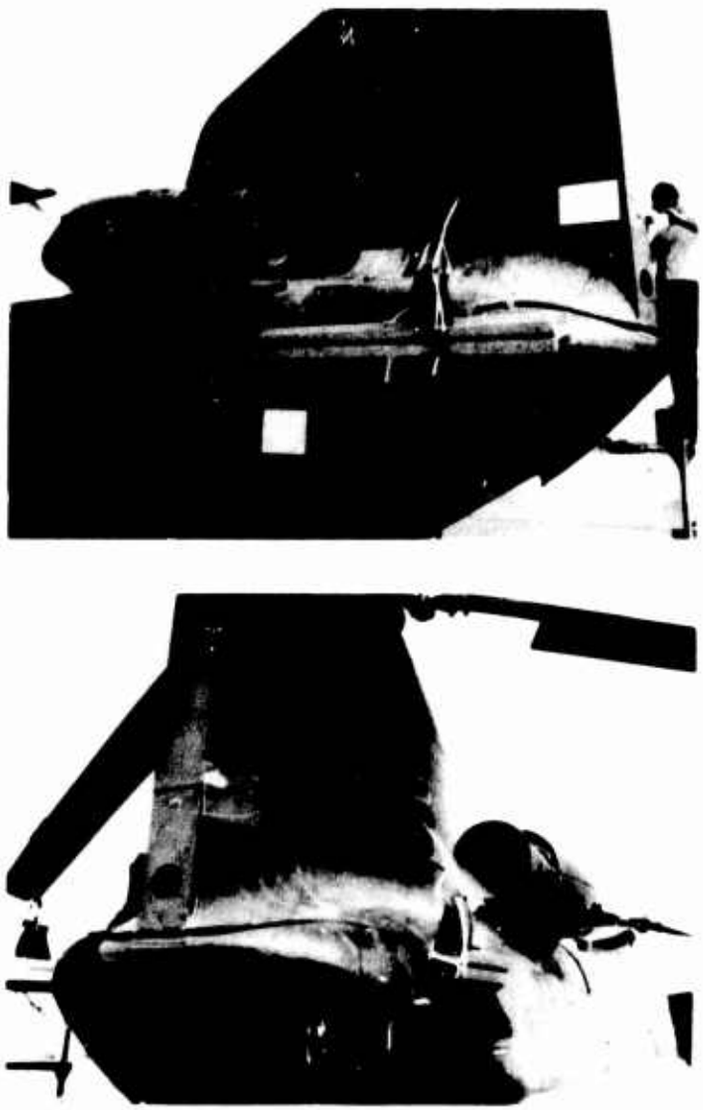

FIGURE 26 PHOTOGRAPHS OF SINGLE-POINT DISCHARGER MOUNTED THREE EXHAUST DIAMETERS BEHIND THE LEFT TURBINE EXHAUST (top) AND IN BOTH EXHAUSTS (bottom)

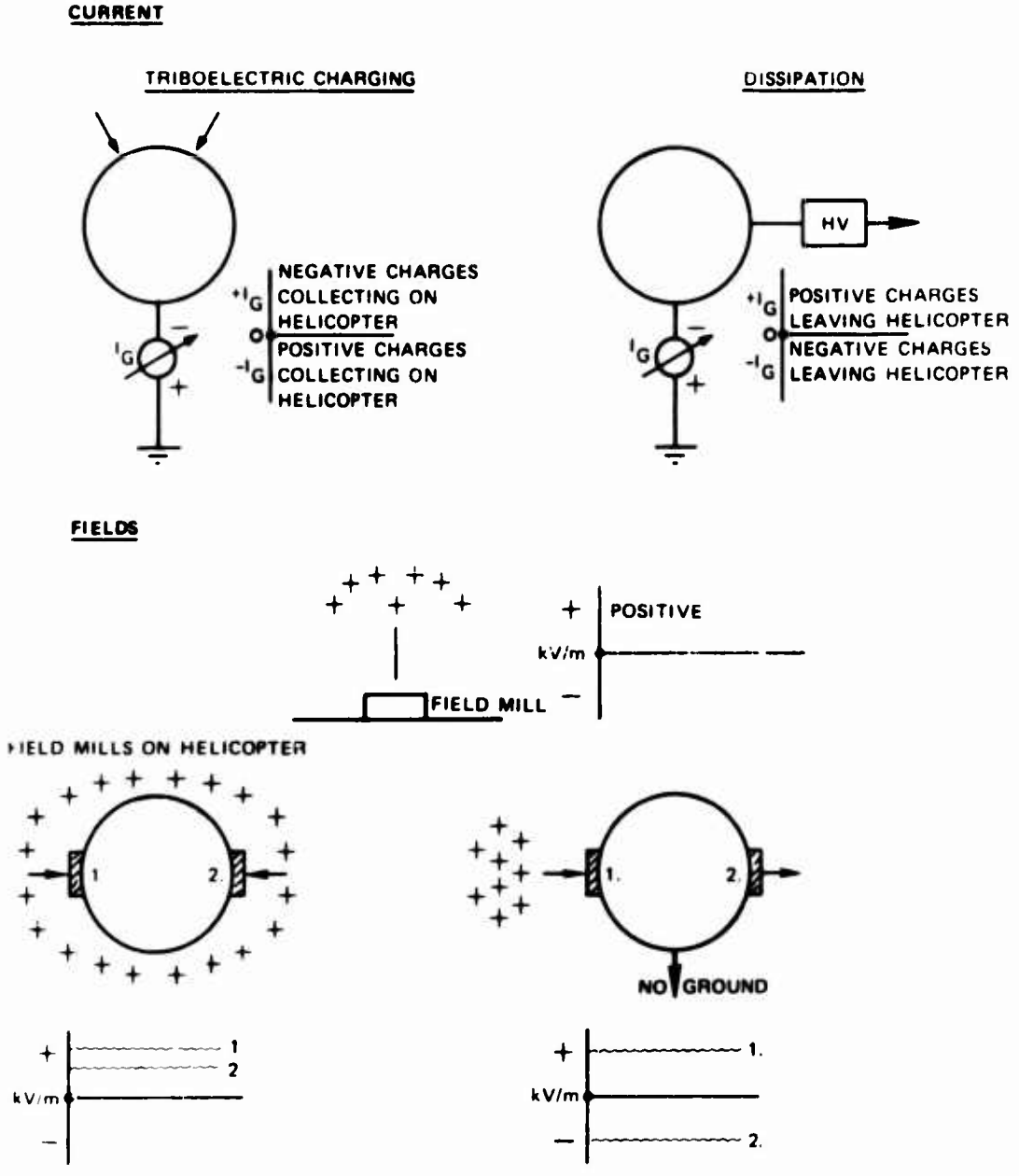

FIGURE 27 SIGN CONVENTIONS FOR CURRENTS AND FIELDS

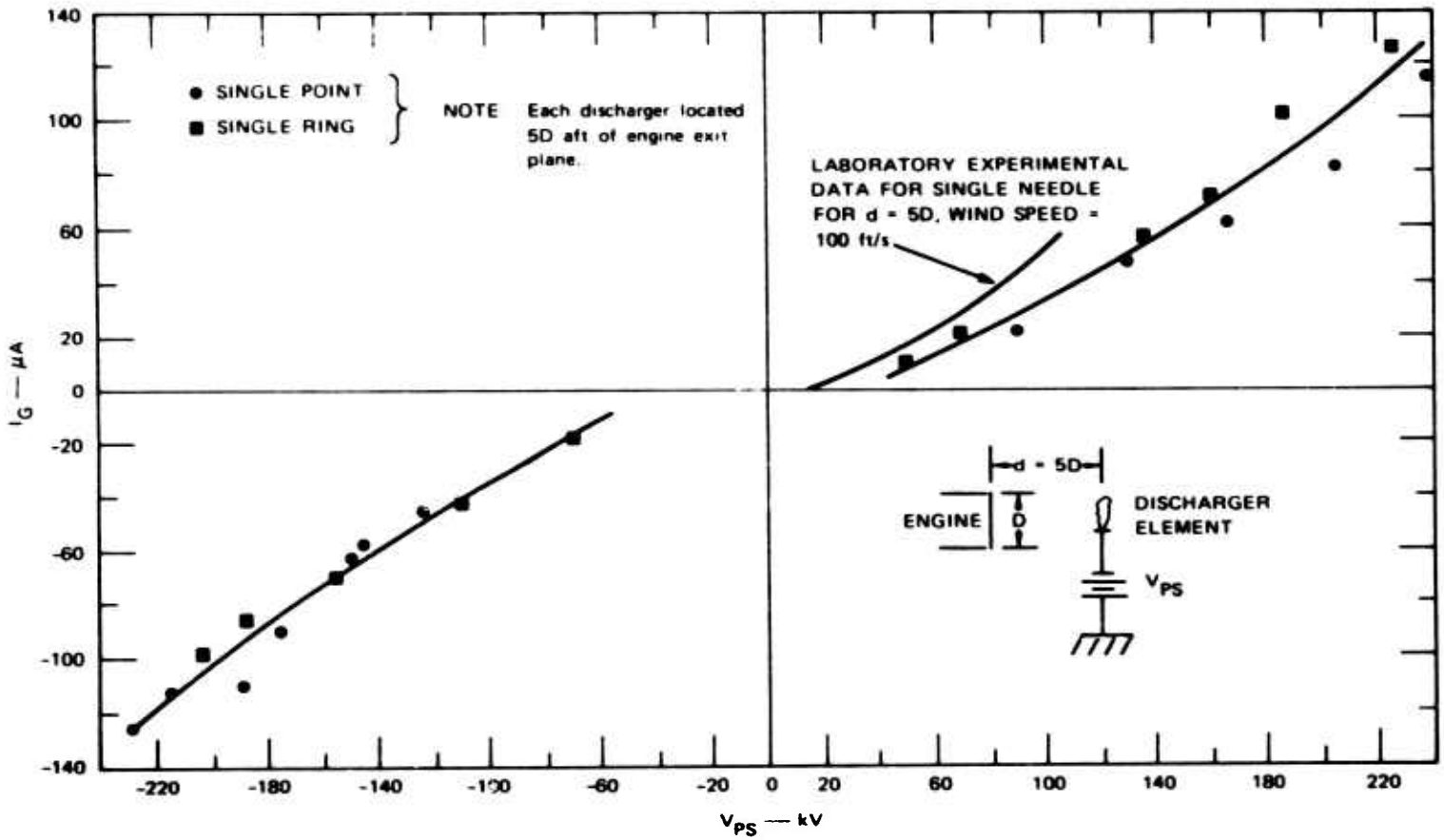

FIGURE 28 FLIGHT-TEST COMPARISON OF SINGLE-RING AND SINGLE-POINT DISCHARGERS IN ENGINE EXHAUST (clean environment)

generate the corona-discharge current required. Thus the engine-exhaust discharger may be considered to be a high-impedance system. (From Figure 27, for V = 200 kV, i = 100 μA; therefore R = 2000 MΩ). In the case of the active discharger developed for jet aircraft,[6] the high wind speed and low air temperature permitted the discharging element to be placed in close proximity to the airframe without any recirculation. There it was possible to achieve discharge currents of 1 mA for power-supply potentials of 60 kV, so that R = 60 MΩ, a much lower impedance.

In a further effort to verify and extend the laboratory work during the flight tests, an investigation was made of the effect on discharge currents of varying the position of the discharging element in the exhaust plume. The results of such a flight-test experiment are shown in Figure 29. Here, in agreement with the laboratory results, we see that increased net discharge current can be achieved by increasing the spacing from 2-3/4D to 5D. In addition, it was found that, with the ring at d = 2-3/4D, it is sufficiently close to the fuselage that flashover occurred from the ring to the fuselage at voltages in excess of 120 to 160 kV, depending on the power-supply polarity. Increasing the spacing to d = 5D increased the net discharge current at the lower voltages and, at the same time, permitted the full power-supply voltage of 220 kV to be applied to the discharger.

Figure 30 illustrates the results of an investigation of the degree to which dischargers located in one engine interact with and limit the current that can be discharged from an identical system in the other engine. The results of this experiment indicates that, on the CH-47, the engines are sufficiently far apart that, at the lower power-supply voltages, discharging in both exhausts doubles the discharge current. At the higher discharge-current levels there is some interaction, and the current discharged from two engines is not quite twice the current

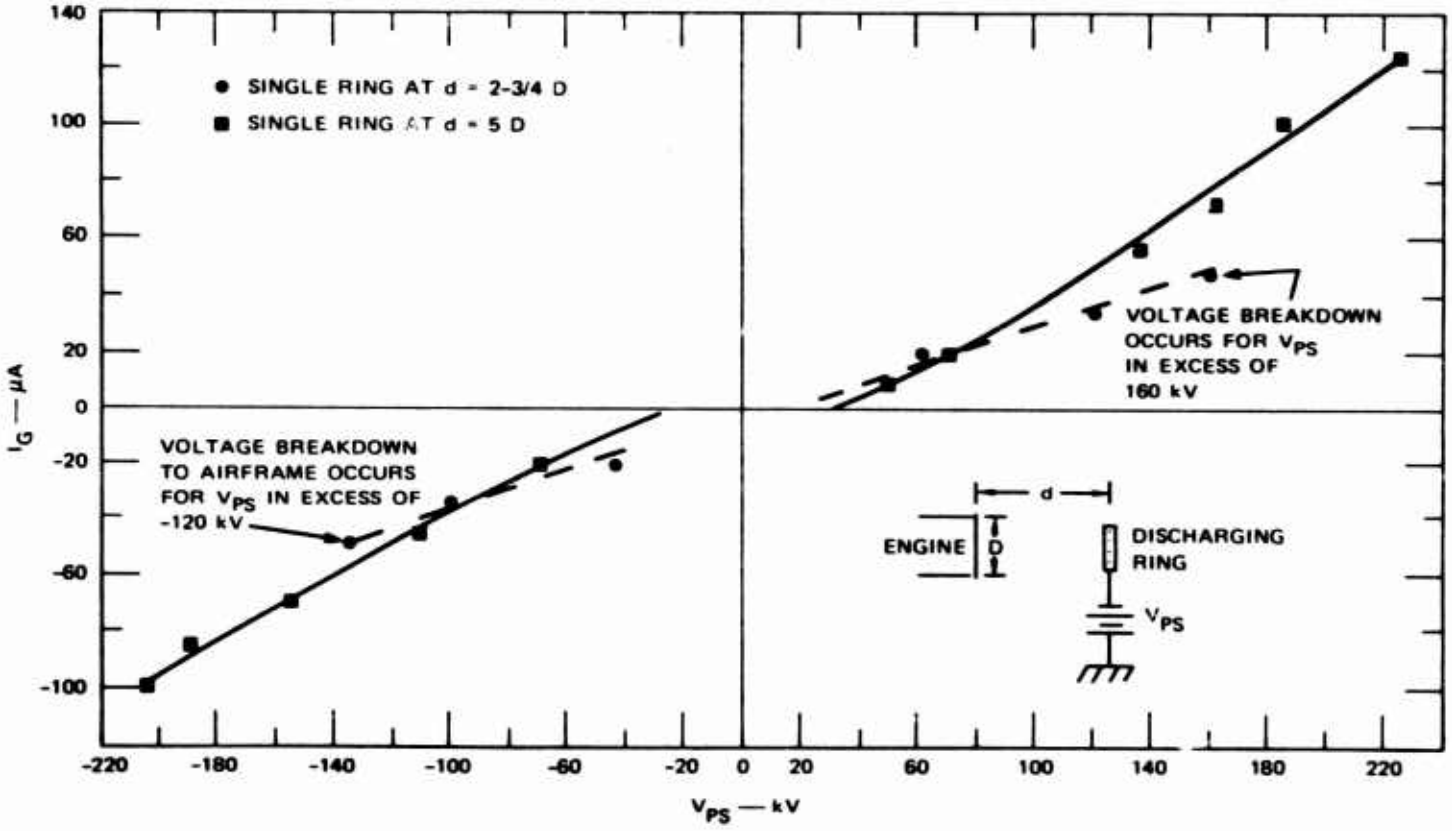

FIGURE 29 FLIGHT-TEST INVESTIGATION OF EFFECTS OF DISCHARGING ELEMENT AS A FUNCTION OF DISTANCE AFT OF ENGINE EXIT PLANE (clean environment)

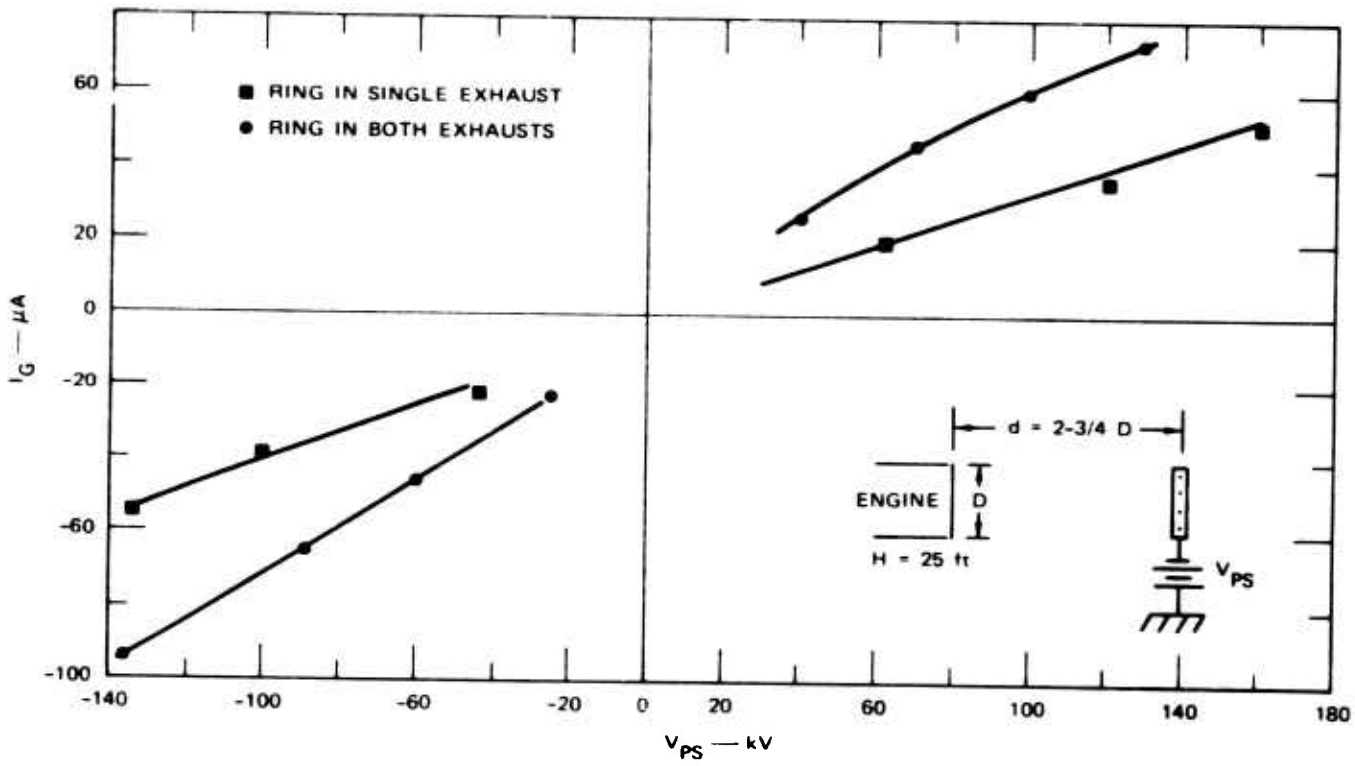

FIGURE 30 FLIGHT-TEST COMPARISON OF DISCHARGE CURRENT FROM DISCHARGING ELEMENTS IN ONE vs. TWO ENGINE EXHAUSTS (clean environment)

discharged from a single engine.

As part of the flight-test program, investigations were made of the effects of hover altitude on discharge current. Results of such investigations using a single-ring discharger located at d = 5D in the engine exhaust are shown in Figure 31. The data for 100-ft and 50-ft hover altitudes are very similar, and are characterized by a single line of best fit in the figure. The 25-ft hover data indicate a substantially higher current for the same applied voltage. This result probably stems from the fact that at 25 ft altitude the discharged ions are less effective in screening the discharge point and thereby limiting the net current as follows. From the 25-ft altitude, the ions more rapidly reach the earth's surface, where they are recombined. Also their image charges in the earth screen them more effectively from the discharger at 25 ft altitude than they do at 50 or 100 ft altitude.

The results of tests with the outrigger discharger system in a clean environment are shown in Figure 32. Comparing Figure 32 with Figure 29 or 31, we find that, at a given power-supply voltage, the outrigger system discharged roughly twice the current discharged by the single ring at d = 5D.

For some of the tests, the discharging system was arranged in the "maximum dissipation" configuration, in which the outrigger system and the ring located at d = 5D in the engine exhaust were both connected to the power supply. The results of such tests are shown in Figure 33. Comparing these data with those of Figures 32 and 31 we find that the "maximum dissipation" current is very nearly equal to the sum of the current discharged by the outriggers alond and the ring alone. Referring again to Figure 33, we observe that there is considerable difference between the data at each of the hover altitudes. It is not clear why this should be so, since the effect is not so pronounced for either of

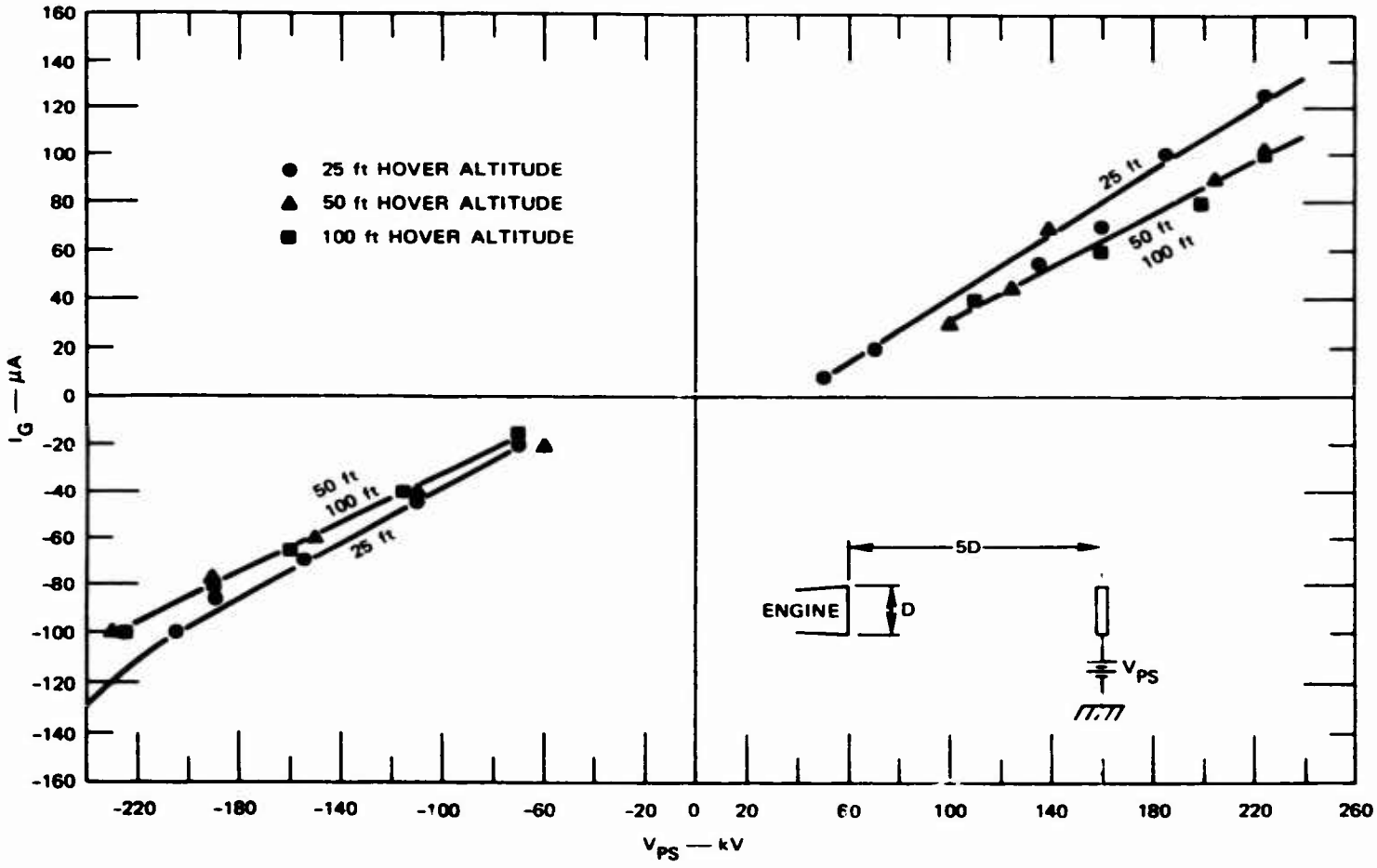

FIGURE 31 FLIGHT-TEST INVESTIGATION OF DISCHARGE CURRENT AS A FUNCTION OF HOVER ALTITUDE FOR THE RING DISCHARGER MOUNTED IN THE LEFT EXHAUST, FIVE DIAMETERS BEHIND THE EXIT PLANE (clean environment)

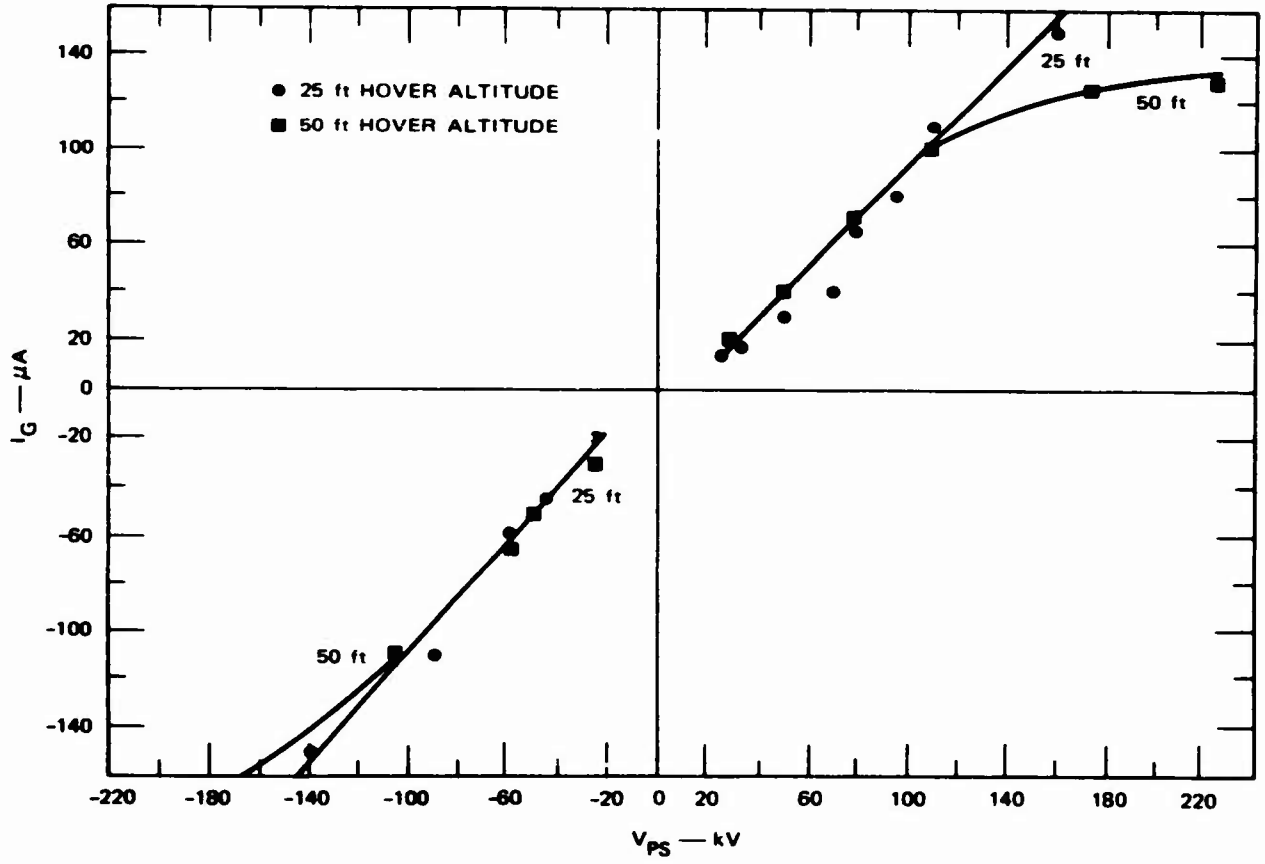

FIGURE 32 FLIGHT-TEST INVESTIGATION OF OUTRIGGER DISCHARGER CURRENTS AS AFFECTED BY HELICOPTER HOVER ALTITUDE (clean environment)

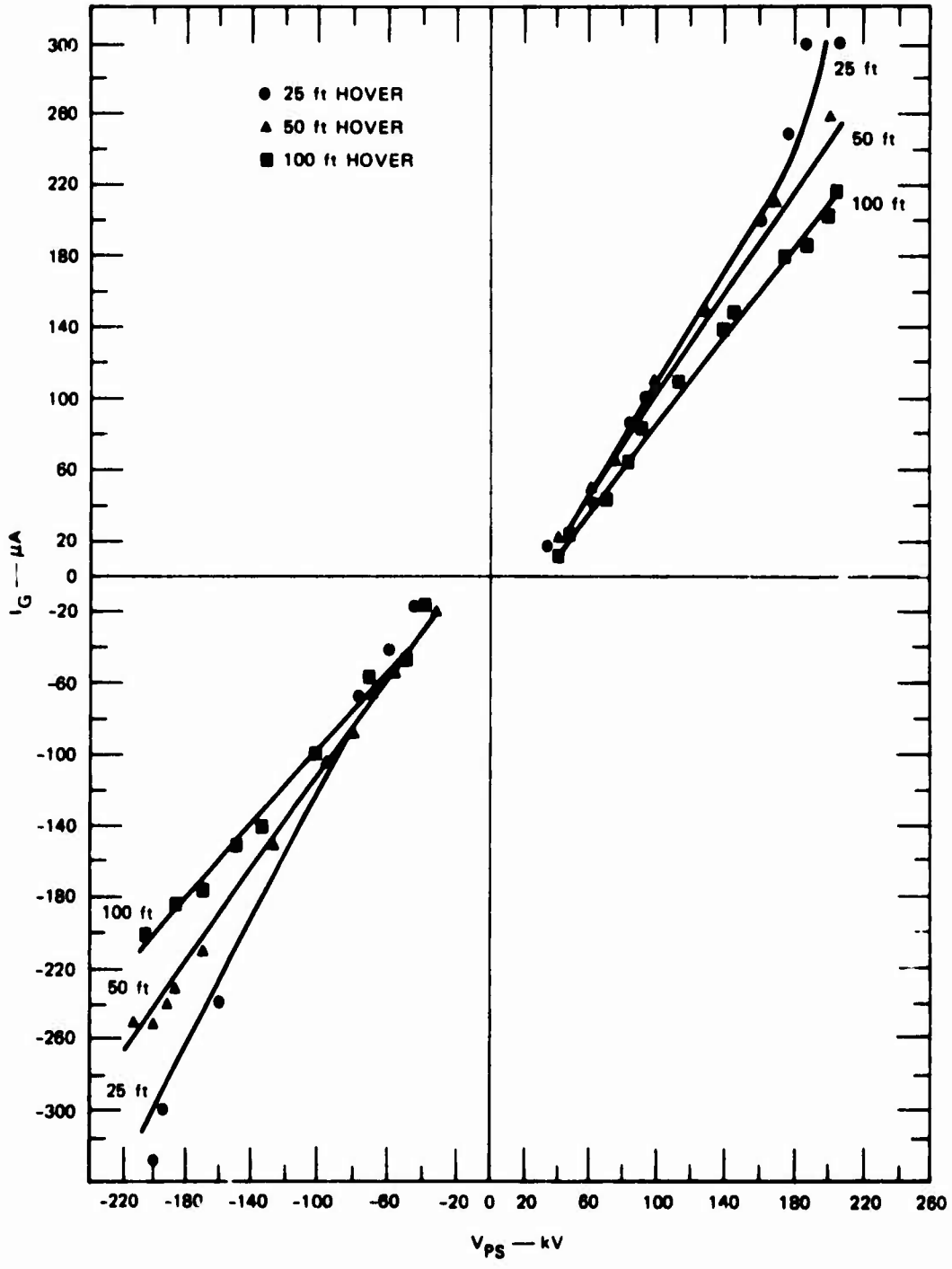

FIGURE 33 MAXIMUM-DISSIPATION FLIGHT TESTS USING OUTRIGGER SYSTEM AND SINGLE RING AT d = 5D (clean environment)

the dischargers used singly. It is felt that, perhaps when larger absolute values of current are discharged, the problem of space-charge-current limitation by the ion cloud assumes increased importance. In this case any process that gets rid of the space charge or minimizes its effects assumes added importance.

Dissipation testing was also carried out in a dusty environment generated by hovering over freshly disked sand, as shown in Figure 34. Results of such tests using the outrigger system are shown in Figure 35. The ground current flowing when the power-supply voltage is set to zero represents the frictional charging current to the helicopter. (This is the current we would like to be able to dissipate with the active discharge system.) By adjusting the power-supply voltage, it is possible to increase the ground current, set it to zero, or even to reverse its polarity. The dusty-area hover data are equivalent to the clean-environment data displaced appropriately to account for the frictional charging current.

Similar tests in the dusty environment were carried out with the ring discharger in the left turbine exhaust, five nozzle diameters aft of the exit plane. The results of these tests are shown in Figure 36. For positive power-supply polarity, the data are equivalent to the clean-environment data (displaced appropriately to account for the frictional-charging current). For negative power-supply polarity, on the other hand, the hover ground currents under dusty conditions are less sensitive to power-supply-voltage changes than under clean conditions. The reason for the decreased sensitivity is not clear. (Actually, it is possible that the data of Figure 36 are distorted by the nonconstancy of the frictional charging. If charging current changes during the course of a data run, it can make the I_G-vs.-V_{PS} curves appear to be steeper or shallower than they actually would be under constant conditions.)

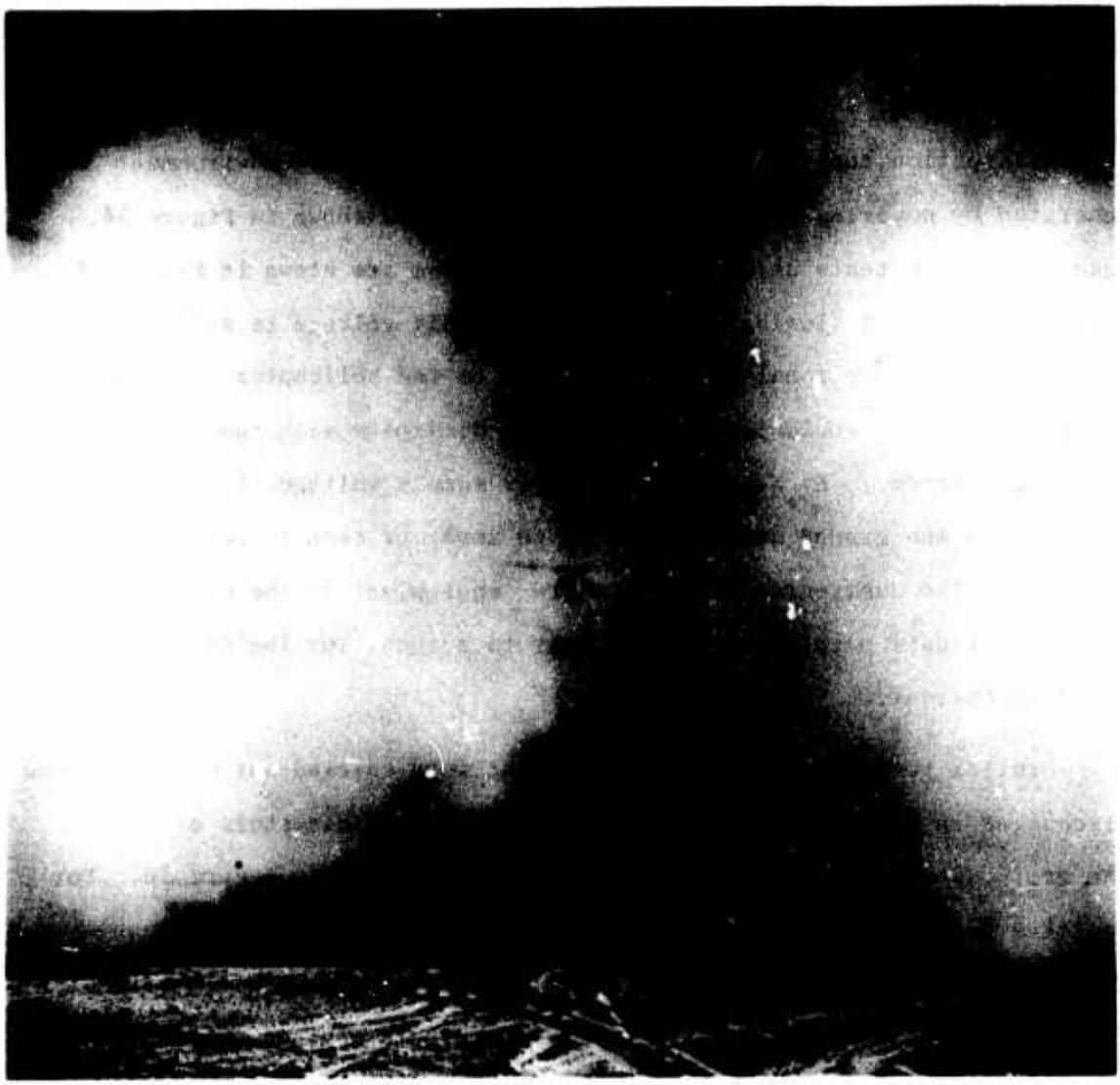

FIGURE 34 PHOTOGRAPH SHOWING FLIGHT-TEST OPERATION AT PHILLIPS DROP ZONE

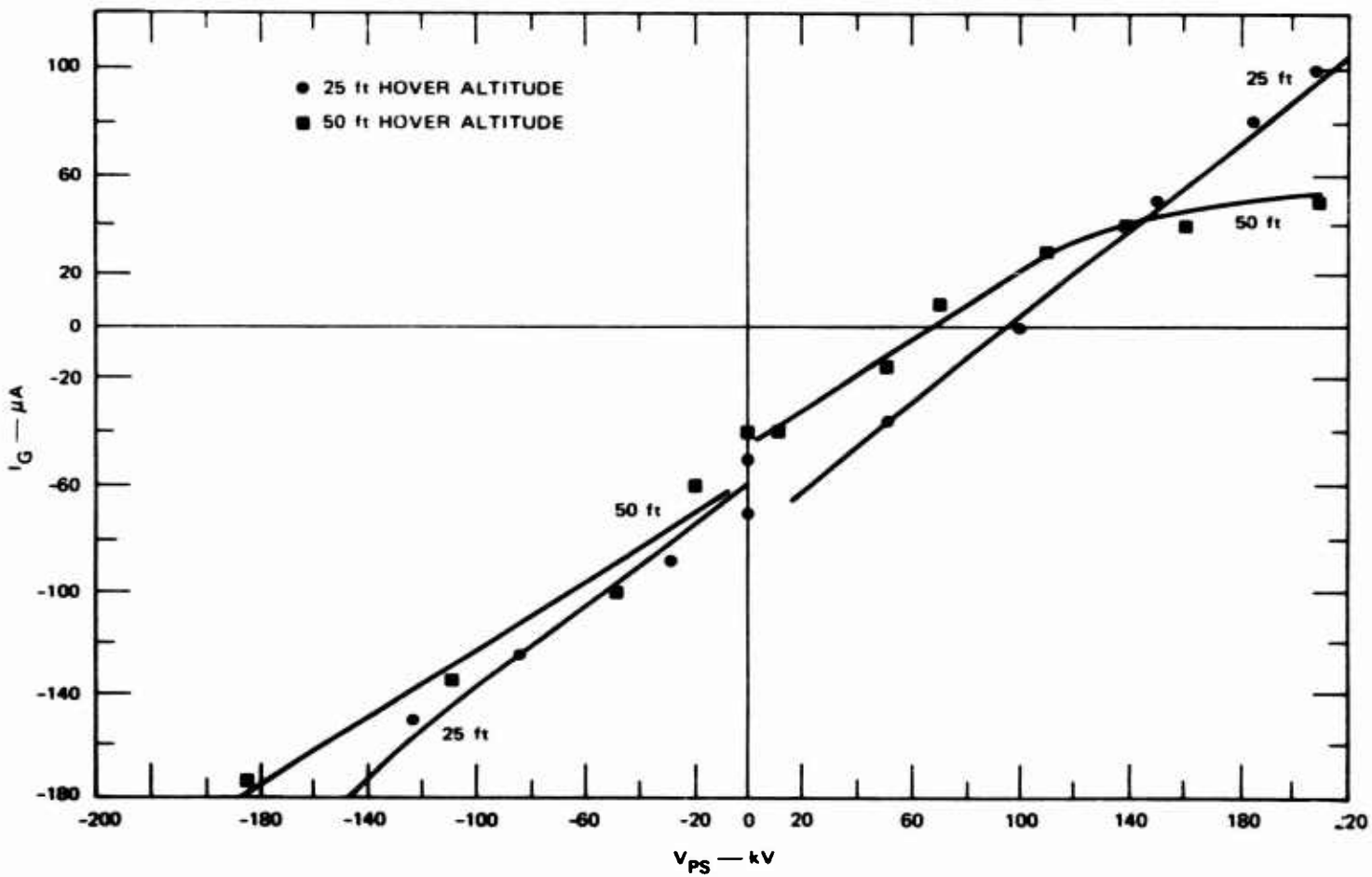

FIGURE 35 FLIGHT-TEST INVESTIGATION OF CURRENT DISSIPATION USING OUTRIGGER DISCHARGERS, AS AFFECTED BY HELICOPTER HOVER ALTITUDE (dust environment)

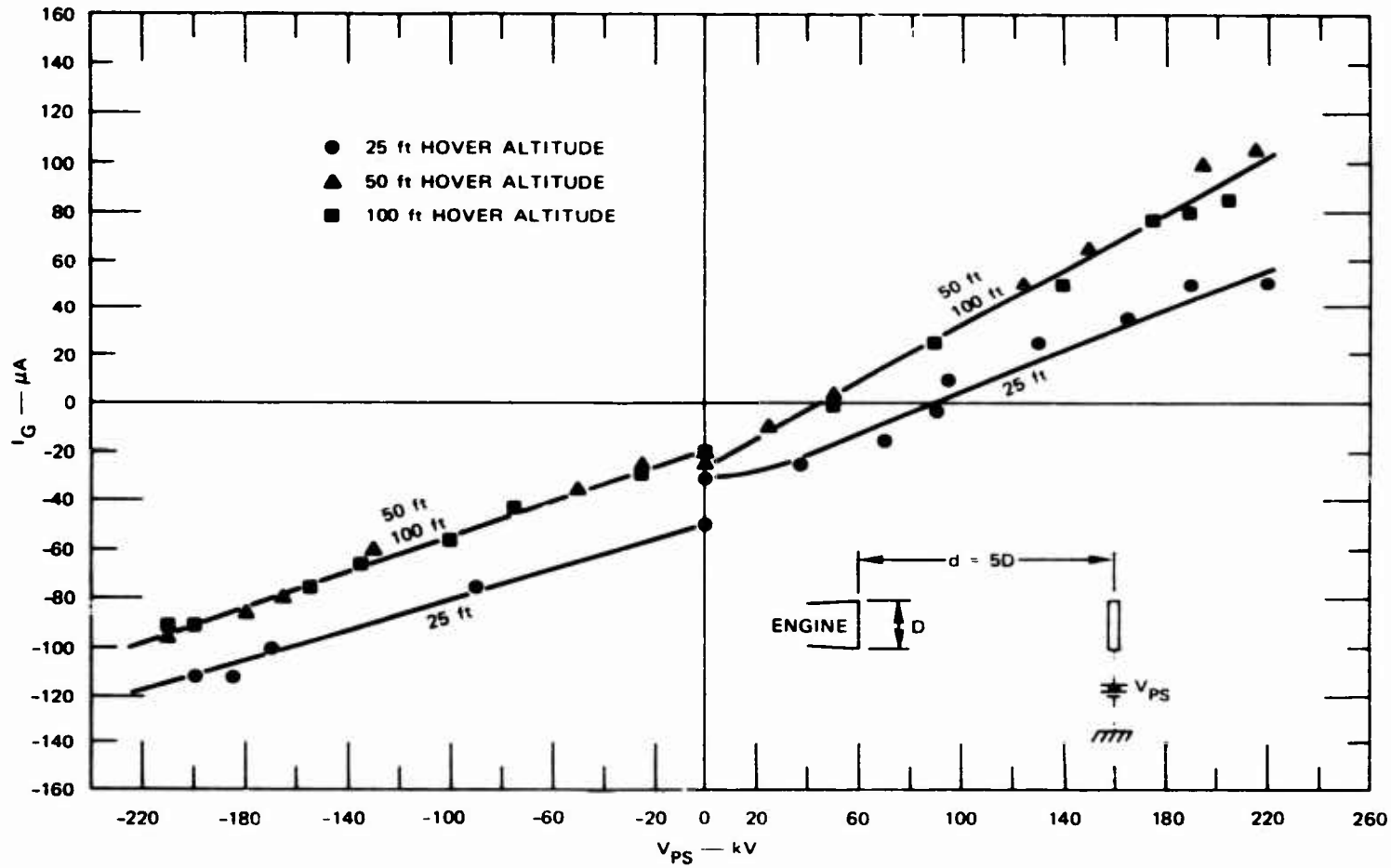

FIGURE 36 FLIGHT-TEST INVESTIGATION OF CURRENT DISSIPATION USING TURBINE DISCHARGER AS AFFECTED BY HELICOPTER HOVER ALTITUDE (dust environment)

The degree to which the SRI flight-test data and ground-test data compare with previous experiments[7] by others is shown in Figure 37. It

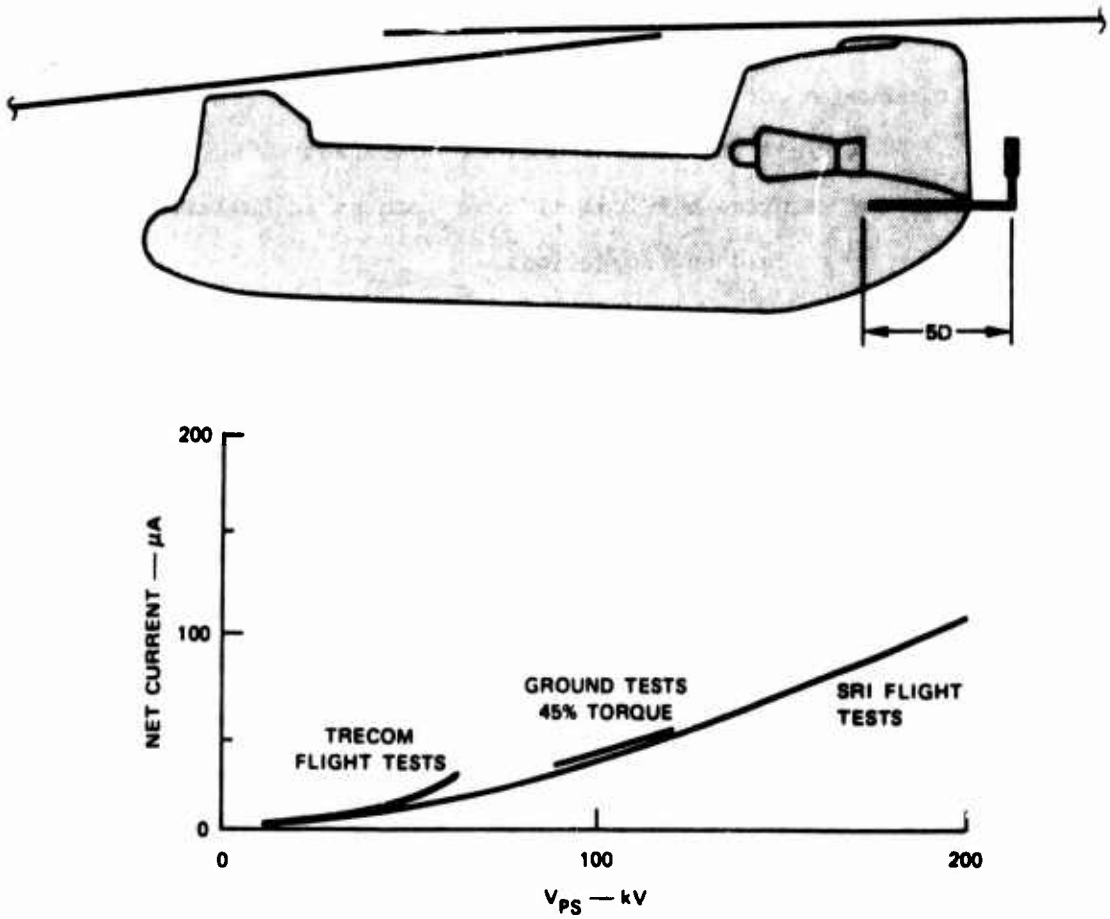

FIGURE 37 COMPARISON OF SRI FLIGHT AND GROUND DISCHARGER TESTS WITH PREVIOUS FLIGHT-TEST DATA

is seen from this figure that there is excellent agreement at low dissipator voltages, but at about 50 kV the curves begin to diverge.

The discharger data discussed above indicate that dissipation of 600 μA net current into the Boeing 301 HLH turbine exhaust appears feasible. The HLH will have three turbine exhausts; each exhaust is approximately twice the diameter of the CH-47 exhaust, and the exhausts

do not pass along the fuselage skin, which will minimize recirculation. Therefore, locating dischargers in each of the three exhausts, five exhaust diameters behind the nozzle (from either the ring or single point) should provide the desired 600 μA.

Although the outrigger discharger discussed earlier produced a higher net discharge current than either the ring or single point in the exhaust, it is felt that this technique would not be suitable on the HLH since the required physical size of such an installation to obtain 600 μA (net) would be impractical.

D. Sensor-Fidelity Flight Tests

One of the most difficult problems associated with the development of a satisfactory active discharging system is that of devising a sensing scheme capable of providing an indication of the helicopter-to-ground potential under all operational conditions. Typical environments include dust, dry snow, electrified rain, and the ion cloud generated by discharge from the dissipator element. Ideally, the sensing element should function without any connection to the ground. A field meter or "field mill" immediately suggests itself as the sensing device.

In considering the workability of a simple field-meter sensing scheme, it is argued that if a charged body is suspended in charge-free, field-free space, there is a unique relationship between the electric-field intensity at a particular point on the body, and the potential of that body. In particular, the fields are zero when the potential is zero. In this case, a field meter is an ideal device for measuring the potential of the body. At the other extreme, if we allow any arbitrary distribution of charges and applied fields around the body in question, there is no unique relationship between electric-field structure about the body, and its potential to ground. Thus, no measurement we can make <u>on the body</u> can tell us its potential.

In planning this program, it was felt that the actual operational situation would lie somewhere between the two extremes discussed above. It was observed, further, that it would be fruitless to try to settle the question of sensing either by purely analytic methods or by laboratory experiments since the problem involves the interaction among poorly understood frictional-charging processes, complex airflows, and tortuous recombination processes. Accordingly, no effort was made to investigate the sensing problem in the laboratory or during the Vertol CH-47 ground tests.

For the flight-test investigation of sensor fidelity, the helicopter was equipped with a total of four electric-field meters (field mills). The field mills are visible in Figures 21 and 25. The overall arrangement of the field meters is shown in the sketch in Figure 38. Provisions were made to suspend Field Meter #1 from the helicopter by means of a nylon rope passed through the cargo hatch. This arrangement simulates the mounting of a field meter on the helicopter cargo hook. It was argued that this arrangement minimized the amount of charged material between the sensor and earth, and would therefore have considerable promise of sensing the true helicopter-to-ground potential.

Field Meter #2 was located on the underside of the helicopter near the nose in the region often used in the past for field-meter installations. This field meter serves to tie together data from this experiment with earlier work. Field-Meter #3 was installed on the side of the fuselage roughly centered in both the vertical and fore and aft directions. Field Meter #4 was mounted on the top of the fuselage roughly centered fore and aft, and slightly to the left of the fuselage center line. The purpose of Field Meters 3 and 4 was to investigate the possibility of using multiple field-meter installations to sort out the effects of charged dust and ion clouds in the vicinity of the hovering helicopter and to infer from multiple field-meter readings the true helicopter-to ground

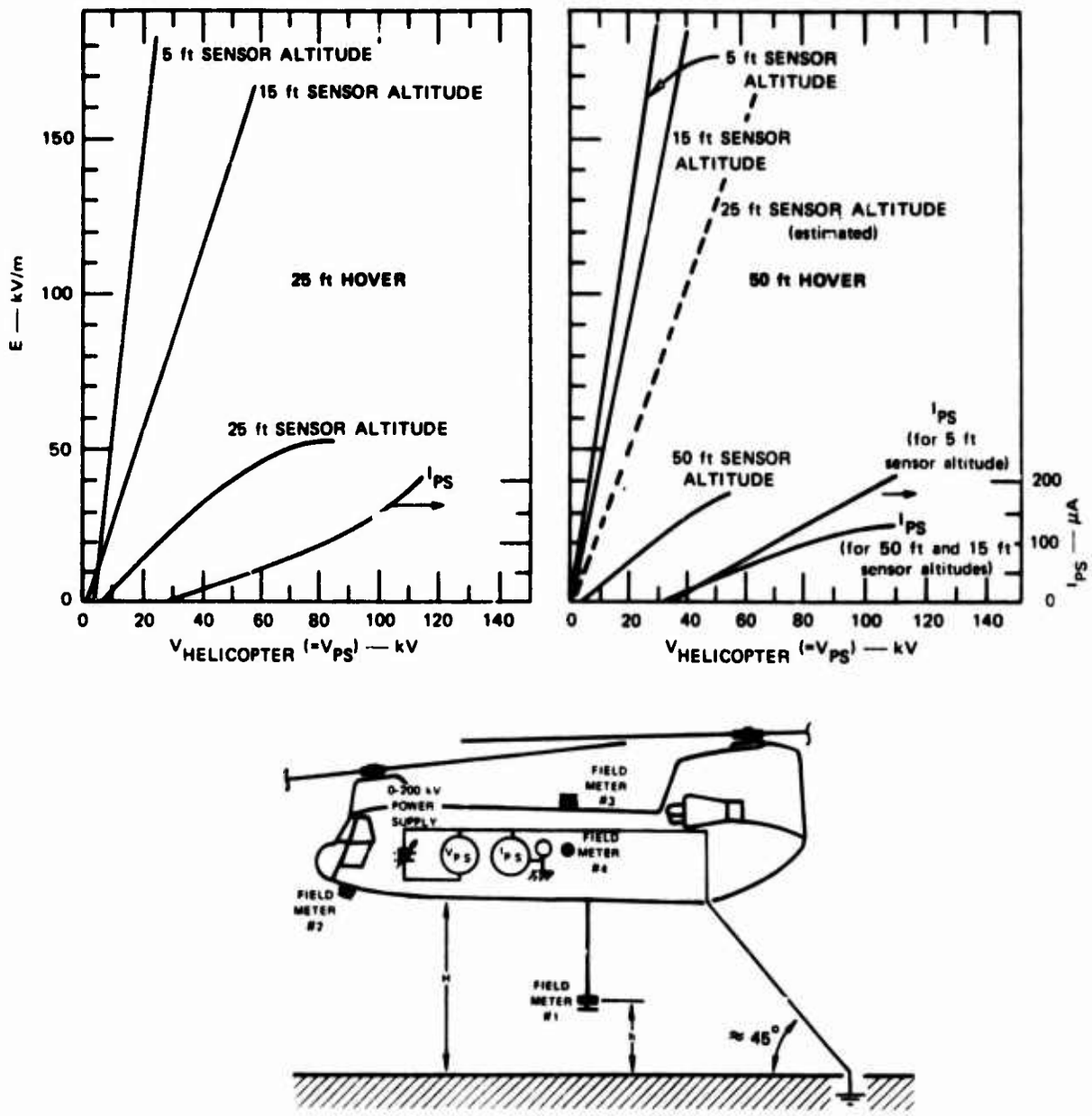

FIGURE 38 FLIGHT-TEST CALIBRATION OF CARGO-HOOK FIELD METER

potential.

The sensor-fidelity instrumentation system included a set of five ground-based field meters that for all but one of the tests, were arrayed under the hovering helicopter. This field-meter system permitted study of the way in which discharge ion and charged dust clouds are distributed and how they affect the electrostatic-field structure in the vicinity of the helicopter. Two basic ground field-meter arrangements were used during the sensor-fidelity tests. For any particular test, the configuration employed is given in the figure that shows the data from that test.

The most fundamental sensor-fidelity flight-test experiment (illustrated in Figures 38 and 39) consisted of determining the relationships between the various field-meter readings and the aircraft potential. For this experiment, the ground wire was connected to the power-supply high-voltage terminal. In this way, the helicopter potential with respect to ground is simply the power-supply voltage. The connection to the power supply was actually made, by connecting a piece of 20-gauge hookup wire to the discharging-element mount. (The discharging element was removed for these tests.) The wire led to a ground stake aft of the helicopter, so that during hover the ground wire remained well aft of the helicopter as shown in the drawing.

Figure 38 presents the results of measurements on the cargo-hook field meter. First we observe that a positive field-meter indication is obtained upon the application of a positive power-supply voltage. This is in keeping with the sign convention for field meters illustrated in Figure 27, where a positive charge above the field meter is interpreted as a positive field indication (this is the convention employed by atmospheric electricians). Since the power supply is connected to the outside world, a positive supply voltage "charges the world positively" with respect to the field meter. Next, we observe that, for a given

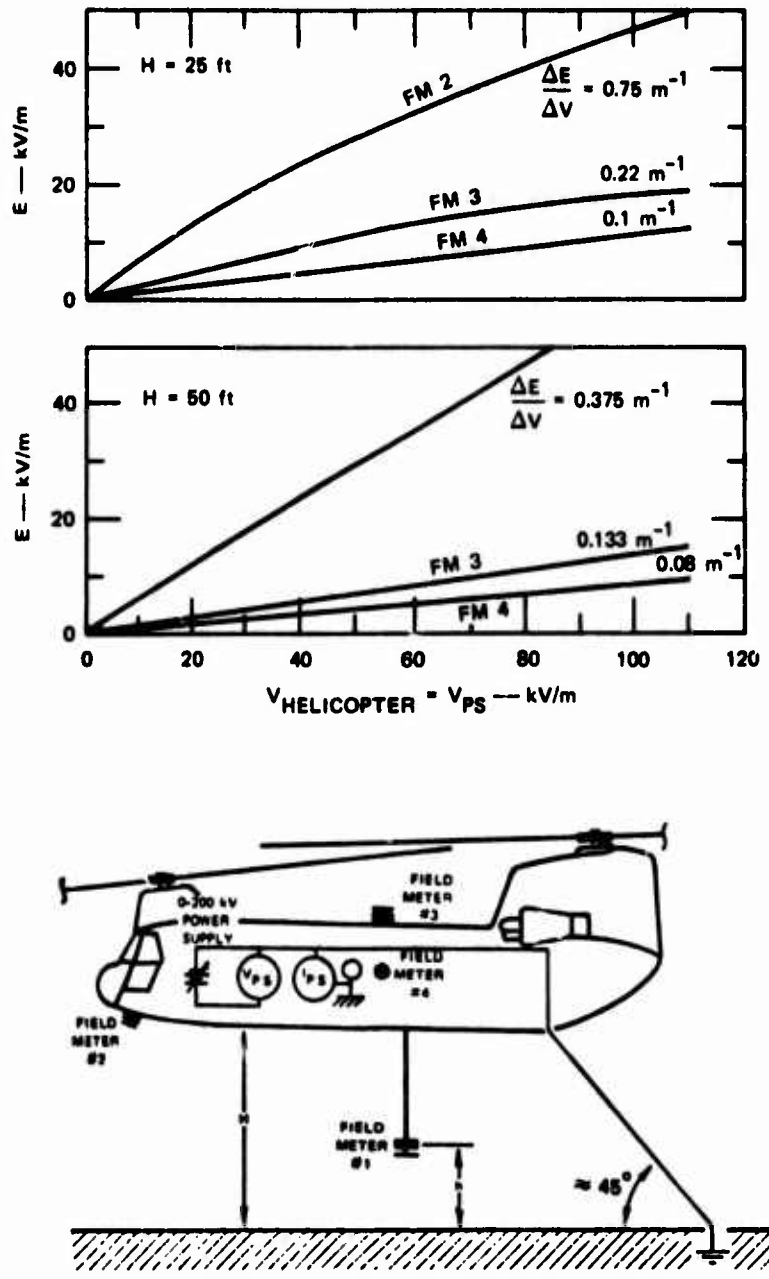

FIGURE 39 FLIGHT-TEST CALIBRATION OF HELICOPTER FIELD METERS

voltage and hover altitude, the field-meter reading depends critically on the field-meter sensor altitude, h. As h is decreased, the protrusion of Field Meter #1 increases so that it produces a greater concentration of field about itself. For very small h, the proximity of the ground further enhances the field.

A word of caution is appropriate here regarding the degree of reliance that should be placed on the precise values of the #1 field-meter readings. In comparing the data at H = 25 and H = 50 for h = 5 we observe that the field meter is more sensitive at the 25-ft hover altitude. This may result from errors in the actual hover and sensor altitude stemming from the way the experiment was conducted. For example, to achieve h = 5 at H = 50, 45 ft of the nylon support rope were played out, and the helicopter was hovered at 50 ft. Thus an error of a few feet in hover altitude introduces the same absolute error into the sensor altitude. Since there is a factor-of-10 difference in the two nominal altitudes h and H, the percent error in h will be 10 times the percent error in H. It is likely therefore that the slope of the curve for h = 5 at the 50-ft hover altitude should actually be somewhat higher than shown.

Returning to an inspection of Figure 38, we find that E_1 varies linearly with V_{PS} until corona threshold evidenced by non-zero power-supply current is reached, and some corona current is discharged. At this time the slope of the curve decreases. Physically this behavior can be explained as follows. The aircraft is charged negatively with respect to the earth so that, to the field meters, the outside world looks positive and they give a positive indication. When corona threshold is reached, negative charge begins to leave the tips of the rotor blades and is driven toward the ground by the rotor downwash. This negative charge in the vicinity of the helicopter makes the outside world look less positive, so that the field-meter reading is reduced.

(This same effect of corona space charge was reported[8] in connection with hovering tests conducted on CH-34C and UH-1A helicopters.) The effect is apparent only on the data for h = H because at h = 5 and h = 15, the field-meter output saturates before corona threshold is reached.

Calibration data for the three fuselage-mounted field meters are shown in Figure 39. Their behavior and sensitivities are similar to those of Field Meter #1 when it is at fuselage level (i.e., for h = H).

The results of these field calibration measurements were checked in a laboratory experiment, and the results of this experiment are reported in Appendix I.

In another set of experiments, the helicopter was grounded and hovered over an array of ground field meters as shown in Figure 40. These tests were carried out in a "clean" area (that is, an area in which there was no dust stirred up by the hovering helicopter). Current was discharged from the outrigger discharger and readings were made of electric-field intensities both on the aircraft and on the ground array. With this arrangement the helicopter is held at ground potential at all times so that there is no contribution to the electric-field structure from net charge on the helicopter. Thus, in the absence of perturbing influences, the airborne field meters should read zero. The only sources of electric field around the helicopter are the potential applied to the discharging element, and the space charge generated by the discharge ion cloud. In a laboratory-model experiment, the relationship between a voltage V applied to the discharger and the electric field E_n it produces at a sensor location n, was determined and is given in Table II. Comparison of these tabulated values of E/V with the slopes of the lines shown in Figure 39 shows that the electric field produced by the discharger (and measured at the various field-meter locations) is small compared to the measurement of the true electric field. Thus, the large

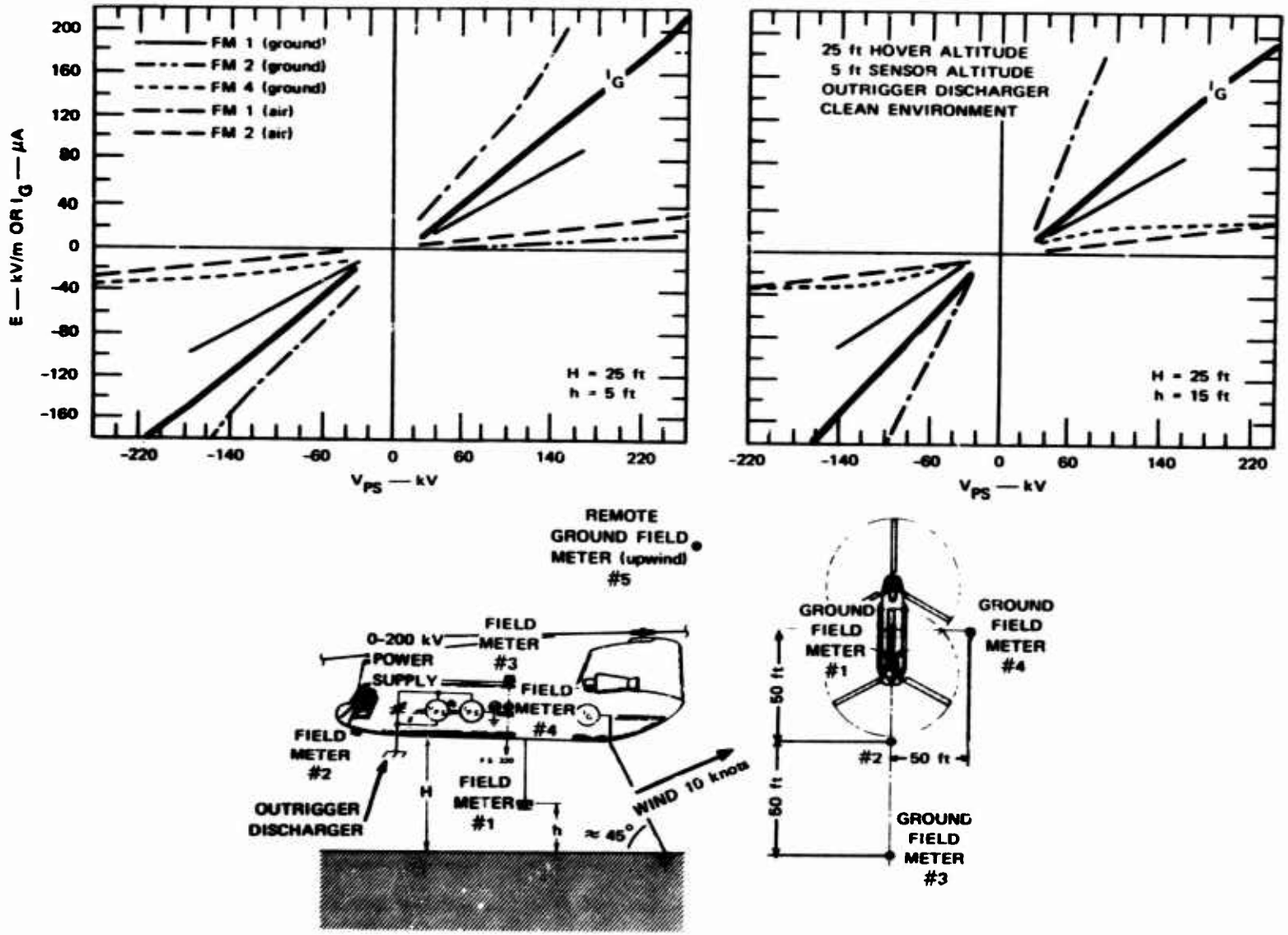

FIGURE 40 SENSOR-FIDELITY FLIGHT TESTS WITH OUTRIGGER DISCHARGER (clean area)

Table II

RELATIONSHIPS BETWEEN OUTRIGGER VOLTAGE AND ELECTRIC FIELD AT VARIOUS SENSOR LOCATIONS

Airborne-Field-Meter Location (n)	E/V (m^{-1})
1	Not determined
2	0.04
3	0.03
4	0.02

electric fields measured on the airborne field meter in Figure 39 are predominantly due to the ion cloud generated by the discharger that is blown around the various field mills by the rotor-wash. Further examination of Figure 40 shows that the ion cloud produced by the outrigger discharger is blown down into the ground array, giving large values for the electric field.

In an effort to better understand the effect of the discharger-produced ion cloud, additional experiments were carried out using various discharger locations. Figure 41 shows the result of one such experiment in which the discharger in the left engine exhaust was used to supply the ions. It can be seen from this figure that the ion-cloud perturbation of airborne Field Meter #1 reading is somewhat smaller with the ring than with the outrigger discharger shown in Figure 40. The ring-discharger ion cloud has a markedly smaller effect on airborne Field Meter #2 than does the outrigger-produced cloud. This difference is attributable to the fact that the ion cloud produced at the outrigger location is blown about in relative close proximity to the #1 and #2 airborne field meters, whereas the ring discharger located far back

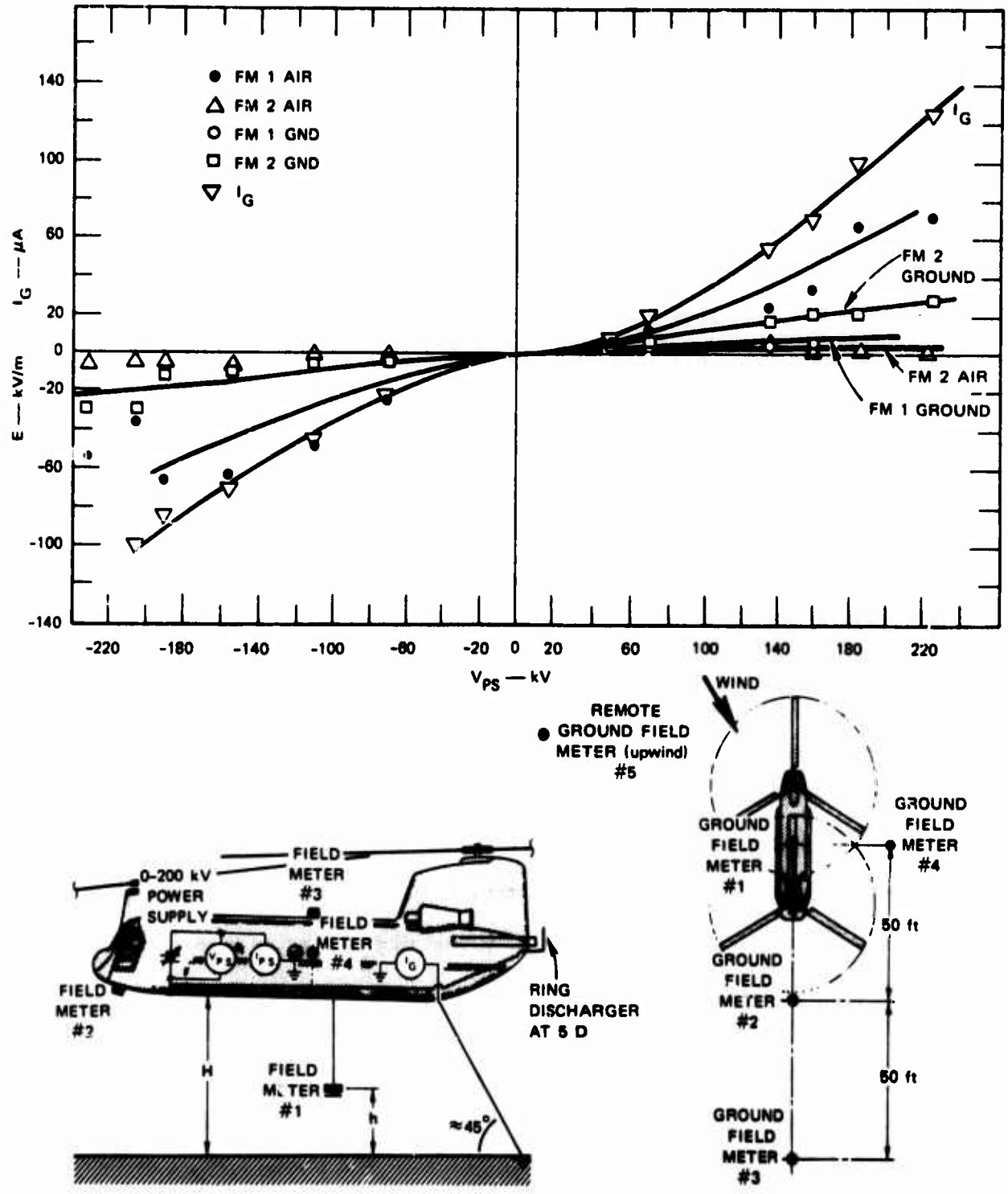

FIGURE 41 SENSOR-FIDELITY FLIGHT TESTS USING RING AT 5D FOR ARTIFICIAL CHARGING

produces an ion cloud that, due to the engine exhaust and rotor down-wash flow pattern is driven away from the #2 airborne field meter and to a lesser extent away from the #1 airborne field meter.

The relation between a voltage applied to the ring discharger and the electric field E_n measured at sensor location n was determined in a way similar to that used for the outrigger discharger (see Table II). The coupling factors for the ring discharger, expressed in terms of the ratio E/V, was less than 0.02 for all airborne-field-meter locations. It can be seen from this that the electric fields measured by the various airborne sensors (see Figures 38 and 39) were only very slightly influenced by the ring-discharger electric field and were principally due to the ion-cloud space charge. The extent of the migration of the ion clouds can be observed in the ground field meters. Referring again to Figure 41, it is seen that the #2 ground field meter gives a higher field reading than does the #1 ground field meter (the #2 ground field meter was beneath and somewhat behind the ring discharger; the #1 ground field meter was directly beneath the CH-47 cargo hatch). The results of these tests indicate that in order to correctly infer the helicopter potential, it is essential that the field-meter location be chosen such that there is minimal effect from the discharger ion cloud, since the field meter cannot differentiate between the "desired" electric field due to aircraft-to-ground potential and an electric field generated by an ion-produced space charge.

As indicated above, it appears that even airborne Field Meter #2 is strongly enough influenced by the discharge-product ions to indicate fields of 5 kV/m or so. The HLH electrostatic-discharge objective is to maintain energy transfers, upon contact with the ground, of less than 1 mJ. It can be seen from Figure 39 that the potential inferred from 5 kV/m (H = 25 ft) is about 6.7 kV. If one assumes a helicopter self-capacitance of about 2000 pF, and if the helicopter was not grounded

and was actually using such an active system, the actual energy transfer upon ground contact would be about 45 mJ, or about 50 times that of the design objective. Therefore, "minimal effect" at field-meter location #2 means that the field measured there would have to be less than about 1 kV/m. It is noted here that during the Yuma tests, the ambient (i.e., naturally occurring) electric field was often about 100 V/m under conditions of nearly cloudless days, and that shortly before a thunderstorm the ambient field increased to approximately 1.2 kV/m.

The sensor-fidelity tests were extended to determine the effects of a dusty operating environment on the performance of the field meters. The helicopter was operated in an area of plowed desert sand at the Yuma Proving Ground to reflect a severe natural charging environment.

Before an understanding of the various observed phenomena was possible, it was necessary to determine the effects of blowing dust in the absence of the helicopter. This was accomplished during a series of "fly-by" measurements. The ground array of field mills was laid out in its usual configuration and the helicopter was used as a wind source to blow the dust over the sensors. The helicopter was flown past the ground array, at an altitude of 50 ft on the upwind side, at a speed that was slow enough to allow a good-sized dust cloud to develop, and yet fast enough so that the dust cloud did not rise to contact any part of the helicopter. After a trial-and-error period, this speed was determined to be about 5 knots, and several fly-bys were made, as shown in Figure 42. The results of these fly-bys were consistent, and the ground field mills indicated that as the dust cloud blew across the surface of the earth it became positively charged, as shown in the graph inset in Figure 42. The dust cloud's movement over the surface can be observed in the graph from the time-to-peak for each field meter, and it is seen that Field Meter #3 peaks first and #1 peaks last, which agrees with the direction the dust cloud was blown. The speed of the cloud's

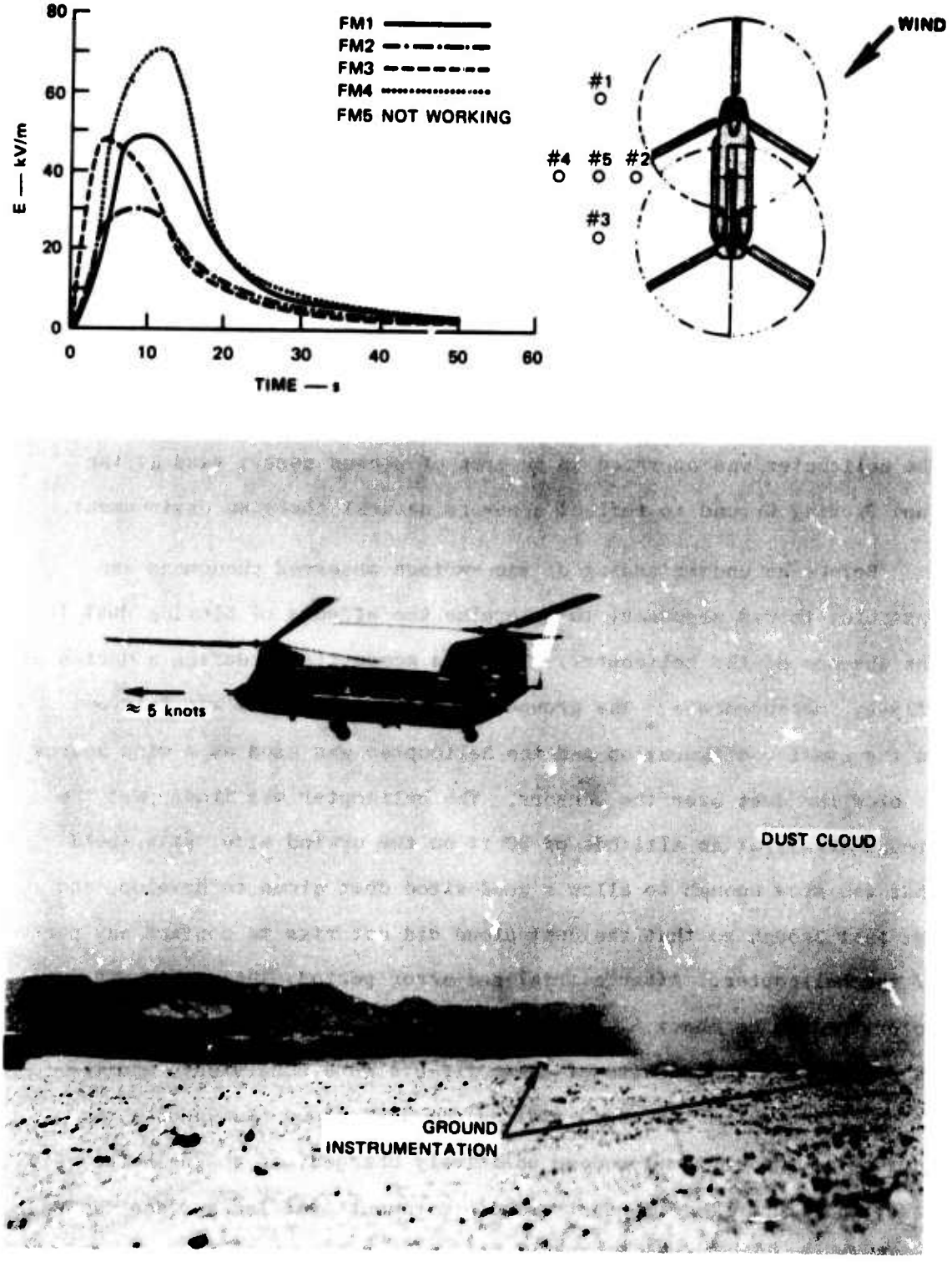

FIGURE 42 HELICOPTER FLY-BY INVESTIGATION OF DUST-DUST TRIBOELECTRIC-CHARGING EFFECTS

movement along a line between field-meters #3 and #4 can be easily calculated to be about 10 ft/s, since these mills were about 70 ft apart. The airborne instrumentation was not used during these tests.

The initial natural-charging sensor-fidelity tests were made at various hover altitudes and Field Meter #1 altitudes with the helicopter grounded. During these tests, the electric fields on the airborne and ground systems were recorded as a function of time. Results typical of the observed electric fields are shown in Figure 43 for a hover altitude of 50 ft and the Field Meter #1 altitude of 25 ft. It should be repeated here that the hovering helicopter was kept at ground potential through the ground line, and therefore any measured electric field other than zero represents an error in the measurement of the helicopter-earth electric field. Figure 43 shows the charging current, I_G, the airborne-field-meter data and the ground-field-meter data recorded over a 35-s period. Time = 0 denotes roughly where the takeoff occurred, and the hover altitude of 50 ft over the ground array was established at approximately 15 s. It is observed from this figure that I_G, the charging current, rapidly increases to about 300 μA and then at about t = 15 s slowly begins to decay. This decay is due to the rotor wash blowing the dust away from the measurement site. It is also observed from this figure that, except for sporadic instances, all of the ground field meters and airborne field meters #1, #3, and #4 measured positive electric fields. This is in agreement with the fly-by tests discussed earlier, and it indicates that the field meters were looking into a region of positive (relative to the helicopter) charge, according to our sign convention (see Figure 27). The negative electric field measured by the airborne #2 field meter was unexpected, but it is now felt that this behavior could be due to the frictional charging of the plastic cockpit canopy and the proximity of Field Mill #2 to that canopy.

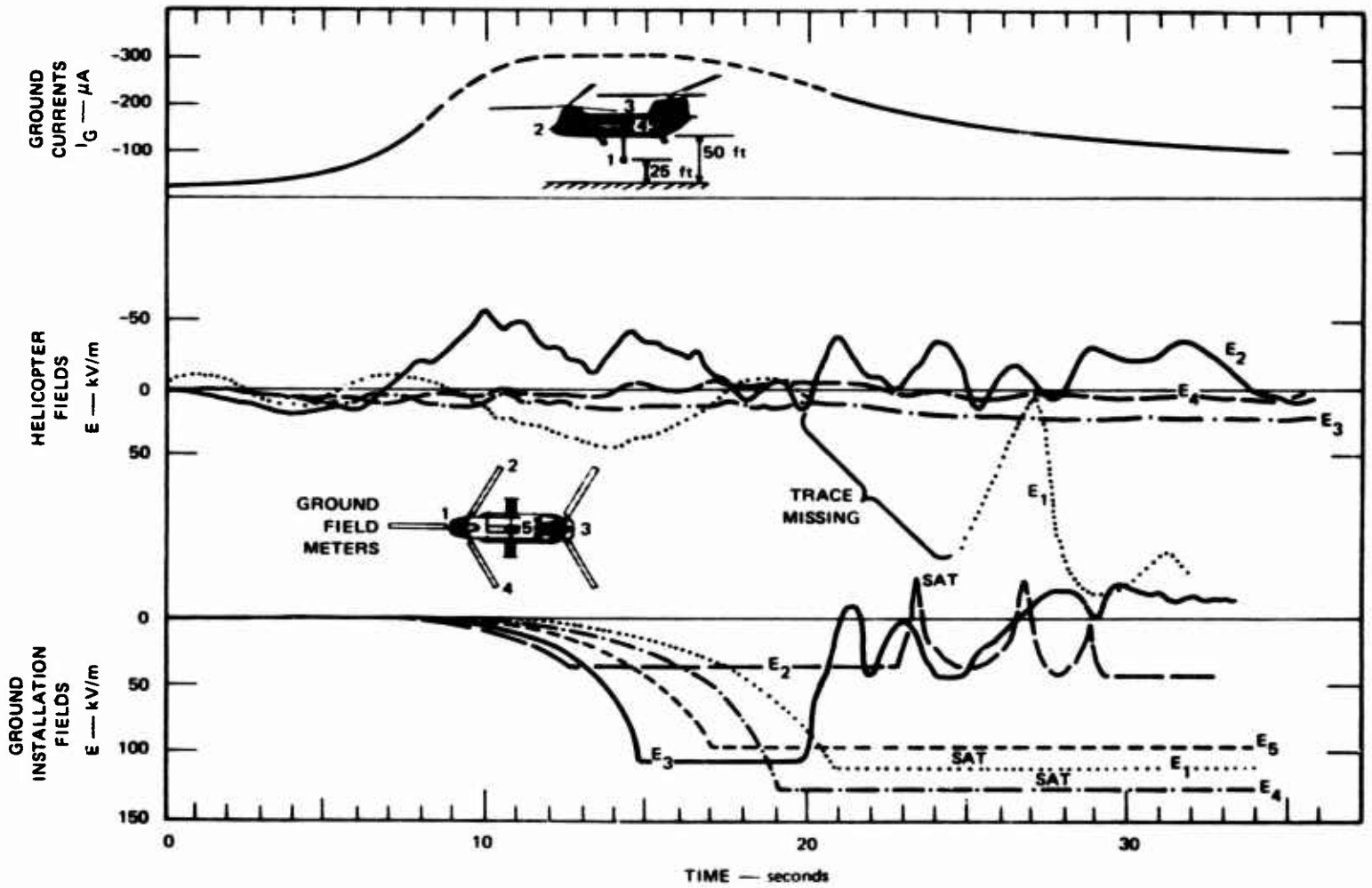

FIGURE 43 OBSERVATION OF ELECTRIC FIELDS ON VARIOUS SENSORS MEASURED AS A FUNCTION OF TIME

A laboratory experiment was performed to examine this hypothesis in more detail. A field mill was set up in the vicinity of a charged sheet of plexiglass to simulate the cockpit canopy. The plexiglass was then sprayed with powdered walnut shells (to simulate dust) which, when sprayed, acquired a positive charge. The observed results were that the plexiglass acquired a charge that was the algebraic sum of its quiescent charge and the charge on the shells. This summing process continued until the charge on the plexiglass became saturated, and plastic-to-air discharges began. It is felt that this experiment supported the notion discussed above. The convective flow patterns produced by the rotors tend to limit the amount of dust (around the canopy and Field Meter #2) that has been blown up directly from the surface of the earth (i.e., the lower cockpit canopy and Field Meter #2 are in a stagnation region). The triboelectric processes occurring on the rotor blades, on the other hand, tend to strip positive charges from the dust and send the (now) negative-charged dust downward in the rotor-wash; these negative charges are then deposited on the canopy, which gives rise to the negative measured electric field.

Although the general behavior of the fields measured by the field meters was similar for each sortie flown in the dust, the specific behavior was sufficiently random that no definite conclusions could be drawn about the effects of sensor location, inferred potentials, and other factors. To describe such random processes, it is profitable to employ statistical methods. Accordingly, the variation of field measured as a function of time was statistically analyzed for each airborne field mill, and the results are given below. A detailed account of the methods used in this analysis is given in Appendix II.

All of the sorties flown in the dust were evaluated for possible use in the statistical compilation shown below, in an attempt to find data that would represent "unbiased" operating parameters. Examples of data excluded were data that represented "climbing-to-hover" conditions,

data in which the hover altitude was uncertain, data contaminated by the presence of dissipator ions, and data in which the desired field meter failed. This selection process resulted in a total of about 9 minutes of data (one sample per second) for Field Meters #2, #3, and #4 and about 2 minutes of data for Field Meter #1. Although these times reflect only a small portion of the total times spent in hover, they were deemed adequate because after a couple of minutes of data, the change in statistics with an increasing number of samples became small.

Since the helicopter was electrically grounded during these operations, it is known that any field (and, hence, inferred A/C potential) other than zero represents an error. The data given in Table III represent an effort to determine the extent of this error which is of interest in the calculation of discharge energies. The table is a short statistical summary of the hover-in-dust data that were examined in detail. (The symbols in the table are those normally used in a statistical work and are explained in Appendix I.) Table III indicates that the mean error indicated by Field Meter #2, for example, at the 50-ft hover altitude was 26.4 kV/m (field) or 48 kV (potential inferred from Figures 38 and 39), and the standard deviations were 14.6 kV/m (field) and 26.6 kV (potential). Table III can be read in a similar manner for the other sensors and hover altitude.

Although the field (or potential) means and standard deviations are useful from an information point of view, they can be misleading if a normal distribution is assumed when calculating inferred discharge energies. A plot of the actual frequency distribtuion (histogram) for the inferred potentials (see Appendix II) shows that the data represent a very poor approximation to a normal distribution in most cases, and that a more suitable distribution would be required to permit an adequate analytic investigation of the inferred discharge-energy probabilities.

Table III

STATISTICAL COMPILATION OF DATA MEASURED BY
AIRBORNE FIELD METERS WHILE HOVERING IN DUST AT 25 AND 50 FT
(Helicopter Grounded, Dissipators not Used)
(Field Meter #1 at Half Hover Altitude)

Field Meter	Hover Altitude (ft)	E/V	N	$\bar{E}$ (kV/m)	σ_E^2 $(kV/m)^2$	σ_E (kV/m)	$\bar{V}$ (kV)	σ_V^2 $(kV)^2$	σ_V (kV)
#1	25	2.86	139	80.7	3180.9	56.4	28.2	307.0	19.7
	50	2.45	103	84.8	3120.3	55.9	34.6	520.1	22.8
#2	25	0.75	142	27.4	238.7	15.4	36.6	424.2	20.6
	50	0.55	530	26.4	214.0	14.6	48.0	708.7	26.6
#3	25	0.22	77	17.8	4.8	2.2	81.0	100.4	10.0
	50	0.133	489	15.7	19.8	4.5	118.0	1113.6	33.4
#4	25	0.1	77	4.1	6.3	2.5	40.9	629.4	25.1
	50	0.08	489	3.3	4.7	2.16	41.4	729.0	27.0

After investigating several histograms, it was decided that the only distribution that could be used without calculating higher-order moments would be the actual frequency distribution of the data involved.

Table IV shows the results of discharge-energy-probability calculations carried out utilizing the raw data summarized in Table III. Table IV shows, for a given discharge energy ($E_{disch} = \frac{1}{2}CV^2$), the potential at which this energy level occurs (inferred from Figures 38 and 39), and based on a numerical integration of the histogram (carried out on the SRI XDS 930 computer), the probability that the specified energy will be equalled or exceeded. The calculations assume a helicopter self-capacitance of 2000 pF. Table IV shows that, for the 50-ft hover altitude, Field Meter #1 has the lowest probability for a given energy, and that Field Meters #2 and #4 are about equal. The 25-ft hover data show that Field Meter #1 is best, again, but that all the field meters at any

hover altitude exhibit a high probability of indicating fields equivalent to energies approaching potentially lethal levels.

Table IV

DISCHARGE-ENERGY PROBABILITY CALCULATIONS INFERRED FROM FIELD-METER DATA FOR A HELICOPTER HOVERING IN THE DUST

(Field Meter #1 at Half Hover Altitude)

Energy (mJ)	Potential (kV)	Probability $P > E_{disch}$							
		FM #1		FM #2		FM #3		FM #4	
		Hover Altitude (ft)							
		25'	50'	25'	50'	25'	50'	25'	50'
1	1.0	0.99	0.97	1.0	1.0	1.0	1.0	1.0	1.0
5	2.2	0.97	0.95	0.99	1.0	1.0	1.0	1.0	1.0
10	3.2	0.96	0.92	0,99	1.0	1.0	1.0	1.0	1.0
50	7.1	0.88	0.86	0.97	0.98	1.0	1.0	1.0	1.0
100	10.1	0.79	0.85	0.95	0.96	1.0	1.0	1.0	1.0
500	22.4	0.53	0.62	0.74	0.86	1.0	1.0	0.83	0.90
1000	31.6	0.44	0.39	0.55	0.75	1.0	0.99	0.65	0.75
5000	70.7	0.0	0.0	0.08	0.21	0.89	0.96	0.15	0.20
10000	100.0	0.0	0.0	0.00	0.03	0.0	0.85	0.01	0.01

Defining lethal levels of impulse shock is difficult in view of the scarcity of data, and the complex way in which electrical shock affects the body. Ventricular fibrillation, which is the most common cause of death in electric shock cases, occurs at intermediate levels of current. Below this level, only unpleasant sensations are felt, while very strong short shocks will stop a fibrillating heart. Dalziel[9] describes a case in Sweden in which a 22 year old man was killed as the result of receiving the residual charge from the capacitors of a high voltage filter supplying a 150 kW transmitter. The energy received by the victim was estimated to be 24 joules. The same paper discusses other

cases in which people received comparable or higher shocks and survived with burns, unconsciousness, or severe headaches. Dalziel and Lee[10] discuss experiments with dogs which indicate that a 0.1-s current pulse of 200 mA will start fibrillation and that the minimum fibrillating current is related to the duration, T, of the current as $1/\sqrt{T}$. For the case of a charged helicopter with a capacitance of 2000 pF discharged by a resistance of 5000 ohms (body plus ground), the discharge pulse duration is $T = RC = (2 \times 10^{-9}) \times (5 \times 10^{3}) = 10^{-5}$-s. Extrapolating the work of Ref. 10, this means that the minimum fibrillation current is 20A. The initial current from the helicopter charged to 100 kV and discharged through 5000 Ω is $10^{5}/(5 \times 10^{3}) = 20$ Amp. Thus the higher energy levels of Table IV are approaching a very dangerous regime, and cannot be considered acceptable.

The calculations for Table IV were made using data that were taken with the helicopter grounded; therefore, they represent an error quantity that reflects the magnitude of the error expected if the helicopter were operated ungrounded, using an active sensing and dissipation system to keep the indicated aircraft-to-earth potential at zero volts.

These large errors in aircraft-potential determination are due to the cloud of charged dust particles swirling about the aircraft, and influencing the field-meter readings in the same way they were influenced by the ion cloud created by the outrigger discharger discussed earlier.

In an additional attempt to understand the relation between helicopter potential and the measured electric fields, natural charging with the helicopter grounded was observed as discussed above and then the ground line was disconnected, allowing the helicopter to acquire a charge. Figure 44 shows data typical of these tests. As in the previous figure, t = 0 denotes roughly the time of takeoff to hover; hover was established over the ground arrays at approximately t = 15 s.

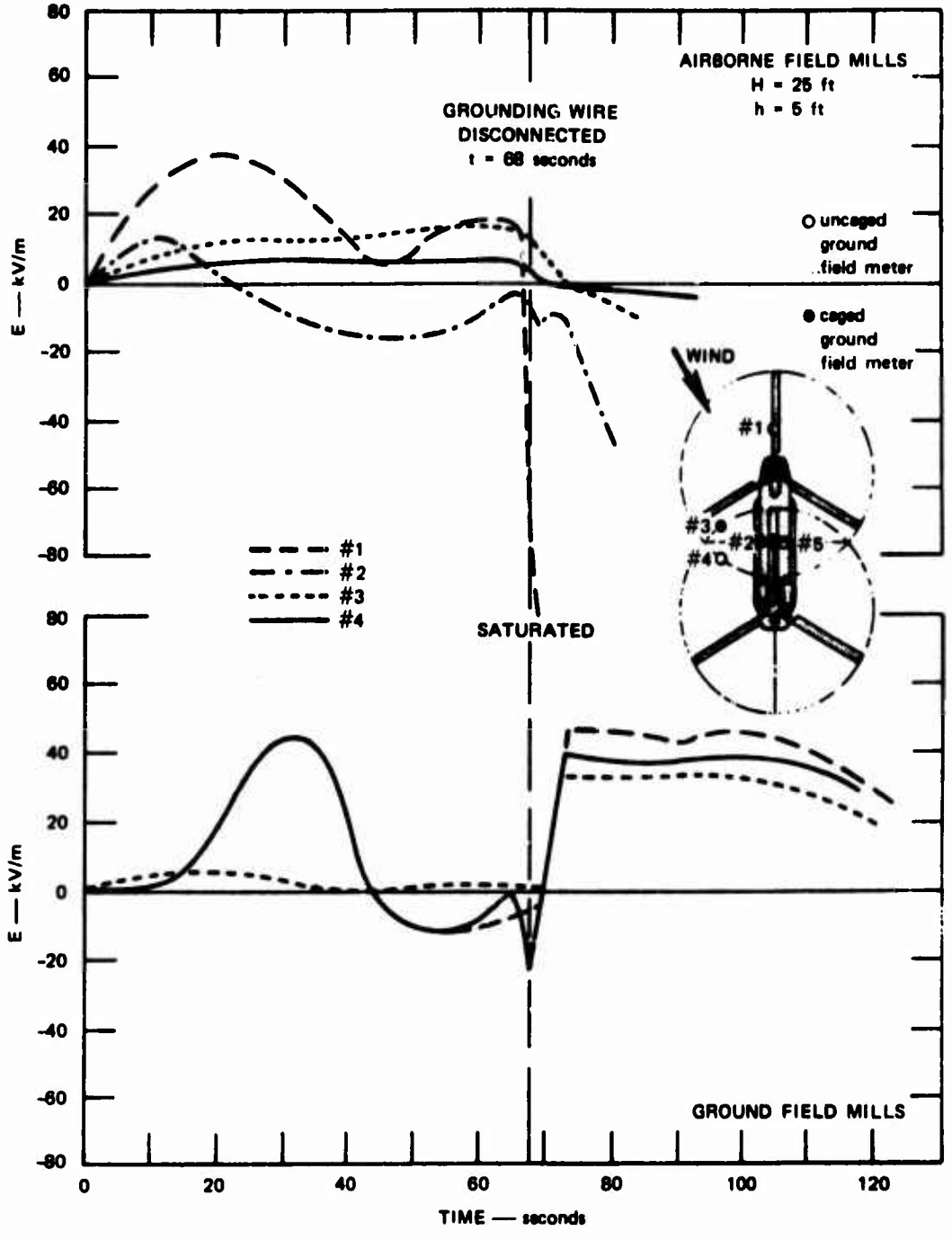

FIGURE 44 MEASURED ELECTRIC FIELD AS A FUNCTION OF TIME DURING GROUND-DISCONNECT EXPERIMENT WHILE HOVERING IN DUST

It is observed from Figure 44 that the behavior of the airborne and ground field mills is similar to behavior to that of Figure 43 before the ground line was disconnected. When the grounded line was disconnected at t = 68 s it is observed that the airborne field meters indicate a negative charge. This is consistent with the idea that, after the ground line is snapped, the helicopter begins to acquire a positive charge from the previously charged dust and from its own triboelectric process during the rotor-blade collisions with the dust particles. After contacting the helicopter the dust particles blow down and away with a reduced positive (or zero, or negative) charge. This cloud then appears negative to the airborne field meters, because the meters measure field with respect to the helicopter. The field meters in the ground array, however, are still looking into a positive electric field due to the positively charged dust, and the (now) acquired positive charge on the helicopter.

In an attempt to try to separate the "true" electric field of the helicopter from the electric field produced by the charged-dust-cloud space charge, an experiment was conducted in which selected field meters were surrounded by a grounded wire-mesh netting. The effect of this "cage" around the field meters would be to shunt most of the true electric field to ground while allowing the charged dust particles to freely blow into the cage, thereby measuring the field due to the ion-cloud space charge. The shunting of the electric field, while having a minor effect on the fields from the dust within the cage, was determined in a laboratory experiment to have reduced the gain of the field mills to external fields by a factor of 20. The field meters chosen for "caging" were #2 and #4 on the ground array and #1 on the helicopter. The results of this experiment showed that the fields inferred from the "caged" and "uncaged" field meter data were comparable. This result is significant because the caged field meter readings were

multiplied by 20 to obtain equivalent uncaged readings. Since the caged field meters were exposed to essentially the same dust environment as the uncaged field meters, this means that errors from extraneous effects (such as field meter insulators charged by impinging dust) associated with operating a field meter in a charged dust environment were down by a factor of at least 20 below the measured values.

Additional ground-disconnect experiments were carried out in the "clean" area to verify the dust measurements made in Phillips Drop Zone. The results of these clean tests are shown in Figure 45 for a 25-ft hover altitude, with a 5-ft #1 sensor altitude. A low, negative-polarity power-supply voltage was used during these tests to try to obtain about the same average magnitude of "artificial" charging as obtained during hovering in the dust. It can be seen from this figure that, prior to the ground disconnect, the airborne field meters are, as expected, looking into a small negative-ion region due to the down-washed negative-ion cloud produced by the ring discharger mounted five exhaust nozzle diameters behind the left engine. The ground array, it is observed, is also measuring a very small negative field. The ground Field Meters #2 and #4, and airborne Field Meter #1, were caged in this experiment. At t = 22 s the grounding wire was snapped and it is seen that the airborne field meters indicate an immediate increase in the observed field. This is consistent with previous experiments, and it shows that the helicopter is becoming more positively charged than the environment around it. It is also seen that the ground field meter indicates an increasing positive charge, which suggests that the electric field from the helicopter becomes much stronger and overpowers the field due to the ion space charge. At about t = 40 s it is observed from the figure that the measured fields begin to decrease in magnitude even though the voltage supplying ions to the discharger remains constant. It is felt that this is attributable to the fact that the helicopter

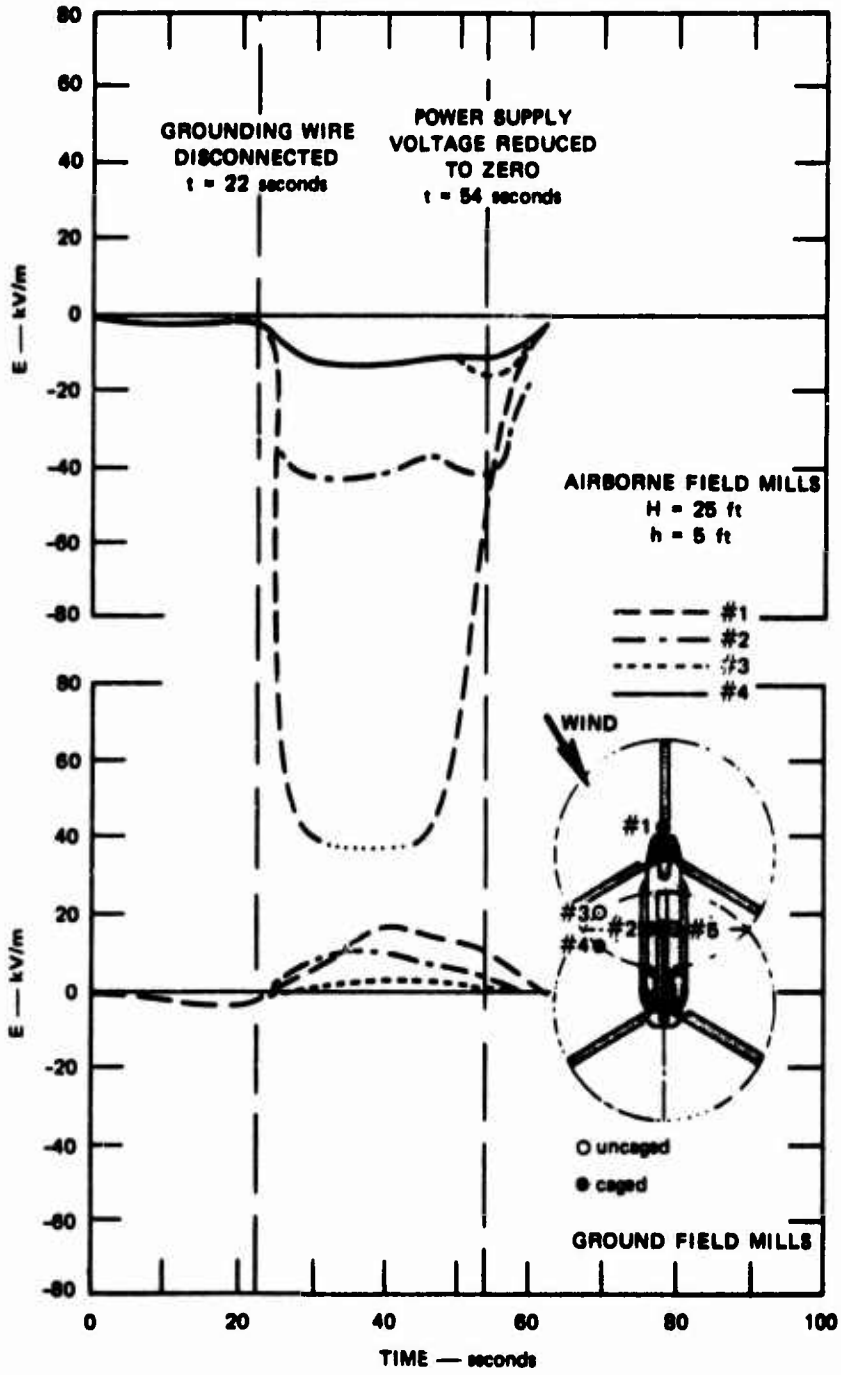

FIGURE 45 MEASURED ELECTRIC FIELD AS A FUNCTION OF TIME DURING GROUND-DISCONNECT EXPERIMENT WHILE HOVERING IN A CLEAN AREA

acquires enough charge to put it into corona, and the corona tends to lower the observed fields.

An experiment to determine the effects of wind on sensor operation was performed and the results are shown in Figure 46. During this experiment the helicopter was grounded and hovered first facing into a 35-knot wind at an altitude of 25 ft at Phillips Drop Zone. Using the ring discharger at 5 diameters behind the left engine exhaust, the natural charging current was nulled and the airborne and ground fields were measured. Then, while maintaining the same position over ground Field Meters #2 and #5, the helicopter was pivoted 90 degrees to the right, so that the wind was blowing on the left side of the helicopter, and the nulling experiment was repeated. The results of this experiment verified previous assumptions made about the wind effects. It can be seen from this figure that when the helicopter is hovering into the wind, airborne Field Meters #1 and #2 measure a higher field than is observed during the hover when the wind is broadside to the helicopter. It is also observed that Field Meters #3 and #4 measure comparable fields in both orientations. These data indicate that the ambient wind does play an important role in the movement of the discharge ions, but that even a 30-to-35-knot wind is not sufficient to blow all of the discharge ions away from the sensors. The ground field meters indicate that, because of geometry (see Figure 46), as the helicopter is turned broadside to the wind only a small net effect is observed.

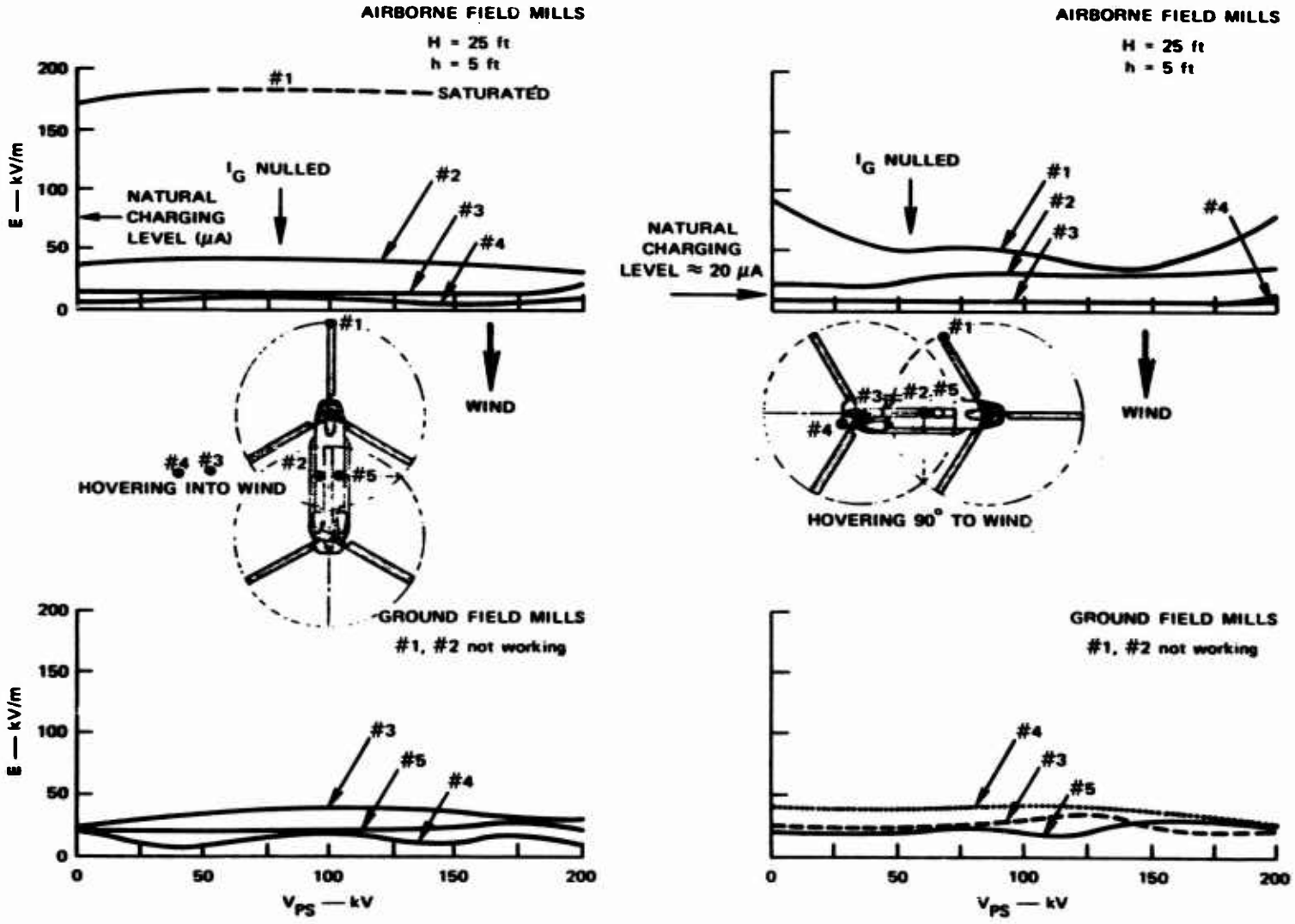

FIGURE 46 FLIGHT-TEST COMPARISON OF EFFECTS OF WIND ON FIELD-METER READINGS DURING NULLING EXPERIMENT

IV CONCLUSIONS

The experiment discussed above has shown excellent agreement between laboratory tests, ground tests, and flight tests. It has demonstrated that laboratory work is a useful and economical tool for investigating concepts related to discharger operation and design.

Laboratory tests and flight testing have confirmed that discharger designs capable of discharging at least 600 μA net current (the HLH design goal) are probably achievable for application to the Boeing 301 HLH helicopter. These tests have also indicated that existing discharger technology is sufficient to achieve that goal.

The flight-test data taken during the Yuma tests and the laboratory measurements program indicate that optimum discharger designs for the 301 HLH would be those that have the discharging electrode standing isolated in the exhaust flow. These designs allow one or more corona points to be inserted into the turbine exhaust at a location as far removed from the fuselage as possible, to minimize recirculation, yet close enough to the turbine exhaust nozzle to provide strong convective flows to remove the discharged ions. Moving the discharger far out into the exhaust plume allows large displacements from the fuselage and, in addition, it allows the discharger to be in a region of low temperature and therefore lower ion mobility which aids the discharging process.

The flight tests conducted at the Yuma Proving Grounds indicate that accurate sensing of the helicopter-earth electric field by a simple field meter or by an array of meters is very difficult to achieve when the helicopter is operating in an environment containing charged ions,

and other solutions to the problem might be more feasible, and should be thoroughly investigated.

A remote-sensing infinite-impedance voltmeter, for instance, could be suggested as one possible solution to the problem. In this scheme the voltmeter (a field mill) could be located inside the helicopter and the sensing accomplished by means of a high-resistance weighted thread that would contact the ground and allow a direct measurement of the helicopter-earth potential to be made. In this scheme, the frictionally charged dust and the discharger ions would have no effect on the measurement, and a zero potential could be established and maintained.

The need for a sensing device would be eliminated altogether if the helicopter were grounded through a wire to ground. The grounding could be accomplished by firing an arrow, with the grounding wire attached, from the helicopter to ground, or by allowing suitably protected personnel on the ground to attach the ground wire to a grounded stake.

Electric-field measurements made with sensors located on the nose, side, top, and on the cargo hook have shown that the field meters generally provide inaccurate measurements of field in the presence of charged ions, charged dust particles, or even the ion cloud generated by the discharger, which is attempting to reduce the helicopter potential.

The data obtained during the dust-hover operations indicated that discharge energies approaching near-lethal levels would be inferred from the field mills when the actual helicopter potential was maintained at zero volts by using a ground wire.

It was shown that the smallest of these field-meter inaccuracies, at high active dissipator currents, could lead to energy transfers more than fifty times greater than the HLH design objective of 1 mJ.

An array of field meters located beneath the hovering helicopter indicated that although the electric field emanating from it can be accurately determined when there is no natural charging taking place, the ground sensing problem becomes just as much a problem as the airborne sensing when the helicopter is in the presence of dust.

Appendix I

LABORATORY ELECTROSTATIC MEASUREMENTS

The field-meter-calibration experiment performed during the flight-test portion of this study provided a relationship between the helicopter-earth potential and the electric field meter outputs (see Figures 38 and 39).

To simplify the installation task as much as possible, the field meters were installed completely on the surface of the skin as shown in Figure 22. With this mounting technique, it is not necessary to cut holes in the helicopter skin so that field meters can be placed wherever the experiment dictates without having to consider the structural or mechanical problems that would arise in a flush field meter installation. Since the field meters mounted on the helicopter protruded about 4 inches beyond the surface of helicopter skin, it was apparent that the electric-field lines would tend to concentrate around the field mills. This concentration of field would give rise to a higher indicated electric field than would be observed if the field mills were mounted flush with the fuselage.

In order to determine how the concentrated field (or "face field," E_{face}) was related to the fuselage field (or skin field, E_{skin}) a laboratory experiment was performed to measure this relation. This experiment consisted of mounting a field meter on a ground plane in a protruding fashion, similar to that done on the CH-47, and immersing this unit into a large (5 ft-by-5 ft) parallel-plate electrostatic cage. The potential between the plates was then varied, and the field-meter output recorded. Since the potential (as measured by an electrostatic

voltmeter) and the cage dimensions were accurately known, the actual electric field applied was precisely known.

The field meter was then mounted flush in the ground plane of the cage, and the experiment was repeated. By comparing the relative outputs of the field meters for these two configurations at a specified incident field, the values E_{face}/E_{skin} can be observed. The results of this experiment are shown in Figure 47 and it is seen that E_{face}/E_{skin} is about 2.5.

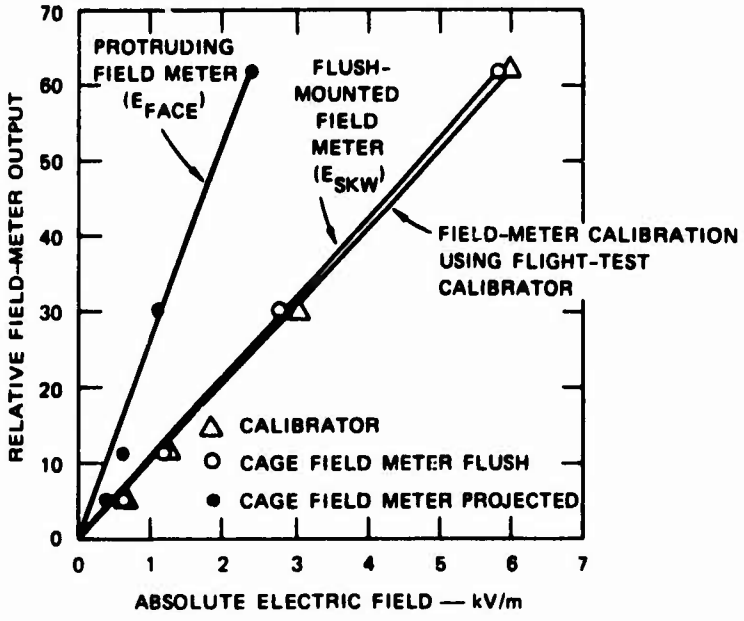

FIGURE 47 COMPARISON OF RESPONSES OF FLUSH-MOUNTED FIELD METER WITH RESPONSES OF PROTRUDING FIELD METER

A related experiment was performed at this time to determine the accuracy of the field-meter calibrator used during the Yuma flight tests. The field-meter calibration box used during the flight tests consisted

of two 12-by-12-inch parallel plates separated by a distance of 10 cm. When a potential, V, was applied between these metal plates, an electric field, E = V/0.1 volts per meter was established in the region between them. One of the plates had a hole cut in it to permit the passage of the field meter vanes when the calibration assembly was placed over the field meter sensor head. With the calibrator in place, the field meter sensor head was in effect flush-mounted in one of the calibrator plates. Since the calibrator had to be carried around from place to place, it had to be made small to insure portability. There was some concern about the adequacy of the size of the plates used and how well they would provide a good calibration with minimal effect from fringing fields. The laboratory experiment to determine the accuracy of the field-test calibrations consisted of calibrating a field mill with the portable calibrator and then calibrating it with the electrostatic cage. The additional line shown in Figure 47 shows the results of this experiment, and it is seen that the difference between the electrostatic cage and the calibrator is insignificant.

It is important to consider the significance of these laboratory measurements in terms of the helicopter experiment. All of the data in the report are presented in terms of "face field" including Figures 38 and 39. Thus, in calculating vehicle potentials from flight data, it is not necessary to convert the data to skin fields provided Figures 38 and 39 are used to convert from field to potential. If, on the other hand, one is interested in the value of the electric field at the skin to compare it to the results of calculations, or if one is interested in the response he would obtain from a flush-mounted field mill, he should convert the field meter reading in question to "skin field" by dividing it by 2.5.

To provide a check on the relationships between helicopter potential and the electric fields at the field meter locations, the laboratory

model measurements illustrated in Figure 48 were conducted. A $\frac{1}{48}$ - scale model (sprayed with silver paint to render it conducting) was suspended at a scaled hover altitude H/48 above a ground plane in the laboratory. In configuration 1, high voltage was supplied to the helicopter via a coaxial cable with the shield grounded. (This arrangement closely duplicates the situation shown in Figures 38 and 39 where a grounded wire led from a high voltage connection on the helicopter to ground.) The electric field intensity at a field meter location was measured by touching a small conductor (the nut of a 4-40 screw mounted on a $\frac{1}{8}$ inch-diam. teflon rod) to the point in question and measuring the charge transferred to the probe using a vibrating reed electrometer. The charge transferred is proportional to the field intensity. Absolute field determinations were made by calibrating the charge transfer probe in the known static electric field between a pair of parallel metal plates. The results of such a set of measurements are shown in Table V together with full-scale CH-47 data from Figure 39 adjusted to represent skin field.

It is observed from this Table that the agreement between E_{skin}/V measured in the Yuma flight tests and E/V from the Configuration #1 model measurements is good for Field Meters #2 and #3. The agreement between the measurements for Field Meter #4 is much poorer. This stems from the awkward location of #4 between the drive-shaft tunnel and the edge of the fuselage. In such a multiply-curved location, rapid field variations occur, and a small error in positioning the charge transfer probe in the laboratory results in a large error in the measured field.

Measurements were made using high voltage Configuration #2 of Figure 48 in an effort to assess the influence of the flight test ground lead in modifying the electrostatic fields about the helicopter. In Configuration #2, the high voltage lead to the power supply was a

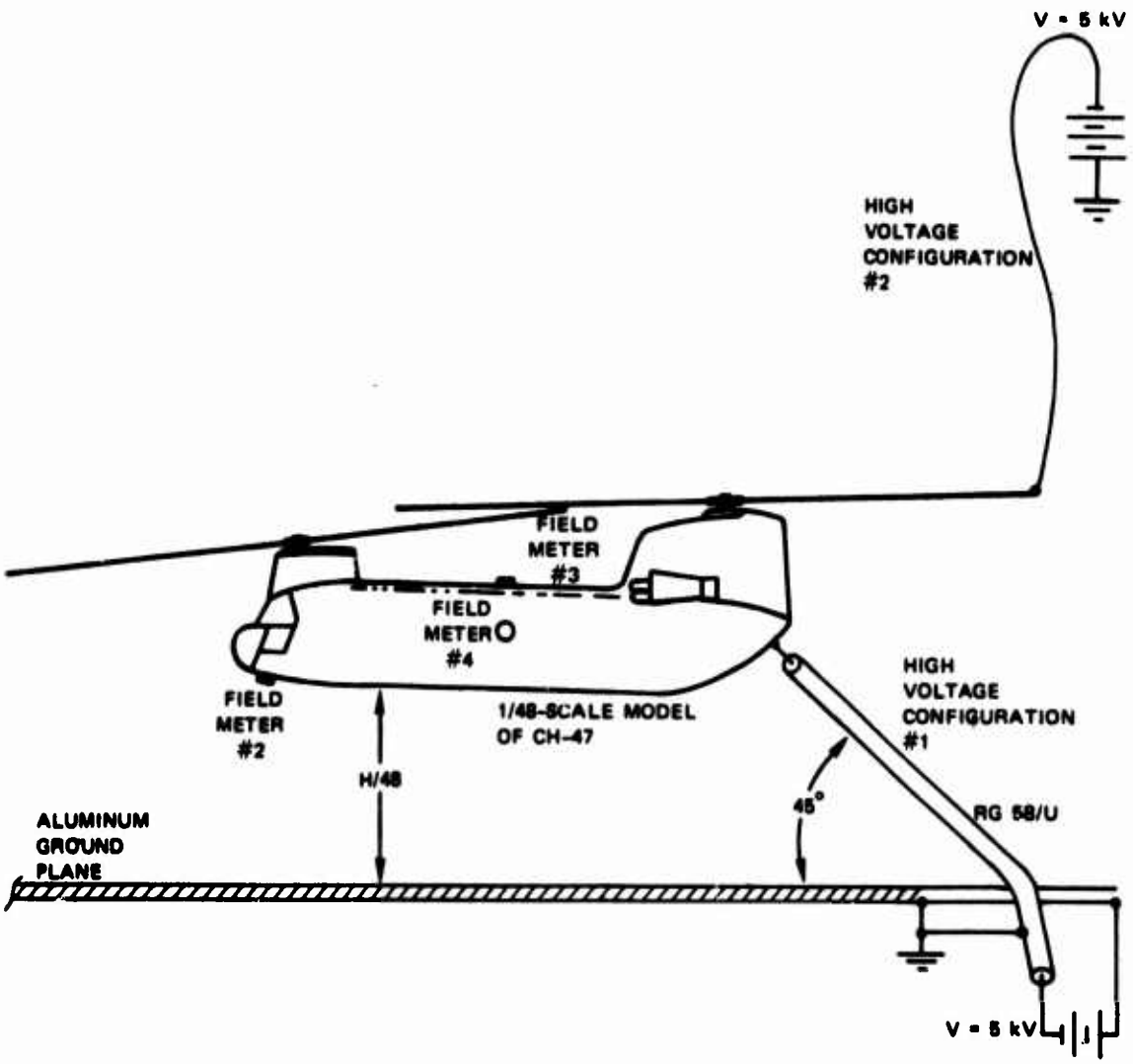

FIGURE 48 LABORATORY CALIBRATION OF FIELD METER LOCATIONS

Table V

Comparison of Electric Fields Measured on a Model and on a Full-Scale CH-47

Field Meter	Full Scale Aircraft $\frac{E_{skin}}{V}$ (m^{-1})	Laboratory Model Config. #1 $\frac{E}{V}$ (m^{-1})	Laboratory Model Config. #2 $\frac{E}{V}$ (m^{-1})	
1		NOT DETERMINED		
2	0.307	0.399	0.423	H = 25 ft
3	0.096	0.087	0.094	
4	0.044	0.096	0.084	
1		NOT DETERMINED		
2	0.241	0.357	0.343	H = 50 ft
3	0.06	0.077	0.081	
4	0.035	0.079	0.078	

#22 awg wire connected to a rotor blade tip and dressed upward and away from the helicopter to minimize the effects of its presence. Comparing the results of Configuration #1 and #2 measurements, in Table V it is evident that the presence of the heavy coaxial cable leading down from the aircraft model had very little effect on the electrostatic field structure. Since the OD of the braid on the RG 58/U cable is 0.15 inch, this means that the ground cable diameter on the full-scale aircraft could have been 48 x 0.15 = 7.2 inch without appreciably affecting the field distribution about the aircraft. Actually the ground lead shown in Figures 38 and 39 was a #20-gauge, so its presence could not have had measurable effect on the aircraft field structure.

Appendix II

A STATISTICAL EXAMINATION OF THE ELECTRIC FIELD MEASURED BY A HELICOPTER HOVERING IN A DUSTY ENVIRONMENT

Since the random nature of the measured electric fields precludes definitive statements about the effects of field-mill location, sensor accuracy, and so on, based on the instantaneous values of the fields, statistical methods are ideally suited to provide estimates of the most probable values of field (or potential), and the variance and standard deviation of the fields or potentials.

By using statistical inference, it becomes possible to arrive at conclusions about the parameters of an infinite population based on the information contained in samples.

Fundamental equations in statistical methods[11] are the first and second moments, or the mean and the variance, respectively.

The sample mean describes the "most probable" value of a set of data and is given by

$$\bar{X} = \frac{1}{N} \sum_{i=1}^{N} X_i \qquad (4)$$

where X_i is a sample from the population, and N is the total number of samples.

The sample variance describes the "variability" of the data samples from the mean value and is given by

$$\sigma^2 = \frac{1}{N-1} \sum_{i=1}^{N} (X_i - \bar{X})^2 \qquad (5)$$

The sample standard deviation is the square root of the sample variance and is denoted as σ.

If the sample set is sufficiently large so that it represents an accurate estimate of the population, and if the population has data values that are distributed "normally", the mean and variance completely describe the population. If, on the other hand, the distribution is not normal, the population can only be analytically described by calculating 3rd, 4th, 5th, or higher-order moments. An alternative to the n^{th}-order-moments method is to use the frequency distribtuion in its raw form, without attempting to find a "typical" analytical description. The probability-distribution functions found in this way might be somewhat non-physical in character, in that they might have discontinuous end points and so on, but it was felt that due to the nonuniformity of the observed distributions, this technique would be appropriate for estimating indicated error probabilities in the calculation of discharge energy.

The "correct" selection of data for use in this analysis is quite important. Statistical methods require that the samples be chosen in such a way that they are "unbiased"--that is, that no individual sample in the population be chosen or rejected on the basis that it is "more" or "less" typical than any other sample. An examination of the time histories of the measured field data showed that a great deal of care had to be exercised in selecting the data to be sampled if it was to be "unbiased" yet correctly represent the desired operating configuration. Much of the data had to be rejected because it was contaminated by the presence of dissipator ions produced by a dissipation or sensor-fidelity test underway or just completed. Other data were rejected because they were gathered during the climb portion of the climb-to-hover and the altitude was constantly changing. Similarly, the other

data were rejected if the radar-altimeter trace on the oscillograph indicated widely varying or uncertain altitudes.

A total of 12 dust-hover operations were examined for usable data and a net time of about 9 minutes of data were available for Field Meters #2, #3, and #4 at the 50-ft hover altitude; the longest continuous set of data for this condition was about 4 min, 20 s, and the rest of the time the data samples were selected from six other, shorter continuous data groups. The Field Meter #1 data at 25*ft consisted of a total of about 1 min, 42 s of data, of which the longest continuous set was 41 s in duration. Although the total number of points evaluated for Field Meter #1 was considerably smaller than the total number of points evaluated for Field Meters #2, #3, and #4, it was deemed adequate because the frequency distributions from Field Meters #2, #3, and #4 did not change very much after a couple of minutes of data had been gathered. (* 50 ft. hover altitude)

Since the search for usable data was such a time-consuming process, the 25-ft-altitude data were limited to about 2 min, 20 s for Field Meters #1 and #2, using the rationale above.

The data for Field Meters #3 and #4 was limited to about 1 min, 18 s, even though a lower confidence level had to be placed on the sufficiency of the samples because the data were not available. The reason for this was that during the Yuma tests, Field Meters #1 and #2 were deemed more important that #3 and #4, and often an equipment failure in the middle of a hover operation required that we use the #3 or #4 field-mill electronics in the #1 or #2 position.

In all the cases above, the data samples were chose at 1-s intervals Figure 49 shows a typical oscillograph record containing the raw data, and it illustrates some of the selection criteria discussed above.

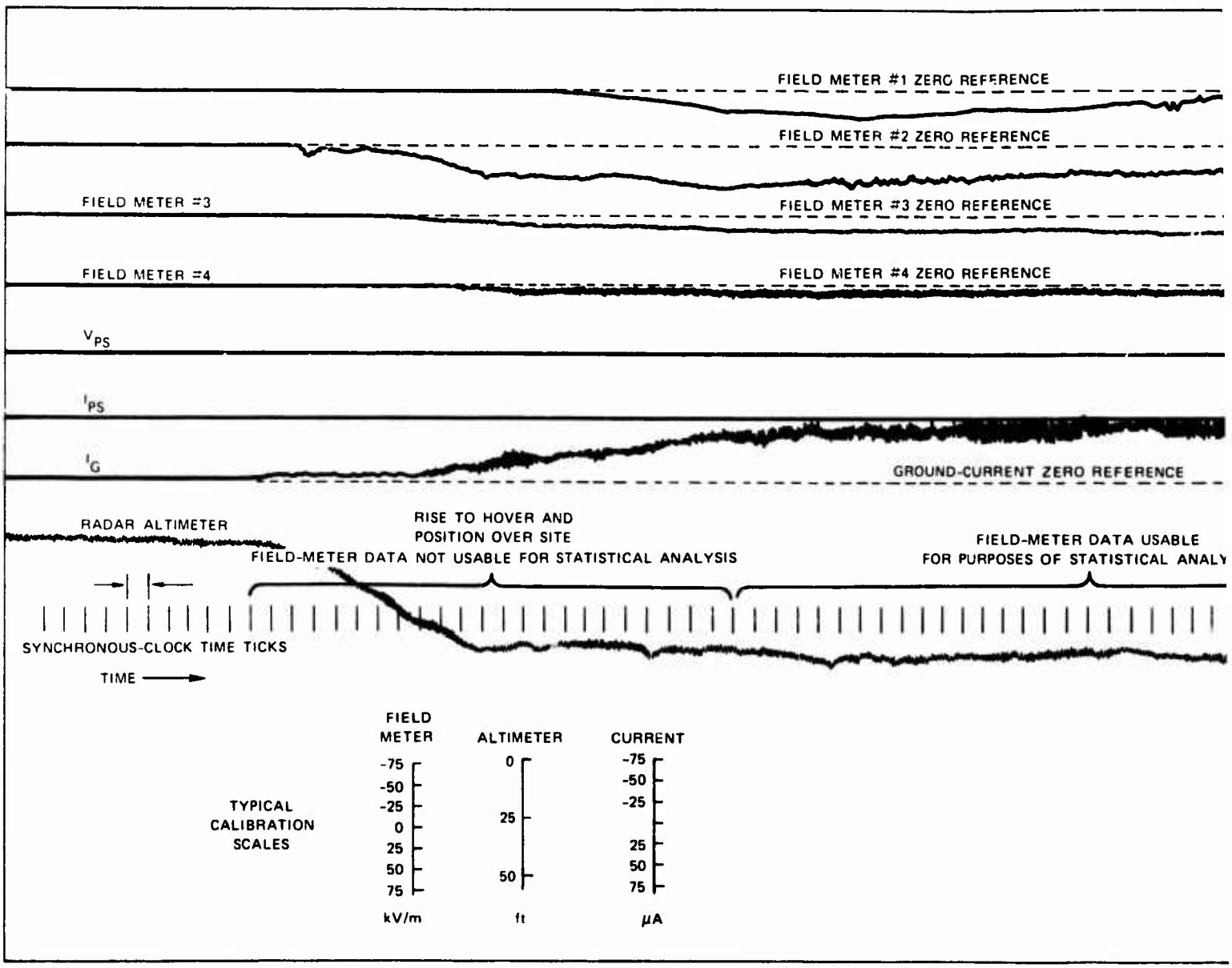

NOTE. Airborne oscillograph traces not shown for field-meter high-gains, static traces, and patch currents

FIGURE 49 TYPICAL OSCILLOGRAPH RECORD (raw data) SHOWING FIELD-METER DATA, GROUND CURRENT, RADAR ALTIMETER, AND CLOCK SIGNAL AS FUNCTIONS OF TIME

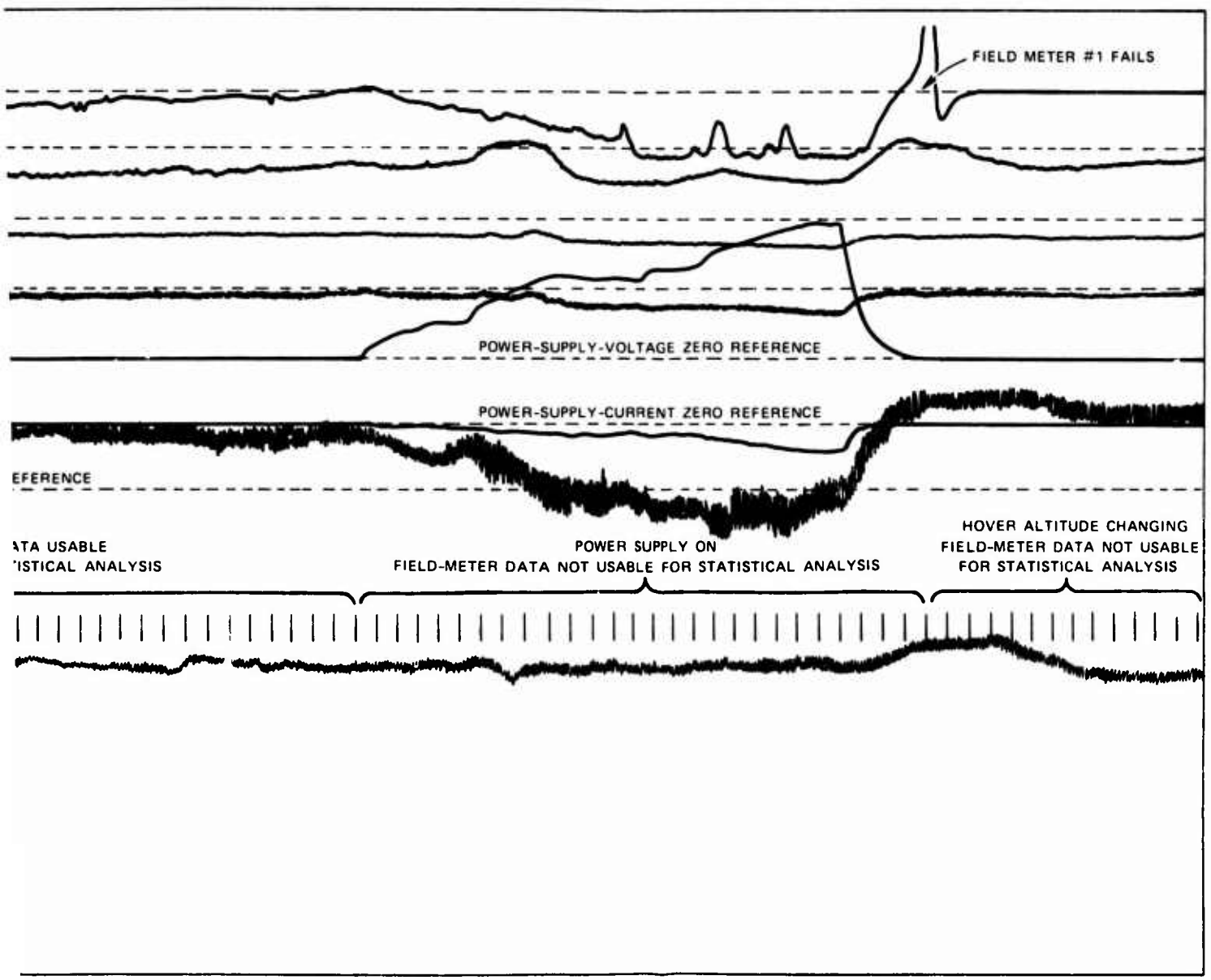
FIELD METER #1 FAILS
POWER-SUPPLY-VOLTAGE ZERO REFERENCE
POWER-SUPPLY-CURRENT ZERO REFERENCE
EFERENCE
ATA USABLE
ISTICAL ANALYSIS
POWER SUPPLY ON
FIELD-METER DATA NOT USABLE FOR STATISTICAL ANALYSIS
HOVER ALTITUDE CHANGING
FIELD-METER DATA NOT USABLE
FOR STATISTICAL ANALYSIS

Since the ultimate goal of this statistical analysis was to estimate the inferred aircraft potential error as it relates to the calculation of discharge energy, the electric-field values read from the raw dust-hover data were converted to potential by using Figures 38 and 39 (see main text), and a computer program was written to analyze this data.

Frequency distributions, or histograms, were plotted for all of the data used, and Figure 50 illustrates a typical electric-field histogram generated from Field Meter #1 data at 15 ft. with 25 ft. hover alt.

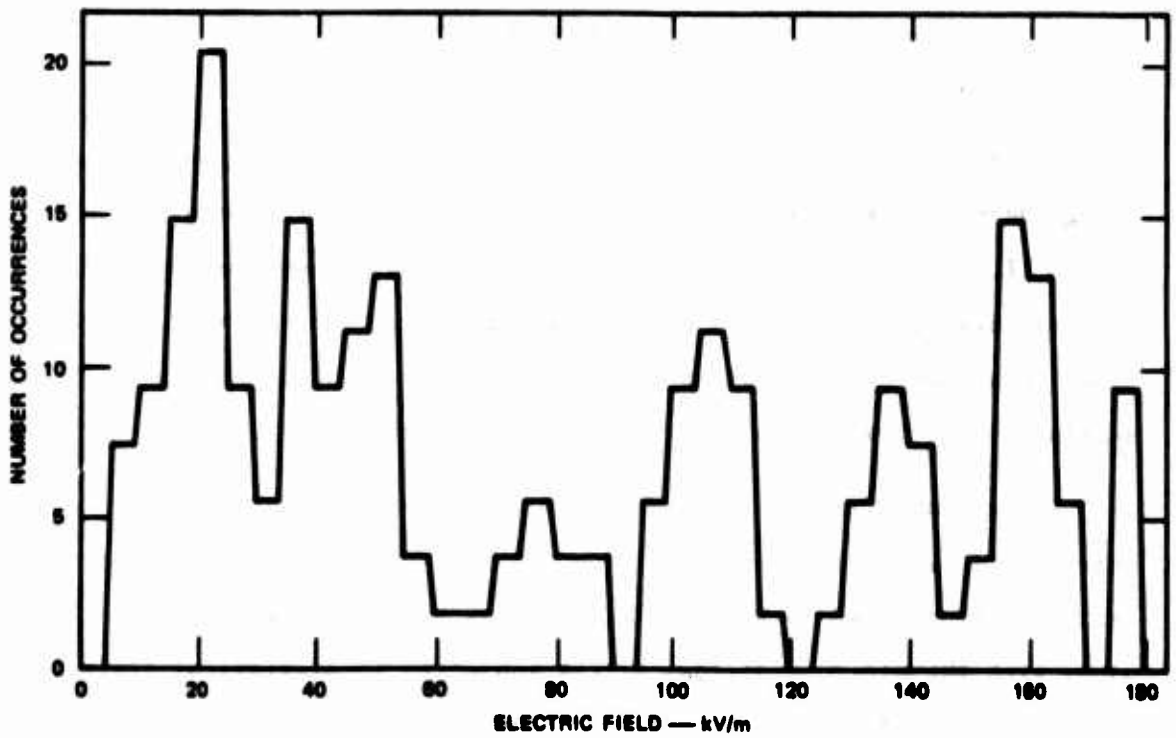

FIGURE 50 ELECTRIC-FIELD HISTOGRAM FOR HELICOPTER HOVER OPERATION IN DUSTY ENVIRONMENT — FIELD METER #1, H = 25 ft, h = 15 ft

Horizontal axis shows measured electric field (in kV/m) and the vertical axis shows the frequency with which a specified electric field was measured. It is observed from this figure that the values of electric

field are not shown as discrete lines, but have a width of 5 kV/m. The selection of the proper sample width is somewhat empirical. It should be wide enought to allow a "smooth" distribution function, but narrow enough so that important detail is not overlooked. The sample width of 5 kV/m shown in this figure has these qualities, and a 5-kV/m (field) or 5-kV (potential) sample width was used throughout this Appendix.

The electric-field histogram shown in Figure 50 was converted to a potential histogram by using the E/V calibrations shown in Figures 38 and 39 and this is shown in Figure 51. Figures 51 through 58 show potential histograms based on the sampled field data and are the basis for the discharge-energy probabilities reported in Table IV of the main text.

Overdrawn on each of the histograms is a normal curve generated by using the calculated values of mean and standard deviation reported in Table III. It can be observed from these figures that a normal distribution is not a very good approximation to the histograms shown, and that an integration of the normal curve would lead to substantial errors in the inference of energy probability.

The ground current, I_G, was recorded on the oscillograph as a function of time, along with the electric fields as described in the text and illustrated in Figure 49. Since I_G was varying with time along with the electric fields, it was subjected to statistical analysis in a manner similar to that done for the electric fields, in an attempt to use the ground-current statistics to normalize the electric-field data. Table VI shows a statistical summary of the ground-current data and Figures 59 and 60 show the ground current histograms for the 25-ft and 50-ft hovers. Examination of this table and the figures shows that the means and distributions of I_G are remarkably similar and illustrate clearly the phenomenon observed during the testing at Yuma: Large

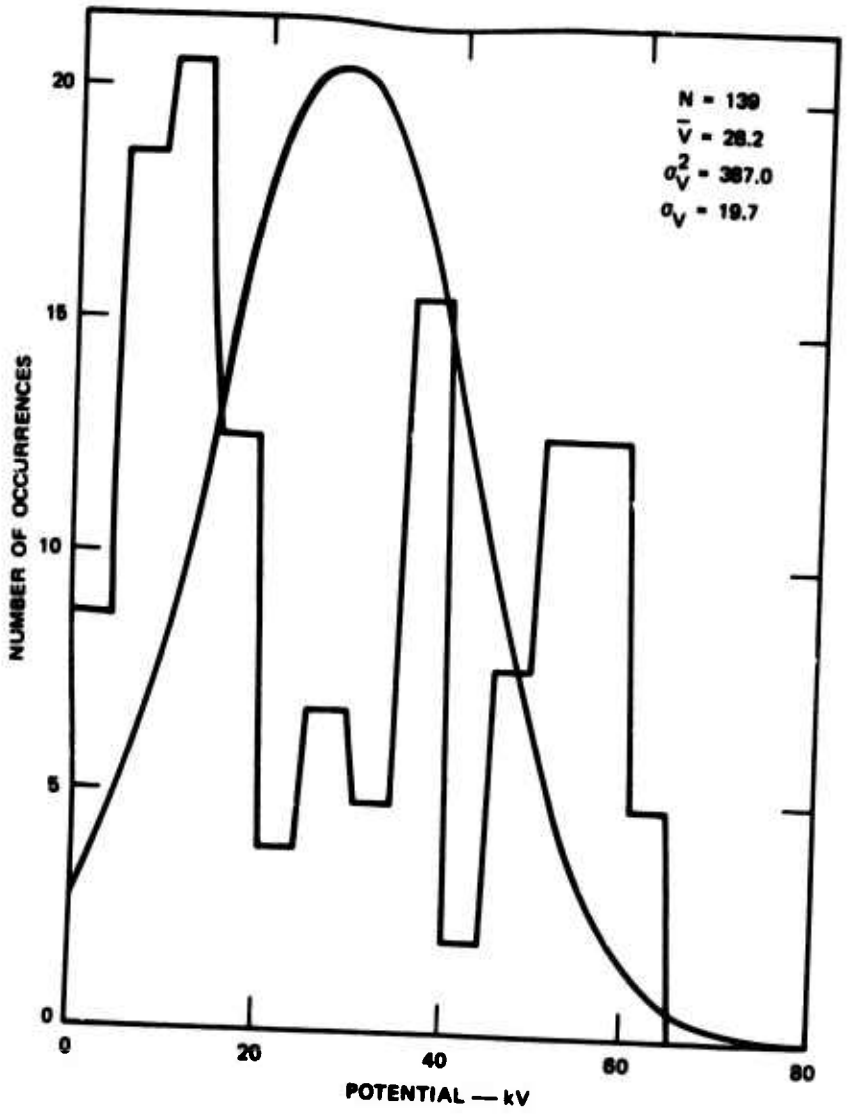

FIGURE 51 POTENTIAL HISTOGRAM FOR HELICOPTER HOVER OPERATION IN DUSTY ENVIRONMENT — FIELD METER #1, H = 25 ft, h = 15 ft

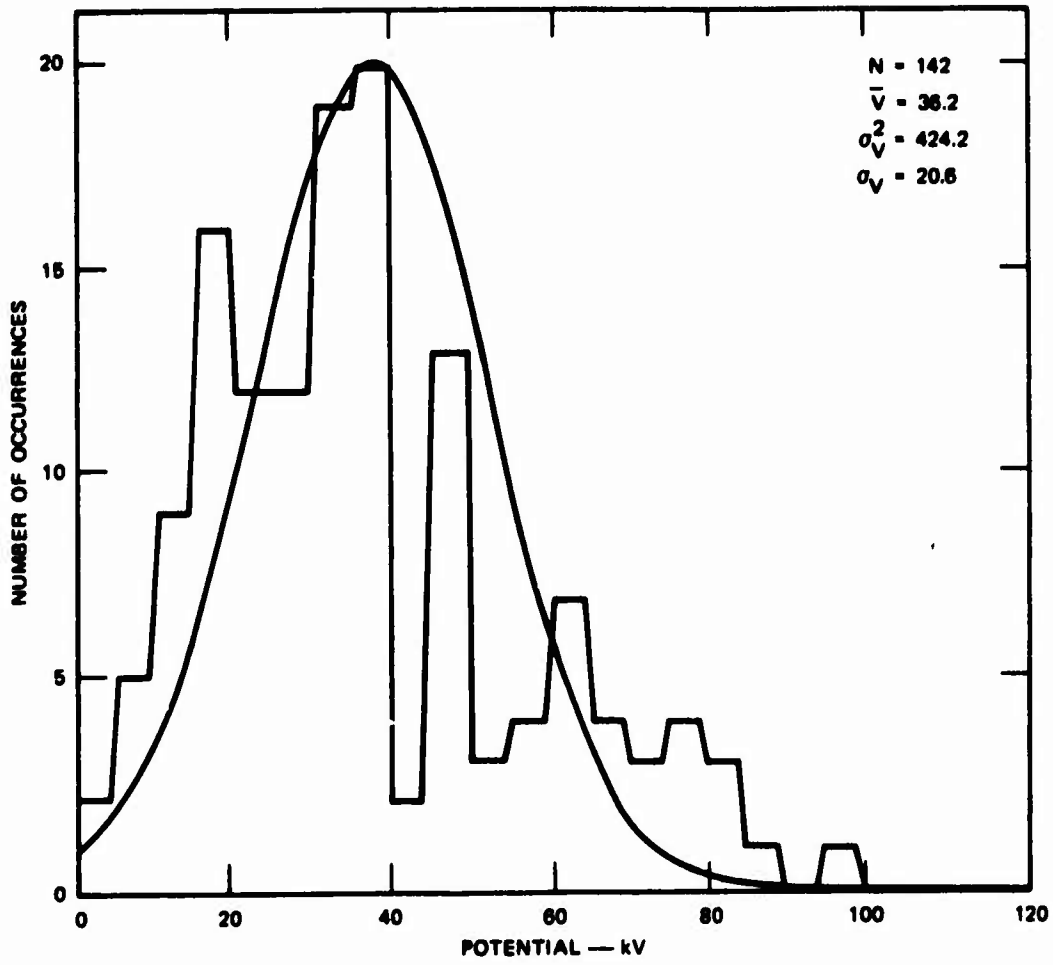

FIGURE 52 POTENTIAL HISTOGRAM FOR HELICOPTER HOVER OPERATION IN DUSTY ENVIRONMENT — FIELD METER #2, H = 25 ft

Table VI

STATISTICAL SUMMARY OF OBSERVED GROUND CURRENT DURING HELICOPTER HOVER OPERATIONS IN A DUSTY ENVIRONMENT

Hover Altitude (ft)	N	$\overline{I_G}$ (μA)	$\sigma^2_{I_G}$ $(\mu A)^2$	σ_{I_G} (μA)
25	142	112.0	5387.6	73.4
50	429	112.4	4173.2	64.6

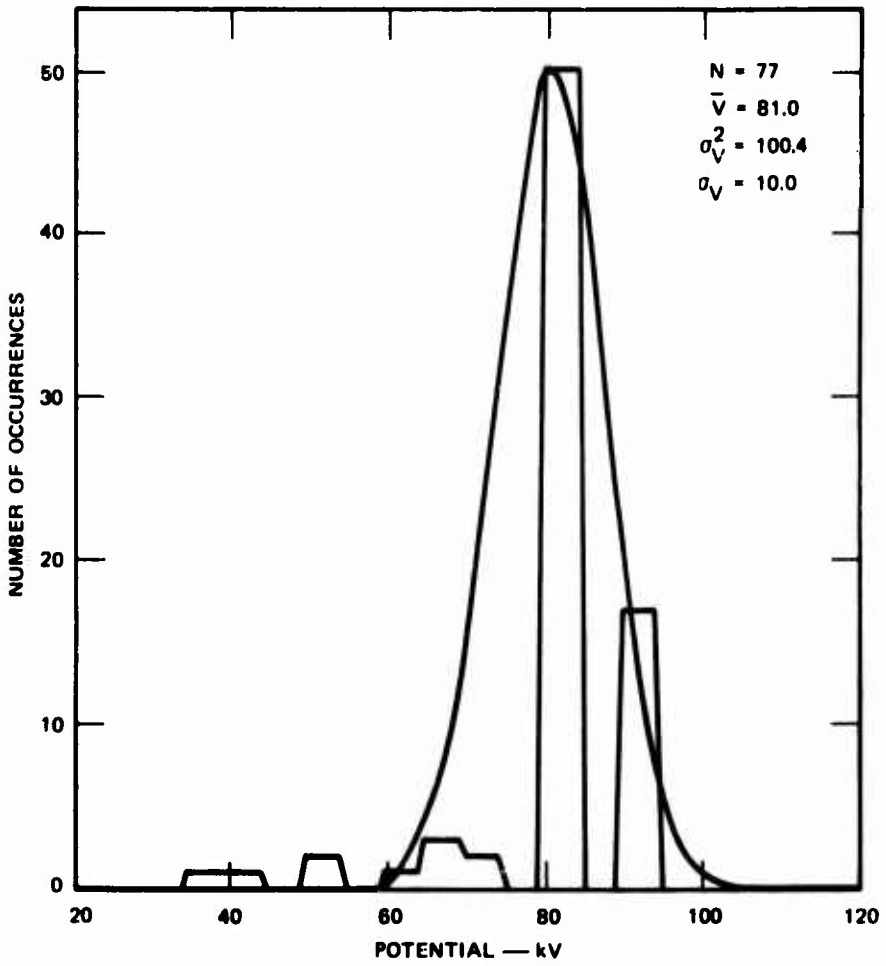

FIGURE 53 POTENTIAL HISTOGRAM FOR HELICOPTER HOVER OPERATION IN DUSTY ENVIRONMENT — FIELD METER #3, H = 25 ft

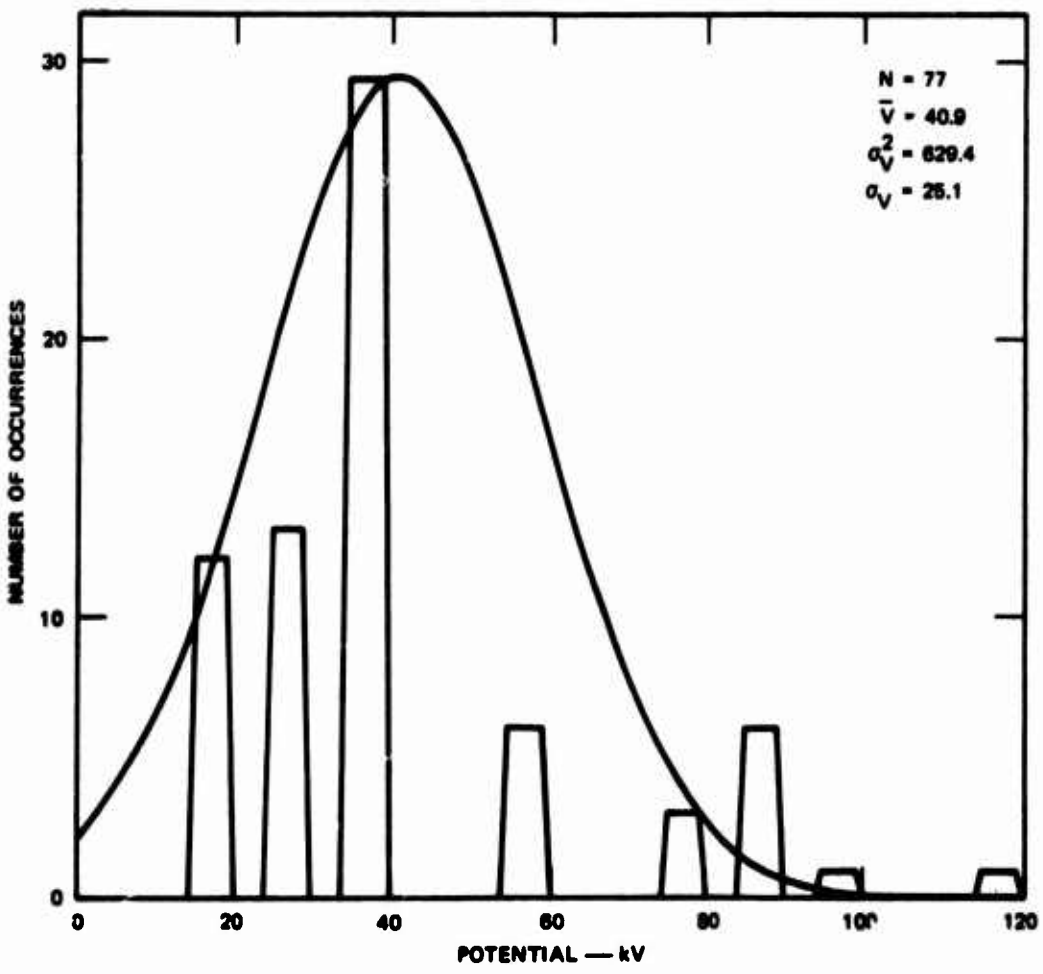

FIGURE 54 POTENTIAL HISTOGRAM FOR HELICOPTER HOVER OPERATION IN DUSTY ENVIRONMENT — FIELD METER #4, H = 25 ft

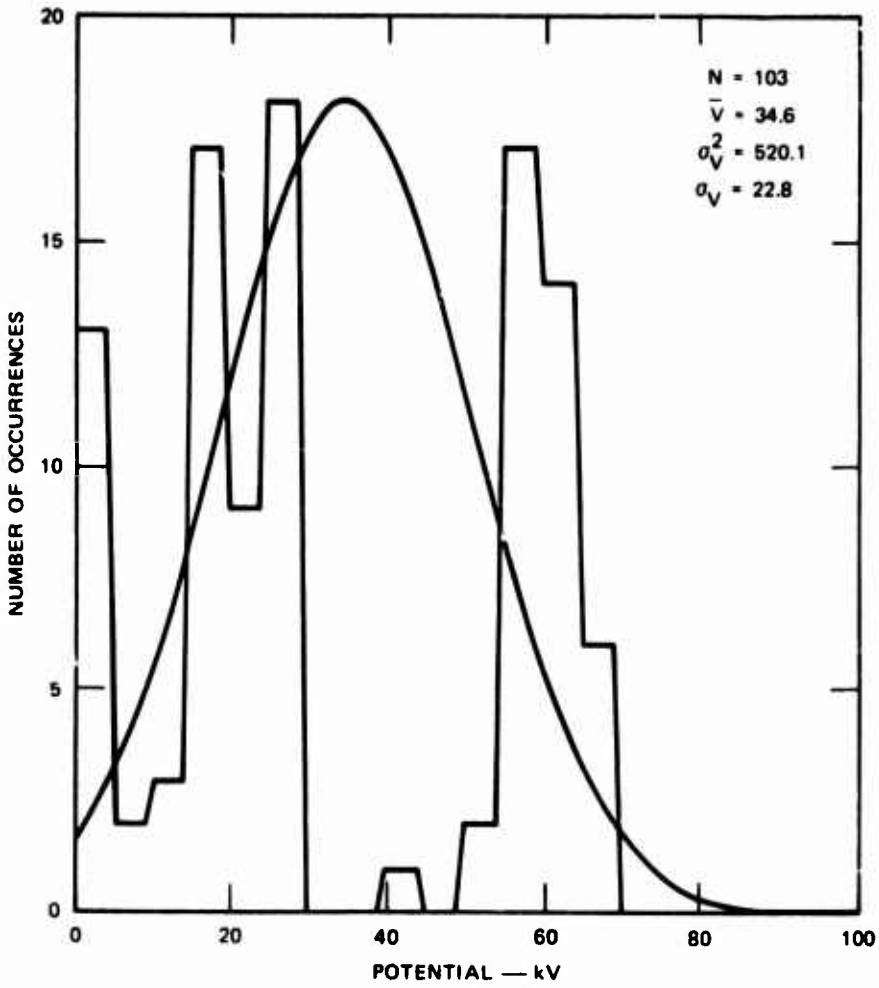

FIGURE 55 POTENTIAL HISTOGRAM FOR HELICOPTER HOVER OPERATION IN DUSTY ENVIRONMENT — FIELD METER #1, H = 50 ft, h = 25 ft

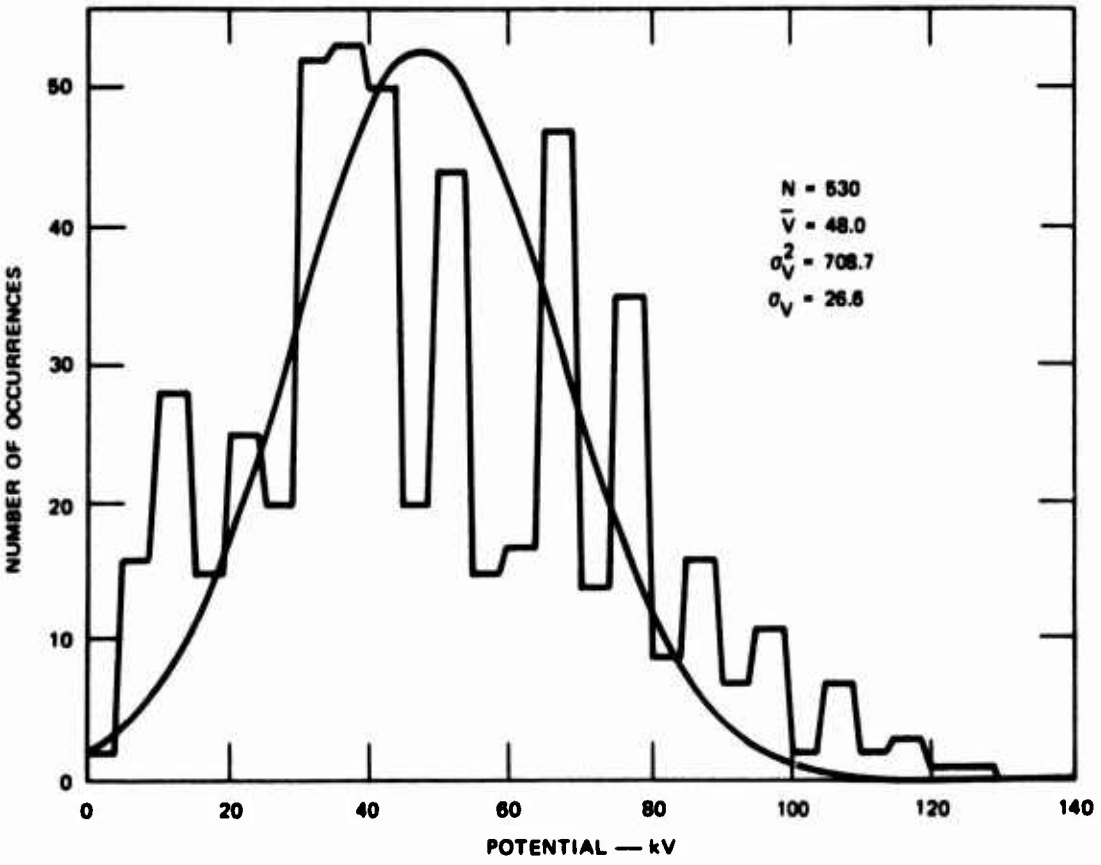

FIGURE 56 POTENTIAL HISTOGRAM FOR HELICOPTER HOVER OPERATION IN DUSTY ENVIRONMENT — FIELD METER #2, H = 50 ft

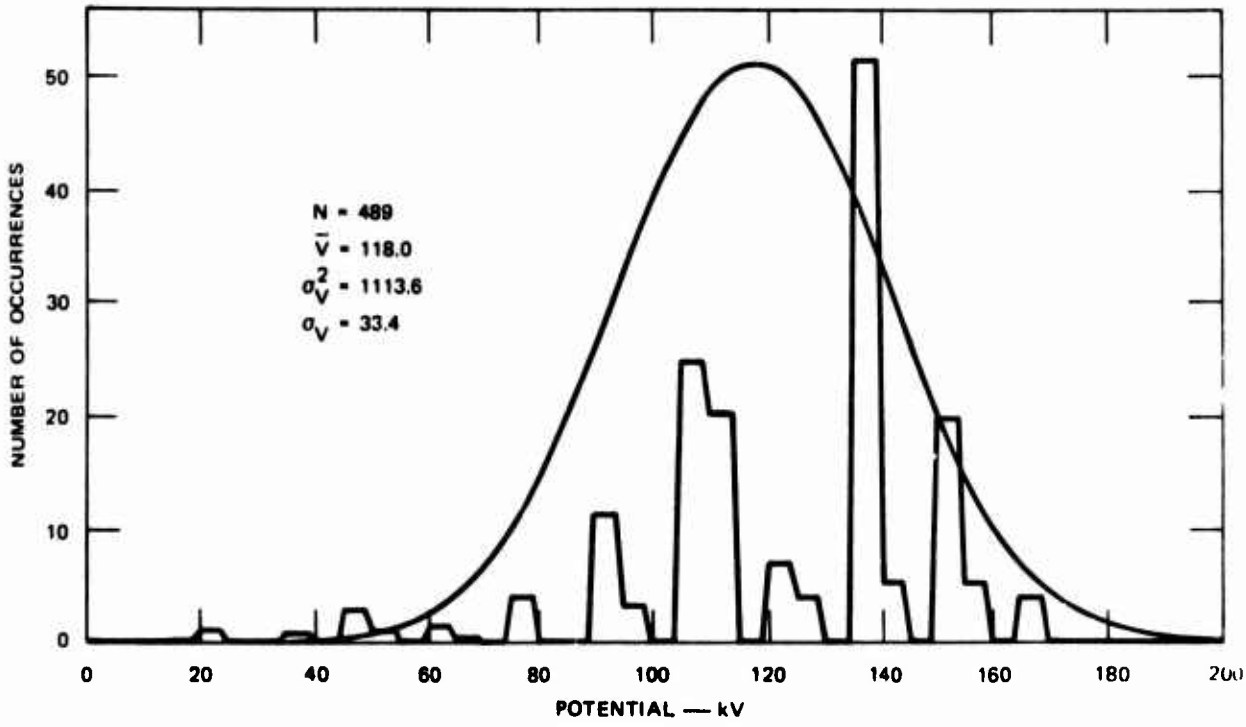

FIGURE 57 POTENTIAL HISTOGRAM FOR HELICOPTER HOVER OPERATION IN DUSTY ENVIRONMENT — FIELD METER #3, H = 50 ft

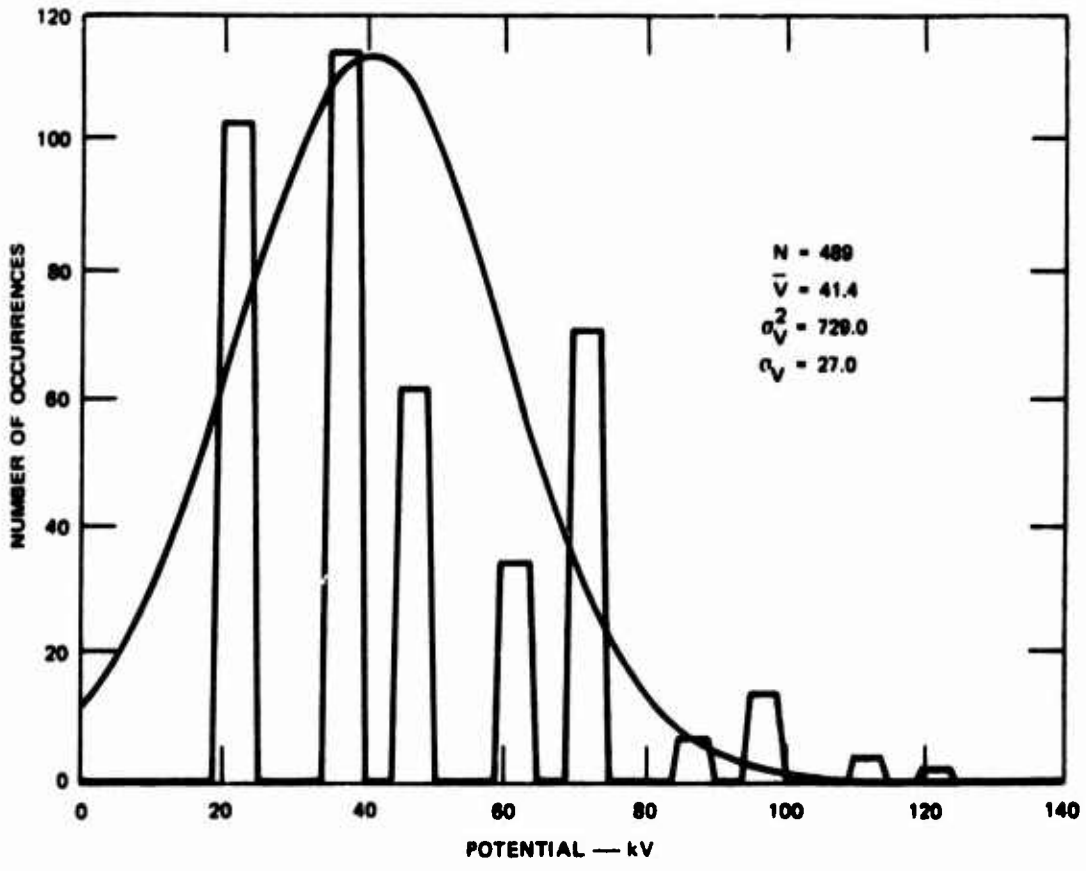

FIGURE 58 POTENTIAL HISTOGRAM FOR HELICOPTER HOVER OPERATION IN DUSTY ENVIRONMENT — FIELD METER #4, H = 50 ft

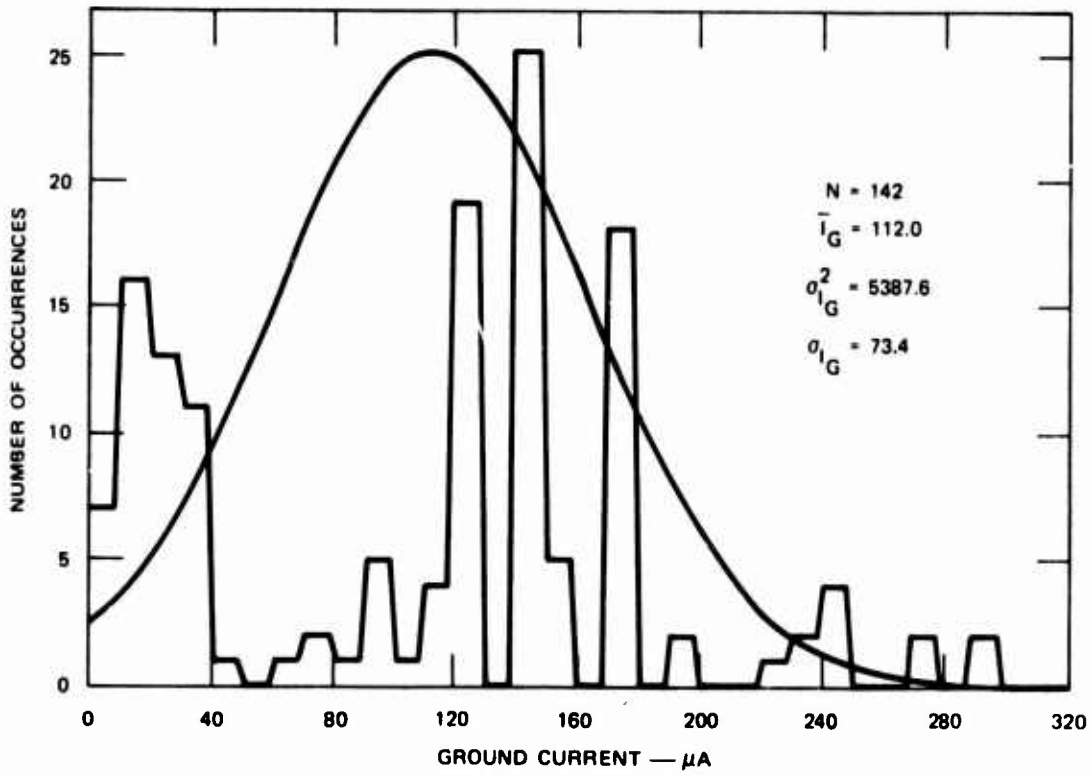

FIGURE 59 GROUND-CURRENT HISTOGRAM FOR HELICOPTER HOVER OPERATION IN DUSTY ENVIRONMENT — A/C GROUNDED, H = 25 ft

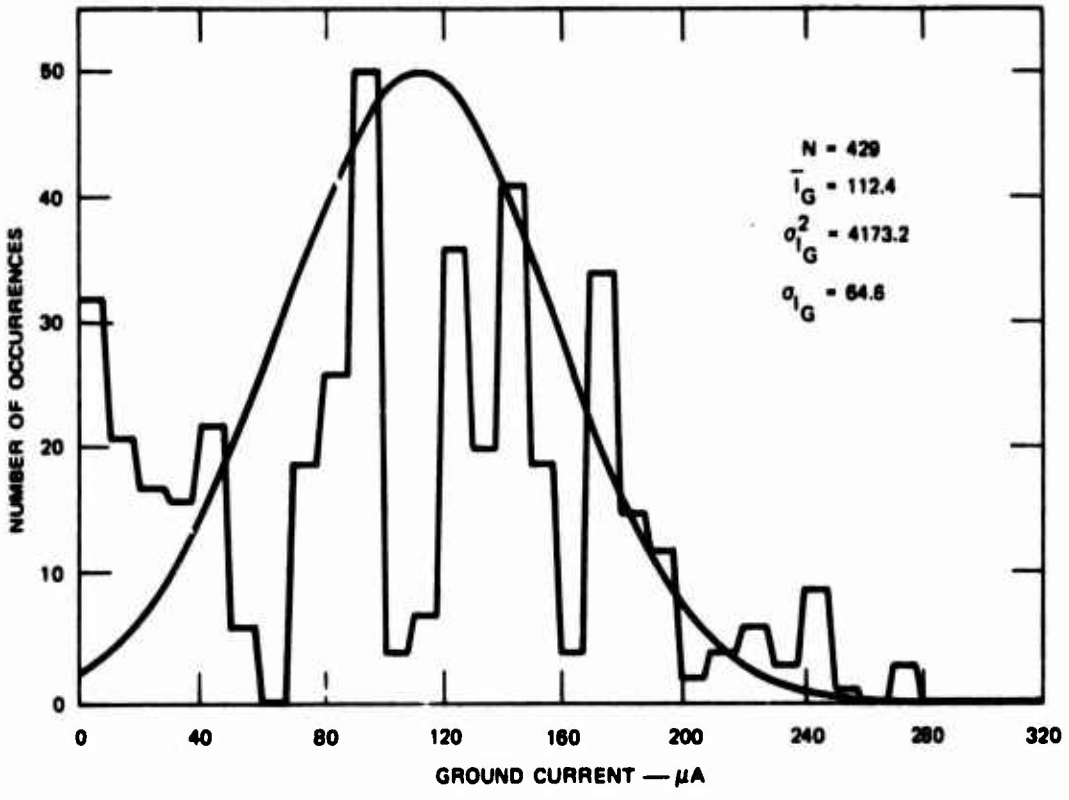

FIGURE 60 GROUND-CURRENT HISTOGRAM FOR HELICOPTER HOVER OPERATION IN DUSTY ENVIRONMENT — A/C GROUNDED, H = 50 ft

I_G's (> 250 μA) were observed infrequently, and only immediately after plowing the test site, but moderate (≃150 μA) and low (≃20 μA) I_G's were frequently observed. Very seldom, however, were I_G's of between 40 and 80 μA observed.

In order to present the potential distribution normalized to the mean value of ground current, 112 μA, a plot of ground current vs. potential was examined to determine if there was any correlation between the measured currents and fields. Figure 61 shows this I-V diagram for Field Meter #2 at the 50-ft hover altitude. It is seen from this figure that some slight positive correlation does exist, but it was felt that this correlation was too small to justify weighting the potential histograms to normalize them to a constant ground current of 112 μA.

The probability of a specified discharge energy was then calculated by a numerical integration of the potential histograms shown earlier (Figures 51 to 58 and the results are reported in the main text (Table IV The calculations presented assumed a helicopter self-capacitance of 2000 pF, and since the discharge energy is directly proportional to capacitance, Table IV can be used to obtain a probability for any other capacitance merely by scaling the energy appropriately.

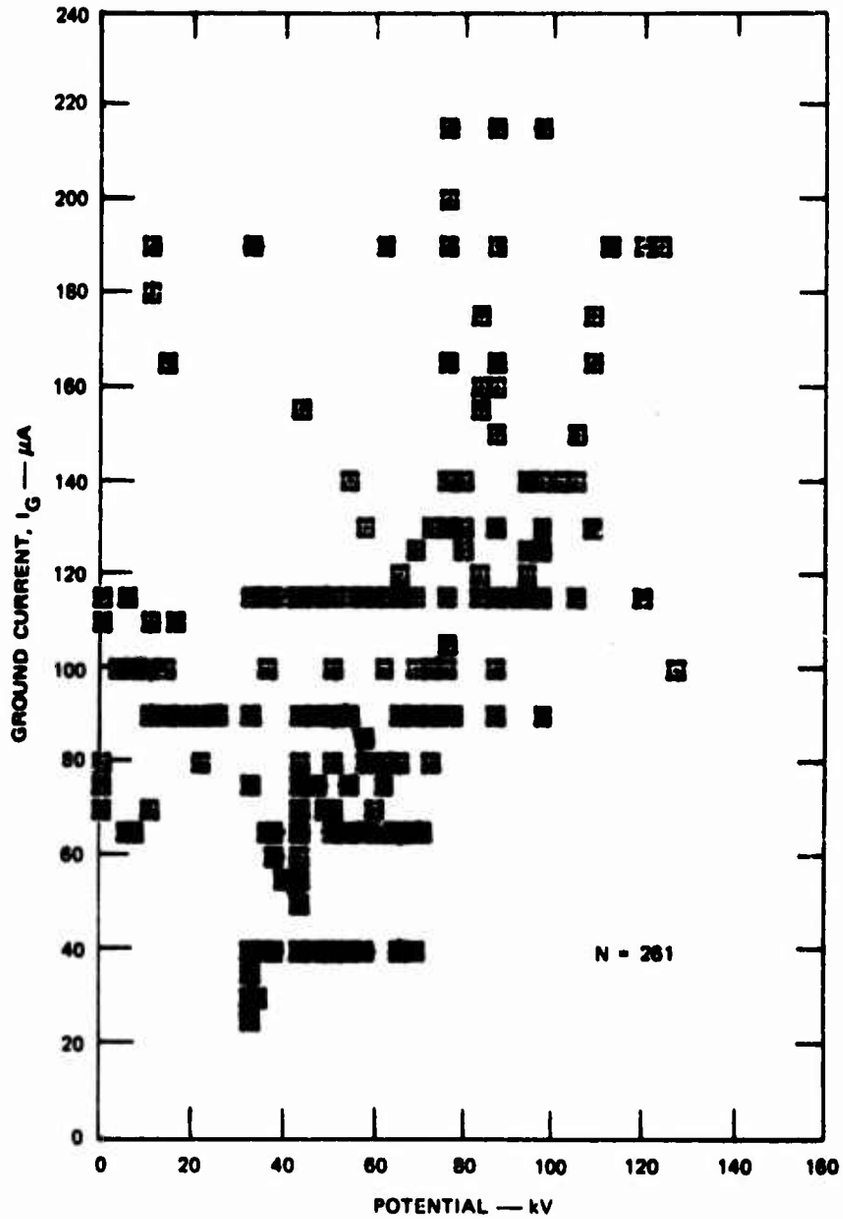

FIGURE 61 MEASURED GROUND CURRENT vs. INFERRED POTENTIAL FROM FIELD METER #2 FOR HELICOPTER HOVER OPERATIONS IN A DUSTY ENVIRONMENT — H = 50 ft

Special consideration was given to the statistical analysis of the error voltage and discharge energy of the helicopter, hovering in the dust cloud, with the simulated cargo hook and Field Mill #1 approximately 5 ft. over the ground. Three flights (#24, #25 and #27) have given good oscillograph records for a hovering altitude of 25 ft. and sensor altitude of 5 ft. over the desert. Table VII shows the test results:

TABLE VII

Charging Current and Available Record Time

for H = 25 ft., h = 5 ft.

Charging Current	Record Time
20 to 40 microamp	35 seconds
40 to 130 microamps	38 seconds
125 to 300 microamps	117 seconds

Out of the above record time (divided into 1 second intervals) a composite histogram was prepared which shows mean error of 11 K volt peaked around 10 KV. Probability of errors are shown in Table VIII:

TABLE VIII

Energy mJ	Probability P E Discharge
5	0.96
10	0.93
50	0.79
100	0.60
500	0.15
1000	0.08

For discussion of the physiologic effects of the above energy see Page 110 and 111. The data contained in Table VIII show, that even at the lowest practical altitude of the sensor over the ground surface, the discharge energy will be unacceptable for a significant percentage of time.

There are no good data available for a hover altitude of 50 ft. and the sensor at 5 ft. over the desert due to the fact that 5 ft. over the desert the Field Mill #1 was in the densest dust cloud and accidentally contacted the ground surface several times. This field meter had many failures which make evaluation of the sensing error under above conditions unreliable and unavailable.

ACKNOWLEDGMENTS

The authors wish to acknowledge the personnel of the Yuma Proving Ground for their support during the flight-test operations and the U.S. Army CH-47 flight crew from Ft. Rucker; aircraft commander W/O Jim Mitchell, who bore the brunt of 15 hours of hover in the dust, and his crew, Capt. Roy Swan, W/O Ron Girdir, SP/6 Andy Bell, and SP/4 Bob Smith for their outstanding effort and enthusiasm during the flight operations. The authors also wish to thank Mr. Greg Wilson and Mr. Erv Hunter of Boeing-Vertol for their efforts in the seemingly-never ending problem of obtaining parts for the test helicopter, and for going out of their way to lend assistance to us whenever it was needed. We also wish to thank Mr. Charles King and Mr. Larry Dolen of Boeing-Seattle for the excellent job they did in instrumenting the test helicopter.

The authors also wish to acknowledge the many stimulating conversations with Mr. B. J. Solak of Boeing-Vertol, who participated in the flight tests, and to thank him for providing much insight into the practical consideration of helicopter cargo handling in the triboelectric environment.

We also wish to acknowledge Mr. Tim McCullough and Mr. Dave Granger of SRI for their support during the various phases of testing and for assisting with the massive data-reduction tasks.

REFERENCES

1. T. R. Andrews and R. H. Forrest, "Evaluation of Active Electrostatic Discharger Mounted on the Engine Exhaust of a Helicopter," Technical Report 71219, Royal Aircraft Establishment, Farnborough, England (November 1971).

2. H. W. Liepmann and A. Roshko, Elements of Gas Dynamics, (John Wiley & Sons, Inc., New York, N.Y., 1967).

3. J. E. Nanevicz, "Plan for the CH-47 Flight Tests at Yuma, Arizona," SRI Project 1657, Stanford Research Institute, Menlo Park, California (May 1972).

4. J. E. Nanevicz, et al., "Experimental Development of Dynamic Static Discharger System for Large Jet Aircraft," AFAL-TR-67-313, SRI Project 6129, Stanford Research Institute, Menlo Park, California (November 1867).

5. C. Becker, "Investigation of CH-54A Electrostatic Charging and of Active Electrostatic Discharger Capabilities," USAAVCABS Technical Report 69-90, Contract DAAJ02-69-C-0102, US Army Aviation Material Laboratories, Fort Eustis, Virginia (January 1970).

6. J. E. Nanevicz and G. R. Hilbers, "Flight Test Evaluation of an Active Discharger System," Interim Technical Report 1 (Phase II), Contract F33615-68-C-1359, SRI Project 7104, Stanford Research Institute, Menlo Park, Calif. (February 1970).

7. "A High-Performance [illegible]ostatic Discharger for Helicopters," TRECOM Technical Re[illegible]3-43, Dynascience Corporation, Blue Bell, Penn. (December 196[illegible].

8. W. G. Hoover, "Loran D Electrostatic RFI and Null Field Discharger Flight Tests," Granger Associates, Palo Alto, Calif. (January 1967).

9. C. F. Dalziel, "A Study of the Hazards of Impulse Currents," Proc. AIEE, pp 1037 - 1043 (October 1953).

10. C. F. Dalziel and W. R. Lee, "Lethal Electric Currents," IEEE Spectrum, pp 44 - 50, (February 1969).

11. W. J. Dixon and F. J. Massey, Jr., Introduction to Statistical Analysis, (McGraw-Hill Book Company, Inc., New York, N.Y., (1951).

APPENDIX II

FLIGHT-TEST EVALUATION OF HELICOPTER CARGO-HANDLING SYSTEMS PASSIVE STATIC-ELECTRICITY DRAINAGE

ABSTRACT

A series of flight tests were performed to investigate the critical components of a passive, grounding-line, electrostatic-discharge system. It was found that the unexpectedly low contact resistance of various surface materials (loose sand, hard-packed desert, asphalt, and concrete) allowed residual helicopter potentials of, generally, less than 5 kV to be achieved.

A series of tests designed to evaluate the physiological response to electrical shock showed that HLH residual potentials of less than 14 kV could be considered reasonable design goals, and that these could be achieved with the grounding-line technique, for the materials tested.

CONTENTS

ABSTRACT 151

LIST OF ILLUSTRATIONS 153

LIST OF TABLES 155

ACKNOWLEDGEMENTS 156

I INTRODUCTION 157

II INSTRUMENTATION 161

A. Aircraft Instrumentation 161

B. Ground System 166

C. Discharger System 168

III CONTACT RESISTANCE OF SOIL 172

IV FLIGHT EVALUATION OF CANDIDATE DISCHARGING SYSTEMS . . . 176

A. Grounding Pole 176

B. Grounding Line 177

V PHYSIOLOGICAL RESPONSE OF ELECTRIC SHOCK 189

VI RADIO-FREQUENCY INTERFERENCE PRODUCED BY THE GROUNDING-LINE CORONA ELEMENT 195

VII ELECTRIC-FIELD-METER DATA 209

A. Airborne Field Meter 209

B. Ground Field Meters 211

VIII DEMONSTRATION PROGRAM 216

IX CONCLUSIONS 218

Appendix A--CHRONOLOGICAL SUMMARY OF FLIGHT PROGRAM 220

REFERENCES 224

ILLUSTRATIONS

62	General Aircraft Config.used During Tests-Clean Area	162
63	General Aircraft Configuration Used During Tests-Dusty Area	163
64	Photograph of Parallel-Plate Infinite-Impedance Voltmeter Showing Current-Measurement System Atop the Plates . . .	165
65	Ground Instrumentation Used During Sorties into Phillips Drop Zone	167
66	Photograph Showing Typical Ground Pole and Ground Line Used During the Discharging Tests	169
67	Schematic Representation of Technique Used to Obtain Surface-Material Resistance Data	173
68	Resistance as a Function of Voltage for Various Surface Materials	174
69	Text Matrix Showing Permutations of Techniques Used to Evaluate Performance of the Grounding Pole	177
70	Matrix of Configurations and Conditions Used to Evaluate Effectiveness of Grounding-Line Techniques	179
71	Comparison of CH-47 and CH-54 Helicopter Potential versus Charging Current	184
72	Aircraft Configuration Used to Measure Physiological Response to Electric Shock	190
73	Helicopter Configuration Used to Evaluate Series Resistance in Cargo-Hook Line to Protect Handler	192
74	Helicopter Configuration Used During RFI Measurement Program Showing Possible Corona-Producing Areas	196
75	Typical System Noise Spectrum Showing Coherent Broadcast and Beacon Stations Above Amplifier/Receiver Noise Spectrum	198
76	Helicopter Noise Spectra for Various Helicopter Voltages.	200
77	Photograph Showing Painted Stripe of "Aqua-Dag-E" on CH-47 Blade and Installation of Granger Associates 611-1D P-Static Dischargers on Rotor-Blade Trailing Edge.	202

78 Noise Spectra for Various Helicopter Voltages During Operation with P-Static Dischargers Mounted on Trailing Edge or Rotor Blades 203

79 Noise Spectra for Various Helicopter Voltages During Operation with P-Static Dischargers Mounted on the Trailing Edges and Tips of the Rotor Blades 205

80 Photograph Showing Granger Associates 611-1D P-Static Discharger Attached to the Tip of a CH-47 Rotor Blade . . . 206

81 Noise Spectra Measured for Corona Termination on Grounding Line Extended to 50 ft Below the Helicopter and for Termination Retracted into Aircraft 208

82 A Comparison of Potential Histograms Generated from Dust Hover Data 209

83 Potential-Difference Histogram Indicating Dust-Cloud-Induced Errors Measured by a Hovering Helicopter 210

84 Charging-Current Histogram 211

85 Electric-Field Histogram Data (Ground Field Meter No. 1) . 212

86 Electric-Field Histogram Data (Ground Field Meter No. 2) . 212

87 Electric-Field Histogram Data (Ground Field Meter No. 3) . 213

88 Electric-Field Histogram Data (Ground Field Meter No. 4) . 213

89 Electric-Field Histogram Data (Ground Field Meter No. 5) . 214

90 Mean Electric Field of Dust Cloud as a Function of Distance from Helicopter--Phillips Drop Zone 215

LIST OF TABLES

Table		Page
IX	Hook Current and Residual Helicopter Voltage Data Obtained by Using Ground-Pole Discharger	178
X	Effects of Various Surfaces and Surface Conditions on Grounding-Element Performance	180
XI	Summary of Natural Triboelectric-Environment Grounding Measurements (Discharging Element Dropped into Dry, Plowed Desert)	182
XII	Tabulation of Particle Potential, Capacity, and Maximum Stable Charge Assuming a Spherical Shape	187
XIII	Physiological Response of Subject Evaluating Anticipated Electrical-Shock Levels After Grounding Aircraft with Discharging Device	191

ACKNOWLEDGMENTS

The authors wish to acknowledge the excellent performance of both the U.S. Army flight crew and their faultless helicopter. The crew, commanded by Capt. R. Donaldson went far beyond their regular duties to assist us in the difficult conditions of heat, dust, and long hours at YPG. SRI also wishes to acknowledge the support provided us by YPG personnel without which, the program could not have been accomplished.

The authors also wish to acknowledge the stimulating and spirited conversations with Mr. B. J. Solak who shed much light on the practical considerations of helicopter operations and who consented to act as guinea pig during the electrical shock phase of the program.

The authors also want to acknowledge Mr. Charles King of Boeing/Seattle for his help during the measurement and analysis portions of the program. Mr. King's direct approach to solving complex problems did much to allow the authors to successfully complete this project.

Further acknowledgment must be given to Mr. David Granger of SRI who was of immeasurable help to the authors during the experimental and data-analysis phases of the program.

I INTRODUCTION

For many years it has been known that when an aircraft (fixed- or rotary-wing) operates in an environment containing particulate material (snow, ice crystals, fog, rain, dust, etc.), there is a high probability that the aircraft will become electrified due to triboelectric (i.e., frictional) charging. This accumulation of charge will increase the potential of the aircraft to a level beyond which further charging results in corona discharges from various parts of the airframe to the surrounding air. The electrical characteristics of these discharges are, of course, dependent on the air pressure in the vicinity of the corona point and the geometry of the corona source region. On aircraft not equipped with special discharging devices, the corona from the airframe generates noise that can interfere with radio equipment. Also on a normal aircraft, the energy released in the discharge that occurs on contact with the ground can prematurely detonate explosive devices or ignite flammable materials.

The solution to this problem for fixed-wing aircraft has generally been to install low-noise active or passive corona-discharge devices that also lower the aircraft potential to acceptable levels. These devices utilize a nonrecirculating discharge system in which the rapid flow of air over the aircraft surfaces is used to carry away the ions created by the corona discharge to maintain a low potential using a low-threshold (hence, low-energy) device.

With increased use of helicopters in cargo operations and the increasing size of helicopters the hazards encountered by cargo handlers and ground personnel become acute, since the capacitance (and hence the

energy released on discharge) is proportional to the size of the helicopter.

The size of presently used cargo helicopters has already caused some problems during sling-load operations in triboelectric environments.[1] These problems include personnel being knocked off their feet by electrical shock when touching the cargo hook, and other miscellaneous complaints of hand injuries consisting of split tips and edges of fingers and nails. Obviously, if such problems can be caused by helicopters of the sizes used today, much larger helicopters such as the Boeing 301 HLH* could cause grievous problems that demand solution.

Early in 1972, SRI and Boeing Vertol undertook a study to determine the feasibility of discharging a charged helicopter by active means.[2] The main thrust of this study was to ultimately apply an active system to the Boeing 301 HLH, but of course, it would have applied to any large helicopter.

An active discharge system consists of an aircraft-potential sensor controlling the discharge system, which utilizes a high-voltage bipolar power supply to provide discharge ions to lower the aircraft potential. SRI experience[3],[4] using the active discharging technique indicated that it worked well for fixed-wing aircraft, because the discharge ions released at the extremities of the aircraft are carried away by the slipstream and cannot recirculate back to the aircraft or linger near the aircraft.

The 1972 helicopter discharge investigation[2] indicated that the active system worked well on helicopters in a charge-free environment, but when it was operating in a natural triboelectric environment the

---

*Heavy Lift Helicopter.

charged (dust) particles swirling beneath the hovering helicopter confused the aircraft-potential sensing system, and erroneous potential information was generated. The magnitude of this erroneous potential information was subjected to statistical analysis, and it was found that very dangerous shocks could result if the active system was used during conditions of moderate-to-high (>50 μA) charging currents. However, these tests and previous tests[5,6] did indicate that satisfactory performance of an active discharge system is possible during conditions of low and very low triboelectric charging.

Since it was determined that an active discharging scheme would not work satisfactorily under conditions of high triboelectric charging, a passive discharge scheme using direct earth contact was proposed. Boeing-Vertol, together with subcontractors, set out to devise various techniques for using the passive, direct-contact approach.

The present program was undertaken to evaluate various discharging schemes under actual flight conditions, and to demonstrate the effectiveness of several of the selected techniques. Additional work was done to obtain information about the magnitude of the Radio Frequency Intereference (RFI) produced by the discharging elements, and by the helicopter itself. During the course of the discharger evaluations it became evident that pure numbers about the residual voltage (after discharge) on the cargo would be meaningless unless one could relate these voltages (and hence discharge energies) to physiological responses to moderate energy shocks that might be experienced by a cargo handler. Accordingly, the human response to electrical shock was investigated.

Additional electric field measurements were made of the dust cloud produced by the hovering helicopter. These data were used to investigate some of the physical processes that occur in the cloud and it also served to help tie this measurement program to the flight-test program undertaken previously.[2]

The soil-resistance measurements, discharger evaluations, demonstrations, RFI tests, and shock-hazard evaluations presented below were conducted at Laguna AAF, Yuma Proving Ground (YPG), Yuma, Arizona during the months of May and June 1973. The helicopter used for the flight tests was a CH-47C, S/N 15022, provided by the U.S. Army Aviation Test Board, Fort Rucker, Alabama.

II INSTRUMENTATION

The instrumentation required to accomplish the program described above can be divided into three categories: aircraft system, ground system, and discharger system.

A. Aircraft Instrumentation

The CH-47C was instrumented to provide measured quantities of aircraft surface electric field. ($\vec{E}_{nose}$), aircraft potential, (V_{acft}), charging current (I_{chg}), discharge line current (I_{hook}), and RF spectral content. The configurations used during the program varied somewhat, depending on the measurement needs, but basically two configurations were used as shown in Figures 62 & 63. Figure 62 illustrates the configuration used during tests in the "clean" area, (a large concrete tie-down pad), and Figure 63 illustrates the configuration used when tests were made in the Phillips Drop Zone (the "dusty" area--a large expanse of heavily plowed sand).

It can be seen from this figure that the principal difference between the clean- and dirty-area configurations is the presence of a high-voltage power supply that was used only during the clean area tests. This supply, a Universal Voltronics BAL200-5.5-S was rated at 1.1 kVA (200,000 V at 5.5 mA) and was used to simulate natural charging effects during operation in the clean area. The use of this supply allowed a thorough evaluation of candidate discharging elements and techniques to be made over nearly all anticipated voltages, currents, and surface conditions, without the inconvenience of operating the helicopter in a natural charging environment.

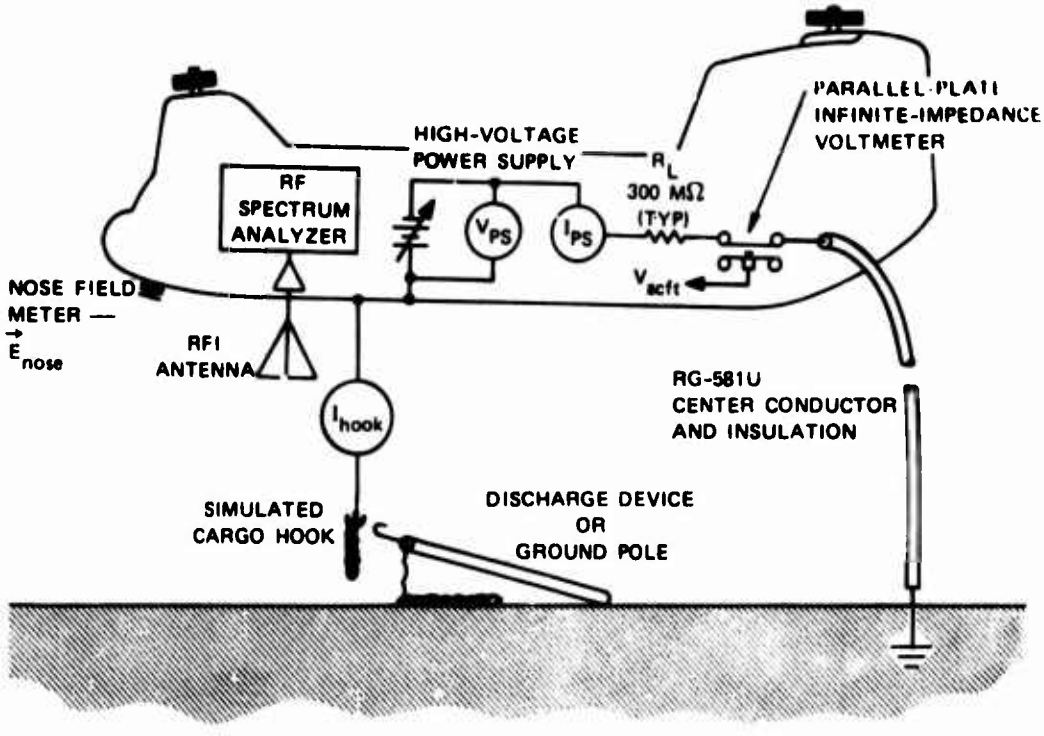

(a) CLEAN AREA (C-130 Tie-Down Pad)

FIGURE 62 GENERAL AIRCRAFT CONFIGURATION USED DURING TESTS

The electric field meter, mounted on the far-forward lower fuselage section, measured the electric field strength at this position on the skin. When used in the clean area, the nose field mill served as a redundant device to infer aircraft potential from the measured fields. When it was used during dust operations (the natural triboelectric environment), the mill served to help tie the data gathered during these tests to those gathered during previous helicopter-in-dust sorties.[2] For a description of the principle of operation of such an electric field meter the reader is referred to an earlier SRI report.[3]

The parallel-plate infinite-impedance voltmeter illustrated in Figures 62 & 63 consisted of a field meter mounted in one of a pair of parallel plates spaced 37 cm. (Each plate was ringed with a 4-inch-diameter

toroid to prevent corona discharges from the edges of the plates.) Using the rule of thumb, "one megavolt arcs one meter in air," this spacing was deemed adequate to hold off the anticipated artificially and naturally produced potentials of about 300,000 volts or so. The separation between the plates was maintained by four teflon rods 5 cm in diameter. In order to ensure that the voltmeter was indeed "infinite impedance," periodic leakage-current tests were made by connecting the high-voltage supply across the voltmeter plates. The ratio of the voltage applied (200 kV) to the measured leakage current determined the plate resistance due to leakage current. This value was never less than $\approx 2 \times 10^{10}$ ohms, and was obtained after a sortie flown in a heavy dust cloud that covered the teflon support rods with a very sparse coating

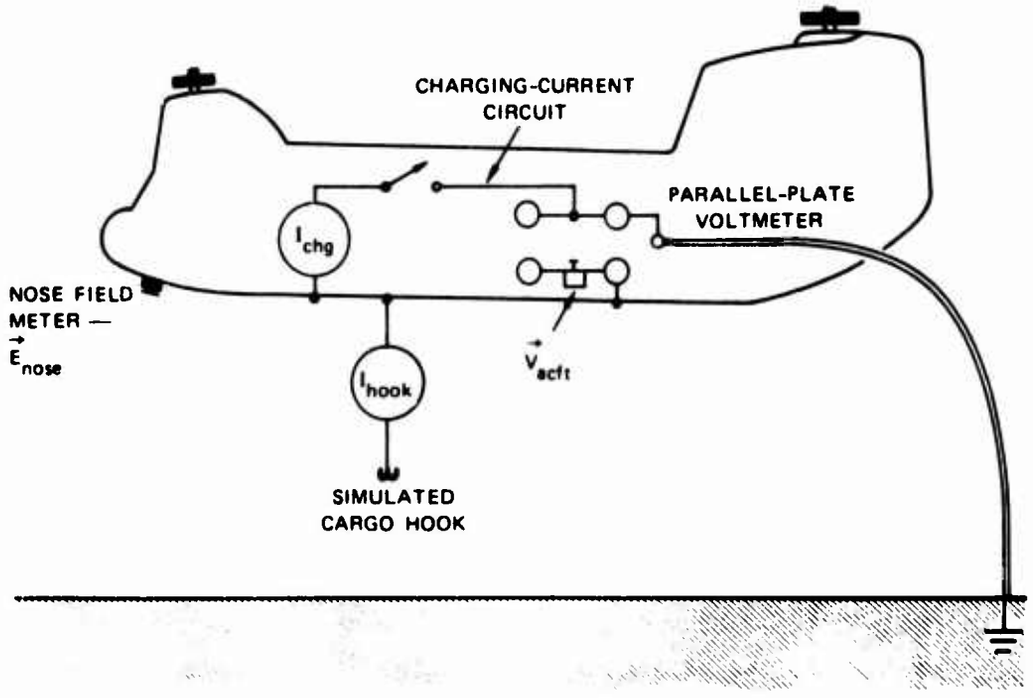

(b) DUSTY AREA (Phillips Drop Zone)

FIGURE 63 GENERAL AIRCRAFT CONFIGURATION USED DURING TESTS (Concluded)

of dust. The implications of this measurement are that the "loading" of the parallel-plate circuit by the leakage current was small and would not affect the operation of the voltmeter. It should be mentioned here that the current measured was indeed leakage current and not corona current--a fact that was confirmed by attempting to detect corona noise with the use of the RF receiver. In order to establish this fact, an antenna was rigged near the parallel plate and the spectral data were observed as increasing voltage was applied between the plates. No spectrum changes were observed over the full voltage range of the power supply. A photograph of the parallel-plate toroidal system is shown in Figure 64 It can be seen in this photo that the separation between the plates is comparable to the dimension of a plate. The parallel-plate area in comparison with the distance is too small to allow the assumption of a uniform field between the plates. The uncertainty regarding field structure was overcome by calibrating with the high-voltage supply and measuring field-meter output in terms of potential applied to the infinite-impedance voltmeter as discussed below.

Physically attached to the top of the parallel-plate voltmeter was a solenoid-driven contactor. This mechanism, which was housed in an oil bath and was corona-protected, was used only during the sorties flown in the dust. It allowed the charging current, I_{chg}, to be measured by the test operator when such a measurement was desired, by grounding the helicopter through the switch and microammeter.

The cargo-hook current, I_{hook}, was determined by rigging a wire-carrying nylon rope lowered through the rescue hatch. The simulated cargo hook was electrically connected to the airframe through a microammeter. This technique allowed the current flowing through the (simulated) cargo-hook line to be separated from the net current measured by the power supply or by the charging-current meter circuit located atop the parallel-plate toroid.

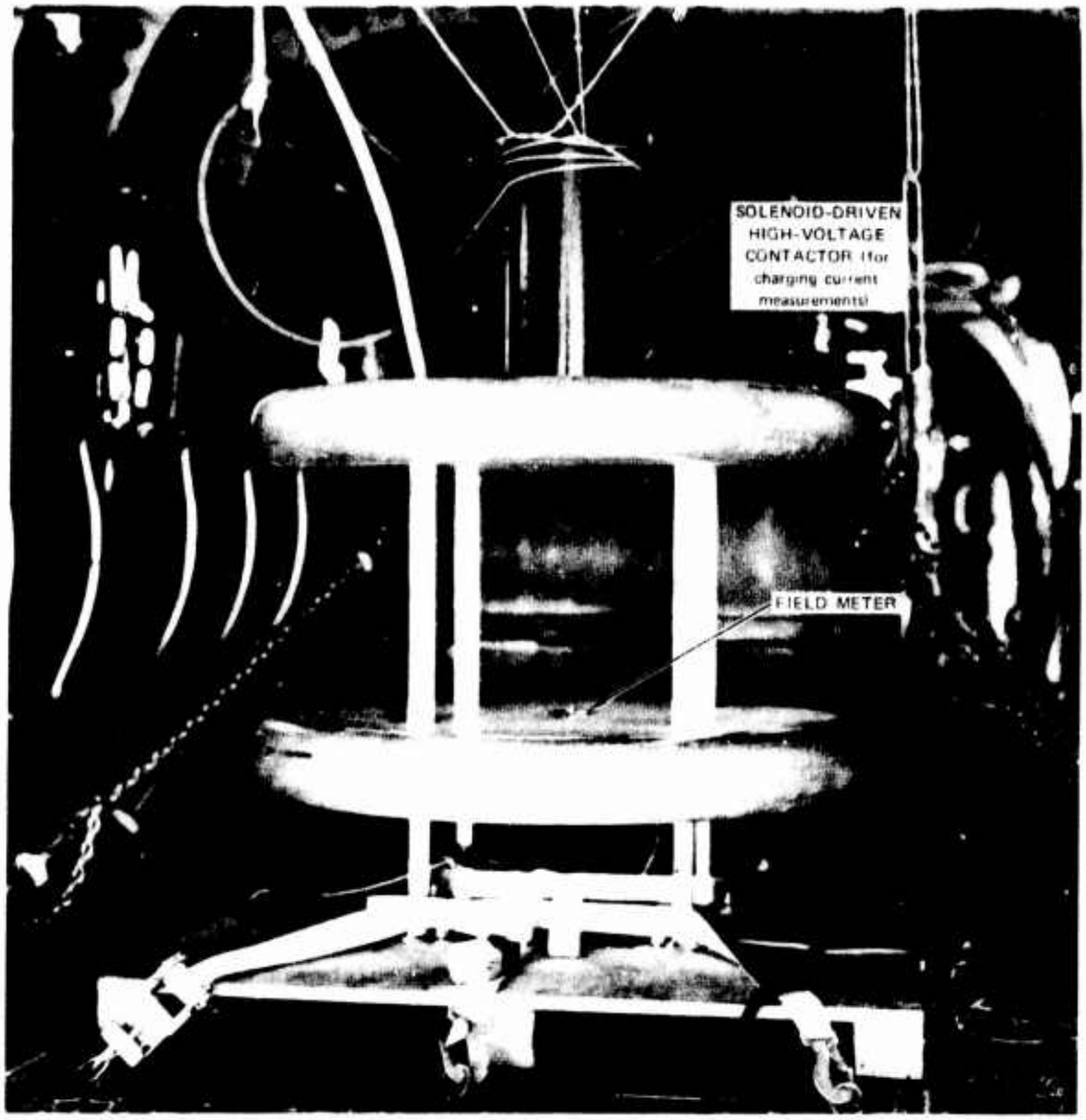

FIGURE 64 PHOTOGRAPH OF PARALLEL-PLATE INFINITE-IMPEDANCE VOLTMETER SHOWING CURRENT-MEASUREMENT SYSTEM ATOP THE PLATES

The RF receiver used to obtain RFI data was an HP 8553 spectrum analyzer using an 8552 IF section and 141T display section. An antenna was built and attached to the underside of the helicopter.

This arrangement allowed a measurement and comparison of the RFI produced by the helicopter and by the helicopter plus grounding-line

element to be made for various aircraft potentials; this is fully reported in the text below.

Current-sensitive instruments (hook current, net current, and charging current) were calibrated daily using a constant-current source designed for this task. The electric-field-sensitive instruments (nose and parallel-plate field meters) were calibrated using the high-voltage power supply while at hover. Although a calibrator device was available to use on these meters, the anticipated electric fields of hundreds of kV/m were far greater than the maximum field of 6 kV/m available from the calibrator, and would have required extrapolation. Since extrapolation could have been misleading under some circumstances, it is felt that using the power supply as a calibration tool gave much more accurate results. This technique allowed the parallel-plate fields to be interpreted directly in terms of potential. The nose field meter was calibrated in a similar fashion while at a hover altitude of 25 ft. It should be noted, however, that prior to dust sorties the nose field mill was calibrated in terms of field so that the dust measurements would be meaningful, and could be compared to the data obtained by the ground array of field meters.

All of the various measured quantities discussed above were recorded on a CEC-5-119 oscillograph so that permanent data records would be obtained.

B. Ground System

A ground array of electric field meters was deployed beneath the helicopter during many of the dust sorties to obtain information about the electrification processes occurring within the dust cloud. Based on photographs taken during the previous flight test,[2] it was known that the dust cloud stirred up by the helicopter was similar in shape

to an oblate spheroid with a radius of, perhaps, 300 to 500 ft and a height of about 100 to 200 ft. This information together with the dust-cloud electrification data obtained previously led to the deployment of the ground array as illustrated in Figure 65 This arrangement allowed data to be sampled from various parts of the cloud to obtain the most data from a limited number of sensors.

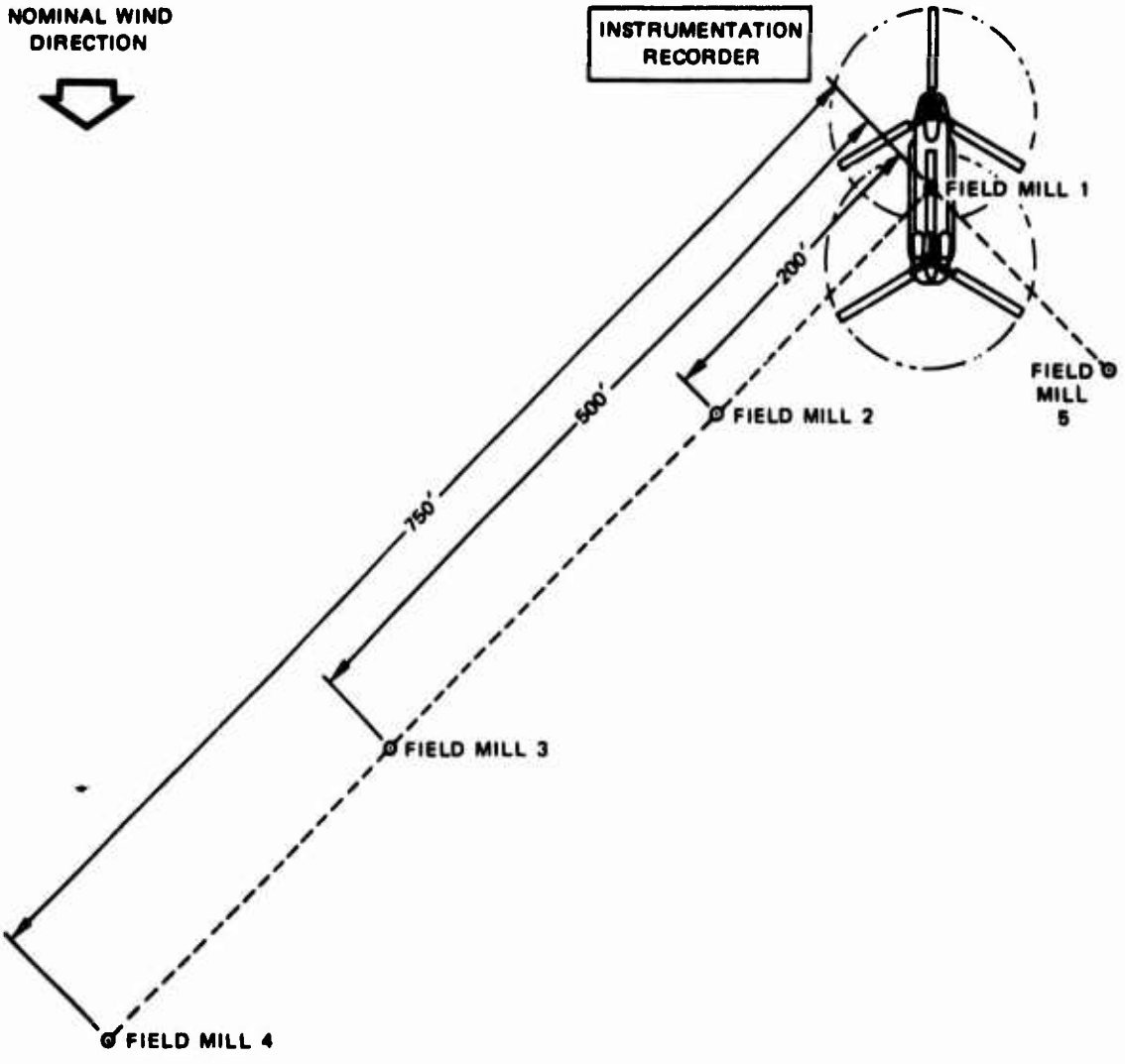

FIGURE 65 GROUND INSTRUMENTATION USED DURING SORTIES INTO PHILLIPS DROP ZONE

The ground field meters were similar to the one used on the aircraft, and except for differences in gain, were identical to each other. The gain of each field meter was adjusted according to the anticipated electric fields based on previous measurements. Since the dust cloud becomes less dense the further one moves from the source region, the electric fields produced by the charged dust particles will similarly decrease. The gain of each field meter was therefore adjusted to compensate for the anticipated field fall-off to allow good resolution of the fields.

Pre- and post-flight calibrations of the field meters were made every time the ground array was used, and were performed by using the field calibrator unit described above. All the ground field-meter data were recorded on a CEC 5-119 recorder located on the ground and synchronized with the airborne recording system via a pair of quartz clocks, one located in the helicopter and the other on the ground.

C. Discharger System

The Boeing Company obtained various "sets" of discharging elements through a subcontractor, The Truax Company. Each "set" consisted of interchangeable components and, when connected together, formed a specific discharge "system." The components consisted of a damage-resistant link, a current-limiting resistor, a weighting element, and a termination device. The design intent of these "grounding lines" was to attach them to the cargo hook and use them to discharge the helicopter to acceptable potential levels through earth contact prior to the handling of the cargo hook by cargo handlers.

An additional type of discharger evaluated was the "grounding pole," a shepherds-hook arrangement whereby the cargo handler could contact the hook or cargo and discharge the helicopter through a line resting on the earth's surface.

As described above, the purpose of these flight tests was to demonstrate that the discharger designs and techniques were workable and to evaluate the designs and recommend a preferable design, if any. The preliminary design idea was to use the "grounding line" for unprepared site operations and the "grounding pole" over prepared sites. A typical grounding line and grounding pole scheme that was evaluated is shown in Figure 66

The damage-resistant link was a flexible piece of 1/4-inch steel cable, 21 inches long, and covered with an abrasion-resistant plastic sleeve. The purpose of this link was to absorb most of the wear and

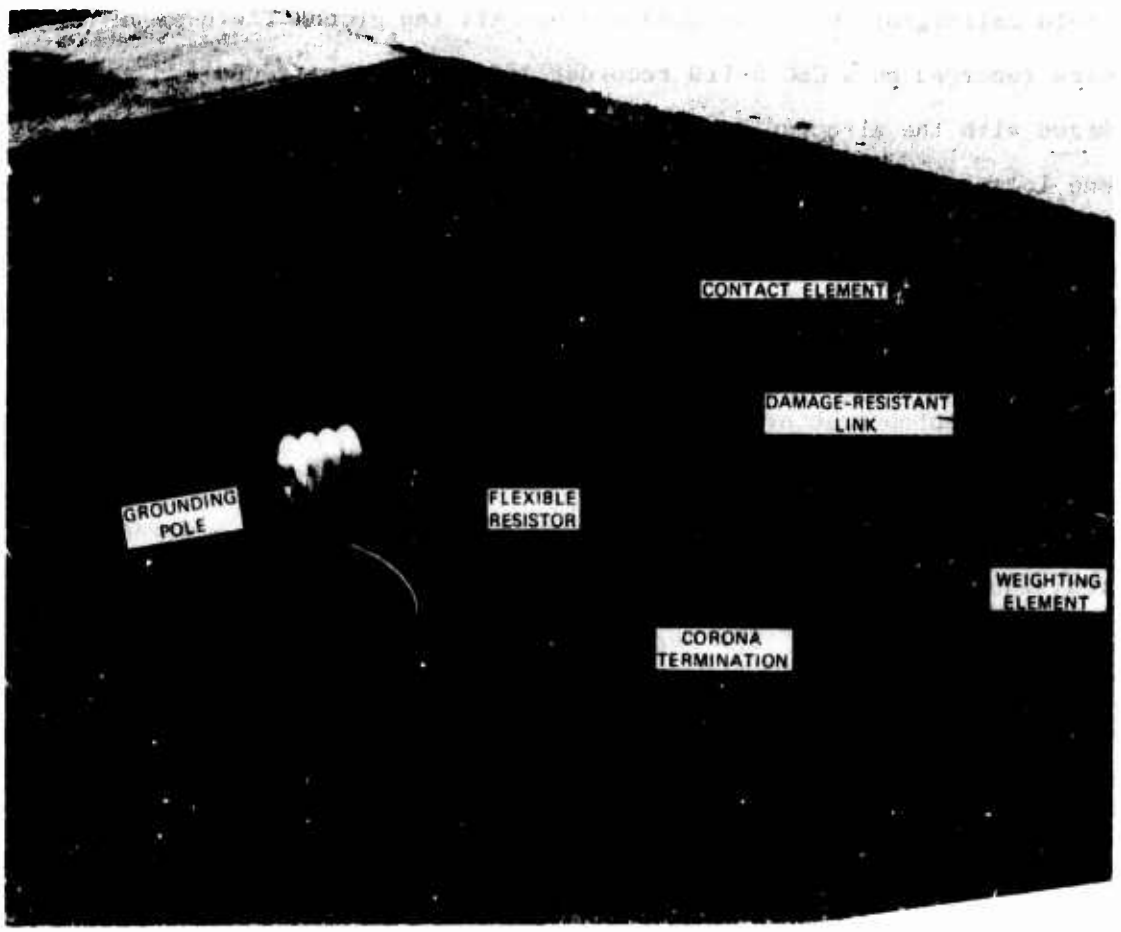

FIGURE 66 PHOTOGRAPH SHOWING TYPICAL GROUND POLE AND GROUND LINE USED DURING THE DISCHARGING TESTS

tear due to inadvertent ground contact of the cargo hook and to provide an electrical connection between the hook and the rest of the assembly.

The flexible resistor was a 5-ft length of 1/4-inch nylon rope covered with a carbon-impregnated polyurethcyne coating. The purpose of this resistor (which, for evaluation purposes, came in values of 15 MΩ , 20 MΩ, and 37 MΩ) was to act as a current-limiter in case the handler accidentally touched it before the weighting element and termination touched the ground. The values of resistance chosen for this resistor were obviously a compromise. The resistance had to be chosen high enough so that in the case of accidental contact the cargo handler would not be severely shocked, yet low enough so that the helicopter could be discharged to an acceptably low potential after ground contact.

The weighting element was a 2-ft-long section of steel chain. Its function was to add enough mass to the end of the grounding line so that it would not whip around in the rotor-wash of the hovering aircraft. The chains supplied by the Truax Company were available in five different weights: 0.42, 0.75, 2.5, 6.2 and 10 lbs/ft. Practical considerations described below limited the evaluation to the lightest three chains because the others were too heavy. An additional type of "weighting element" evaluated was a 3-ft-long, 1-MΩ flexible resistor. The basic design of this resistor was similar to that of the resistors described above except that fine, short steel wires protruded through the resistor about every inch along its surface to act as a corona discharger and ground-contact element. This element was referred to as a "spiked resistor" and is described later in the text.

The terminations that were evaluated were a corona brush, an aircraft P-static wick discharger, a 10-inch-diameter corona-suppressing ball, and no termination (i.e., the chain-end only). The purpose of

the termination was threefold: To provide a precontact method of reducing the helicopter potential through corona discharge; to provide a mechanism for breaking through the soil's surface crust to obtain a lower resistance; and to ensure that the termination end, if accidentally touched, would not injure the handler.

The three systems described above were used in various ways at different times, depending on the measurement needs, to perform the program described below.

III CONTACT RESISTANCE OF SOIL

In order that the grounding-line, grounding-pole, and shock-measurement programs conducted at YPG have a more universal basis for comparison with other similar programs, an extensive series of contact resistance measurements were made.

The materials subjected to these tests included concrete, asphalt, rocks, hard-packed dry desert, and loosely-plowed desert. It was felt that these surface materials were typical of the kinds of materials likely to be encountered during normal flight operations. Also, because of the arid desert conditions, the resistance values obtained would be "worst-case" values and place an upper bound on the possible range of contact resistance expected from surface materials of these types.

The resistance measurements were performed by connecting the high-voltage power supply between a "good" ground (a tie-down/grounding stake) and a 2-ft section of chain at the end of a long piece of RG-58/U cable. The chain was then arbitrarily dropped onto the candidate surface about 40 ft away from the ground rod and the measurements were made. This process was repeated several times on the same surface to ensure that representative data were obtained. Figure 67 illustrates schematically the technique used to obtain the resistance data.

The power-supply voltage was varied and the voltage, V_{ps}, and power supply current, I_{ps}, were recorded. Resistance data were then obtained as the ratio of V_{ps} to I_{ps}, and are shown plotted in Figure 68 as a function of applied voltage for the various surfaces. These data were somewhat of a surprise because of the nonlinear behavior of the resistance

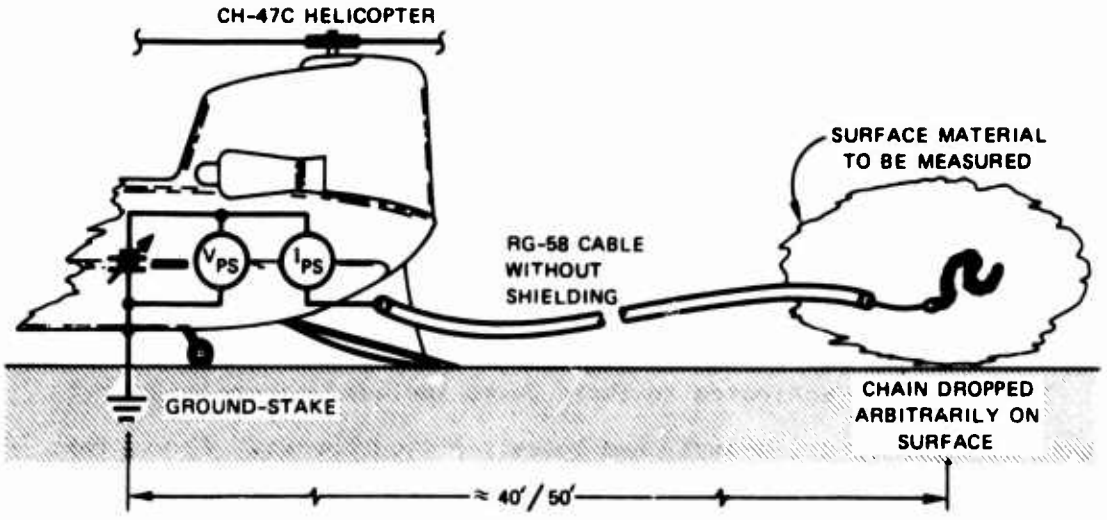

FIGURE 67 SCHEMATIC REPRESENTATION OF TECHNIQUE USED TO OBTAIN SURFACE-MATERIAL RESISTANCE DATA

with voltage. The low-voltage resistance data obtained for the concrete and soft desert, however, agreed well with resistance data reported earlier.[2]

The nonlinear behavior shown in the figure, apparently stems from the incremental breakdown of insulating coatings on the constituent particles. The resistance, at a given voltage, for a given material is a measure of the strength of this insulation.

The exceptionally low values of resistance obtained from measurements in the dusty area probably indicate that a moist substratum of sand lay beneath the surface, and evaporation of this moisture was prevented by the fine silt-like sand on the surface.

The data shown in the figure for hard desert and asphalt are truncated at 10 kV and 15 kV, respectively. The reason for this was that for higher potentials the candidate material broke down electrically. The data shown for the resistance of rocks terminates at 45 kV because

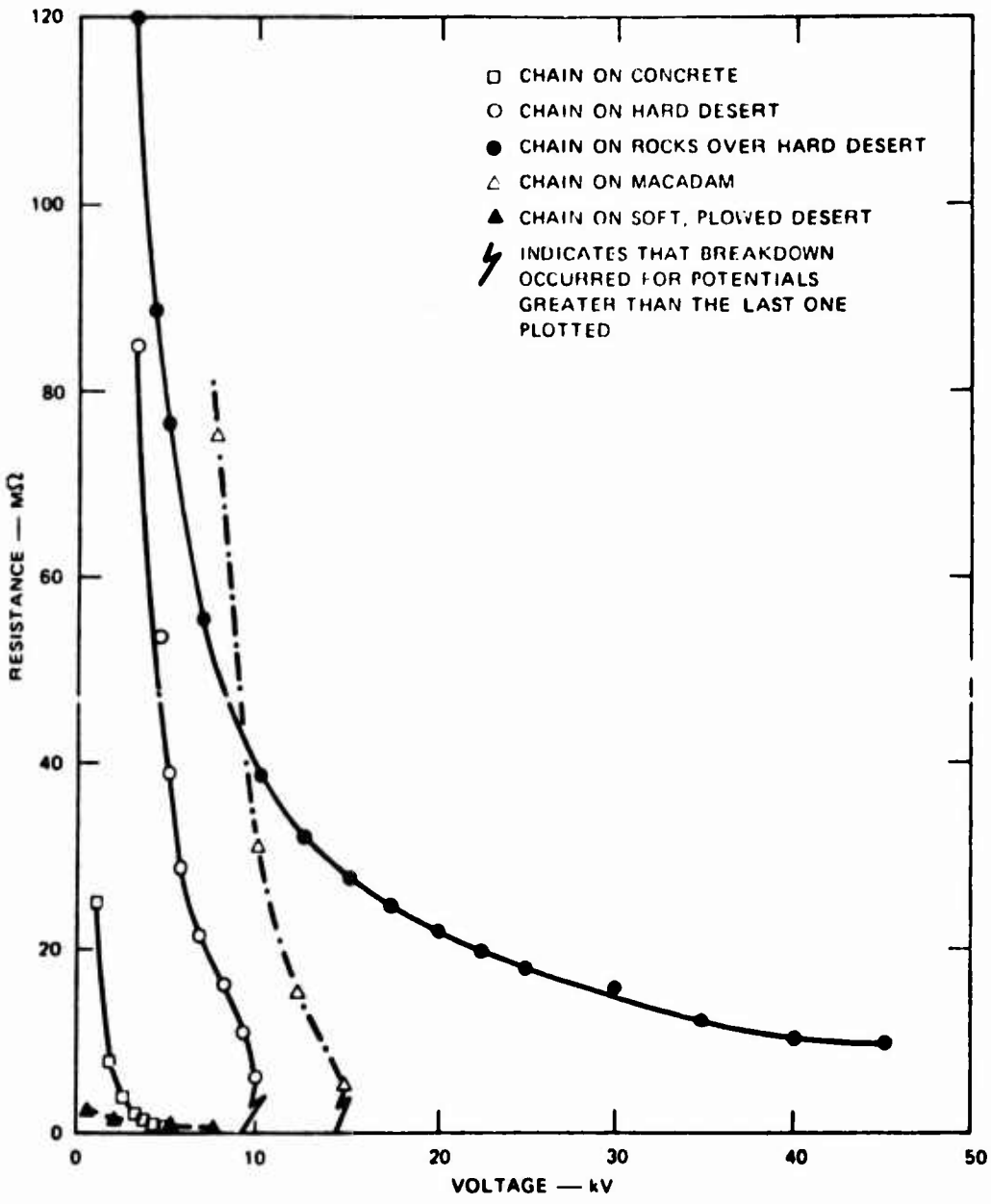

FIGURE 68 RESISTANCE AS A FUNCTION OF VOLTAGE FOR VARIOUS SURFACE MATERIALS

above this value the power-supply-current limit was reached and further increase in voltage was not possible. At 45 kV, however, the rocks showed no evidence of an impending large-scale breakdown to reduce the contact resistance below 10 MΩ.

The implications of these data are that grounding techniques involving, say, macadam, will not be as effective as grounding to concrete or the hard desert, as long as the breakdown potential is not exceeded. When the breakdown potentials of the materials are reached, however, the grounding techniques should all be essentially equivalent in terms of residual potential on the aircraft.

This proved to be generally true as described in the text below, except that the asphalt proved to be an inferior conductor as compared to desert or concrete for all initial helicopter potentials. It is believed that the reason for this is that the movement of the helicopter and the rotor-wash kept moving the grounding element after initial contact was made, preventing the current flow along the original contact path.

It should be mentioned here that, during the dirt measurements, only the desert near YPG was subjected to these tests. Since this soil is typically arid but fertile it is possible that less arable soil such as silica-based sand might lead to much higher values of contact resistance with a resulting increase in residual aircraft potential.

IV FLIGHT EVALUATION OF CANDIDATE DISCHARGING DEVICES

As described earlier, two basic discharging techniques were to be used: (1) In prepared site areas, where generally uniform surfaces would be available, a grounding pole (very similar to a shepherds hook) or a grounding line would be used; and (2) at unprepared sites, a grounding line would be used. The grounding-line concept would rely on a line, free-hanging from the cargo hook to touch the ground and thus reduce the helicopter potential. The grounding pole, however, required at least one person on the ground to touch the cargo, or cargo hook, with the shepherds hook, and to hook-up or otherwise manipulate the cargo.

The grounding devices were thoroughly evaluated over the range of voltages and surface types appropriate to their anticipated use.

A. Grounding Pole

The grounding pole was evaluated over a dry concrete surface. The measurement technique was to raise the aircraft potential to the desired level using the power supply; then to touch the simulated cargo hook (a 10-kg aluminum block) with the pole The residual potential on the aircraft could then be determined by measuring the voltage between the plates of the parallel-plate voltmeter. A matrix of the grounding-pole test permutations is shown in Figure 69.

The results obtained by using the grounding pole over dry concrete are shown in Table 1. When R_L, the current-limiting resistor, and the power-supply voltage were changed, the charging current could be varied over a wide range. It is seen from the figure that the hook current

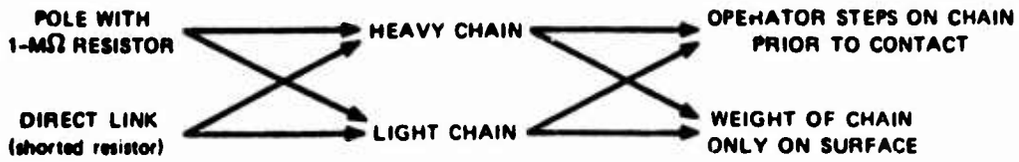

FIGURE 69 TEXT MATRIX SHOWING PERMUTATIONS OF TECHNIQUES USED TO EVALUATE PERFORMANCE OF THE GROUNDING POLE

(the charging current if a perfect earthing was made) varied from 138 μA to 590 μA, and that the residual aircraft potential, over this range of current, generally stayed less than 10 kV, even for initial potentials as high as 175 kV. The residual potential is the key number in describing the capability of a given discharge system.

These tests indicated that the grounding-pole technique was a viable design and could be used satisfactorily in any of the configurations tested, although the heavier chain (contact element) did give slightly better results. A marginal improvement was also obtained when the grounding-pole handler stepped on the chain to increase the contact pressure, although the overall decrease in residual voltage would probably not warrant mandatory use of this technique.

B. Grounding Line

The various grounding-line elements were thoroughly evaluated over their range of anticipated use. A matrix of the various test configurations and conditions is shown in Figure 70. Evaluations performed over concrete, macadam, and hard desert indicated that all of the grounding-line "systems" were of about equal effectiveness after earth contact was established.

Table IX

HOOK CURRENT AND RESIDUAL HELICOPTER VOLTAGE DATA OBTAINED BY USING GROUNDING-POLE DISCHARGER

Power-Supply Voltage (kV)	Lightweight Chain				Heavy Chain			
	Chain on Surface		Operator's Weight on Chain		Chain on Surface		Operator's Weight on Chain	
	Hook Current (μA)	Residual Voltage (kV)	Hook Current (μA)	Residual Voltage (kV)	Hook Current (μA)	Residual Voltage (kV)	Hook Current (μA)	Residual Voltage (kV)
50	138	10	145	10	300*	7	310*	7*
100	570*	5.5*	575*	4*	300	9	300	9
150	470	9	485	5.5	475	8	475	8
175	540	11	570	10	590	7.5	575	10

*R_L = 150 MΩ instead of the usual 300 MΩ.

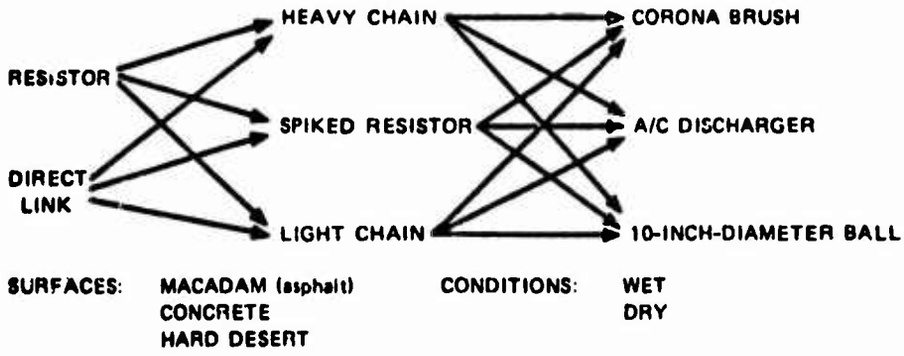

FIGURE 70 MATRIX OF CONFIGURATIONS AND CONDITIONS USED TO EVALUATE EFFECTIVENESS OF GROUNDING-LINE TECHNIQUES

A serious drawback of the light or unweighted elements was revealed during these tests. The element, hanging from the simulated cargo hook was blown about severely by the rotor-wash both in the air, before ground contact, and on the ground, after contact. The effects of this were that a good ground could not be maintained when using the "spiked-resistor" or lightweight chains as grounding elements. The severity of this movement was such that it was likely that, had there been a cargo handler beneath the helicopter, he could have been injured due to the whipping motion of the contact elements.

The results obtained above indicated that the best (simplest and most effective) discharge element was just a moderately heavy chain hanging from the cargo hook, without termination or resistor. This configuration was used to examine the effects of different surfaces and surface conditions on the discharge "system" capabilities. The results of these measurements are shown in Table X for a clean environment, with artificial charging being produced by the power supply. The "dry" surface was the unperturbed state of the material to be used for the test, and a "wet" surface was obtained by pouring 10 gallons of water over the surface to make a very large puddle that was further dispersed by the down-wash from the rotor blade.

Table X

EFFECTS OF VARIOUS SURFACES AND SURFACE CONDITIONS ON GROUNDING-ELEMENT PERFORMANCE

Surface Material	Initial Aircraft Potential (kV)	Dry Surface			Wet Surface		
		I_{ps} (μA)	I_{hook} (μA)	$V_{residual}$ (kV)	I_{ps} (μA)	I_{hook} (μA)	$V_{residual}$ (kV)
Macadam (asphalt)	50	150	125	9	160	155	0
	100	300	265	15	325	315	0
	150	500	430	17	525	500	0
Hard desert	50	180	170	0	160	135	0
	100	325	315	0	350	335	0
	150	500	500	0	500	500	0
Concrete	50	150	140	5	160	155	0
	100	325	300	7	350	325	0
	150	500	485	8	525	500	0

It can be seen from this figure that the dry macadam surface was the only material that allowed the aircraft potential to remain above 10 kV, which is in good agreement with the expected values based on the resistance measurements made earlier (see Figure 66). It can also be observed that all wet surfaces maintained the residual potential at 0 volts for all initial (ungrounded) potentials.

The data in Table X indicate that the grounding-line technique seemed to work quite well (with the exception noted) for all of the different configurations evaluated in the artificial charging environment.

Subsequent to these findings it was of interest to determine whether the same results could be obtained in the natural triboelectric-charging environment. A series of measurements were conducted in the Phillips Drop Zone to evaluate the various grounding-line techniques described above. Blowing dust offers a satisfactory medium in which to study the general triboelectric charging process; it is readily available, and it offers reasonably repeatable test conditions. SRI and others[5,6] have previously used dust to good advantage for this purpose, but of course it will not substitute for all triboelectric environments. For example, dust may not suitably simulate all aspects of frictional charging by dry snow. A summary of results of the grounding measurements in the dust environment is presented in Table XI. The data presented in this table are averages of the data taken during the evaluation of a given configuration, to avoid overwhelming the reader with individual data points and evaluations. The overbar (—) indicates that an average was taken, $\bar{I}_{chg}$ is the net charging current to the aircraft due to the dust cloud, $\bar{I}_{hook}$ is the current flowing in the simulated cargo-hook line after ground contact was made, $\bar{V}_{acft}$ is the helicopter potential measured prior to the ground contact by the discharging element, and $\bar{V}_{resid}$ is the residual aircraft potential after earth contact by the grounding element. The disparity between I_{chg} and I_{hook} stems from the fact that

Table XI

SUMMARY OF NATURAL TRIBOELECTRIC-ENVIRONMENT GROUNDING MEASUREMENTS

(Discharging Element Dropped into Dry, Plowed Desert)

Grounding-Line "System"	$\bar{I}_{chg}$ (μA)	$\bar{I}_{hook}$ (μA)	$\bar{V}_{acft}$ (kV)	$\bar{V}_{resid}$ (kV)
14-MΩ resistor, light chain, A/C discharger	90	79	55	1.1
14-MΩ resistor, heavy chain, corona brush	76	31	70	2.6
14-MΩ resistor, spiked resistor, 10-inch-diameter ball	135	125	85	4.8
Heavy chain, corona brush	133	128	78	0
Light chain, A/C discharger	110	106	67	0.2
Spiked resistor, 10-inch-diameter ball	150	140	98	1.5
Heavy chain	180	180	98	0.9

these two measurements were not made at the same time. Since the charging current was not steady, the difference between $\bar{I}_{chg}$ and $\bar{I}_{hook}$ is indicative of the variability of the charging current.

It is observed from this table that all of the residual aircraft potentials are less then 5 kV, and that residual potentials obtained when a chain element was used for grounding are much less than 5 kV.

A problem encountered here and throughout the rest of the program was that the flexible resistor increased in value by as much as a factor of four, apparently due to the stress placed on it by the weight of the chain and the bending of the resistor caused by its movement beneath the helicopter. This was measured and is illustrated by comparing the data with and without the "14-MΩ" resistor. The residual

voltage with the resistor is much higher than would be expected by calculating the IR drop of the resistor and adding it to the residual potential obtained without the resistor.

The charging current obtained during these measurements was only moderate in comparison with the anticipated charging current of 600 μA on the HLH. However, since these data agree well with the artificial-charging measurements reported earlier, and with the expected residual potential values based on the soil-resistance data, the authors believe that these data could successfully be extrapolated to higher aircraft potentials and charging currents without difficulty.

The charging current produced by the dust cloud and the resultant helicopter potential were routinely measured during operations at Phillips Drop Zone. A plot of these measured data is shown in Figure 71. A "least squares" curve through the data points shows that the helicopter potential increases almost linearly with charging current to about 80 kV. and then begins to curve. Extrapolation shows this curve asymptotically approaching 160 to 180 kV for very large charging currents. Since the potential-versus-current data obtained in the dust were unlike the data taken in the artificial environment, appropriate checks were made to be sure that the differences were not due to instrument or measurement error. No such errors were found. Previous experience[7] indicated that high potentials were generated by charging currents as low as 10 μA. The data of Ref. 7, however, were obtained using a CH-54 test vehicle. Since the discharge characteristics of a helicopter depend on details of blade design (which affects corona threshold) and on engine exhaust characteristics (which affect discharge through the conductivity of the exhaust), one should not expect data obtained on one aircraft to apply in all details to another helicopter type. SRI's experience with CH-47s in a clean environment indicates that the threshold of measurable corona current is approximately 75 kV, and that in

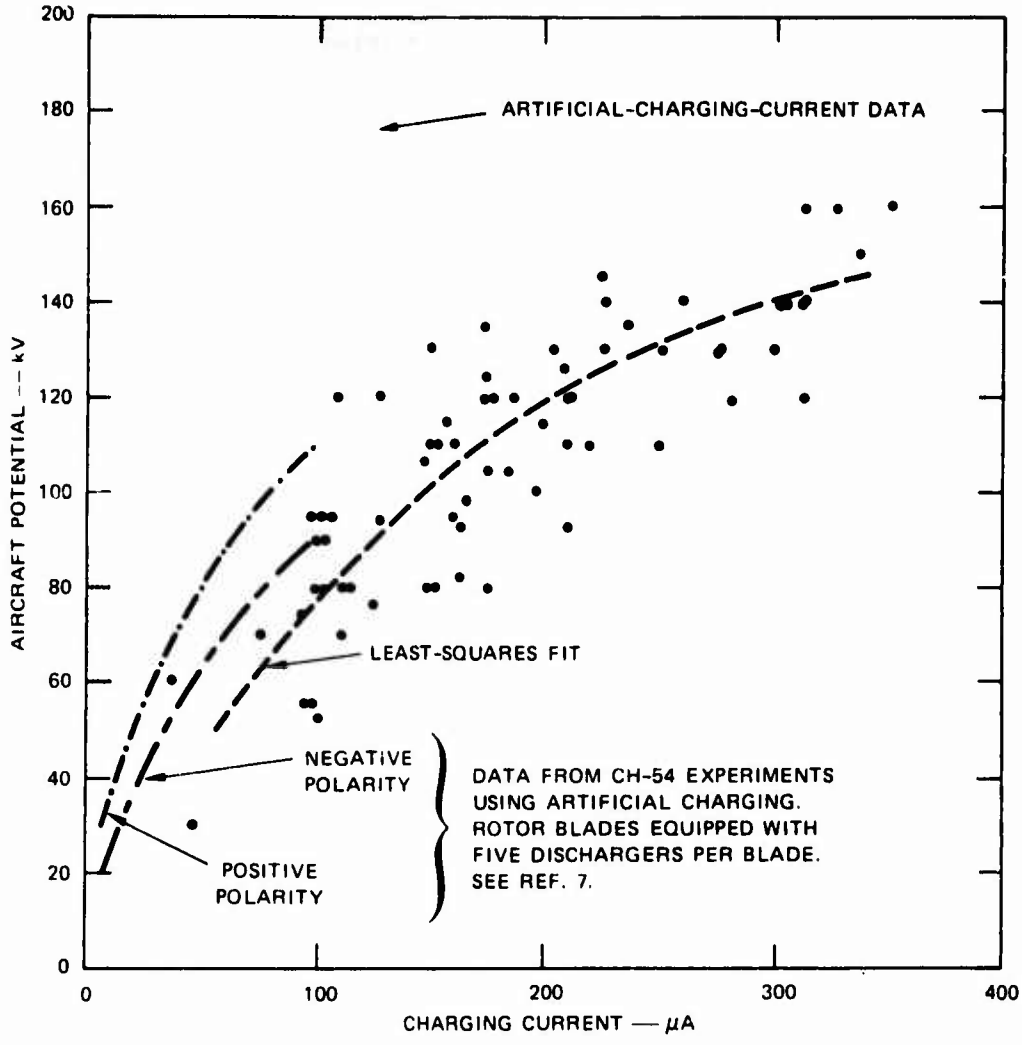

FIGURE 71 COMPARISON OF CH-47 AND CH-54 HELICOPTER POTENTIAL VERSUS CHARGING CURRENT

Data points obtained from CH-47 sorties flown in natural charging environment.

order to maintain a helicopter voltage of 200 kV the helicopter had to be charged at a rate of about 100 to 150 μA. This is different from the CH-54 data by about a factor of two or so, and can be explained by considering the blade design. The CH-54 blade utilizes a continuous aluminum sheet around the trailing edge and an aluminum tip cap. The CH-47, on the other hand, has a rectangular trailing edge, and a square tip (i.e., the tip is a truncated airfoil). Since the corona discharges

will begin in these high field regions, it is clear that the CH-47 could easily have a corona threshold factor of two or so lower than the CH-54, minimizing the observed I-versus-V differences.

The differences observed between aircraft potential measured in the natural charging environments cannot be fully explained, because of insufficient knowledge about the electrified dust cloud and its contribution in changing the air resistance between the helicopter and ground. It can be seen from Figure 7 that the change in effective space resistance between the 50-μA and 300-μA charging currents is about a factor of two (from 10^9 Ω at 50 μA to 5×10^8 Ω at 300 μA). This is a small change, achievable if sufficient conduction ions are present in the electrified dust cloud.

Further insight into the reasons for the observed difference between the CH-47 helicopter discharge characteristics in the clean environment and in the dust environment may be gained by consideration of the results of CH-54 experiments of Ref. 7. There it was found that the addition of five passive dischargers per blade on the CH-54 greatly reduced the aircraft potential required to discharge a given current, and made the discharge characteristic nonlinear at low charging rates. Data from the discharger-equipped CH-54 have been plotted in Figure 7 for comparison. It is evident that the discharging characteristic of the discharger-equipped CH-54 is quite similar to that of the CH-47 operating in the dusty environment. This comparison of the CH-47 and CH-54 data appears to indicate that the presence of the dust cloud has the effect of reducing the aircraft voltage needed to discharge a given current to the same degree as would the addition of a set of low-corona-threshold dischargers.

A possible explanation for the observed modification of helicopter discharge characteristics by the dust cloud follows from the observation

that the dust cloud is highly charged and that it is composed of very small dust particles. A microscopic examination of the dust blown up from Phillips Drop Zone showed that the particles range in radius from 0.0001 inch to about 0.010 inch with the greatest number of them appearing in the 0.001-inch to 0.002-inch range. The particles were of random shape, some with sharp, irregular projections, and others with smoother but well defined edges.

Since the cloud's conductivity is a function of the number of free ions between the helicopter and ground, a simple argument can be made that supports the view that the dust cloud is weakly ionized, and may contain enough conduction (high-mobility) ions to maintain the potential at a value below that achievable when no, or little, dust is present.

It is well known that the maximum potential to which a sphere may be raised is equal to the radius of the sphere times the electrical breakdown field--that is,

$$V_{max} = a\left|\vec{E}_{max}\right| \quad . \tag{6}$$

In air, $\vec{E}_{max}$ is about 3×10^6 V/m. If one assumes that the dust particles are spherical, a calculation of their maximum potential may be made. (Actually, as particle size begins to approach the mean free path for air molecules, $\vec{E}_{max}$ increases above 3×10^6 V/m. For the range of particle sizes considered here, however, the increase is a factor of only two or so, and the simpler argument of a constant value of $\vec{E}_{max}$ will be used.) The capacitance of the sphere can be calculated and an estimate of the maximum charge on the sphere can be obtained.

These values were tabulated for the range of particle sizes observed in the Yuma dust and are shown in Table XII. Flight-test measurements of the charge acquired by individual cirrus-cloud crystals (100 to 200

Table XII

TABULATION OF PARTICLE POTENTIAL, CAPACITY, AND MAXIMUM STABLE CHARGE ASSUMING A SPHERICAL SHAPE

Radius		V_{max}	C	Q
Inch	Meters	Volts	Farads	Coulombs
0.001	2.54×10^{-5}	76	2.8×10^{-15}	2.13×10^{-13}
0.005	1.27×10^{-4}	381	1.4×10^{-14}	5.33×10^{-12}
0.010	2.54×10^{-4}	762	2.8×10^{-14}	2.13×10^{-11}

microns in diameter) indicate that they acquire charges of the order of 10^{-11} coulomb.[8,9] Thus it is very likely that dust particles will also acquire charge considerably in excess of the maximum stable level. Charges in excess of the stable level can be acquired because for the small particles under consideration, breakdown of the air cannot occur immediately. (An electron must be present in the immediate vicinity of the particle in order to start the breakdown process. As the particle size decreases, the occurrence of such a chance electron takes progressively more time.) It has been shown[10] that, for a particle of 0.001-inch radius, charge in excess of the stable maximum can reside for a period of roughly 0.1 s. Thus, particles acquire excess charge on impact. They move away from the point of impact, and, ultimately, electrical breakdown of the air in the immediate vicinity of the particle occurs, relieving the excess charge and generating highly mobile ions of the same sign as the initial charge on the dust particle. These ions are available to migrate to the helicopter and help discharge it at low voltage.

Thus, it appears that the continual charging and discharging of the dust particles results in a conductive medium that effectively shunts the helicopter to ground through a large, diffuse resistor,

maintaining a potential lower than that observed in the absence of the dust cloud, for a given charging current. This phenomenon, of course, is strongly dependent on the cloud's particle density, which may result in the nonlinear behavior shown in Figure 71. SRI's laboratory experience has also indicated that the amount of triboelectric charging obtained is dependent on the type of material used. For example, lycopodium powder produces very high triboelectric charging when blown over an object, whereas powdered walnut shells do not give as much charging. This indicates that actual helicopter charging would be similarly affected, and that another set of data might be obtained if the tests were performed in, say, snow.

The evaluation of the grounding pole and various grounding lines revealed that all of the devices employed worked satisfactorily, with some qualifications. The grounding line worked best when it consisted simply of a heavy chain hanging from the end of the flexible resistor. Operationally, the use of a corona termination was superfluous because a noticeable increase in the precontact current from the line was observed only immediately before contact when the corona element was very close to the ground. Since the grounding line worked so well in reducing the helicopter potential, it is felt that the use of the grounding pole should be eliminated in favor of full-time use of the grounding line.

V PHYSIOLOGICAL RESPONSE TO ELECTRIC SHOCK

Early in the course of the program it became obvious that a discussion of aircraft residual potentials and discharge energies would be meaningless unless a person's response to these quantitites was understood, and therefore a program to determine this response was developed.

Two basic questions were asked during this phase of the program: (1) what would be the highest permissible residual potential on the aircraft that would permit a person to carry out cargo duties when the aircraft was (nominally) grounded through use of one of the discharging devices evaluated, and (2) what series resistance should be present on the cargo-hook line to protect the cargo handler in case he should accidentally touch the grounding line before it makes ground contact?

To answer the first question, the helicopter was configured as shown in Figure 72 and the test was performed over dry concrete.

The test was conducted by bringing the helicopter up to some potential, V, with the power supply. The (barefooted) person beneath the helicopter then touched the simulated hook and noted his response to the stimulus; V was then increased and the test repeated. This continued until the subject terminated the test. A table of helicopter voltages, CH-47 discharge energies, and the person's observations about the shock levels he felt are shown in Table XIII.

It can be seen from this table that the subjects' comments about the degree of shock felt agrees well with the data published by Dalziel.[11,12] Since the measurements were made using a CH-47 (with a capacity of about 1000 μμF), an additional column is included in the

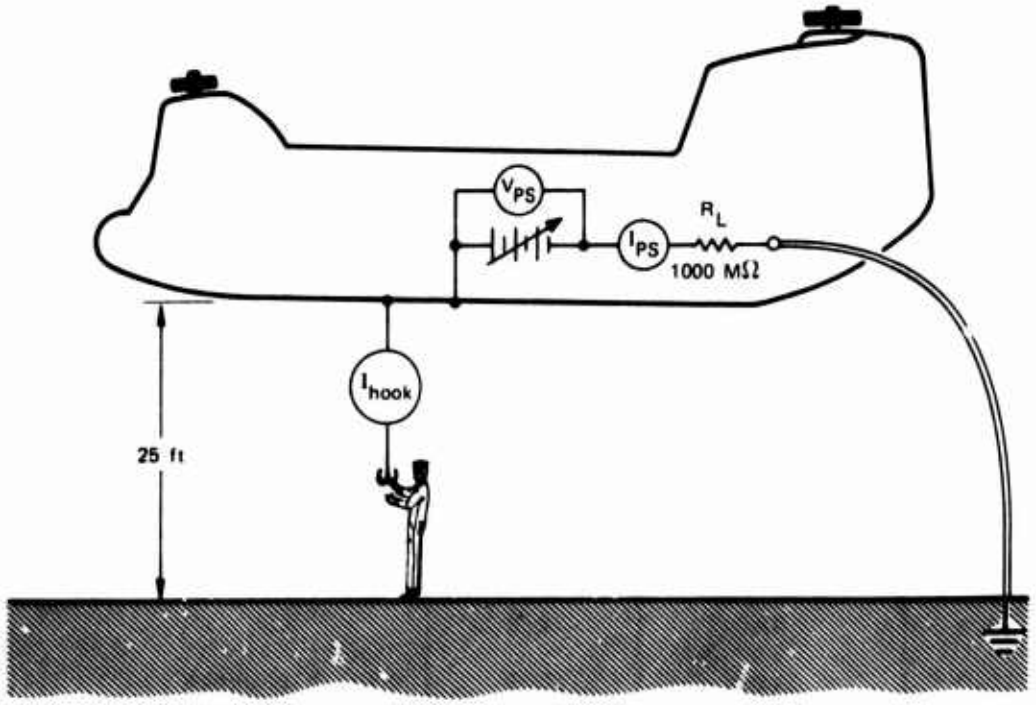

FIGURE 72 AIRCRAFT CONFIGURATION USED TO MEASURE PHYSIOLOGICAL RESPONSE TO ELECTRIC SHOCK

table that specifies, for a given discharge energy, the appropriate potential to obtain that discharge energy, assuming a helicopter capacitance of 2000 μμF (the estimated capacity of the Boeing 301 HLH).

In an additional test performed along these same lines but extending the energy range, two subjects were used. Subject D experienced a severe shock in the ankles and wrist accompanied with chest-muscle contraction at 25 kV, while subject B experienced this same phenomenon at 30 kV. It should be noted here that all tests of this nature began at very low voltages and were incremented in no more than 2.5-kV steps. Additional precautions were taken when these tests were performed by having a medic standing by at the test site in case anything unforeseen should happen.

These tests clearly indicated that the grounding-line and grounding-pole technique could reduce the potential sufficiently so that a cargo

Table XIII

PHYSIOLOGICAL RESPONSE
OF SUBJECT EVALUATING ANTICIPATED ELECTRIC-SHOCK LEVELS
AFTER GROUNDING AIRCRAFT WITH DISCHARGING DEVICE

Aircraft Voltage (kV)	CH-47 Discharge Energy (mJ)	Equivalent HLH Voltage (kV)	Comments
2.5	3	1.8	
5.0	12.5	3.5	
6.0	20	4.5	(Dalziel threshold)
7.5	28	5.2	"Slight shock"
10.0	50	7.0	"Shock in fingers"
12.5	78	8.8	
15.0	112	10.2	"Sensible shock"
17.5	152	12.5	"Shock felt in wrist"
20.0	200	14.0	"Distinct shock felt in wrist and ankles"
23.7	250	16.0	"(Dalziel: Strong shock, not dangerous)"
30.0	450		Boots arc over (see text)

Note: Assumed capacities CH47 1000 pF; HLH 2000 pF.

handler would experience, at most, an unpleasant but not dangerous shock.

In order to determine the value of a series resistance to protect the cargo handler in the event that he should touch the grounding line prior to its earth contact, a measurement was devised using a 10-MΩ series resistance, to evaluate this question. Obviously, any choice of a resistor is a compromise. If the resistance is very high, the cargo handler is protected, but after ground contact, the residual potential

is also high and direct contact with the helicopter could result in a serious shock. On the other hand, a low resistance (or no resistance) provides the lowest possible residual potential, but offers no personnel protection. The resistor used for this test was a large rigid resistor whose resistance remained constant throughout all these tests at 10 MΩ.

The helicopter configuration used for this test is shown in Figure 73. The experiment was performed in a manner similar to that of the

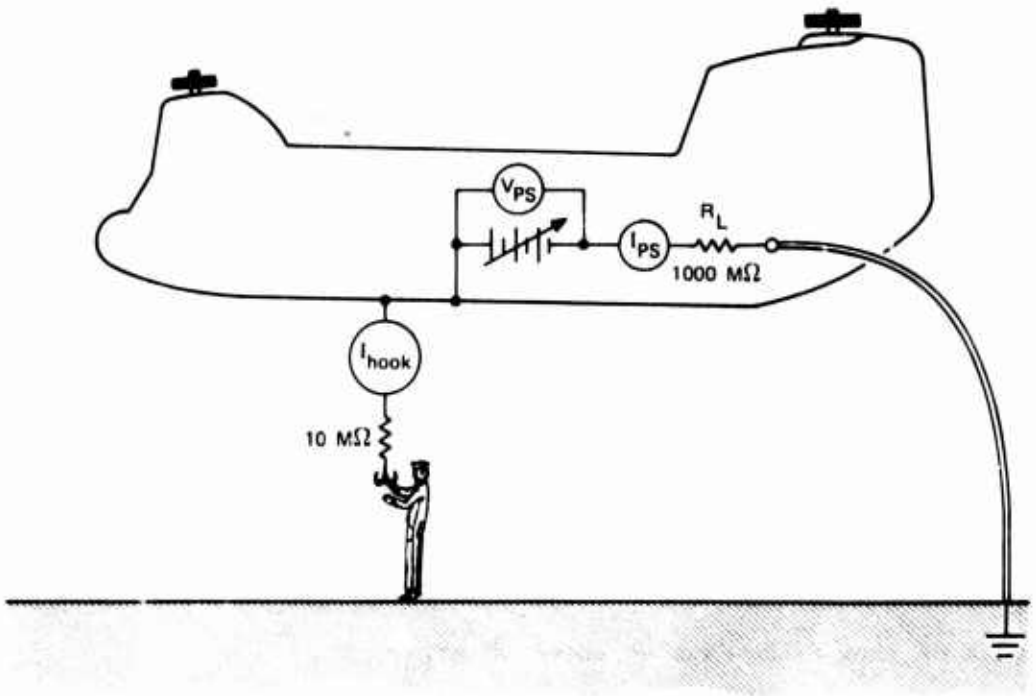

FIGURE 73 HELICOPTER CONFIGURATION USED TO EVALUATE SERIES RESISTANCE IN CARGO-HOOK LINE TO PROTECT HANDLER

previous test above. At 30 kV the subject felt nothing, but by 80 kV a burning sensation could be felt in the fingers. At 120 kV the burning sensation had increased in intensity to the point at which the subject considered the sensation equivalent to a severe shock and did not want to continue.

The two tests confirmed earlier suspicions about the levels of tolerable shock and clearly demonstrated that the residual aircraft potentials obtained during the grounding-line and grounding-pole evaluations were reasonable and should provide the cargo handler with a reasonable degree of safety from shock. A 5- to 10-MΩ series resistance results in a good compromise; the residual potentials are kept low for moderate charging currents, while at the same time the handler is provided current protection for most of the anticipated potential levels.

An experiment related to the shock tests was performed to determine what personnel protection, if any, should be recommended to ensure maximum safety for the cargo handler. Since most military boots are of rubber-soled construction, it was conceivable that a handler could charge himself up to the point where the soles of his boots would breakdown, thereby defeating some of the safety the grounding line offered if the breakdown potential was high enough.

The experiment consisted of determining the breakdown potential of a pair of typical rubber-soled boots by connecting the voltage power supply between a ground stake anchored in concrete and the inside of the boot, which was resting on concrete. Two boots were used for these tests and both of them broke down at about 30 kV.

The implications of these tests are that conductive-soled boots could probably prevent an unpleasant shock in some isolated circumstances, but generally, their use would be of little benefit. If the helicopter had been previously grounded by use of the grounding line or grounding pole, the handler, wearing rubber-soled boots, would probably receive very little shock because of the low residual potential of the helicopter, as described earlier. If the handler, again wearing rubber-soled boots, were to touch the grounding line containing the series resistor, he could charge to 30 kV and discharge would occur. The shock felt during this

discharge would be small, however, because of the low capacity (and hence, discharge energy) of the human body.

VI RADIO-FREQUENCY INTERFERENCE PRODUCED BY THE GROUNDING-LINE CORONA ELEMENT

Present and future helicopter avionics systems include LF and VLF navigation equipment such as OMEGA, LORAN C/D, and the more common ADF. It is known that radio-frequency interference (RFI), produced by one or more sources of electrical noise can have serious effects on these systems. Loran C/D, for example, becomes "unlocked" when exposed to RFI for more than a few seconds, requiring a lengthy setup period to get it working again. One type of RFI that can produce these error-causing effects is corona, which can be produced by the aircraft when operating in a triboelectric environment. Corona is a series of minute discharges occurring from a region of intense electric field. Corona occurs from places such as sharp-pointed extremities (e.g., rotor-blade tips, trailing edges) or from protruding pitot tubes, antennas, and so on.

For a complete description of corona, and its effects on fixed-wing aircraft, the reader is referred to earlier SRI reports.[8,9]

Since several of the terminations used on the grounding-line discharge system were of a design that would produce corona at relatively low potentials, it was necessary to determine the extent to which this corona would produce RFI, which could interfere with low-frequency navigation and communication systems.

In order to examine the RFI produced by the discharger terminations, a Hewlett-Packard spectrum analyzer was installed aboard the aircraft and configured as shown in Figure 74, connected through an HP 465 preamplifier to an antenna installed on the belly of the helicopter.

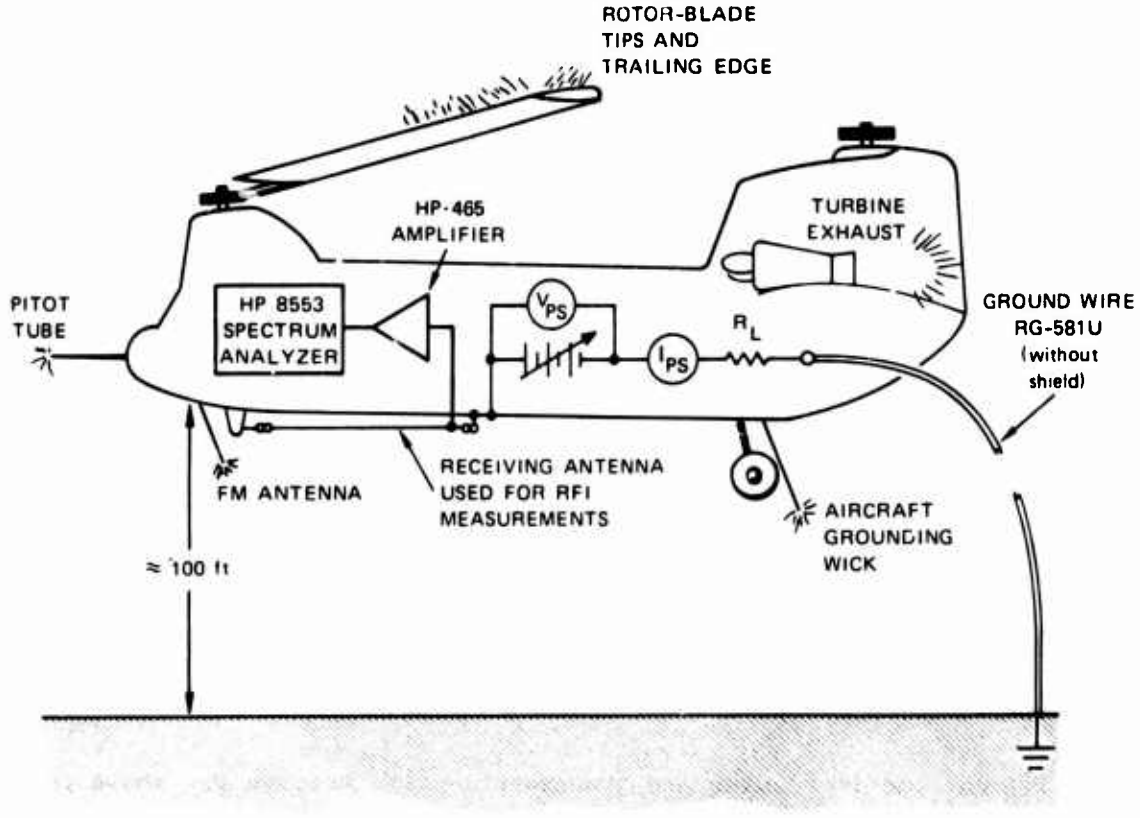

FIGURE 74 HELICOPTER CONFIGURATION USED DURING RFI MEASUREMENT PROGRAM SHOWING POSSIBLE CORONA-PRODUCING AREAS

Corona was produced by using the high-voltage power supply to simulate triboelectric charging and raise the helicopter to the desired potential. A hover altitude of 100 ft assured that the grounding line with its corona termination section could be lowered far enough below the aircraft to prevent shielding of the discharge by the airframe, and allowed the discharge from the termination to be easily detected by the spectrum analyzer as long as the rest of the aircraft was fairly quiet.

Pre- and post-flight system calibrations were made for every sortie flown utilizing the spectrum analyzer. A measure of the efficiency of a receiving system is its ability to discern atmospheric noise above instrument noise. Accordingly, one of the pre- and post-flight checks was to observe a receiver noise spectrum made after disconnecting the antenna and comparing it to the "system" spectrum obtained with the antenna connected. If the receiver noise spectrum was sufficiently low so that atmospheric noise could be observed above the receiver noise, the antenna, preamp, and spectrum analyzer were deemed adequate to make the test. In fact, if the background atmospheric noise is observable, any further attempt to decrease the receiver noise is a waste, since the atmospheric noise places a lower bound on the observable signal.

Typical receiver noise and atmospheric noise spectra are shown in Figure 75. It is observed from this figure that the 0-to-200-kc frequency range contained many coherent broadcast and beacon stations. The actual number of these present and their relative amplitude varied from day to day, and depended on helicopter altitude and location. Before every test described below, however, baseline data were obtained at the location and hover altitude to be used for the test. It should be noted that the actual "atmospheric" noise lies in the null regions between the received stations.

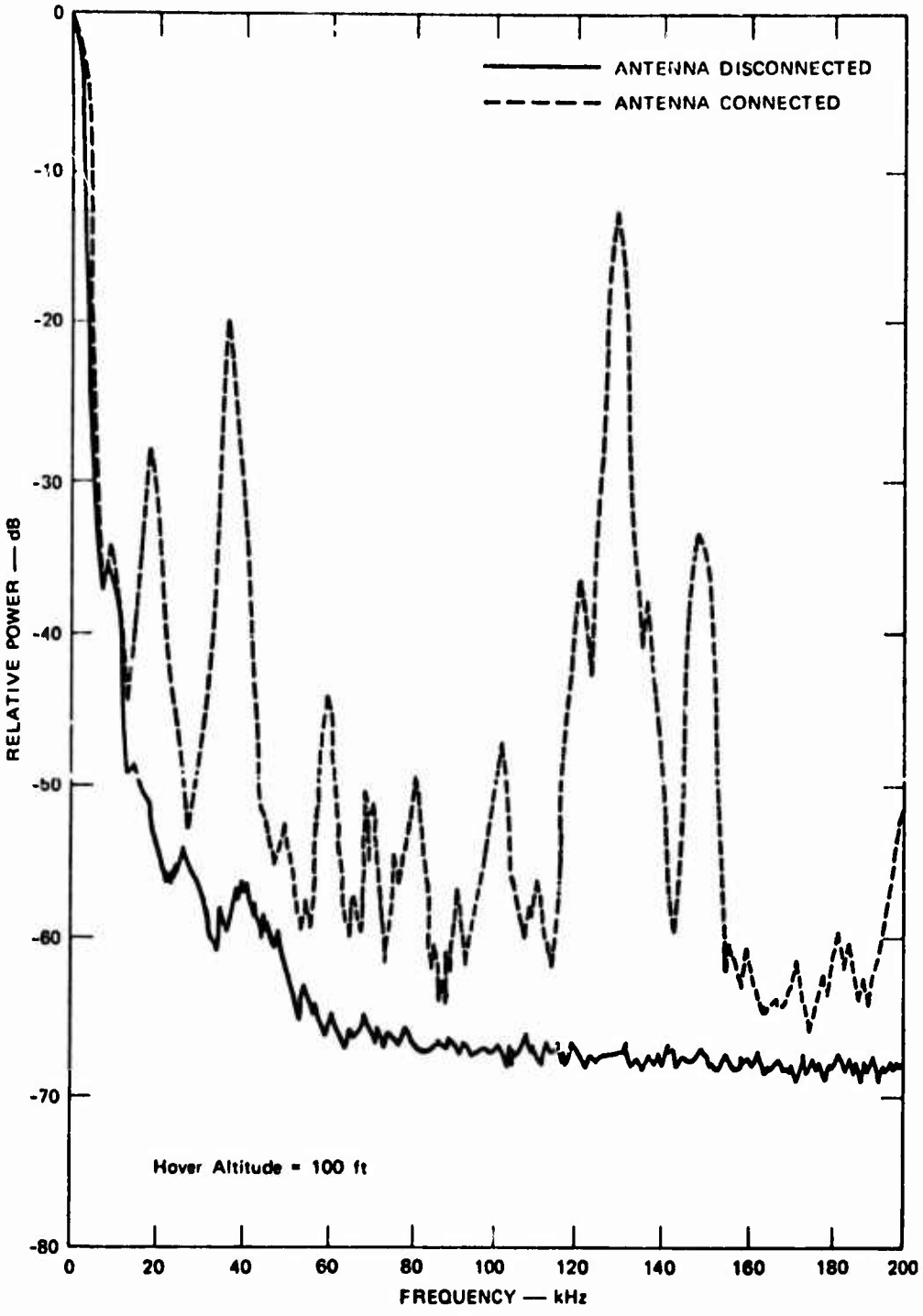

FIGURE 75 TYPICAL SYSTEM NOISE SPECTRUM SHOWING COHERENT BROADCAST AND BEACON STATIONS ABOVE AMPLIFIER/RECEIVER NOISE SPECTRUM

In order to examine the RFI produced by the corona termination hanging from the end of the grounding line, it was necessary to examine RFI produced by the aircraft and to minimize it within the capabilities and scope of this program. Figure 76 shows typical spectra obtained by raising the helicopter potential to 100 kV, 150 kV, and 200 kV, and recording spectra for each of these. The zero-volt spectrum is not shown, because it was only slightly different from the 100-kV spectrum; the power-supply microammeter indicated that corona current began at about 75 to 90 kV, and hence the only real difference is in the peak-to-peak fluctuations of the spectrum at a given frequency.

With the exception of Figure 75, the figures in this section represent only a "best fit" to the data, to allow the reader to observe significant features in the spectrum. In fact, the actual corona spectrum data are quite noisy and not at all smooth, as the figures would indicate. Next to the figure legend, the magnitude of these fluctuations for each voltage is shown; it can be seen, for example, that the peak-to-peak fluctuation of the 200-kV helicopter spectrum of Figure 76 is 10 to 20 dB.

These data indicated that it would be fruitless to attempt to measure the RFI effects of a corona termination in the presence of so much noise generated by corona discharges from the helicopter itself, and steps would have to be taken to reduce the noise.

In order to ensure that the noise spectra observed were attributable to the helicopter, and not the power supply, associated instrumentation, or ground wire, a series of tests were conducted concurrently with the RFI tests. One such test utilized an antenna mounted inside the helicopter close to the power supply and grounding wire and connected to the amplifier-spectrum analyzer. During another check, the grounding wire was brought in close proximity to the RFI antenna mounted on the fuselage belly. No increase in the spectrum was observed during any of these tests,

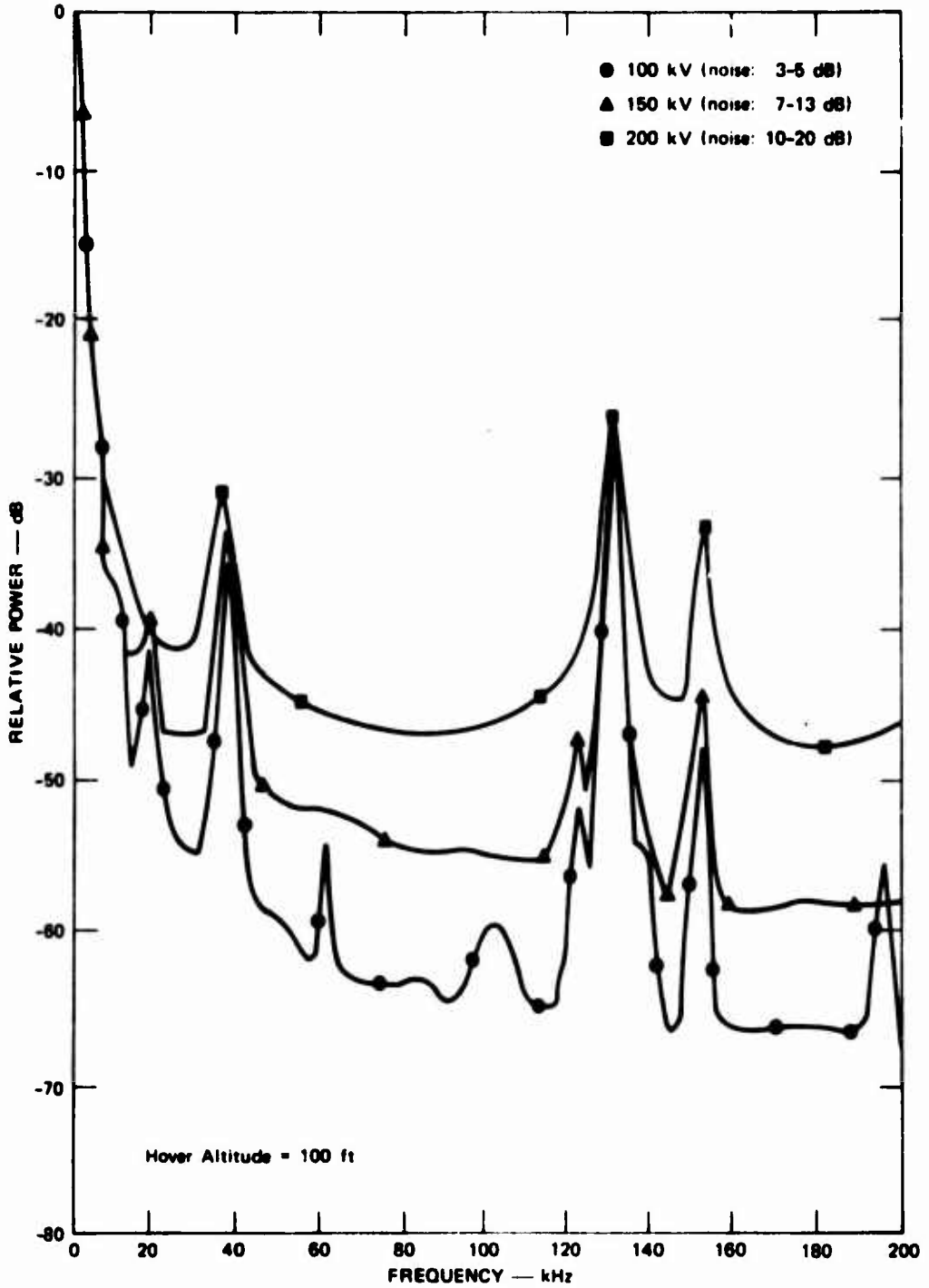

FIGURE 76 HELICOPTER NOISE SPECTRA FOR VARIOUS HELICOPTER VOLTAGES

or during other tests when the aircraft potential was raised as high as 200 kV. These tests indicated that the increases observed in the noise spectrum during regular RFI testing were coming from the aircraft, and not from the high-voltage system.

This helicopter noise occurred throughout the remainder of the testing even though precautions were taken to eliminate some of the more obvious corona-producing points on the helicopter. The end of the FM antenna was heavily taped to prevent corona from the tip, and the grounding wick located near the aft, port landing-gear assembly was effectively removed by taping it up close to the fuselage.

Subsequent to these findings, a Safety-of-Flight release was requested by Boeing Vertol and granted by the U.S. Army Aviation Test Board to install Granger Associates model 611-1D orthodecoupled P-static dischargers to the trailing edges of the rotor blades in accordance with U.S. Army ECOM drawing No. ES-C-202998. For a complete description of the theory of P-static dischargers, the reader should consult Nanevicz, et al.[13] These dischargers were attached according to the drawing, and the trailing edges of the rotor blades were electrically connected to the leading edges (and, hence, airframe) by a coating of "Aqua-Dag E" (a colloidal suspension of carbon particles). After the "Dag" has dried, the resistance between the rotor-blade trailing edges and airframe was no more than 2 kΩ. The original intent was to paint the entire blade surface with Dag. Since the RFI tests were to be performed using artificial charging only, no frictional charging would be occurring on the blade and a strip of Dag between the leading and trailing edge was deemed sufficient. Figure 77 shows the installation of the trailing-edge dischargers on one of the blades, and the Dag strip applied to the blade.

It was believed that under these conditions the charge that accumulated on the aircraft would bleed away through the discharge and thus

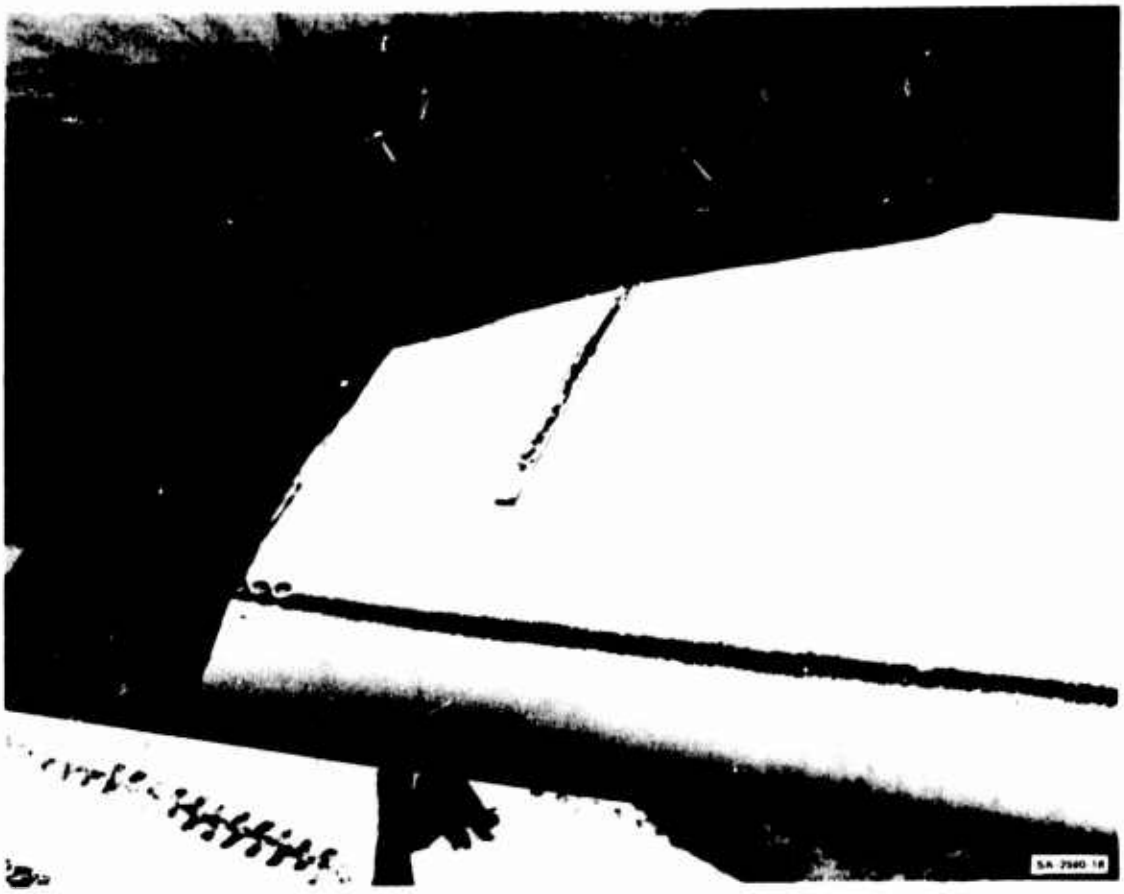

FIGURE 77 PHOTOGRAPH SHOWING PAINTED STRIPE OF "AQUA-DAG E" ON CH-47 BLADE AND INSTALLATION OF GRANGER ASSOCIATES 611-1D P-STATIC DISCHARGERS ON ROTOR-BLADE TRAILING EDGE

quiet the otherwise (electrically) noisy aircraft. This turned out to be only partially true.

Figure 78 shows corona-noise spectra for helicopter potentials of 100, 150, and 200 kV, obtained during tests with the dischargers attached to the trailing edges. It can be seen that the noise decrease achieved by using the trailing-edge dischargers was, perhaps, 10 dB over most of the frequency band. A significant decrease was obtained, however, in the peak-to-peak fluctuations in the spectrums. The 200-kV spectrum of Figure 78 for example, shows fluctuations of 3 to 5 dB, whereas the

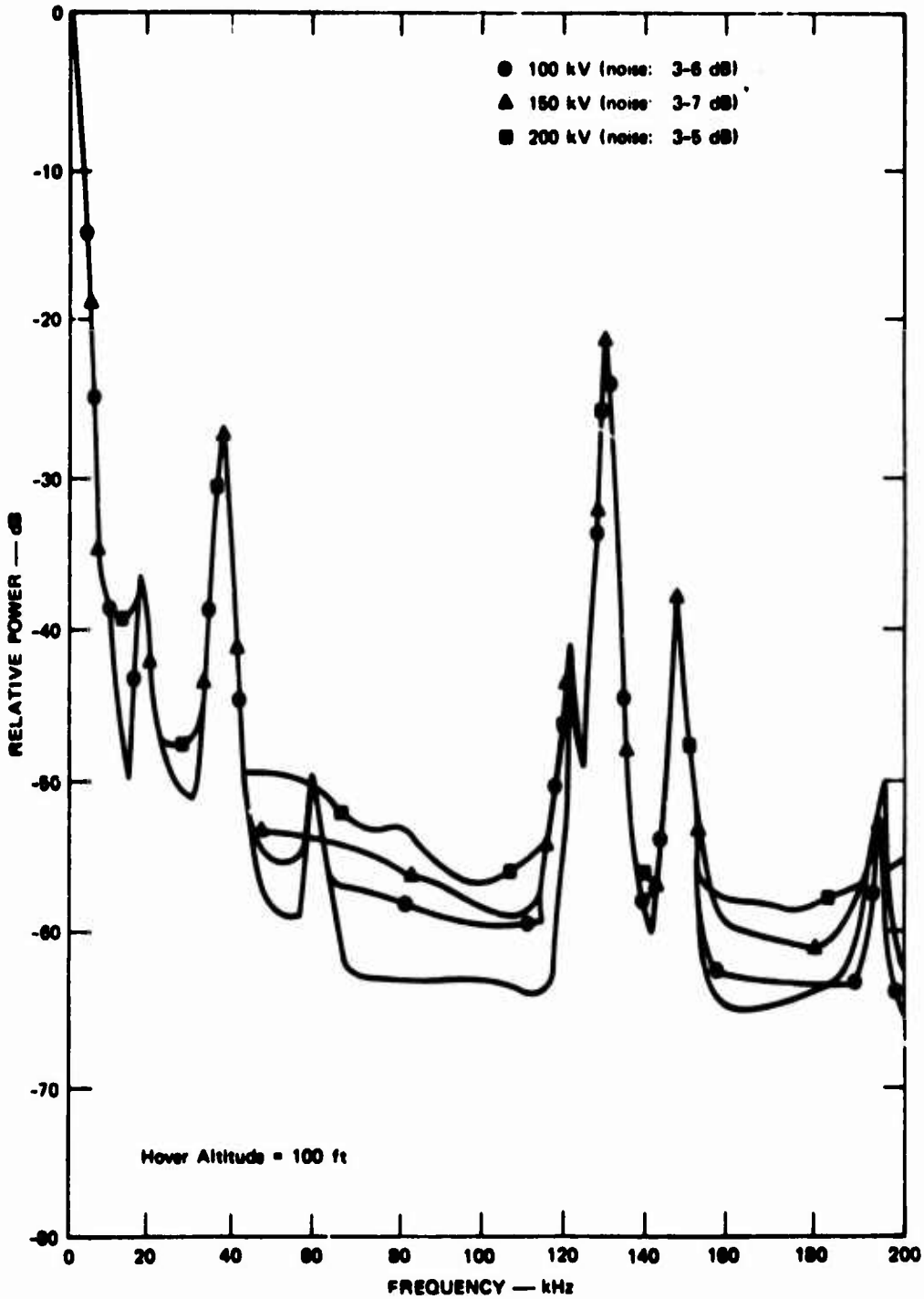

FIGURE 78 NOISE SPECTRA FOR VARIOUS HELICOPTER VOLTAGES DURING OPERATION WITH P-STATIC DISCHARGERS MOUNTED ON TRAILING EDGE OR ROTOR BLADES

spectrum of the unprotected helicopter (Figure 79, shows fluctuations of 10 to 20 dB.

Since there was still significant helicopter noise, it was argued that perhaps a better location for the dischargers was at the blade tip, since the tip is a truncated airfoil section and contained many sharp edges. Also, since this is a region of low pressure the discharge should occur at lower field strengths[14] and, hence, lower aircraft potentials. A Safety-of-Flight release was obtained for these tests and the spectra were measured using both the trailing-edge dischargers and the tip dischargers are shown in Figure 79. A comparison of Figure 79 with Figure 78 shows very little improvement in the spectrum. Figure 80 shows a photograph of the trailing-edge and tip discharger installation.

Although RFI data were not taken during dust sorties, it was observed that the sintered tungsten ends of the P-static dischargers were badly damaged after about one-half hour of operation in the dust. Apparently, collisions with dust particles tended to chip the brittle tips rather than wear them smoothly. During the RFI testing, care was taken to ensure that, although some tips were broken, enough good dischargers were installed to make the evaluation meaningful. Future helicopter operations, however, performed in other than a particle-free environment with discharger-protected blades should consider a less brittle type of discharger needle such as steel, or the dischargers should be oriented in such a way as to shield the pins from the impinging particles.

It should be noted here that during these tests the helicopter pilots reported massive RFI indications in the audio channel of the ADF (the loop function was not tested), and frequently reported UHF RFI during tests at high voltage. Since some spectral noise persisted even after P-static dischargers were attached to the blades, it can only be assumed that other locations on the helicopter were causing the RFI,

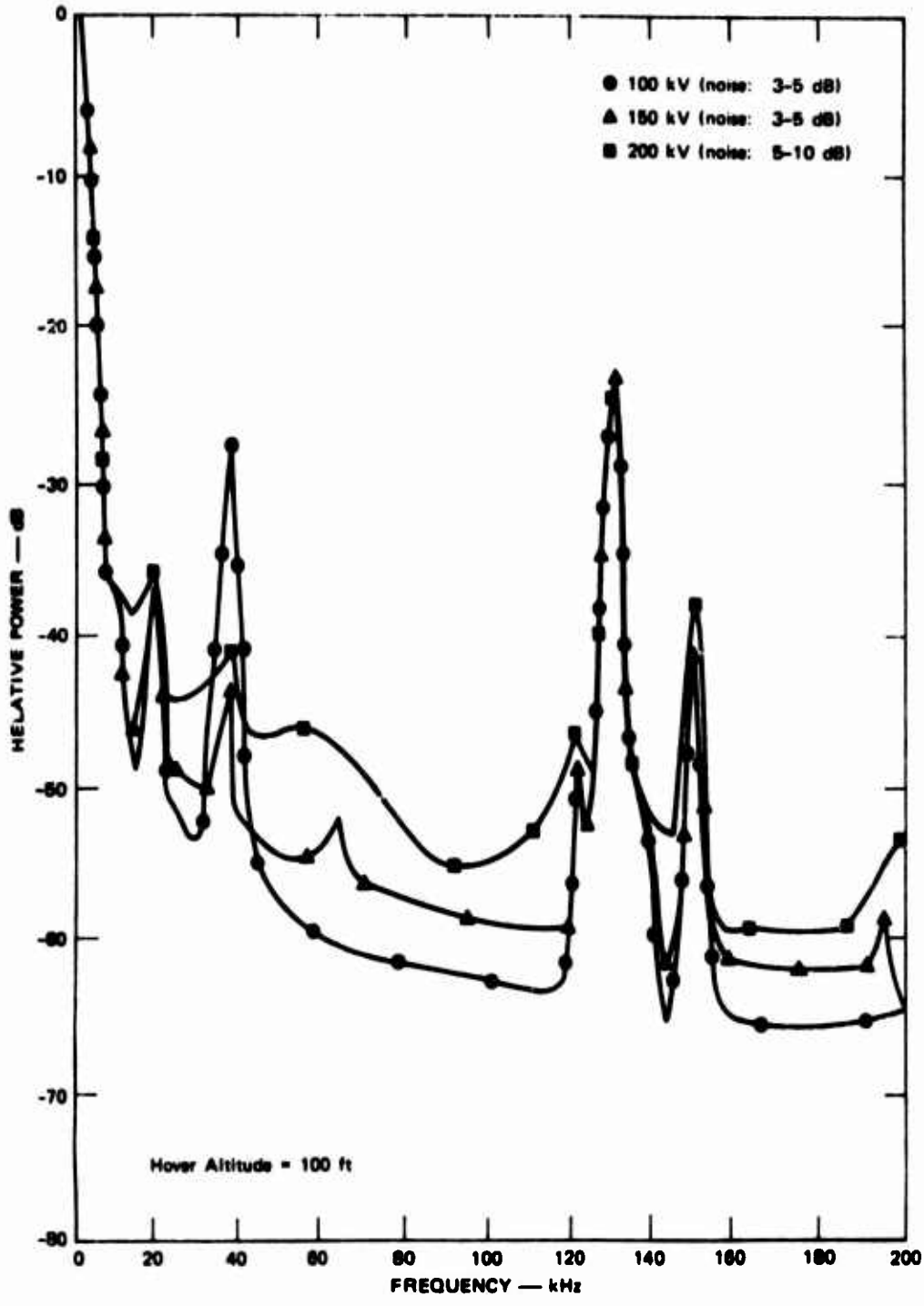

FIGURE 79 NOISE SPECTRA FOR VARIOUS HELICOPTER VOLTAGES DURING OPERATION WITH P-STATIC DISCHARGERS MOUNTED ON THE TRAILING EDGES AND TIPS OF THE ROTOR BLADES

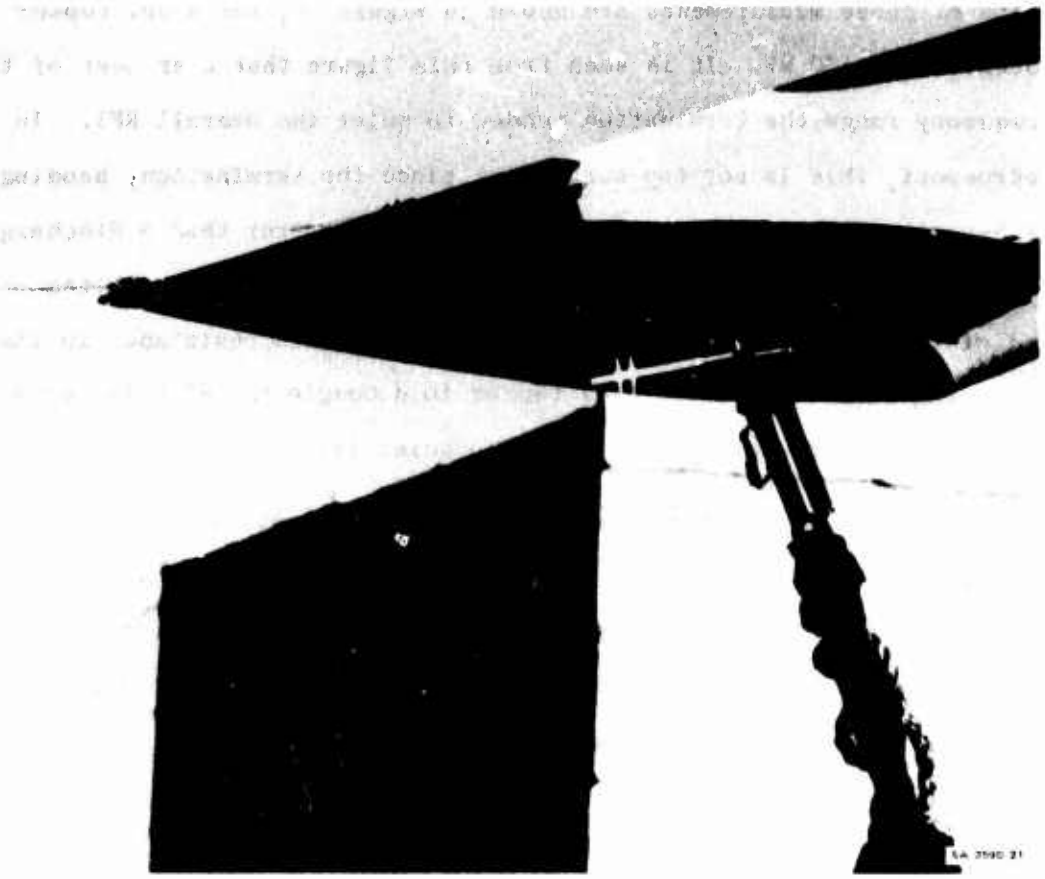

FIGURE 80 PHOTOGRAPH SHOWING GRANGER ASSOCIATES 611-1D P-STATIC DISCHARGER ATTACHED TO THE TIP OF A CH-47 ROTOR BLADE

such as the pitot tube, UHF antennas, FM antennas, or other areas. The location and identification of RFI source regions is time-consuming and difficult, at best. Since it was beyond the scope of this program to identify and quiet these areas, no additional effort was expended in attempts to reduce radio-noise levels.

Since the dischargers reduced the noise by, perhaps 10 to 20 dB over the unprotected helicopter, it was decided to attempt to measure the corona noise of the grounding-line termination. The termination chosen for this measurement was the so called "corona brush," a bundle

of fine, flexible wires fanned out into a brush configuration. The results of these measurements are shown in Figure 81, for a helicopter potential of 150 kV. It is seen from this figure that over most of the frequency range the termination tended to quiet the overall RFI. In retrospect, this is not too surprising since the termination, hanging 50 ft beneath the helicopter, will go into corona sooner than a discharger of similar radius (because the electric field strength terminating on the end of the brush is higher), and because the series resistance in the grounding line (≈ 20 to 40 MΩ) tended to decouple the RF noise generated by corona from the brush, and hence to quiet it.

Similar tests performed with the other terminations (chain, and 10-inch-diameter ball) showed no overall increase or decrease in the noise spectrum and it can be assumed, therefore, that none of these devices would degrade the performance of NAV/COM systems beyond the degradation stemming from helicopter RFI alone.

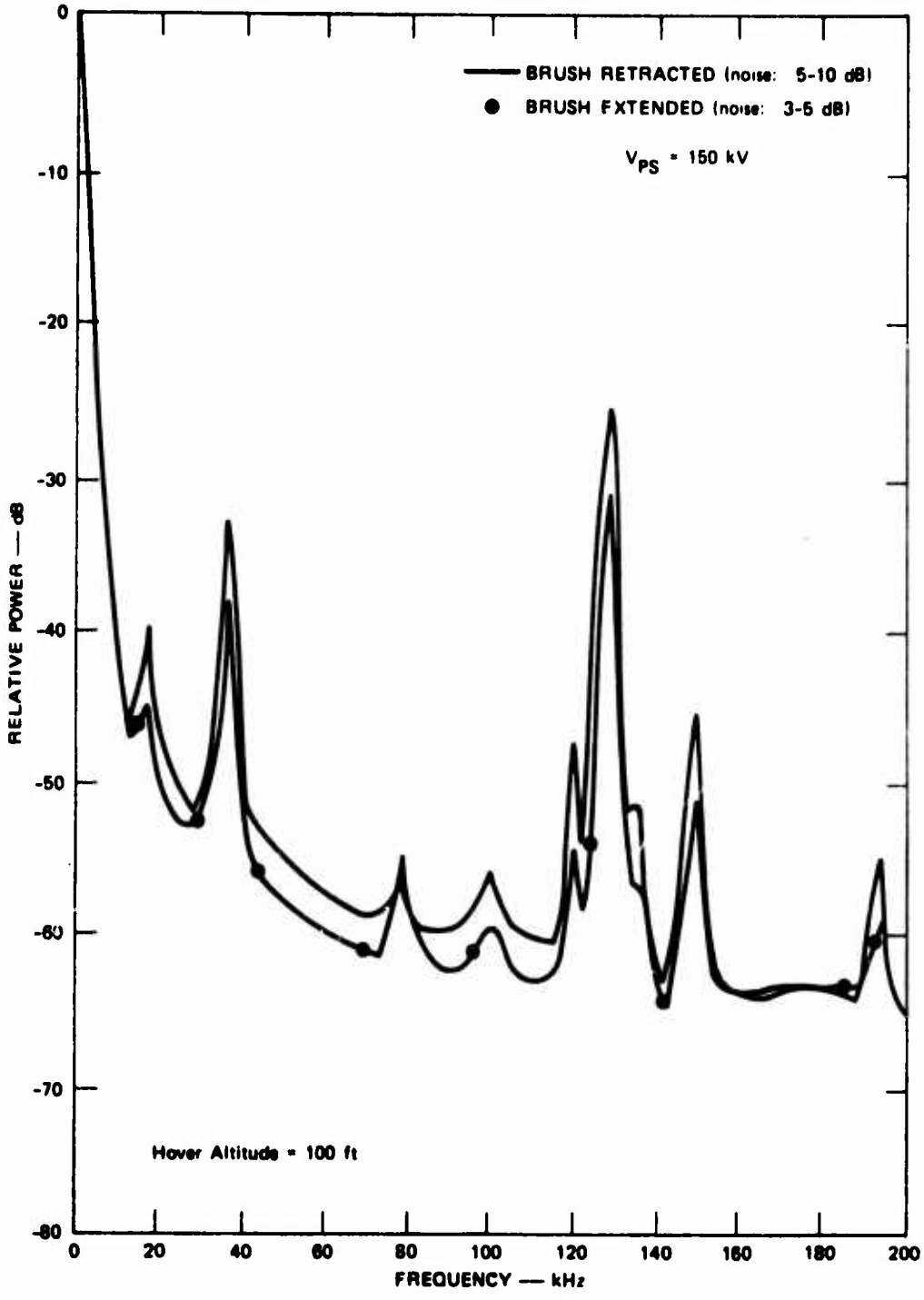

FIGURE 81 NOISE SPECTRA MEASURED FOR CORONA TERMINATION ON GROUNDING LINE EXTENDED TO ≈50' BELOW THE HELICOPTER AND FOR TERMINATION RETRACTED INTO AIRCRAFT

VII ELECTRIC-FIELD-METER DATA

As explained earlier, six electric field meters were used to obtain data about the dust cloud--one on the nose of the helicopter, and five on the ground.

A. Airborne Field Meter

The data from the airborne field meter, obtained during sorties flown in the dust, were statistically analyzed and compared to earlier SRI dust-cloud measurements.[2]

A potential histogram is shown in Figure 82. The solid line in the figure represents the potential distribution inferred from the

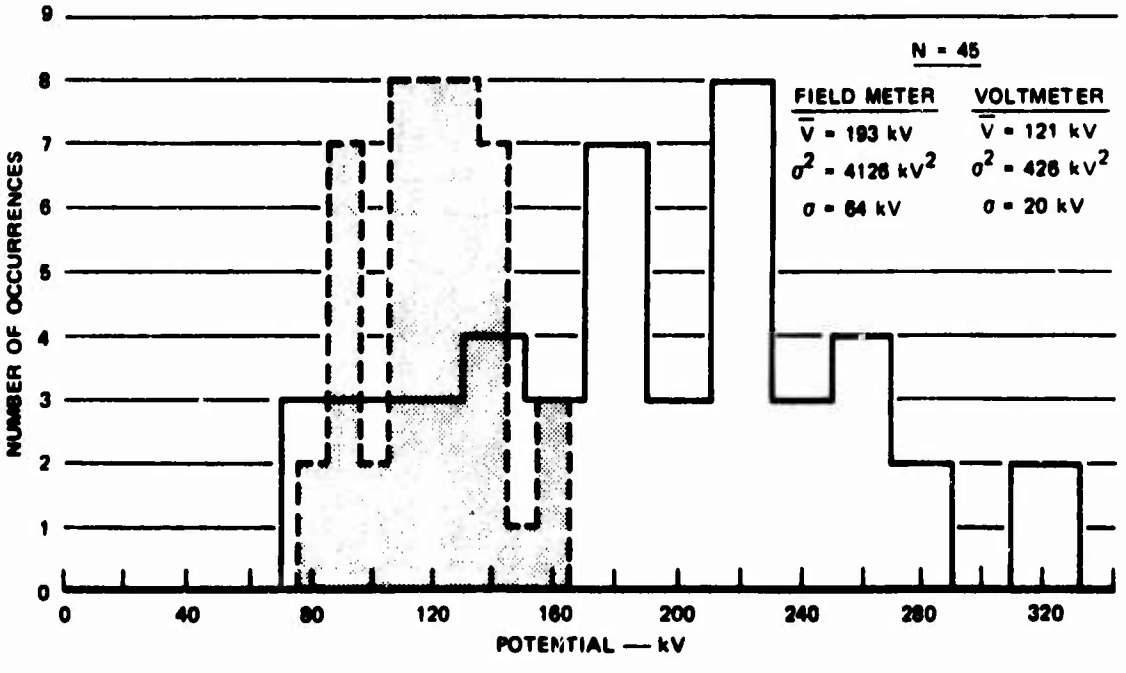

FIGURE 82 A COMPARISON OF POTENTIAL HISTOGRAMS GENERATED FROM DUST HOVER DATA

nose-mounted field meter on the helicopter. The shaded area represents a distribution of the actual helicopter potential measured by the parallel-plate voltmeter. The marked difference between these two distributions indicates the magnitude of the sensing errors produced by the charged dust cloud. The numerical difference between the field-mill-inferred potentials and the actual potentials was calculated and a distribution drawn. These data, shown in Figure 83, can be compared with

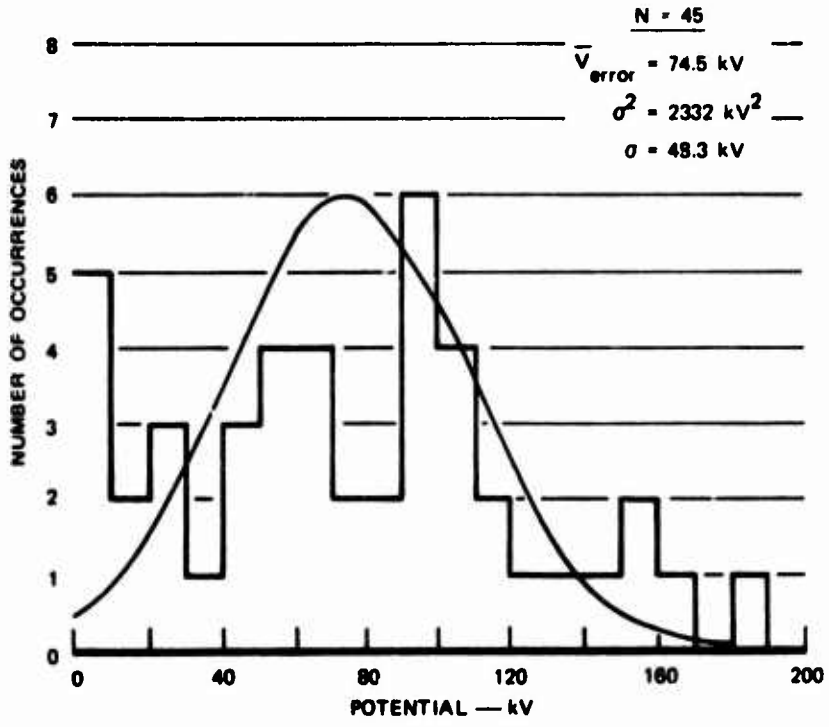

FIGURE 83 POTENTIAL-DIFFERENCE HISTOGRAM INDICATING DUST-CLOUD-INDUCED ERRORS MEASURED BY A HOVERING HELICOPTER

the data in Appendix II. A comparison of the means shows that the mean of the recent data is about twice that of the earlier data, and the standard deviation of the present data is about three times greater then the previous data.

The difference in means is attributable to the difference in charging currents, which was also about a factor of 2 greater than the currents obtained during the previous tests, as illustrated in Figure 84. Since

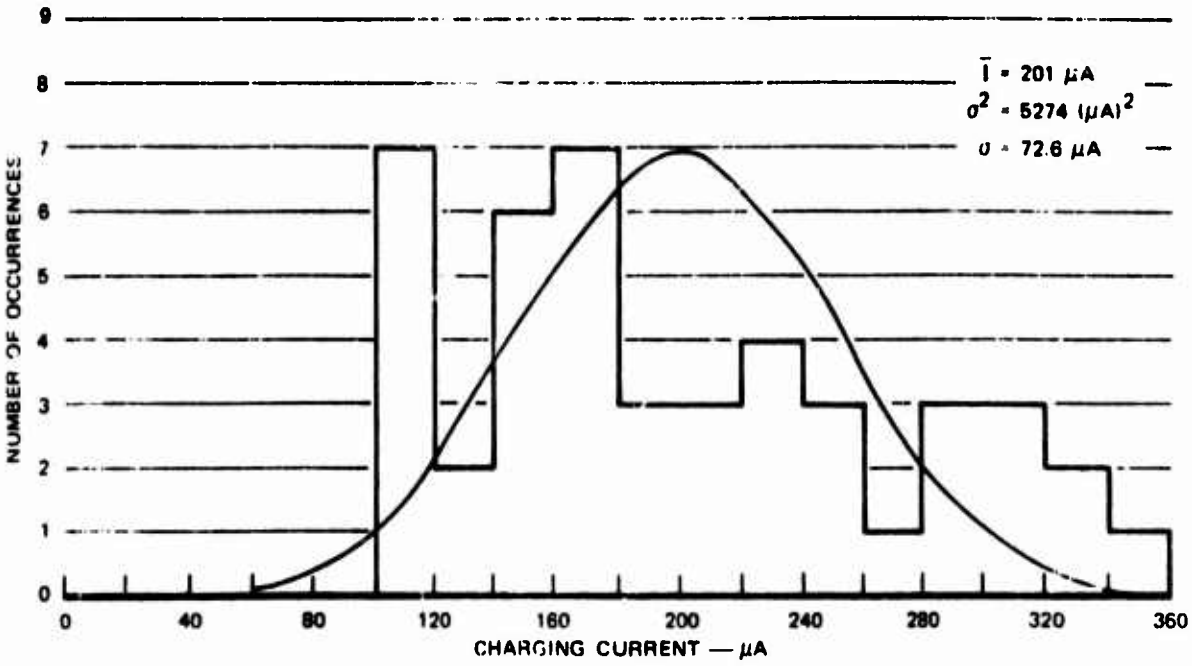

FIGURE 84 CHARGING-CURRENT HISTOGRAM

the standard deviations of the current histograms are the same, it is felt that differences in the deviations of the potential distributions are attributable to the fact that fewer sample points were used in the analysis of the present data.

B. Ground Field Meters

The data from the ground array of field meters were subjected to the same statistical analysis as the airborne data. Figures 85 through 89 show the simultaneous field histograms obtained from the ground field meters. It can be seen from these figures that the data obtained from near the helicopter generally has a wide variance, attributable to the turbulent nature of the rotor wash. The variance of the mill 500 ft away from the helicopter, however, exhibits a small variance, which indicates that the dust cloud surrounding the No. 3 mill was fairly uniform in charge density. The data obtained from the field meter farthest away

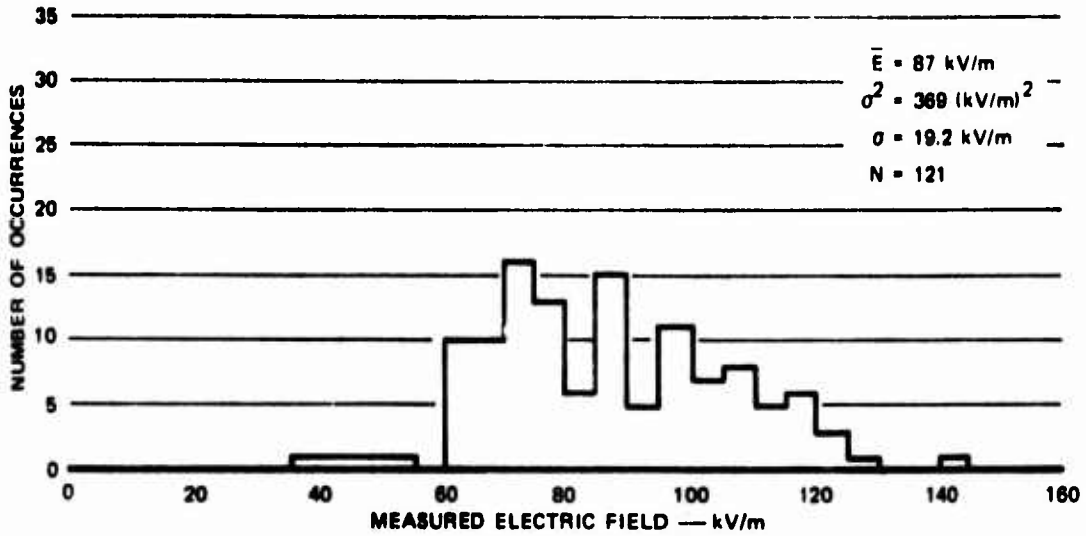

FIGURE 85 ELECTRIC-FIELD HISTOGRAM DATA
Ground Field Meter No. 1.

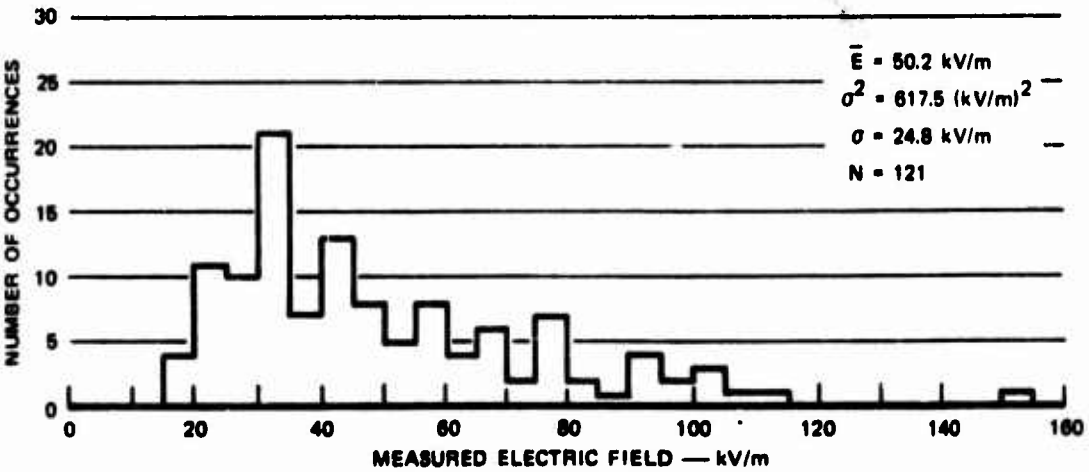

FIGURE 86 ELECTRIC-FIELD HISTOGRAM DATA
Ground Field Meter No. 2.

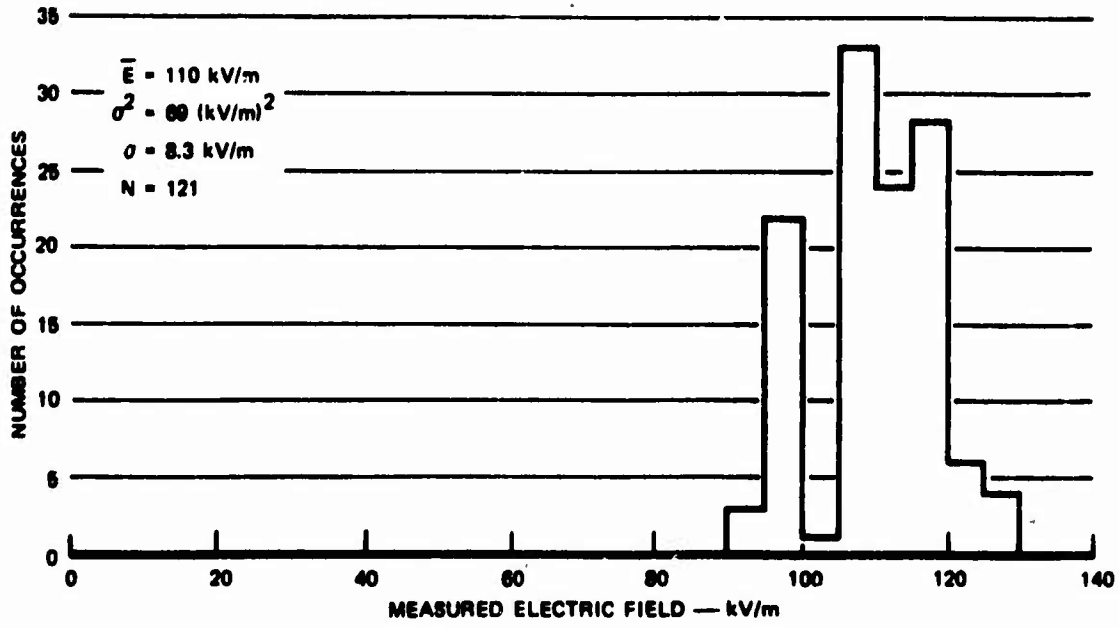

FIGURE 87 ELECTRIC-FIELD HISTOGRAM DATA
Ground Field Meter No. 3.

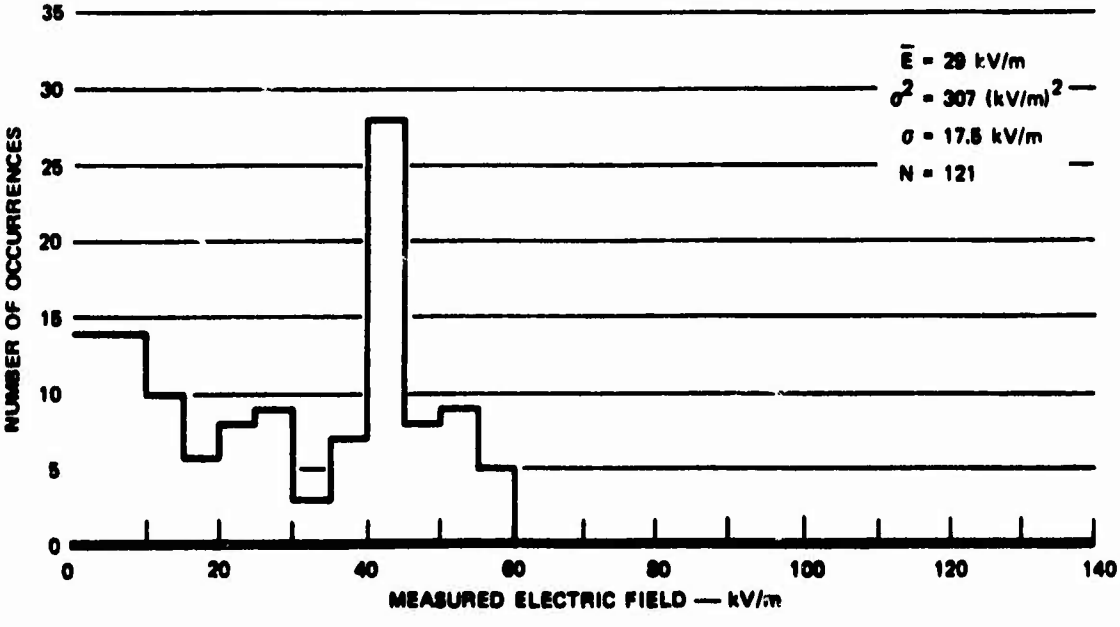

FIGURE 88 ELECTRIC-FIELD HISTOGRAM DATA
Ground Field Meter No. 4.

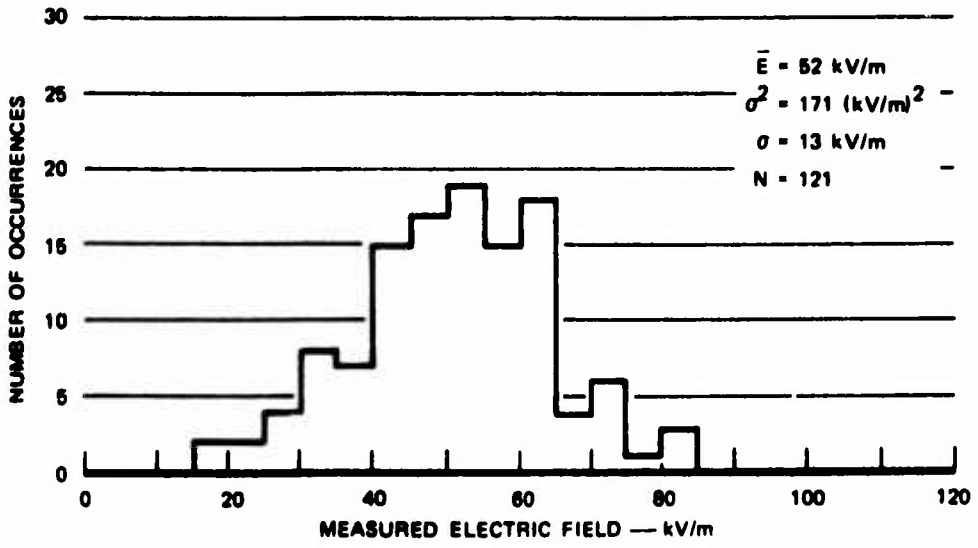

FIGURE 89 ELECTRIC-FIELD HISTOGRAM DATA
Ground Field Meter No. 5.

from the helicopter (No. 4) shows a definite peak in the histogram, with a rather broad shoulder on the low side of the peak. The total time duration of these data is about 2-1/2 min, and the No. 4 mill required about 1 to 1-1/2 min to achieve a steady-state condition. The data obtained after the steady-state condition was reached, although not presented here, exhibited a small variance, indicating that the dust cloud was uniform.

Since the dust cloud was bigger than expected, the field-meter spacing used resulted in undersampling of the cloud. This precluded definitive statements about the cloud's density gradient. Figure 90, however, is a plot of the mean values for the data shown in the previous figures plotted against distance from the helicopter. It can be seen from this figure that a null region exists somewhere around 200 ft from the helicopter and that the cloud's charge density is higher on either side of that point. It can also be seen from this figure that extrapolation of the data yields a well developed dust cloud over 1000 ft in radius.

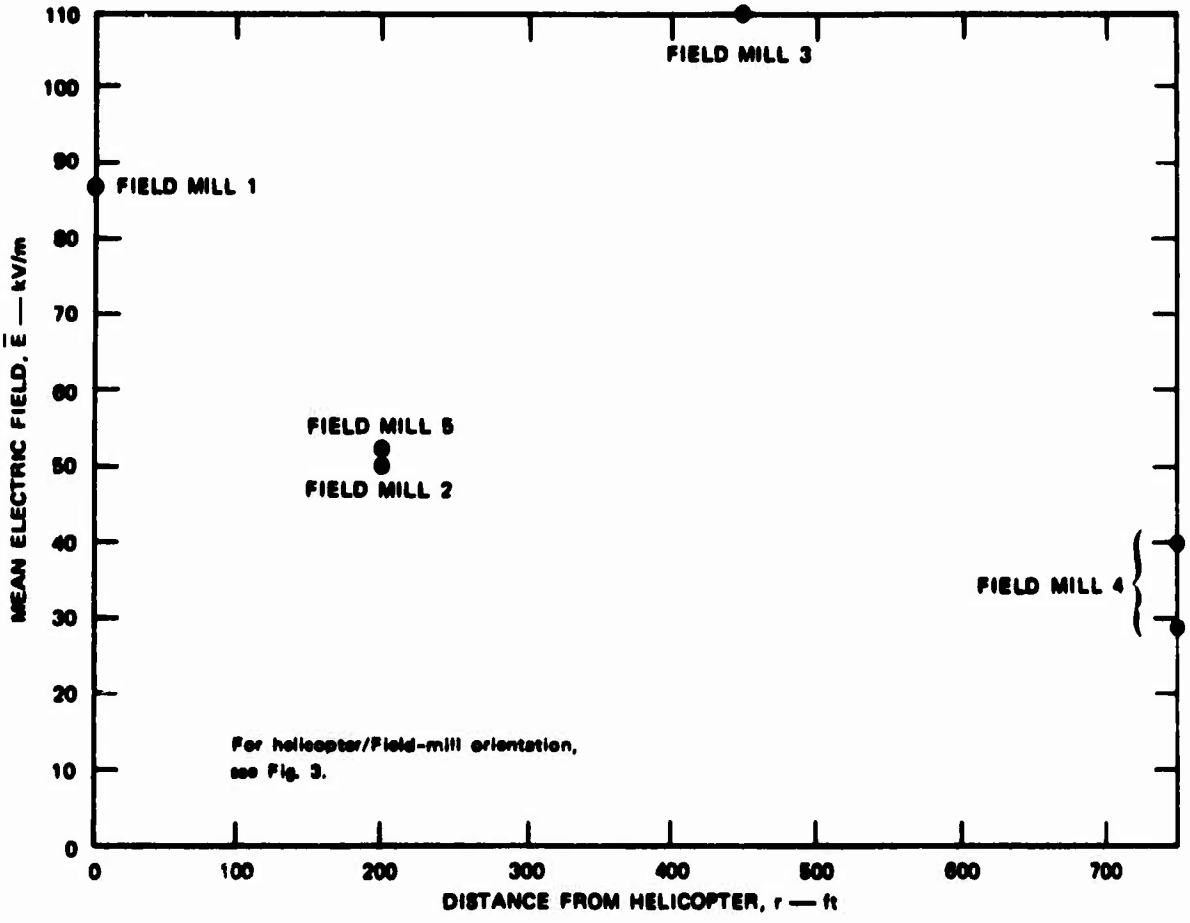

FIGURE 90 MEAN ELECTRIC FIELD OF DUST CLOUD AS A FUNCTION OF DISTANCE FROM HELICOPTER — PHILLIPS DROP ZONE

VIII DEMONSTRATION PROGRAM

At the conclusion of the evaluation phase of the program a demonstration of grounding techniques was provided to representatives of the U.S. Army and the Boeing Company, Vertol Division. The demonstration consisted of practical situations during which the cargo (a CONEX container) and the simulated cargo hook were touched and manipulated by the test witnesses after the helicopter had been discharged by using several of the techniques described earlier.

Present during the demonstration program were Mr. J. Vichness and S. Poteate from the U.S. Army AMRDL; Mr. F. Koch from the U.S. Army AVSCOM; Mr. N. Rothman, Mr. B. J. Solak, and Mr. G. Wilson of Boeing/Vertol; in addition to SRI and flight-crew personnel. Messrs. Koch and Solak volunteered to verify the discharging results by touching the cargo or hook to determine what shock effects, if any, would be felt by a cargo handler during actual Army cargo operations.

The natural-charging demonstrations were performed in the Phillips Drop Zone. The test data show that before the helicopter was discharged by either the grounding line or pole, the helicopter potential reached about 130 kV. Subsequent to the discharging the potential was reduced to less than 1 kV and Mr. Koch and Mr. Solak felt no sensation whatsoever when they touched the simulated cargo hook.

Artificial-charging tests were performed over concrete, asphalt, and hard-packed desert, and were designed to operate at the anticipated HLH charging level of 600 μA, with an initial helicopter potential of about 150 kV. Both the grounding line and grounding pole were used, separately, to discharge the helicopter during these tests. The CONEX container was

similarly discharged using the grounding pole while the helicopter was hovering over concrete. During these tests, only macadam produced a "sensible shock," felt by both Mr. Koch and Mr. Solak, which agrees with the expected results obtained earlier. The hard-packed desert produced a similar, but less intense shock. The subjects felt no sensation at all when the discharging was accomplished over concrete. At the conclusion of the test, both Mr. Koch and Mr. Solak agreed that the grounding techniques used were viable and suitable for actual operations and that the shocks they did feel were well within acceptable limits.

IX CONCLUSIONS

It has been conclusively demonstrated that a passive, resistive grounding-link technique can successfully reduce the potential of an HLH-size helicopter hovering in a triboelectric environment to "safe" residual potentials, even under the most severe of anticipated conditions. These techniques were successfully demonstrated to representatives of the Boeing Company, and the U.S. Army.

A series of RFI measurements were taken to determine the magnitude of the noise produced by the termination hanging from the end of the grounding line. These measurements indicated that the corona produced by the termination did not affect significantly the overall noise level of the helicopter, which was considerable, especially at potentials greater than 150 kV.

The simultaneous aircraft field and aircraft potential measurements conclusively demonstrated the errors obtained by using the field meter to infer aircraft potential. The measurements also confirmed earlier flight-test data indicating that an active discharge system, which relied on remote potential sensing by field meters, was not a viable technique when used in conditions of high triboelectric-charging rates.

The statistical data derived from both the airborne and ground systems indicated that the dust cloud produced by the hovering helicopter during the program was characteristically similar to the cloud reported during SRI's earlier flight-test program in Yuma.

In order that the measurements at YPG could be extended to include most of the probable environments, a series of ground-resistance measurements were made that showed that the resistance of macadam, concrete,

and sand under arid conditions is lower than had generally been believed. The resistance measurements also demonstrated a nonlinear characteristic that would aid discharging under certain conditions.

Since a "safe" level of residual aircraft potential is principally determined by the response of the cargo handlers to electrical shock, a series of shock tests were performed, using human subjects to determine the upper limits of the "safe" regime. It was found that the most severe level of shock that would be considered as "safe" was a discharge energy of about 200 mJ. This corresponds to a CH-47 potential of 20 kV, or an estimated HLH potential of 14 kV. All of the discharger tests performed demonstrated that a residual potential of less than 14 kV could be achieved.

CHRONOLOGICAL SUMMARY OF FLIGHT PROGRAM

The material in this appendix is a chronological summary of the events connected with the flight-measurement program performed under this project, and referred to in the text.

Date (1973)	Flight Number	Oscillograph Record Number	Activity	Flight Time
5/20	—	—	Helicopter arrives at Yuma Proving Grounds.	—
5/21	—	—	SRI and Boeing-Seattle equipment arrives and periodic inspection of helicopter by aircrew begins.	—
5/22	—	—	Installation and ground checkout of airborne equipment. Periodic inspection continues.	—
5/23	—	—	As 5/22.	—
5/24	—	—	Flight test after periodic inspection. SRI and Boeing flight orders OK'd.	—
5/25	1	—	Preliminary airborne equipment checkout and first RFI measurement.	:30
	2	—	Unprotected-aircraft RFI evaluation.	:20
5/26	—	—		
5/27	—	—	Memorial Day week-end; no flight operations.	
5/28	—	—		
5/29	3	2–4	RFI evaluation of discharging-element corona noise in presence of unprotected aircraft.	:25
	4	5–8	As Flight 3.	:20
	5	9–11	Ground-pole evaluation.	:40
5/30	6	12–15	Ground-pole evaluation and RFI measurements.	:20
	7	16	As Flight 6.	:20
	8	17–22	Grounding-line evaluation.	:35

Date (1973)	Flight Number	Oscillograph Record Number	Activity	Flight Time
5/31	9	23-25	As Flight 8.	:30
	10	26-31	Drop-line evaluation under various surface conditions.	:45
	11	32	Testing of physiological reaction to electrical shock.	:20
	12	--	Aircrew familiarization with dust hover operations.	:30
	--	33-34	Rubber-soled-boot electrical breakdown measurements.	--
6/1	13	39-44	Dust-environment measurements of grounding line with various discharger configurations attached.	2:00
6/2	--	--	Week-end; no flight operations.	
6/3	--	--		
6/4	14	45-46	System calibration flight.	:15
	15	47-57	As Flight 13.	1:20
6/5	--	--	Helicopter blades painted with conductive paint. RFI antenna modified. Trailing-edge dischargers attached.	--
6/6	16	62-77	RFI evaluations.	:35
6/7	17	78-81	As Flight 16.	:20
	18	82-87	As Flight 16.	:35
	19	88-90	As Flight 16.	:20
6/8	20	91-101	As Flight 16.	:30
	21	102-103	Testing of physiological reactions to electrical shock.	:20

Date (1973)	Flight Number	Oscillograph Record Number	Activity	Flight Time
6/9	--	--	Week-end; no flight operations.	
6/10	--	--		
6/11	22	104-110	RFI and shock tests.	:45
	23	111-114	As Flight 12.	:45
	24	115-119	RFI evaluation.	:30
	25	120-124	As Flight 24.	:20
6/12	26	125-129	Demonstration of discharging techniques in dust area.	:30
	27	130-135	Demonstration of discharging techniques in clean area.	1:00
6/13	28	136-139	Shock tests.	:20
	29	--	Aborted due to thunderstorm activity.	
6/14	30	140-143	Dust environment measurements under high-charging conditions.	:35
	31	144	RFI evaluation with blade tip dischargers.	:45

REFERENCES

1. "Passive Null Field Dischargers for CH-54 Aircraft," ENSURE Item No. 265, U.S. Army Vietnam, Long Binh, Republic of Vietnam (U).

2. J. E. Nanevicz and D. G. Douglas, "Electric Discharge System," Final Report, Contract CH 700377, SRI Project 1657, Stanford Research Institute, Menlo Park, Calif. (November 1972).

3. J. E. Nanevicz et al., "Experimental Development of Dynamic Static Discharger System for Large Jet Aircraft," AFAL-TR-67-313, SRI Project 6129, Stanford Research Institute, Menlo Park, Calif. (November 1967).

4. J. E. Nanevicz and G. R. Hilbers, "Flight Test Evaluation of an Active Discharger System," Interim Technical Report 1 (Phase II), Contract F33615-68-C-1359, SRI Project 7104, Stanford Research Institute, Menlo Park, Calif. (February 1970).

5. M. C. Becher, "CH-54A Static Discharge Test Program; Evaluation of Dynasciences Active ESD and Granger Passive P-Stat Dischargers," DCR-299, Dynasciences Corporation (Scientific Systems Division), Blue Bell, Penn. (16 April 1969).

6. M. C. Becher, "Investigation of CH-54A Electrostatic Charging and of Active Electrostatic Discharger Capabilities," U.S. Army Aviation Material Laboratories, Fort Eustis, Virginia (January 1970).

7. H. E. Inslerman et al., "Ensure 265 CH-54 (Flying Crane) Electrostatic Discharger Evaluation," ECOM Technical Report ECOM-3120, U.S. Army Electronics Command, Ft. Monmouth, N.J. (April 1969).

8. R. L. Tanner and J. E. Nanevicz, "Radio Noise Generated on Aircraft Surfaces," Final Report, SRI Project 1267, Contract AF 33(616)-2761, Stanford Research Institute, Menlo Park, Calif. (September 1956), AD 109651.

9. R. L. Tanner and J. E. Nanevicz, "Precipitation Charging and Corona-Generated Interference in Aircraft," AFCRL 336, Technical Report 73, SRI Project 2494, Contract AF 19(604)-3458, Stanford Research Institute, Menlo Park, Calif. (April 1961) AD 261029.

10. W. R. Harper, Contact and Frictional Electrification (Oxford University Press, Ely House, London, 1967).

11. C. F. Dalziel, "A Study of the Hazards of Impulse Currents," Proc. AIEE, pp. 1037-1043 (October 1953).

12. C. F. Dalziel and W. R. Lee, "Lethal Electric Currents," IEEE Spectrum, pp. 44-50 (February 1969).

13. J. E. Nanevicz, E. F. Vance, R. L. Tanner, and G. R. Hilbers, "Development and Testing of Techniques for Precipitation Static Interference Reduction," ADS-TR-62-38, SRI Project 2848, Final Report on Contract AF 33(616)6561, Stanford Research Institute, Menlo Park, Calif. (January 1962), AD 272807.

14. J. D. Cobine, Gaseous Conductors, Theory and Engineering Applications (Dover Publications, Inc., New York, N.Y., 1958).

APPENDIX III

GROUNDING LINE

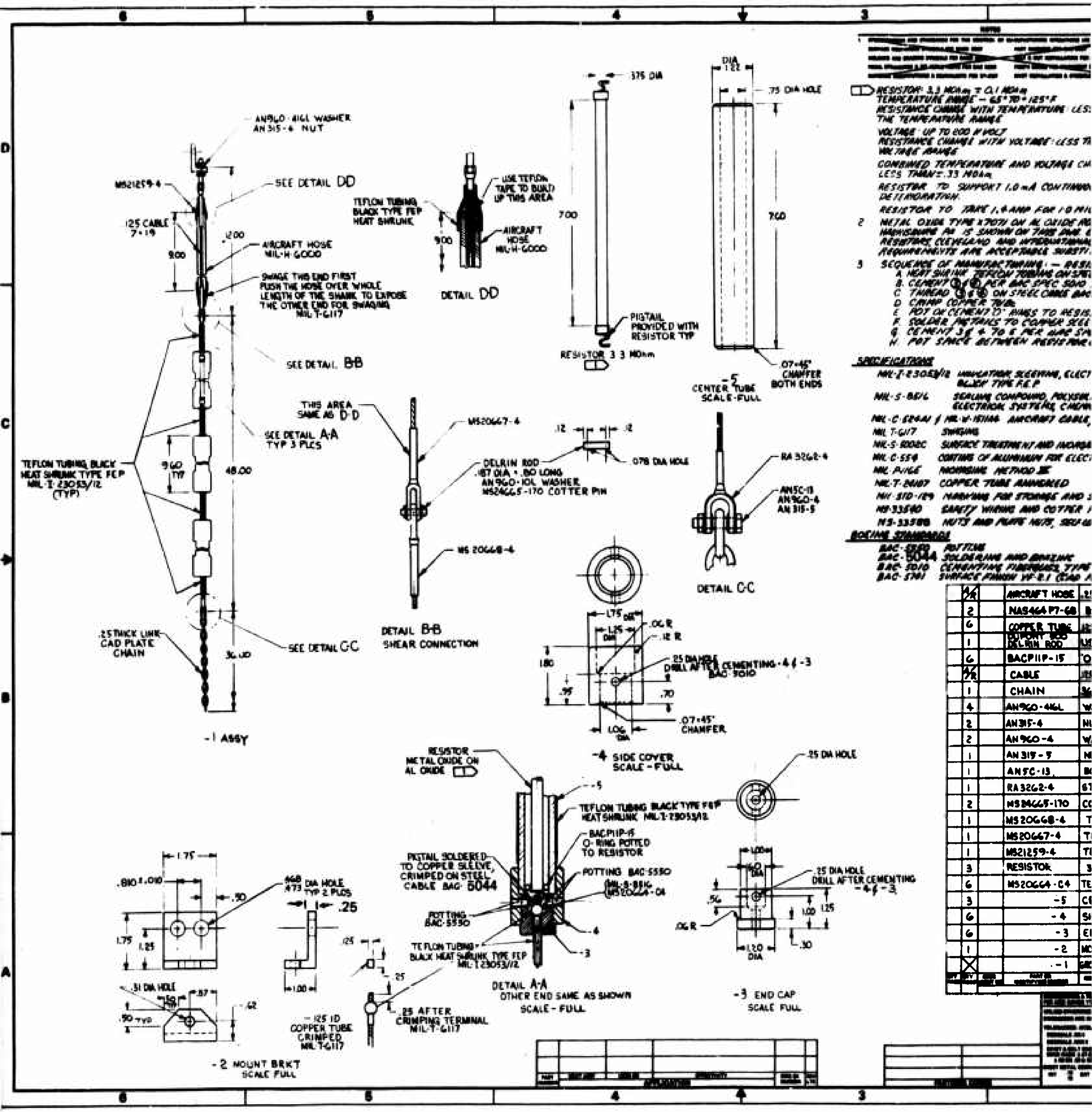

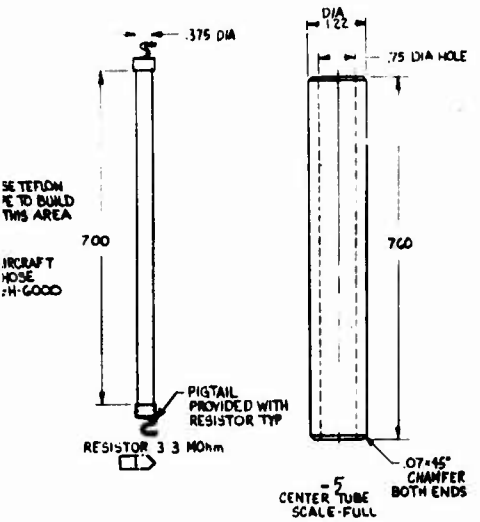

-5 CENTER TUBE
SCALE-FULL

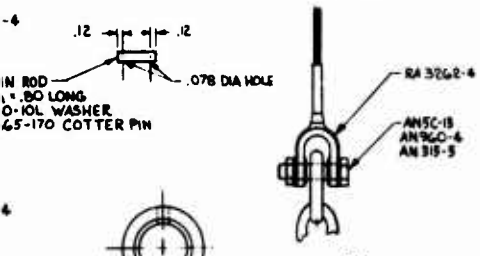

DETAIL C-C

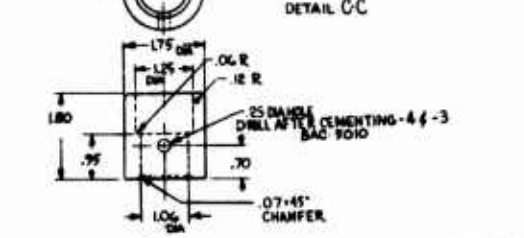

-4 SIDE COVER
SCALE - FULL

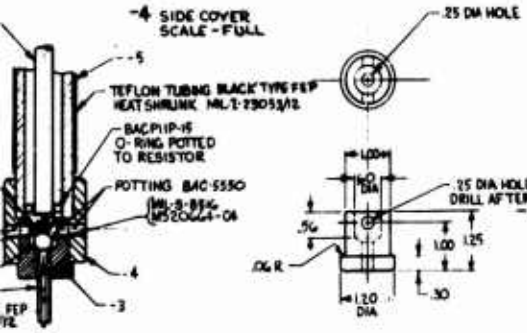

TAIL A-A
THER END SAME AS SHOWN
SCALE - FULL

-3 END CAP
SCALE FULL

RESISTOR: 3.3 MOhm ± 0.1 MOhm
TEMPERATURE RANGE — 65° TO +125° F
RESISTANCE CHANGE WITH TEMPERATURE: LESS THAN 0.083 MOhms FOR THE TEMPERATURE RANGE
VOLTAGE UP TO 600 V VOLT
RESISTANCE CHANGE WITH VOLTAGE: LESS THAN 0.2 MOhm FOR THE TOTAL VOLTAGE RANGE
COMBINED TEMPERATURE AND VOLTAGE CHANGE LESS THAN ± .33 MOhm
RESISTOR TO SUPPORT 1.0 mA CONTINUOUS CURRENT WITHOUT ANY DETERIORATION.
RESISTOR TO TAKE 1.4 AMP FOR 1.0 MICROSECOND WITHOUT DETERIORATION

2 METAL OXIDE TYPE X707H ON AL OXIDE ROD - BY RESISTOR PRODUCTS CO HARRISBURG PA IS SHOWN ON THIS DWG. EQUIVALENT RESISTORS OF VICTOREEN RESISTORS CLEVELAND AND INTERNATIONAL RESISTANCE CO MEETING ABOVE REQUIREMENTS ARE ACCEPTABLE SUBSTITUTES.

3 SEQUENCE OF MANUFACTURING: — RESISTOR ELEMENT
A. HEAT SHRINK TEFLON TUBING ON STEEL CABLE SEGMENTS
B. CEMENT ③ & ④ PER BAC SPEC 5010 TYPE 3B DRILL .25 DIA HOLE
C. THREAD ③ & ④ ON STEEL CABLE BACK TO BACK SWAGE BALL ENDS
D. CRIMP COPPER TUBE
E. POT OR CEMENT 'O' RINGS TO RESISTOR ENDS - INSERT IN TUBE - POT RESISTOR IN PLACE
F. SOLDER PIGTAILS TO COPPER SLEEVES
G. CEMENT 3 & 4 TO 5 PER BAC SPEC 5010 TYPE 3B
H. POT SPACE BETWEEN RESISTOR ENDS AND END PIECES

SPECIFICATIONS

MIL-I-23053/12 INSULATION, SLEEVING, ELECTRICAL, HEAT SHRINKABLE, POLYTETRAFLUOROETHELENE BLACK TYPE F.E.P.
MIL-S-8516 SEALING COMPOUND, POLYSULFIDE RUBBER FOR ELECTRICAL CONNECTORS AND ELECTRICAL SYSTEMS, CHEMICALLY CURED
MIL-C-5424A & MIL-W-15114A AIRCRAFT CABLE, STAINLESS STEEL
MIL-T-6117 SWAGING
MIL-S-5002C SURFACE TREATMENT AND INORGANIC COATING FOR METAL SURFACES OF WEAPON SYSTEMS
MIL-C-554 COATING OF ALUMINUM FOR ELECTRICAL CONDUCTIVITY
MIL P11GE PACKAGING METHOD III
MIL-T-24107 COPPER TUBE ANNEALED
MIL-STD-129 MARKING FOR STORAGE AND SHIPMENT
MS-33540 SAFETY WIRING AND COTTER PINNING, GENERAL PRACTICES FOR
MS-33588 NUTS AND PLATE NUTS, SELF LOCKING AIRCRAFT DESIGN AND USAGE LIMITATIONS OF.

BOEING STANDARDS

BAC-5550 POTTING
BAC-5044 SOLDERING AND BRAZING
BAC-5010 CEMENTING FIBERGLASS, TYPE 3 (SHEAR 500 PSI)
BAC-5741 SURFACE FINISH VF 2.1 (CAD PLATE)

4		AIRCRAFT HOSE	.25 ID .56 to .62 OD	MIL-H-6000		
2		NAS464 P7-6B	BOLT	TEMPORARILY SECURE FOR SHIPMENT		
6		COPPER TUBE	.25 ID × .25 LG	MIL-T-24107 ANNEALED		
1		SUPPORT ROD DEL-RIN ROD	USED AS SHEAR PIN	.38 DIA 80 LONG SHEAR STRESS 500 ± 200 #		
6		BAC P11P-15	'O' RING			
4/6		CABLE	.25 CABLE 7×19	AIRCRAFT CABLE STAINLESS STEEL MIL-C-5424A & MIL-W-83420		
1		CHAIN	36.00 LG	COMMERCIAL QUALITY		VF-2.1
4		AN960-416L	WASHER			
2		AN315-4	NUT			
2		AN960-4	WASHER			
1		AN315-3	NUT			
1		AN5C-13	BOLT			
1		RA3262-4	STANDARD FORK END	TRU-LOC Bridon Amer. Corp Wilkes-Barre, PA		VF-2.1
2		MS24665-170	COTTER PIN			
1		MS20668-4	TERMINAL			
1		MS20667-4	TERMINAL			
1		MS21259-4	TERMINAL			
3		RESISTOR	3.3 MOhm			
6		MS20664-C4	TERMINAL BALL END	STAINLESS STEEL		
3		-5	CENTER TUBE	FIBERGLASS		
6		-4	SIDE COVER	FIBERGLASS Taylor Corp Valley Forge, PA		
6		-3	END CAP	FIBERGLASS		
1		-2	MOUNTING BRKT	AL ALLOY 6061 .25 x 1.0 x 1.75		
X		-1	GROUNDING LINK ASSY			

PARTS LIST

HLH/ATC PASSIVE STATIC ELECTRICITY RESISTIVE GROUNDING LINK

J 77272 SK301-11753

SK301-11753 D

5716